NONLINEAR SEISMIC ASSESSMENT CRITERIA FOR REINFORCED MASONRY STRUCTURES IN CANADA

MARCO CALCAGNO

A THESIS SUBMITTED TO THE FACULTY OF GRADUATE STUDIES IN PARTIAL FULFILMENT OF THE DEGREE REQUIREMENTS FOR THE DEGREE OF MASTER OF APPLIED SCIENCE

GRADUATE PROGRAM IN CIVIL ENGINEERING
YORK UNIVERSITY
TORONTO, ONTARIO

SEPTEMBER 2024

Abstract

The objective of this thesis is to bridge the gap that exists in the field of the assessment of reinforced masonry (RM) structures in Canada under seismic loading. Contrary to common belief, earthquakes pose a significant threat to various regions throughout Canada. Despite this risk, Canada lacks a formally approved seismic risk-based assessment framework for existing RM structures, and instead, rely on U.S. evaluation criteria (NIST, ASCE/SEI -41, TMS 402) for the assessment of structures built to the Canadian design code (CSA S304). The work presented in this thesis aims to validate the extension of the ASCE/SEI-41 codes to the Canadian context, as well as assessing the accuracy and relevance of the empirically defined expressions for estimating the seismic performance indices in masonry construction. This was accomplished through the development of a comprehensive database of over 70 reinforced masonry wall specimens that were constructed and tested in Canadian Academic Institutions. The specimens considered encompassed a wide range of design parameters that proved to be an asset in this investigation as it allowed for a comprehensive representation of RM specifications found in the Canadian built environment. Analytical expressions provided in the U.S. evaluation criteria were programmed into the database and used to estimate the code-based analytical values of flexural and shear strengths, wall stiffnesses, mode of failure, and lateral drift capacities. These values were then compared with the experimentally recorded values and reported failure patterns from the Canadian test specimens, which provided insight into the accuracy and parametric dependence of the true response indices and the predicted values from Code expressions. Convergence of experimental and analytical results would demonstrate that these expressions are able to successfully predict the performance of RM structures and could therefore be seamlessly introduced in ongoing development of a Canadian Code of seismic assessment of Reinforced Masonry structures. A corollary to this is that divergence between analytical estimates and experimental values denote discrepancy in the underlying physical models used to interpret and quantify the response and therefore reconsideration and refinements in the theories are necessary. To explore these cases, detailed nonlinear finite element analysis was undertaken using the ATENA software with the objective to illustrate the role of important design values on the RM wall performance indicators to be used as a basis for the required improvement of the Code Expressions.

Acknowledgements

I want to express my thanks to my Supervisor Dr. Stavroula Pantazopoulou for her commitment to my success and support throughout the journey of completing this thesis. Working under her guidance has excelled my knowledge in the field of structural engineering and I am forever grateful for her patience and dedication. In addition, I am grateful for the contributions made by my committee supervisor Dr. Shooka Karimpour who has been a key figure in the evaluation of my research throughout the past several years.

Being a part of the Department of Civil Engineering at the Lassonde School of Engineering for the past 6 years to obtain my B.ENG and Masters of Applied Science degree has been an amazing experience that I will truly miss. Recognition goes out Riad Rajab for his help throughout the various stages of my graduate journey.

Special thanks to my good friends and colleagues Hadi, Roberto, Sandi and Buddhi who supported me along the entirety of my graduate studies and helped me achieve success. Special acknowledgement goes to Farah Dameh for her amazing teaching and assistance of my numerical work.

To my family and friends, thank you for believing in me throughout my academic endeavours and inspiring me to strive further. I truly would not have been able to accomplish everything I have without them

Finally, to my furry friends Zeus and Stitch. Thank you for being my dedicated study partners and keeping me company on countless late nights of work, I share this accomplishment with you.

Table of Contents

List of Tables

List of Figures

Chapter 1

Introduction

1.0 Introduction

Masonry stands as one of the most dependable building materials with a prevalence that spans around the globe for use in various construction applications. Its long-lasting population is mainly due to its inherent strength, durability and versatility that has made it an appealing material of choice for centuries due to its widespread availability and adaptability. One of its most notable strengths is the ability to be used to its full potential with minimal dependence on large machinery, a characteristic that was used to its fullest throughout history. As a result, many historic buildings and monuments around the world have been constructed from masonry and have stood the test of time, showcasing the longevity and reliability of this building material. From the iconic cathedrals in Europe, to the ancient temples in Asia, masonry structures comprise some of the most iconic structures ever built.

Masonry structures are frequently found in the Canadian built environment, largely in the form of historical buildings and within the modern lower-rise residential industry. Since the early days of its foundation as a country, Canada has been a leading nation in the trade and construction industry, which caused rapid growth that created the need for the development of its urban cities and metropolitan areas. Since Canada was a leader in lumber production at the time due to its rich local forestry environment, many early structures were built primarily out of timber. An overlooked design aspect of these structures at the time was the poor fire performance of wood, resulting in many devastating fires that completely wiped out Canadian cityscapes such as Montreal in 1852, and Toronto in 1904.

Figure 1.1) Aftermath of the Toronto fire of 1904 which destroyed over 100 buildings and caused over $300 million modern equivalent of damages (City of Toronto Archives, 1904)

Following these catastrophic events, building designs were carried out with an inclusion of fire performance considerations, which brought clay and concrete masonry construction into the limelight due to its strength, fire resistance, as well as durability properties. Many of these structures were originally built from un-reinforced masonry (URM), which consisted solely of concrete blocks connected together via mortar joints. The continually advancing construction industry brought forth advancements to this structural system in the form of added internal steel reinforcement bars, leading to the prevalence of reinforced masonry (RM) construction.

Reinforced masonry walls are commonly built from hollow concrete blocks which are then filled with grout, either fully or partially along the length of the wall. Steel bars are then placed inside these grouted voids in both the vertical and horizontal directions, which bonds to the grout and creates one composite unit. The presence of steel reinforcement within the wall provides

significant enhancement to ductility performance and consists of vertical (longitudinal) bars placed in the hollow cells of the masonry cinder blocks, and horizontal (transverse) bars placed either in the mortar joints, or in specially arranged blocks (referred to as knockout units) so as to allow for the passage of the bars through the masonry blocks; the resulting formation is known as bond beams. The final resulting product from this is a robust and durable structure able to withstand various stresses, with additional ductility performance as a result of the added reinforcement.

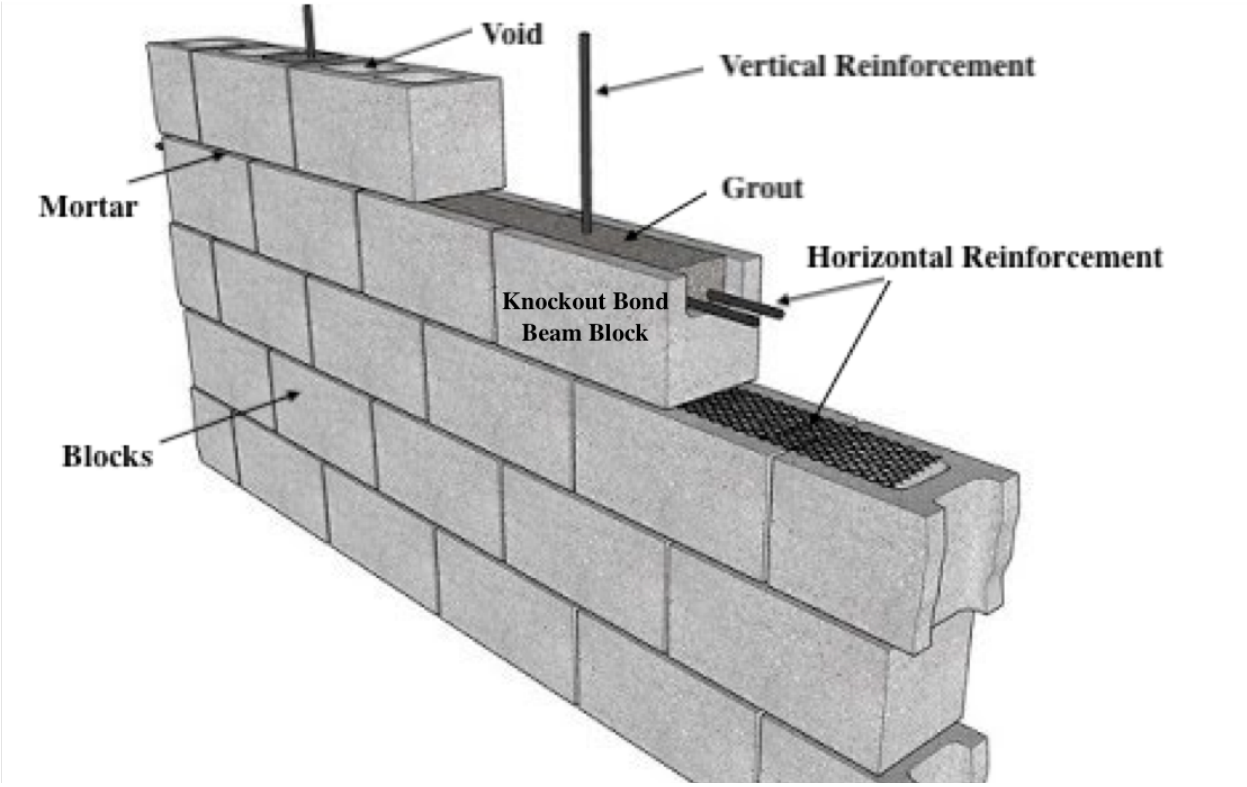

Figure 1.2) Schematic illustrating the arrangement of the vertical reinforcement placed inside the grouted cell voids of masonry blocks and the horizontal reinforcement placed in the grouted courses built with bond beams/knockout units

1.1 Knowledge gaps

In the component form of construction, masonry elements are planar components where the thickness is much smaller than the other two dimensions. As a result, most of the focus in masonry codes is in masonry walls, where these walls may have rather low aspect ratios (shear span to section depth ratio), but seldom reach values that exceed 3. Therefore, masonry walls when loaded in their plane are considered deep members. Despite the placement of reinforcement as described in the preceding, masonry elements are generally under-reinforced (i.e., they often

contain sparsely spaced bars that amount to a low reinforcement ratio over the wall area) and carry relatively low axial load from the overburden weight. On account of these characteristics of detailing, masonry walls are of primary significance (in terms of stiffness and strength) when loaded in their plane of action whereas when loaded normal to that plane their response is that of very slender flexural elements.

These aspects of the masonry wall behavior are particularly important in the case of earthquake loading. Older masonry structures, built to former design codes prior to the introduction of uniform seismic risk in Canada, are at higher risk for developing damage in the event of an earthquake, on account of the intrinsic characteristics of masonry construction outlined above. With each revision of Canadian Codes and redefining the seismic risk of the country, an increasing number of masonry structures have to be checked with regards to their performance and the anticipated level of damage they are likely to undergo in a future event.

Seismic evaluation or seismic assessment of existing structures has gained more attention after the issuing of formal guidelines by NEHRP and FEMA in the US in the early 2000's. The recommended procedures presented in the ASCE/SEI 41-23 document are a culmination of continuous effort for revision and improvement as more and more experimental and seismological data become available. At the same time, reconnaissance reports from field seismic events illustrate points of systemic weakness in older construction methods that are responsible for extensive damage or collapse. The ASCE/SEI-41 procedures are revised on a 5-year cycle and include specific sections dedicated to both Reinforced and Unreinforced Masonry. Canada's NRC (National Research Council) has also started to develop its own set of provisions addressing different structural systems in the Canadian built environment. In all cases, the procedures are classified depending on the increasing level of complexity required for their application as Tier 1, Tier 2 and Tier 3; the three levels are intended to identify, from among the vast number of evaluated structures, those that present specific risks for damage. Tier 3 procedures require detailed analysis of the structural system using a numerical model (either frame or detailed finite element analysis), where component stiffness is specified by the user (either in the form of member stiffness or effective material moduli). By analysing the structural model to an estimated seismic hazard with a preselected probability of occurrence, performance of the individual components is quantified in terms of a performance indicator (either in terms of force demand, or in terms of deformation demand). In the stage of evaluation, these performance indicators are compared against preselected

limit states that have been calibrated from previous test results as quantifiers of the level of anticipated damage, which are referred to as "performance limit states". In the case of reinforced masonry, the various performance limit states, which are associated with minimal damage, repairable damage, and near collapse of the structure, have been determined from collective evaluation of a large database of tests conducted in various universities throughout the United States of America. In the present study, the objective is to check the applicability and relevance of these criteria when used to evaluate Reinforced Masonry Structures in Canada. To obtain an independent evaluation, a database of tests is assembled and studied against the proposed limit states. To avoid overlap and bias of the analysis by considering tests that have been already included in the Database of ASCE/SEI-41 that supported the derivation of the performance criteria and associated limit states, only tests conducted in Canadian Universities were considered in the present work. This also provides the benefit that allows for focus on detailing practices and material properties that are characteristic of the Canadian Masonry Construction Practice.

1.1.1 Physical Properties of Reinforced Masonry

The possible design arrangements that can be chosen for a given reinforced masonry structure are virtually endless, and as a result, the assessment of these structures is an arduous process that requires the use of several design assumptions to make the process objective and unbiased from preconceived notions as to the function of the individual components in the overall system. Whether it be from the minor misalignments of the individual blocks and mortar joints that may occur during its construction process, to the specific amount and pattern of the steel reinforcements used, or the connectivity between blocks and between structural elements at construction joints, there is no way around the numerous tolerances and inaccuracies that could affect the accuracy of the analytical representation of these complex structures. Although masonry structures have been around for centuries, there is still a surprising degree of uncertainty surrounding the exact shear behaviour and distribution of forces that occurs along the interfaces between the individual blocks and mortar joints. This is due to the fact that the engineering analysis of reinforced masonry structures is a multifaceted procedure that demands comprehension of the mechanical properties of all the materials utilised in the design such as the concrete blocks, the specific mortar and grout mixture, the arrangement of the grouting, the properties of the multiple planes of interface and interaction between dissimilar materials, and the steel reinforcement bars.

Understanding the mechanistic behaviour of each component is essential for the calculated response variables to be relevant with reality, however, determining the precise strengths of each of these parameters is a complex task of its own.

Unlike reinforced concrete structures that typically exhibit uniformity along the entire section of the wall, reinforced masonry structures contain irregularities in the form of the individual mortar joints between every block that connect them together to form the wall. These mortar joints are laid by workers all by hand, and as a result, are largely susceptible to human error in the form of varying thicknesses and asymmetries in every direction. This is crucial since joints play a significant role in the crack propagation and load transfer throughout the wall and therefore affect the structural mechanics in a profound manner. Additionally, the design expressions that are followed for the engineering analysis and design of reinforced masonry structures contain limitations and biases owing to (a) the empirical approach in deriving them, and (b) the bounds of the databases that have supported their derivation (this refers to the set of parameter values and combinations thereof, that have been tested by the individual investigators from where the specimens of the database are drawn). It is noted that most of the experimental studies report results from a small group of specimen tests, owing to the fact that conducting a single masonry wall test is a significantly labour-intensive challenge. Therefore, the experimental variability and repeatability of experimental evidence that is sought in other experimental studies that deal with small samples (e.g. cylinders or cubes) cannot be captured in the typical experimental paper that reports test results on wall components. Instead, this variability is captured in this experimental field only through the assembly of databases of tests that are conducted studying the same problem by several different investigators.

This methodology is used in the present work, where the parametric sensitivities of the problem of masonry wall behaviour is captured by crossing the boundaries of the individual studies when combining them into a single dataset. Where the role of certain parameters is not clear in the experimental evidence, answers and clarity are sought in numerical simulation of wall tests after calibration of the numerical models to test results. This approach is also followed in the present study, using the numerical platform known as GiD-ATENA (Cervenka Consulting, 2023). The following sections of this thesis aim to identify how well the data collected correlate with the empirical assessment procedures of ASCE-SEI 41-23, and where discrepancies are noted, further

investigation is pursued using numerical simulation in order to determine how the procedures may be improved when adapted into the Canadian Seismic Evaluation Framework.

1.1.2 Seismic Assessment Provisions

One of the most severe loading events a structure can experience during its lifespan are the demands induced by earthquakes. Within the context of the assessment for reinforced masonry structures under seismic loads, there are specific analysis procedures that are intended to be followed for quantification of the seismic demands of such a structure at a specific seismic hazard level. In Canada, the Tier 3 analysis for seismic evaluation of structures is still being formulated, considering however the procedures already adopted in the US. Contrary to common belief, there are quite a few fault lines that pass through the Canadian topography and bring with them inherent seismic risk, most notably along the western coast, and near some major Canadian cities such as Montreal. Fracking for petroleum extraction has also created seismicity in what is known as "stable Canada" in the prairies. So, in today's reality throughout Canada, there is seismic risk to be reckoned with, having different intensities which may be uniformly commensurate to the severity of requirements reflected in previous construction approaches (i.e., moderate risk in the prairies where requirements were practically non-existent, severe risk in the Western provinces where however the detailing – albeit existing, is now considered below current standards).

The work presented in this thesis intends to contribute to this field through the use of an experimental database of reinforced masonry walls constructed within Canada. The collected experimental data will be vetted and compared against analytical data obtained from the NIST (GCR 17-917-45) and ASCE/SEI-41 (2023), provisions in effort to propose recommendations for the new Canadian framework considering the American provisions for seismic assessment of Reinforced Masonry.

1.1.3 Masonry Design Codes

As is typically standard in the engineering practice, there are many design standards that are set in place to serve as a benchmark to be followed in the engineering design and construction processes which are often used to streamline the processes. Standards exist for all sectors of design and range from a variety of materials and applications, and will generally vary between different geographical regions based on local common practices.

Canada and the United States follow separate codes related to the structural design and analysis of Reinforced Masonry structures. For buildings constructed within Canada, the CSA S304-24 controls current design whereas the TMS 402-22 is followed for buildings constructed within the United States. Although these codes aim to accomplish the same goal of maintaining the safety and welfare of the public by providing recommendations required for adequate construction procedures, there exist several key differences between the two which identify the knowledge gap in the field that is traditionally settled through empiricism. This empiricism restricts their applicability to only structures built within their prospective region of authority and from similar design details as what was present in the data that was considered in their derivation.

The presence of key differences between these two national codes has been a known issue and has provoked the research interest throughout the past several years of several key organizations such as the National Concrete Masonry Association (NCMA, 2024), the Canadian Standards Association (CSA, 2024) and the Canada Masonry Design Centre (CMDC, 2023-2024). An in-depth comparison of these codes will be provided in the upcoming literature review presented in Chapter 2 of this thesis. Furthermore, it is noted that different standards exist for RM structures in Canada and the US, yet a single seismic assessment procedure is currently being applied. To this end, the research presented in this thesis demonstrates an initiative to identify areas of discontinuity between the two standards, possibly emanating from the intrinsic differences in the underlying Codes of RM design and detailing, and attempt to derive recommendations to aid in reconciling these differences.

1.2 Objective

The principle objective of the presented thesis was to assemble an experimental database that comprised of a large set of data taken from Canadian literature regarding the in-plane lateral performance of reinforced masonry walls. This database contained the varying design parameters found in all the walls, with the goal in mind of programming the Canadian CSA and American TMS prescribed design equations for each wall in accordance with these design parameters. The goal in mind for the completion of a database such as this was to compare the analytical estimates determined from such equations with the data that occurred in reality from the Canadian experimental tests. Convergence of results between analytical and experimental response indices would be an indicator that the equations presented in the masonry design codes are appropriate in

determining the response of a reinforced masonry structure in Canada. In the scenario where dissimilar results between analytical and experimental values, an investigation could be carried out to determine what was leading the analytical estimates astray, and potential recommendations for a reworking of these empirically defined expressions could be investigated.

1.3 Methodology

To address the thesis objectives, an experimental database was assembled in an effort to lead the investigation toward overcoming the ambiguities imparted by the empirical expressions of the Seismic Assessment procedures for Reinforced Masonry structures. Tests considered in the database were purely related to the in-plane, lateral resistance of reinforced masonry structures built and tested in accordance with Canadian practice. As such, the data presented in this work is aimed towards a Canadian audience, with experimental and analytical values being represented in limit states design and metric nomenclature unless otherwise specified. By systematically collecting data relating to the physical properties, structural configurations and performance of wall specimens under simulated seismic conditions, a complete picture of the complex interactions of these structures was assembled and analysed. A detailed explanation regarding the collection and processing of the experimental data in the database is presented in the third Chapter of this thesis. Quantitative data metrics of interest from the experimental tests were related to the milestone points of wall performance such as the yield strength and ultimate residual performance point of the wall specimens at respective levels of lateral drift. The goal of the methodology has been to conduct an all-inclusive comparison of the design standards outlined in the Canadian Masonry Design Code (CSA S304-24) and the corresponding American Standard (TMS 402-22) The procedure consisted first of the identification of key differences and knowledge gaps between the two codes, and was then followed by a parametric study of Canadian experimental test data conducted on reinforced masonry wall specimens tested under in-plane, fully reversed cyclic lateral displacements to simulate representative earthquake forces. Convergence of results between the test data and the results from analytical calculations using the reference framework adopted in ASCE/SEI- 41 (2023) is used as a criterion for required improvements in the methodology of seismic assessment.

1.4 Organization of the Thesis

1.4.1 Chapter 1

The first Chapter of this report provides an overview of the conducted research. Beginning with an introduction into reinforced masonry (RM) construction, it begins to address the complexities associated with the seismic assessment of existing RM structures in Canada. The experimental database is briefly introduced and the methodology of research is discussed. This chapter states the primary objective of the database assembly, which is to fill the gap within the Canadian earthquake engineering field by evaluating the applicability of American codes on Canadian RM structures, and expands the scope of the research by introducing the use of numerical models as a means to supplement missing data in ranges of parameters beyond the bounds of the database, after pertinent model calibration.

1.4.2 Chapter 2

In Chapter 2, an in-depth literature review and state of the art discussion is provided. The literature review has been conducted on the codes and standards relevant to the research and provides an overview of the similarities and differences between the CSA S304-24 and the TMS 402-22 codes used for design of reinforced masonry structures in Canada and the US, respectively. With regards to seismic assessment provisions, the two frameworks investigated are the ones presented by the National Institute of Science and Technology, NIST (GCR 17-917-45) and the American Society of Civil Engineers, ASCE/SEI -41 (2023).

In addition, a review of the studies conducted on the reinforced masonry specimens present in the database is provided to observe the construction methodologies, loading procedures and range of design parameters present in the test matrix, which may have a bearing on the estimated response indicators.

1.4.3 Chapter 3

In Chapter 3, a detailed description of the methodology utilised in the development of the database is provided. The chapter begins with a discussion of the background surrounding the objective of the study, then goes into an examination of the specimens considered in the data collection. This examination considers the design parameters of the specimen, such as the material properties, specimen dimensions and reinforcement details, the presence/absence of boundary elements, and the performance of tested specimens. This is followed by a review of the

experimental setup followed by the researchers in the experiments considered in the database, which referred to the test procedures and loading protocols followed. Finally, the milestone points of the load displacement curves obtained from the tests and representing the mechanical response of each specimen is discussed and the significance of their definition as performance indicators is explained.

1.4.4 Chapter 4

The fourth Chapter of this report presents the results obtained from the analysis of the database. It includes calculations of the flexural and shear strength estimates for each specimen obtained through application of code prescribed equations, and provides a comparison against the experimentally recorded values. In addition, it investigates the discrepancies that were found between the recorded failure modes in the experiments and those predicted through analytical estimates while providing insight into the potential reasons for this discontinuity. The comparative analysis discussed in this chapter aims to highlight the need for revisions of the Canadian and American design provisions on account of their differences in assumed values and achieved experimental results.

1.4.5 Chapter 5

The fifth Chapter of this thesis compares the experimental deformation indices (drift or rotation capacities) of the specimens with the estimates obtained after application of the Assessment Frameworks mentioned in the preceding for these parameters. An analysis of several design parameters is considered in an attempt to display the sensitivity of performance with regards to changes of the three key influencing parameters of design in accordance with recommendations provided in NIST (GCR 17-917-45); these being the aspect ratio, vertical reinforcement ratio and axial load ratio. Finally, an analysis is presented for the stiffnesses of the walls, with a comparison made between the experimental values, obtained from the ascending branch of the backbone envelope, and the theoretical values that were computed through analytical equations. Recommendations are provided for the enhancement of convergence between the experimental and analytical values, and a validation for the use of cracked properties in the expressions is presented.

1.4.6 Chapter 6

The sixth Chapter of this report is related to the detailed finite element analysis conducted using the ATENA software. The aim of this portion of the work was to address the open issues regarding the various empirical expressions used for the assessment of reinforced masonry structures such as the analytical stiffness and shear calculations. Through the use of a detailed finite element model, a clearer understanding of the mechanical response occurring along the specimen was obtained, and was used to analyse discrepancies between experimental and theoretical values as well as to explore the response of masonry walls with design variables beyond the range of the database collection. The numerical model used as a basis for the study was developed after verification of a specimen selected from the relevant Canadian experimental literature; verification was based on successful correlation between calculated and experimental response characteristics including prevalent failure mode.

1.4.7 Chapter 7

The final Chapter of this thesis summarizes the findings of the conducted work and makes recommendations into the next steps required from this research to address the discrepancies in code and potentially adapting a Canadian specific seismic assessment framework for existing reinforced masonry structures.

Chapter 2

State of the Art & Literature Review

2.0 Background of Reinforced Masonry Structures

For centuries, societies around the world have faced the task of meeting the demand for housing and facilities on account of the population and urban growth. Due to their ready availability and ease of construction by skilled workers, masonry buildings quickly became the main construction method of choice. In its early days of use, masonry structures were unreinforced and were built from readily available stones present in the area. These stones were often of varying dimensions and as a result, the walls constructed in this manner had a random arrangement of blocks and variation of joints connecting the individual elements. Advancements in this methodology saw the adoption of uniform blocks connected in a much more precise manner which allowed for a more systematic construction process and presented regularity and clean geometry along spans as mortar joints of the same dimensions could be used throughout.

Figure 2.1) Visual comparison between the random distribution of blocks in historic masonry (left) and modern (right) construction

As it was found repeatedly throughout history, these masonry structures lacked sufficient seismic resistance and were susceptible to damage and collapse during earthquakes. This deficiency stemmed from the rigid and brittle nature of the masonry blocks which allowed for ease of cracking and sliding along the individual mortar joints. Following the identification of this deficiency in the structural system, new construction techniques in the early to mid-twentieth century employed the addition of reinforcement to improve the ductility and performance of the masonry. The first form of reinforcement utilised in masonry structures was through the use of timber lacing, which involved placing horizontal timber elements within the masonry courses to tie the individual blocks together and assist in lateral load resistance. From here, early applications saw the implementation of wrought iron bars built into the brickwork of structures, which although the exact contribution towards the force resistance that resulted in their presence was not fully understood at the time, generation of engineers began experimenting on this form of construction to further enhance their design. This eventually led to evolution of the use of steel rebar instead of iron, which were not only placed in the same horizontal manner between courses as the timber laces, but also vertically inside cell voids of the individual masonry blocks. With the inclusion of vertical reinforcements, walls are able to withstand much greater loads as a result of the added flexural strength and attained ductility, as well as better resistance towards lateral forces.

2.1 Seismic Risk in Canada

Out of all the different geographical regions of the world, Canada is often not associated as being a country with severe seismic risk. This assumption is not entirely correct since many regions across Canada are intersected by various fault lines that are susceptible to tectonic plate slippage which has been known to induce seismic activity. Figure 2.2 and Figure 2.3 below illustrates the varying levels of seismic hazard across Canada for spectral accelerations at periods of 0.1 seconds, Sa (0.1), and 0.05 seconds, Sa (0.05). From these Figures, we can see that the greatest seismic intensities, denoted by a red colour gradient, occur along the western coast. In addition, similar, but often lesser, intensities are reported across various regions along the perimeter of the country, with relatively stable regions reported in the middle regions of the landscape.

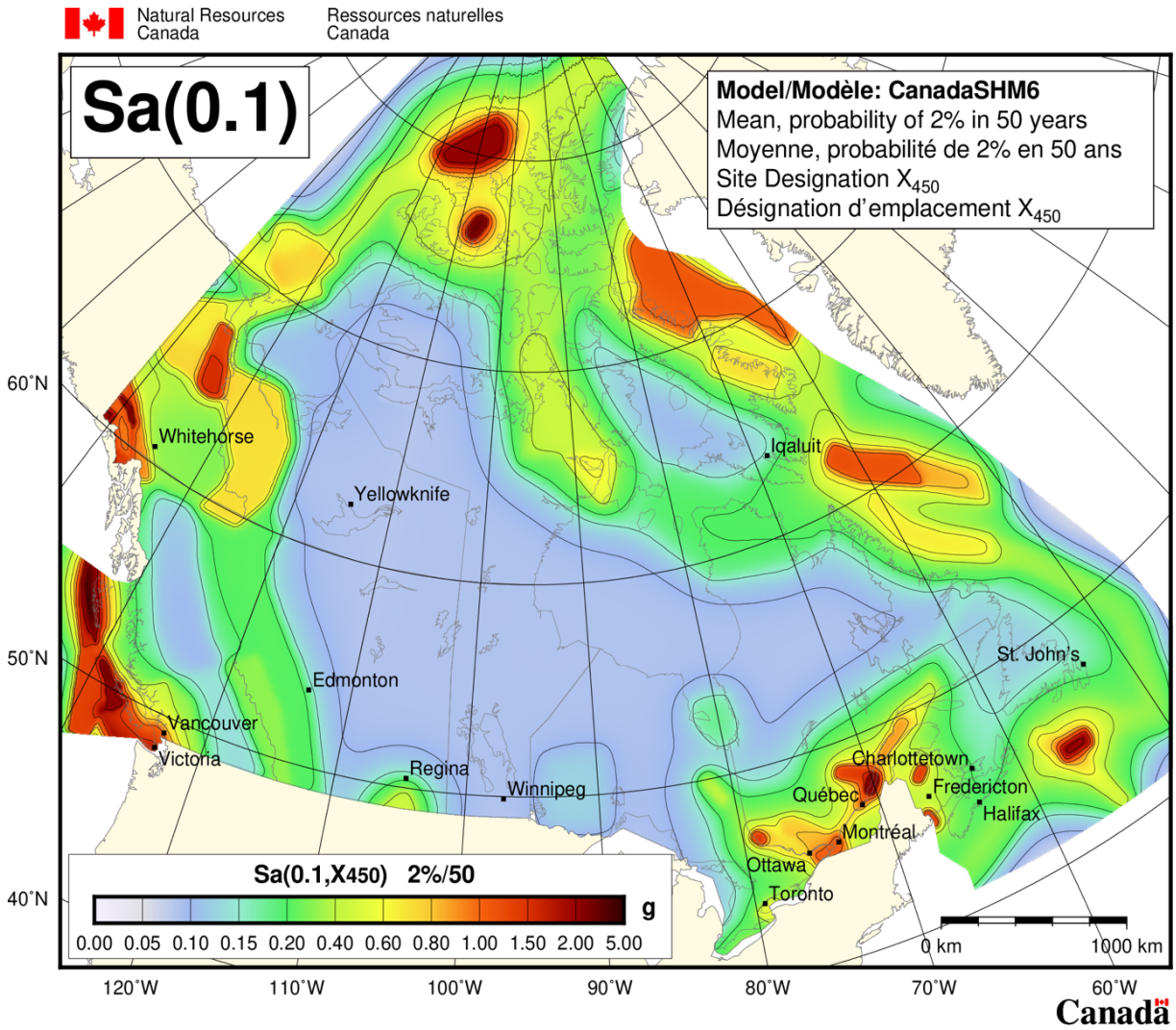

Figure 2.2) 2020 National Building Code of Canada seismic hazard map for spectral acceleration for a period of 0.1 seconds (Mean values of 5% damped spectral acceleration for site designation X_{450} and a 2% probability in 50 years)

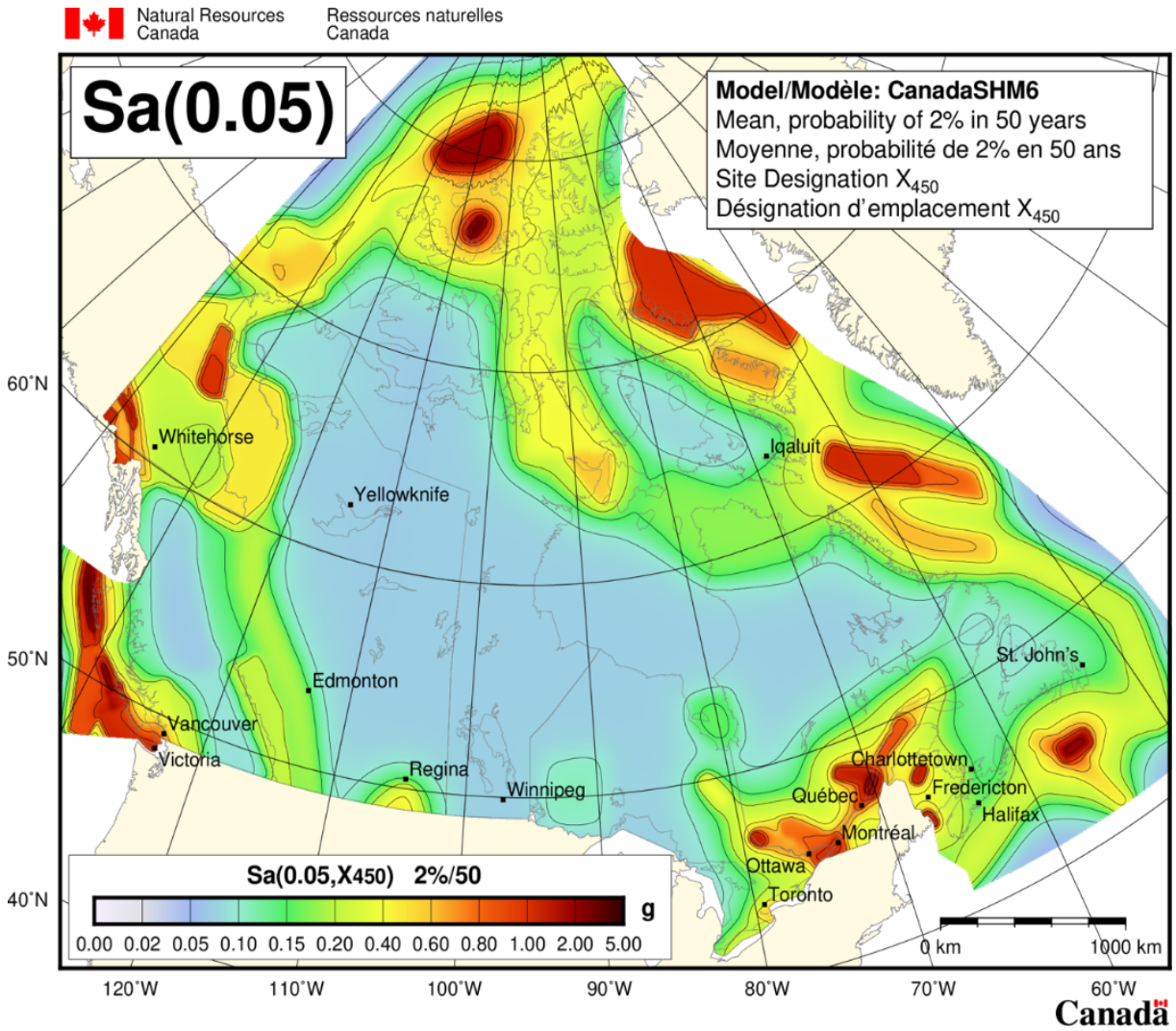

Figure 2.3) 2020 National Building Code of Canada seismic hazard map for spectral acceleration for a period of 0.05 seconds (Mean values of 5% damped spectral acceleration for site designation X_{450} and a 2% probability in 50 years)

It is important to note that due to the increased prevalence of hydraulic fracturing procedures in recent years, subsurface conditions across the country have been altered in a manner that has increased seismic risk throughout the Canadian landscape, even throughout the otherwise stable regions of the country. Fracking involves the injection of high-pressure fluids into the earth's crust in order to create cracks in deep rock formations to allow for natural gas and oil to be extracted. This fracturing of formations can cause earthquakes to occur through slippage of existing faults. The slippage of these faults is often encouraged from the improper disposal of wastewater from these procedures, where large volumes of water is injected into deep underground wells, that can act as a form of lubricant on the fault lines and make them more prone to slippage.

As a result of these factors, the need for a robust methodology for the seismic resilience of masonry structures in Canada is of paramount importance.

Reinforced masonry structures are prevalent in the Canadian built environment, primarily in residential construction due to their reliability and cost-effectiveness, with some of these being historical structures built prior to the 19th and early 20th centuries. These structures have been prone to material degradation throughout the years and might have not been constructed with adequate design considerations, therefore, having a dependable means of prediction of the response of these structures during a seismic event is crucial to promote their longevity and the safety of the general public.

2.2 Performance of Reinforced Masonry Structures

Reinforced masonry structures can exhibit a diverse range of behaviours depending on the selected design method, which can depend on a series of specifications such as the reinforcement layout, the mechanical properties of the steel and masonry constitutive parts, and the severity and orientation of loading. In order to ensure accuracy of the experimental investigation conducted in the present work, the wall specimens considered in the data analyses were reinforced specimens tested under fully reversed cyclic loading, with a wide variety of reinforcement arrangement and design specifications which brought forth a layer of additional statistical confidence in the data.

In reinforced masonry specimens, the inclusion of steel reinforcement bars within the wall aids in the distribution of the shear forces along the height induced from the applied lateral loading that is meant to simulate similar forces that would occur from seismic activity. The performance of each specimen can be classified based on its exhibited mode of failure, which could be either a brittle, force-controlled shear failure, a ductile deformation-controlled flexural failure or a mixed response between the two.

2.2.1 Shear Failure

Shear failure is a common form of response for reinforced masonry structures subjected to earthquake forces. This form of failure is accompanied by brittle diagonal cracking that demonstrates little indication of distress prior to failure, which is why common construction practices often specifically design against this performance mode. Specimens constructed with low aspect ratios (ratio of height to length dimensions), generally less than 0.8, high amounts of vertical (longitudinal) reinforcement, and walls with low amounts of horizontal (transverse) reinforcement

are prone to experience this form of failure. Shear failure occurs when the principle tensile stresses that are induced on the wall specimen from the combined action of the horizontally acting seismic loads and the vertically acting loads owing to the combined effect of the overturning action of the earthquake loads and the overburden gravity loads exceed the specified tensile strength of the masonry.

In terms of the analytical calculations, shear failure is expected to occur when the calculated shear strength of a wall specimen is estimated to be less than its flexural strength, meaning that shear behaviour will occur first and dominate the response of the specimen. Shear failure in a reinforced masonry wall can occur in several different forms based on the specific construction details of the specimen and loading procedures used in the test. For example, walls tested under high axial compressive forces are more prone to failing through diagonal tension cracking of the masonry blocks as opposed to shear sliding along the bed joints. In the context of a shear failure of a reinforced masonry wall, there exist several distinct modes of response that could occur based on the details of the specimen and the combined action and sequence of applied forces.

2.2.1.1 Factored In-Plane Sliding Shear Resistance

Failure due to wall sliding is a possible behaviour that can occur when a portion of the wall slides on a horizontal plane relative to another portion of the wall, typically either between courses at a mortar joint or along the base of the wall at the footing. For the purposes of the investigation at hand, only sliding failure occurring at the base of the wall was considered in the data analysis since this is the location of highest lateral force demand. Computing the shear resistance at every bed joint along the height of the wall is possible but it would exceed the scope of the present work and steer too far from the task of analysing the validity of the current practice in the transfer of foreign American codes to existing Canadian reinforced masonry structures for a seismic assessment context.

This sliding shear failure is characterised by a loss of cohesion and friction at the plane of sliding and results in lateral displacements without substantial deformation along the height of the wall. This form of behaviour is prone to occur in walls subjected to low vertical gravity loads and high lateral forces, such as those located at the ground-level of low-rise buildings. In practice, this form of failure is designed against through the implementation of adequate amounts of sufficiently anchored vertical reinforcement which would resist sliding through dowel action. Additionally,

the sliding resistance is also enhanced by increased depth of compression zone where force transfer occurs by friction.

Figure 2.4) Illustration of a typical sliding plane of a reinforced masonry wall that has failed due to sliding along the mortar-brick interface

Through analysis of numerous specimens considered in the test matrix of the database all tested under varying levels of applied axial stress, sliding shear was most likely to occur at the base of the wall since this is where the maximum shear force is acting. However, it was observed that for wall specimens that were a part of a larger multi-storey building, they could in fact experience a sliding failure towards the top of the wall height given that the gravity loads at the top of the specimen are less than at the base. Without the presence of these compressive gravity forces serving to keep the masonry from sliding through enhanced frictional resistance, the masonry is able to slide along a horizontal plane much easier at a higher course along the height. This finding was confirmed by results obtained from EIDin (2017), where it was found that in the

absence of sufficient vertical reinforcement as well as partial grouting of the wall, it is not possible to mobilize adequate dowel action so as to prevent sliding failure from occurring.

As per CSA S304 provisions, the factored sliding shear resistance of a reinforced masonry wall with sliding occurring at the mortar joints between courses is computed through the following analytical expression:

$$V_r = 0.16\ \phi_m \sqrt{f'_w}\ A_{ucr} + \phi_m \mu P_1 \quad (2.1)$$

For sliding occurring between the base of the wall and the concrete support, the factored in-plane sliding resistance is equal to the frictional coefficient along the sliding plane times the maximum compressive force

$$V_r = \phi_m \mu C \quad (2.2)$$

Where:

ϕ_m - Masonry material factor, which for the purposes of this assessment study, has been set equal to 1

μ - Friction coefficient of the sliding surface, defined as the ratio of the applied compressive force perpendicular to the surface of the frictional force parallel to the surface required to maintain motion

$\mu = 1$ for sliding occurring between masonry to masonry contact such as between courses

$\mu = 0.7$ for sliding occurring between masonry and smooth concrete such as at the connection between the base of the wall and the concrete base

C - Compressive force in the masonry acting normal to the sliding plane (kN)

$$C = P_1 + N \quad (2.3)$$

P_1 - Applied axial compressive load (N)

N - Factored tensile yield force of the vertical dowels that develop a yield strength on both sides of the sliding plane

$$N = A_{vertical,\ total} * f_{y,vertical} \quad (2.4)$$

f'_w - Compressive strength of the masonry wall as a composite unit, which is expressed in these equations in a square root term to approximate the tensile strength (MPa)

A_{ucr} - The uncracked segment of the effective cross-sectional area of the wall that provides shear-bond capacity (mm^2)

$$A_{ucr} = c * t_w \quad (2.5)$$

2.2.1.2 In-Plane Crushing Failure

The second form of shear failure consists of crushing of the blocks, and often occurs on walls with lower aspect ratios. This form of response is typically accompanied with diagonal cracking that propagates through the masonry and mortar joints running parallel to the field of principal compression stresses. Cracks continue to grow as the severity of loading increases which leads to the eventual crushing of masonry along diagonal struts. In addition, improper placement of vertical reinforcement within the wall can fail to provide the necessary confinement to the masonry, creating weak points susceptible to localised crushing. This form of response is known to occur when the compressive strength of the wall (f'_w) is locally exceeded by the applied compressive stresses. It is important to recall that the compressive strength of a reinforced masonry wall is not necessarily equal to the strength of its constitutive parts, but rather is related to the bond between them. This means that for a given reinforced masonry wall specimen, the specified compressive strength (f'_w) is often lower than the compressive strength of the block or mortar used for its construction. The determination of the specified compressive strength of a reinforced masonry wall (f'_w) can be determined through analytical methods that incorporate standard values provided in design tables, or with a more accurate procedure of experimental testing of masonry prisms. These prisms, sometimes referred to as wallettes, are constructed to at least two units high and built with stacked mortar bond and without the presence of any reinforcement. According to CSA S304-24 provisions pertaining to the shear resistance of a reinforced masonry wall, the shear force applied in the wall should not exceed the following empirical limit:

$$V_{crush} = 0.4\phi_m\sqrt{f'_w}b_w d_v \gamma_g \quad (2.6)$$

Where:

ϕ_m - Masonry material factor, which for the purposes of this assessment, has been set to 1

f'_w - Compressive strength of the masonry wall as a composite unit, which is expressed in these equations in a square root term to approximate the tensile strength (MPa)

b_w - Thickness of concrete block used in the construction of the wall (mm)

d_v - The effective depth of the wall cross section, which is taken as the distance from the centroid of tensile reinforcement to the centroid of the compression zone (mm)

γ_g - Grouting factor to account for grouted sections, which has been set to 1 for assessment

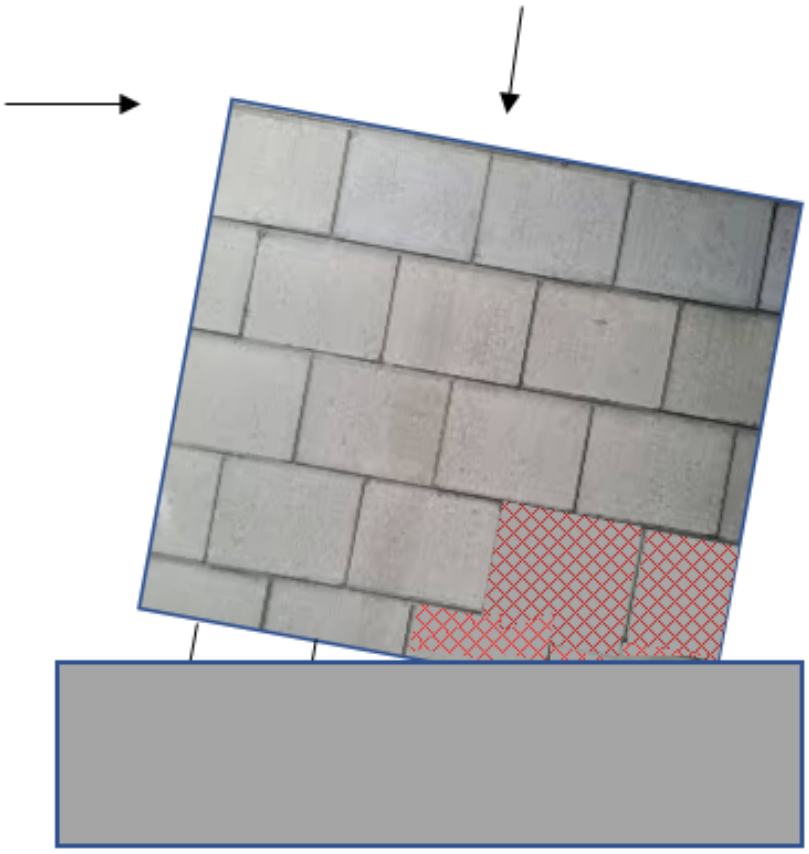

Figure 2.5) Illustration of the isolated crushing blocks of a reinforced masonry wall that has failed due to a shear crushing failure

2.2.1.3 In-Plane Diagonal-Tension Failure

A diagonal tension failure is prone to occur in a reinforced masonry wall when the tensile capacity of the masonry is exceeded by that of the applied shear stresses, leading to the formation of an approximate 45-degree angle crack across the wall. Diagonal-tension resistance is based on strength contributions stemming from the combined action of the masonry units and the steel reinforcements placed horizontally in the cell voids of the blocks and between courses. The contribution from the masonry is mainly established from the masonry walls compressive strength (f'w), the arrangement of grouting, and the design geometry of the specimen, (length, height, block thickness, boundary element dimensions, etc.) while the shear strength contribution stemming from the steel reinforcement is based on the amount, spacing and yield strength of the horizontal bars. The interaction that occurs between the masonry and reinforcement steel creates a composite

action that is able to provide enhanced shear capacity, although the precise contribution from each parameter is currently not well known due to the inherent complexity of reinforced masonry structures and the ambiguities surrounding the current analytical models.

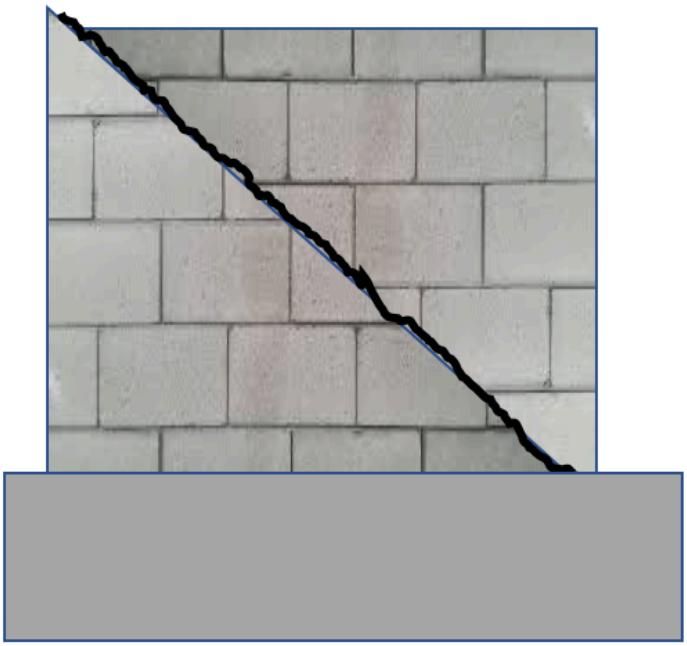

Figure 2.6) Illustration of the diagonal failure of a reinforced masonry wall that has failed due diagonal tension from the yielding of horizontal reinforcement

The following equation that is used to determine the shear strength of a reinforced masonry wall specimen against diagonal tension failure as per CSA S304 provisions is listed below, in which the contribution from masonry components is present in the first term, and steel contributions in the second:

$$V_r = \phi_m * (v_m * b_w * d_v + 0.25P_d) * \gamma_g + 0.6 * \phi_s * A_v * f_y * (\frac{d_v}{s}) \quad (2.7)$$

Where

The shear resistance of the reinforcement is expressed by:

$$V_s = 0.6 * \phi_s * A_v * f_y * (\frac{dv}{s}) \quad (2.8)$$

The shear resistance of the masonry is expressed by:

$$V_m = \phi_m * (v_m * b_w * d_v + 0.25P_d) * x\gamma_g \quad (2.9)$$

ϕ_m - Material factor for masonry, which for the purposes of this assessment, has been set to 1

v_m - Intrinsic shear resistance of plain masonry (running bond), equal to:

$v_m = 0.16 * [2 - (\frac{Mf}{Vf*dv})] * \sqrt{f'_w}$, (MPa) where $0.25 < \frac{Mf}{Vf*dv} \leq 1$ (2.10)

For wall specimens with lower aspect ratio values, that is when the height to length ratio of the wall is less than 1, the upper bound of the limit increases to a value:

$0.4\phi_m\sqrt{f'w}b_w d_v \gamma_g(2 - \frac{Lw}{Hw})$, where $\frac{Lw}{Hw}$ is taken as > 0.5 (2.11)

d_v - The effective depth of the wall cross section, which is taken as the distance from the centroid of tensile reinforcement to the centroid of the compression zone (mm)

$d_v = 0.8*L_w$ (mm) (2.12)

b_w - Thickness of concrete block used in the construction of the wall, referred to as the web width in CSA S304 provisions (mm)

P_d - Applied axial compressive load on the specimen (N)

γ_g - Grouting factor to account for grouted sections, which has been set to 1 for assessment. For partially grouted walls, this value shall be set to the ratio of the effective cross-sectional area of the wall to the gross cross-sectional area of the wall ($\frac{Ae}{Ag}$) (2.13)

ϕ_s - Material factor for steel, which for the purposes of assessment, has been set to 1

A_v - Cross-sectional area of one vertical steel reinforcing bar (mm^2)

2.2.2 Flexural Failure

Ductile flexure failure of walls is known to exhibit notable energy dissipation as a result of cracking, yielding of the vertical reinforcement bars and plastic deformations. In this regard, ductility refers to the measurement of deformation that a structure is able to undergo beyond yielding while not compromising its load carrying capacity. This form of response is generally exhibited by specimens characterized by an aspect ratio of greater than or equal to 1, and a moderate level of applied axial compressive stress, generally within 10 percent of the specified compressive strength of the masonry wall (f'_w). The presence of the steel reinforcement bars, primarily in the tension zone of the wall, helps resist extensive amounts of cracking as the bars will begin to yield and experience plastic deformation as the load progresses. Eventual failure is accompanied by tensile yielding of the vertical reinforcing bars located in the tension zone, combined with toe cracking and potential spalling of blocks and grout in the compressive zone. The inclusion of adequate amounts of vertical reinforcement results in the exceptional ductility of

flexure dominated reinforced masonry walls and allows for significant displacement, which typically consists of an outward bowed profile on the tension side and compressed face on the compression side. This ductile response and effective earthquake-induced energy dissipation capabilities makes this form of response the preferred form of response for a typical reinforced masonry wall specimen.

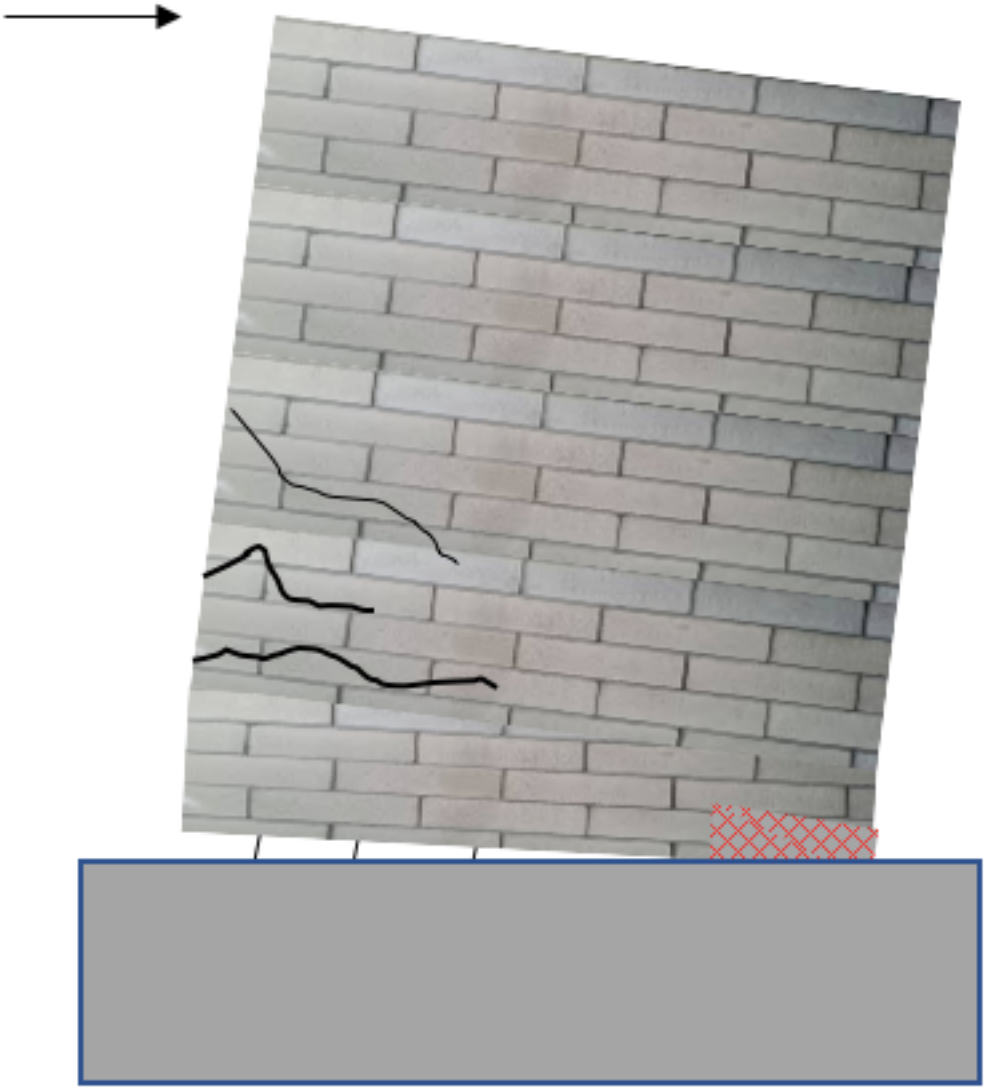

Figure 2.7) Illustration of the flexural performance of a reinforced masonry wall that has experienced flexural cracking on the wall face as a result of the increasing lateral load

Damage from this form of failure is often accompanied with horizontal flexural cracking as well as minor flexure-shear cracks, typically present in the plastic hinge zone. To this end, the plastic hinge zone of a typical reinforced masonry wall is the region where inelastic deformations and flexural rotations occur, and generally requires additional seismic detailing in this region. In terms of the analytical prediction of the flexural strength of a reinforced masonry wall, classical beam theory expressions can be extended and used to estimate the flexural capacity with a reasonable degree of convergence between the experimental values. In regards to the empirical expressions presented in various design codes, most of the experimental data used in their development was obtained on reinforced concrete wall specimens rather than on reinforced masonry specimens, which adds an additional layer of ambiguity to the extension of these empirical expressions.

2.2.2.1 First Principles Flexural Strength

The analytical approach regarding the calculation of the flexural strength of the walls that was followed and implemented into the database was based on first principles assumptions. This method involves fundamental theories based on the mechanics of the materials of reinforced masonry and structural analysis principles, which was used as a basis of comparison between the experimental results recorded in the experiments. First principle calculations consider the stress-strain relationship of the steel and masonry, neutral axis and strain compatibility and equilibrium of forces. The first step of the analysis was to determine the location of the neutral axis (c), which based on first principle assumptions, the strain in the masonry and steel at any arbitrary section must be proportional to their distances along the neutral axis to ensure that plane sections remain plane after bending. It is important to note that for the purpose of analysis, all material factors were set to one, which ensured a consistent baseline during evaluation and allowed for a greater emphasis to be placed on the flexural strength characteristics of the specimens. The flexural moment was determined based on equilibrium between the internal forces within the cross section and was calculated through the application of the following derived equation, which has been adapted from Pantazopoulou (2022):

$$M_{1R} = 0.5c * \alpha_1 f'_w t_w L_w * (1-\beta_1\xi) + 0.7\rho_v(1-\xi)A_n f_y(0.15L_w + 0.35c) + 0.45A_{s,BE}f_y L_w \quad (2.14)$$

Where:

c - Represents the depth of the neutral axis (mm)

$$c = L_w * (0.7\rho_v A_n f_y + P_d + A_{s,BE} f_y)/(\alpha_1 f'_w L_w t_w + 0.7\rho_v A_n f_y) \quad (2.15)$$

α_1 - Coefficient used to determine the equivalent intensity of the stress block

$$\alpha_1 = 0.85\Phi_m\chi = 1 \quad (2.16)$$

f'_w - The average masonry compressive strength of the wall derived from experimental compressive tests of wallette units (MPa)

t_w - Thickness of the masonry block. Since all walls in the database were single wythe specimens, this was also equal to the thickness of the wall (mm)

β_1 - Coefficient that represents the height of the equivalent stress block (Varies based on the compressive strength of the wall)

ξ - Represents the ratio of the depth of the neutral axis (c) to the effective depth of the section (d)

ρ_v - Represents the vertical reinforcement ratio of the reinforcement present within the web of the wall

A_n - The net area of the wall specimens, taken as multiple of the length (L_w) and the thickness (t_w) of the wall. For partially grouted specimens, the net area is not constant for the whole height of the wall, and the area of the voids needs to be accounted for in the ungrouted regions (mm^2)

f_y - Yield strength of the vertical steel reinforcing bars (MPa)

$A_{s,BE}$ - Summation of the cross sectional area of the vertical steel reinforcement present within the boundary elements of the specimen (mm^2)

2.2.3 Mixed Shear-Flexural Failure

A third possible failure mode is a mixed shear-flexural failure mode which occurs when the wall simultaneously experiences combined shear and flexural forms of nonlinear behaviour. This form of response occurs through both tensile yielding of the vertical reinforcement bars as well as diagonal cracking (and the eventual failure) within the compression zone of the wall

specimen. Visual indication of this form of response is through the presence of vertical and horizontal flexural cracking and diagonal shear cracks. Mixed shear-flexure performance experiences the typical bending from a conventional flexure response with an additional contribution from displacements due to shear deformations. It is important to note that the designation for mixed shear-flexural failure of walls examined in the database were given to specimens that exhibited analytical values of governing shear and flexural strengths that were within 5 percent from each other.

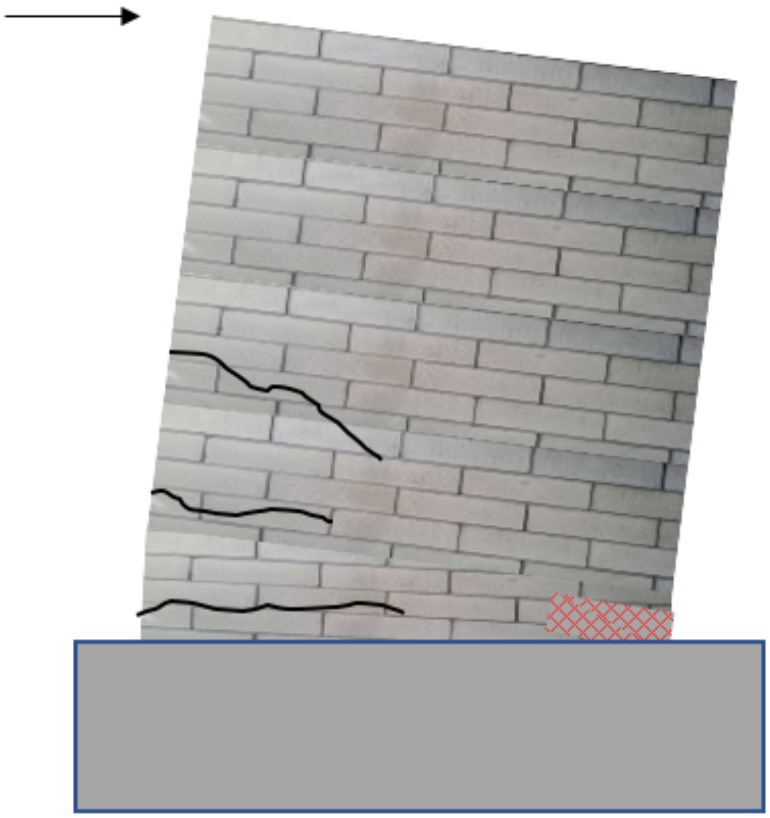

Figure 2.8) Illustration of a mixed shear-flexural performance of a reinforced masonry wall that has experienced flexural cracking on the wall face and well as possible crushing in the toe region

2.2.4 Governing Failure Mode

As it has been established, the mode of failure that a structure can exhibit is based on its detailing and loading, and has an influence on the observed behaviour deformation patterns when nearing the onset of failure. A successful prediction of how a structure will fail is of critical importance in structural design and assessment procedures, and engineers often base their design

choices off this anticipated behaviour to ensure that the structure is well equipped to perform as intended. The failure mode of a reinforced masonry structure is determined from the relative hierarchy of its shear and flexural capacities, where the element will fail in whichever mode it has been most under designed for. To this end, one might predict the anticipated failure mode of the structure throughout the implementation of analytical equations for flexural and shear resistances, where the governing performance will stem from the lowest value. Therefore, it can be said that:

$$Q_{Governing} = \min \{Q_{flex}, Q_{Sliding}, Q_{Diagonal\text{-}Compression}, Q_{Diagonal\text{-}Tension}) \quad (2.17)$$

Where:

Q_{flex} represents the flexural strength of the specimen

$Q_{Sliding}$, $Q_{Crushing}$, $Q_{Diagonal\text{-}Tension}$ are all shear strengths associated with difference mechanisms of behaviour, where the lowest of the three will occur first and is the governing shear mode

Therefore, $Q_{Governing}$ will be the resulting minimum value between the flexural strength (Q_{flex}) and the lowest of the three possible shear strengths (either $Q_{Sliding}$, $Q_{Crushing}$, $Q_{Diagonal\text{-}Tension}$)

2.3 Seismic Assessment Frameworks for Existing Masonry Structures

2.3.1 Preface

Within the field of seismic assessment, the National Institute of Standards and Technology (NIST GCR 17-917-45) and the American Society of Civil Engineers (ASCE ASCE/SEI 41-22) have developed comprehensive provisions and assessment criteria that are aimed for the purposes of seismic assessment of existing reinforced masonry structures. These documents serve as crucial resources that outline a detailed framework for the seismic assessment and performance of structures that are used to ensure that building design is on par with safety standards and can withstand severe ground motions. Given that the design and construction of older masonry buildings was not done with access to the modern seismic considerations in mind, these frameworks are critical in identifying weakness of the structure and predicting the level of anticipated damage. In specific, the outlined approaches are used to determine the specific plastic hinge properties of the idealized structural members and their corresponding elastic stiffness.

2.3.2 Analysis Methods According to NIST Recommendations

The NIST document (GCR 17-917-45) titled "Guidelines for Seismic Risk Assessment and Risk Mitigation" outlines approaches pertaining to the assessment and retrofit methodologies pertaining to the seismic assessment of reinforced masonry structures. These methodologies recommend an approach for the assessment of masonry structures that is similar in nature to those used in the case of reinforced concrete beams and columns. That is, the complete moment curvature relationship of elements is defined through lateral force and drift expressions. According to the beam-column modelling concept, the main component of response involved the rotation of the member chord as a consequence of flexural curvature, in addition to shear deformations. In this context, deformation is measured from the deviation of the member from its chord as depicted in Figure 2.9. This deformation, which is measured as an angle (in radians), is referred to as lateral drift ratio or simply drift.

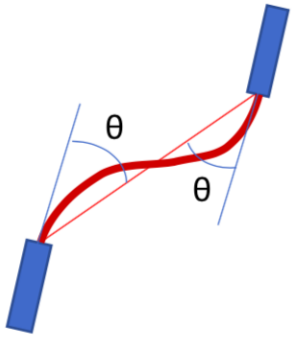

Figure 2.9) Definition of drift ratio (θ) on a deformed frame member, adapted from Pantazopoulou (2023)

The resistance curve of a structural element represents the force-displacement correlation, and can be used as a means to predict how the element will behave during loading, as well as how the strength resistance degrades as a result of the increasing deformation. These curves can be derived though moment curvature relationships, and by adopting the beam-column modelling-concept, the flexural response can used as a reference standard for constructing the resistance curve of the member. According to the NIST provisions, the backbone envelops requires user input at specific coordinates of response, namely at the location of peak flexural response (M_{max}, ϕ_m) and at post peak values of 75 percent (M_{75}, ϕ_{75}) and 50 percent (M_c, ϕ_c) of maximum response, where the point at 50 percent refers to the crushing occurring in the compression zone of the wall.

From the diagrams illustrated in Figure 2.10 below, a typical cross section of a rectangular wall is shown of a specimen for the analysis of axial loading and flexural action across its strong direction plane. Through discretization of the wall cross-section into individual layers, the stress-strain relationship can be analysed in each layer, a convenient method of analysis for complex cross-sectional footprints such as a partially grouted reinforced masonry wall. In addition, a complete moment curvature diagram is depicted for a typical wall section analysed through such a layered analysis procedure.

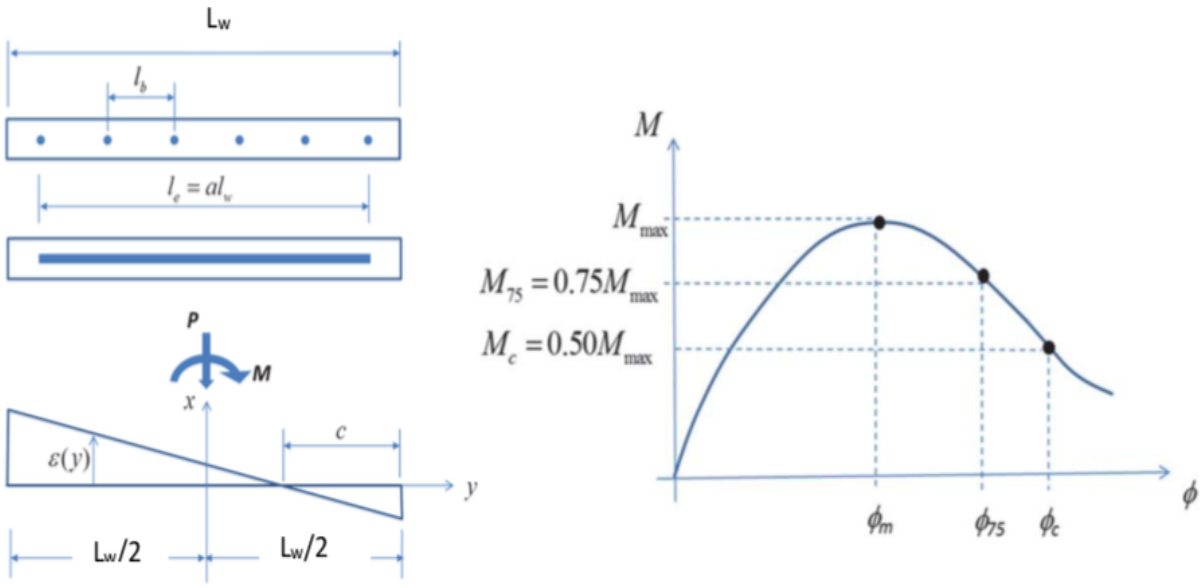

Figure 2.10) Moment curvature relationship of a reinforced masonry wall with milestone points identified [Adapted from Pantazopoulou (2023)]

2.3.2.1 NIST Backbone Envelopes

For a typical rectangular reinforced masonry wall tested under lateral loading, such as the case of the specimens considered in the database, the wall is treated in analysis as a statically determinate cantilever model as illustrated in the series of illustrations below. In this model, the wall is fixed at the base, and due to the lateral loads applied at the top of the wall, the wall experiences in-plane deformations. From Figure 2.11 below, the definition of the effective height (H_e) of the wall is set as the distance from the point of maximum moment (base of the wall) to the

point of zero moment (location of lateral load), which for a cantilever model, is equal to the shear span (and the specimen height) of the wall.

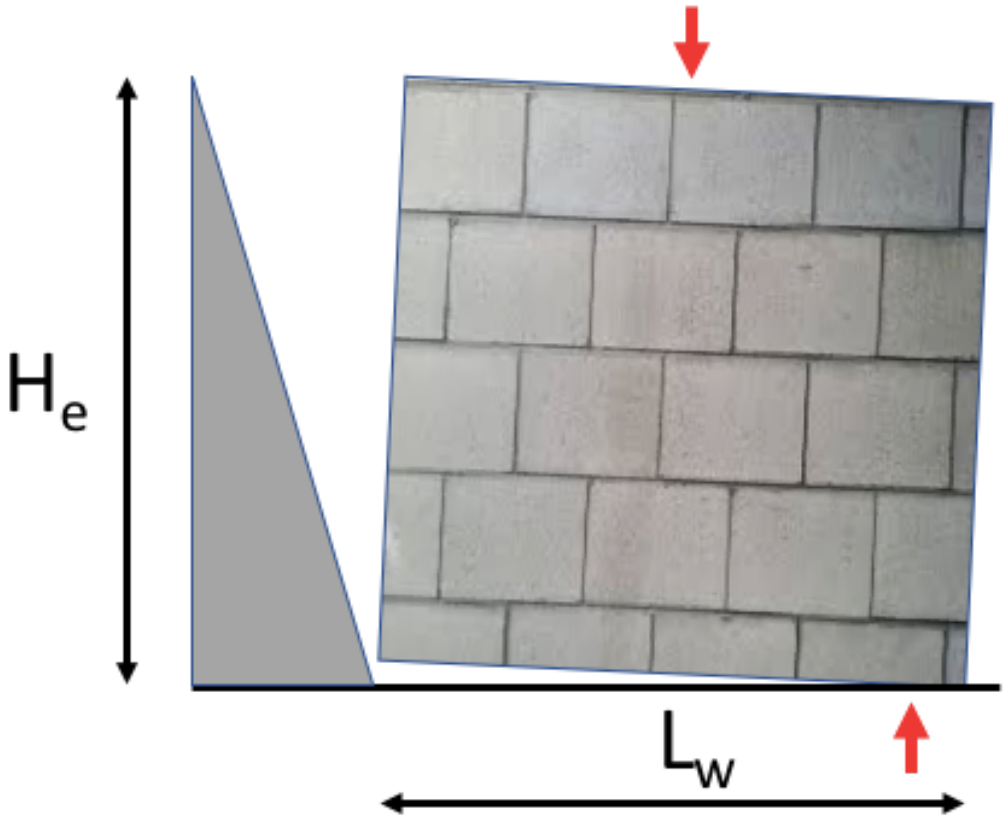

Figure 2.11) Schematic diagram of a cantilever model of swaying in-plane wall with effective height (H_e) and wall length (L_w) definition depicted

Based on the outlined moment-curvature analysis relationships, specifically at points located at the peak, 75 percent and 50 percent of post-peak, as outlined above, the backbone curve can be formed for the force displacement relationship based on the experienced failure mode exhibited by the specimen. The NIST provides definitions for backbone envelope curves for both flexure and shear dominated walls, and are established through reference of the following four milestone points. In a similar manner to the descriptions addressed previously, flexural failures for walls bent in their plane occurs primarily due to the previously mentioned theoretical concepts bending moments and is characterized by the yielding of the vertical bars. The attainment of a flexural failure is typically targeted to experience a more ductile form of response, such as is evident in the outlined backbone envelope below. Shear failure on the other hand is a much more

brittle form of failure and can occur from a variety of mechanisms such as the sliding along a horizontal plane or the yielding of horizontal reinforcement.

NIST guidelines recommend a uniform manner to define the milestone points on the response envelope of RM wall experiments so that the corresponding coordinates (drift ratio values at yield, maximum and nominal ultimate limit state) may be comparable across different specimens. The resulting multilinear plots that connect the characteristic milestone points are referred to as backbone curves and are used for modelling the nonlinear response of reinforced masonry walls in pushover analysis of RM structures using frame-modelling idealizations, as per the popular software (e.g. SAP2000). Figure 2.12 below depicts the recommended backbone curve for members dominated by flexure and by shear respectively.

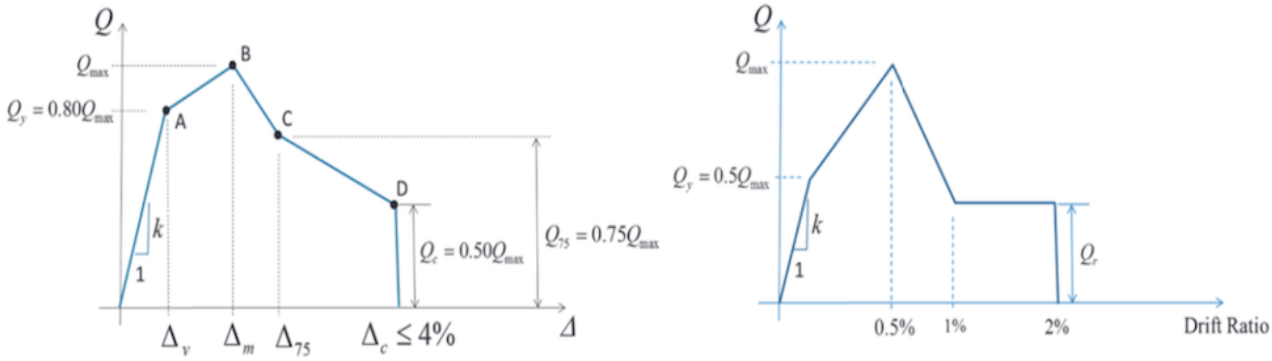

Figure 2.12) NIST backbone response envelopes for reinforced masonry walls. (a) Flexure dominated response; (b) Shear dominated response (Adapted from Pantazopoulou (2023)

Four distinct points are noted on these curves, labelled from A to D. Looking first at the backbone envelope for flexure dominated walls, the first point (A) is associated with the yielding point of the specimen. It is set at the point on the envelope with ordinate equal to 80 percent of the maximum load on the ascending branch of response. This point indicates the onset of plastic deformation in the specimen. In comparison, for shear dominated specimens, this yielding point occurs much earlier at 50 percent of the maximum load. The following point B represents the maximum applied load during the testing (Q_{max}) for flexure dominated specimens this occurs at the corresponding displacement at peak, but for shear dominated specimens this is set to correspond to a drift of 0.5%. Point C is located on the descending post peak segment of the envelope curve and is located at 75 percent of the maximum load for the flexure dominated

envelope and 50 percent of the maximum load for the shear dominated envelope. The fourth and final point D is the residual point at an ordinate of 50 percent of Q_{max} for both envelopes. For flexure dominated specimens, the abscissa is the drift capacity of the specimen at 50% of the peak load which is not taken more that 4%, whereas in the case of shear dominated specimens the plateau extends from 1% to 2% drift.

Milestone Point	Point A	Point B	Point C	Point D
Shear: $Q = \frac{M}{He}$	$Q_y = 0.8 * Q_{max}$	Q_{max}	$0.75 * Q_{max}$	$0.5 * Q_c$
Displacement: Δ	Δ_y	Δ_m	Δ_{75}	$\Delta_c \leq 0.04 * H_e$
Drift Ratio: $\theta = \frac{\Delta}{He}$	$\theta_y = \frac{\Delta y}{He}$	θ_m	$\theta 75$	$\theta_c \leq 4\%$

Table 2.1) Milestone point definitions on the prescribed NIST backbone curves

Even though these figures have been developed using American provisions and have been presented by the NIST, an American corporation. The derivation of these curves has been achieved through experimental databases that considered American test data, and yet, these curves are widely recognized by Canadian practitioners given that there are no equivalent curves that have been developed to specifically tailor to Canadian experimental data. To provide a means of validation of these curves on Canadian structures, the prepared database contained in this thesis attempted to recreate the curves presented by the NIST through consideration of strictly Canadian data.

To check the consistency of the proposal represented by the above figure, the collection of recorded envelopes of the database experiments were plotted as shown in Figures 2.13, 2.14 and 2.15. Each curve's ordinates were normalized to the respective peak value; the objective here was to examine the spread into the deformation (drift) axis and to associate this spread to the dominant mode of failure. In Figures 2.13, 2.14 and 2.15 below, lateral drift vs. the normalized experimental load have been plotted and grouped based on the observed failure mode during experimental testing with the objective to compare the levels of drift that were recorded in the Canadian literature with the values that are assumed in the American NIST assessment framework, with the hope that appropriate convergence between levels of drift will be observed. After all, if these backbone

envelope curves are to be applicable to the Canadian practice, then they ought to provide an appropriate representation of the reality that has been recorded in the experimental tests.

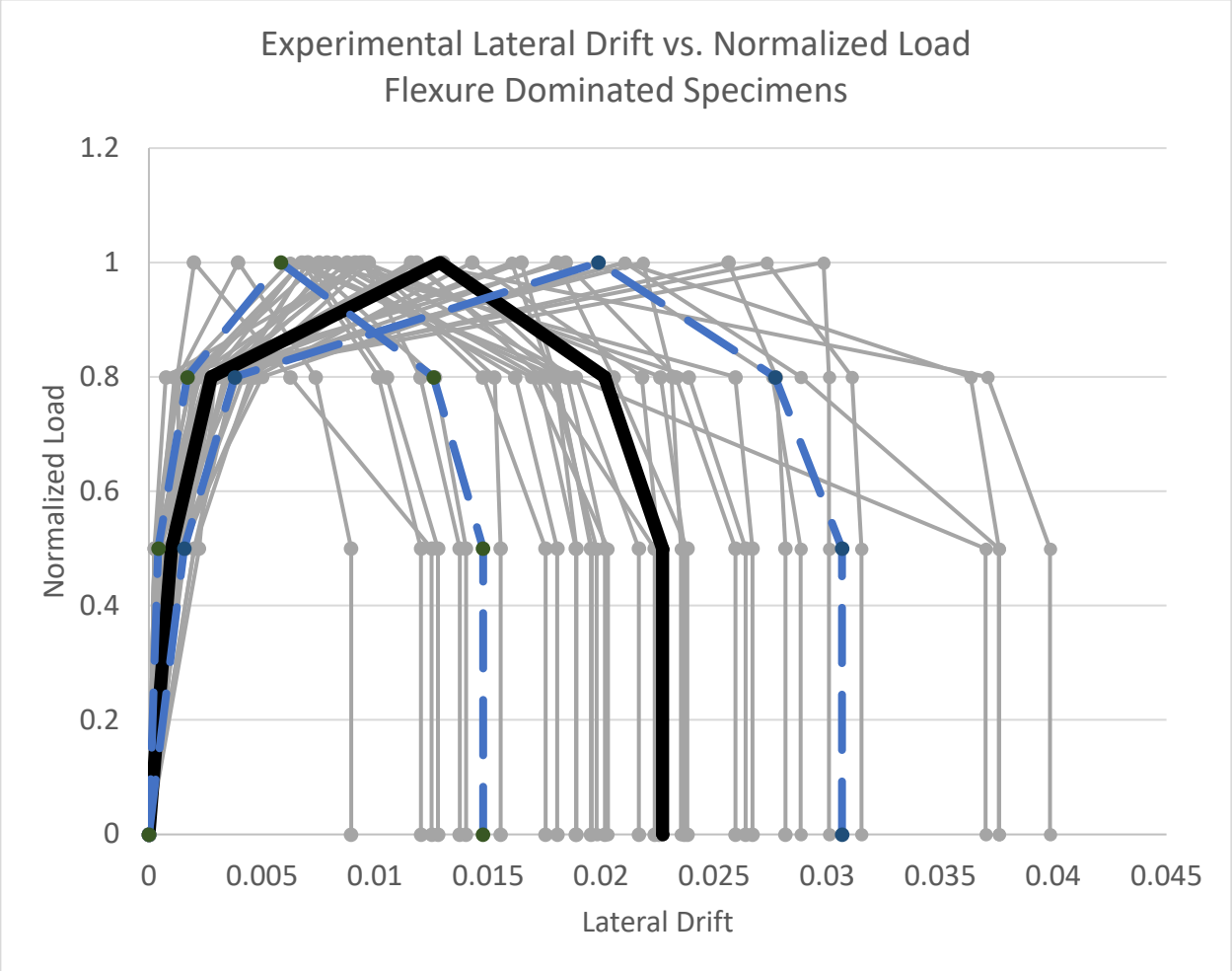

Figure 2.13) Experimental lateral drift ratio vs. peak normalized load of flexure dominated specimens considered in the database: Drift ratios at failure range from 1% to 4%.

Looking first at the flexure dominated walls in Figure 2.13 above, we can see that a wide range of drift levels were covered by the considered experiments for a range between around 1 percent to 4 percent, with a mean value of 2.25 percent shown in the thick black line and standard deviation lines shown in blue. If we recall, the NIST backbone curve presented levels of drift for flexure dominated walls to be in the magnitude of 4 percent, but evident in the data considered in the database, this value was seldom reach by the tests. This discrepancy highlights the fact that these backbone curves presented in the NIST assessment framework, which has been derived based on American experimental tests, does not accurately align with experimental performances of that from Canadian experimental tests. This discrepancy can be attributed to fundamental flaws

within the NIST framework that fail to appropriately depict the response of reinforced masonry structures, as well as due to the differences that exist between the American and Canadian building practise as a result of the differences in seismic risk.

	$\theta 0.5_{u\ +ve\ Pre}$	$\theta 0.8_{u\ +ve\ Pre}$	θ_{Peak}	$\theta 0.8_{u\ +ve\ Post}$	$\theta 0.5_{u\ +ve\ Post}$
Mean	0.0001	0.003	0.013	0.020	0.023
Standard Deviation	0.0006	0.001	0.007	0.008	0.008
Mean - St.Dev	0.0004	0.002	0.006	0.012	0.015
Mean + St.Dev	0.0016	0.004	0.020	0.028	0.031

Table 2.2) Mean and standard deviation values for the milestone points of the flexure dominated specimens

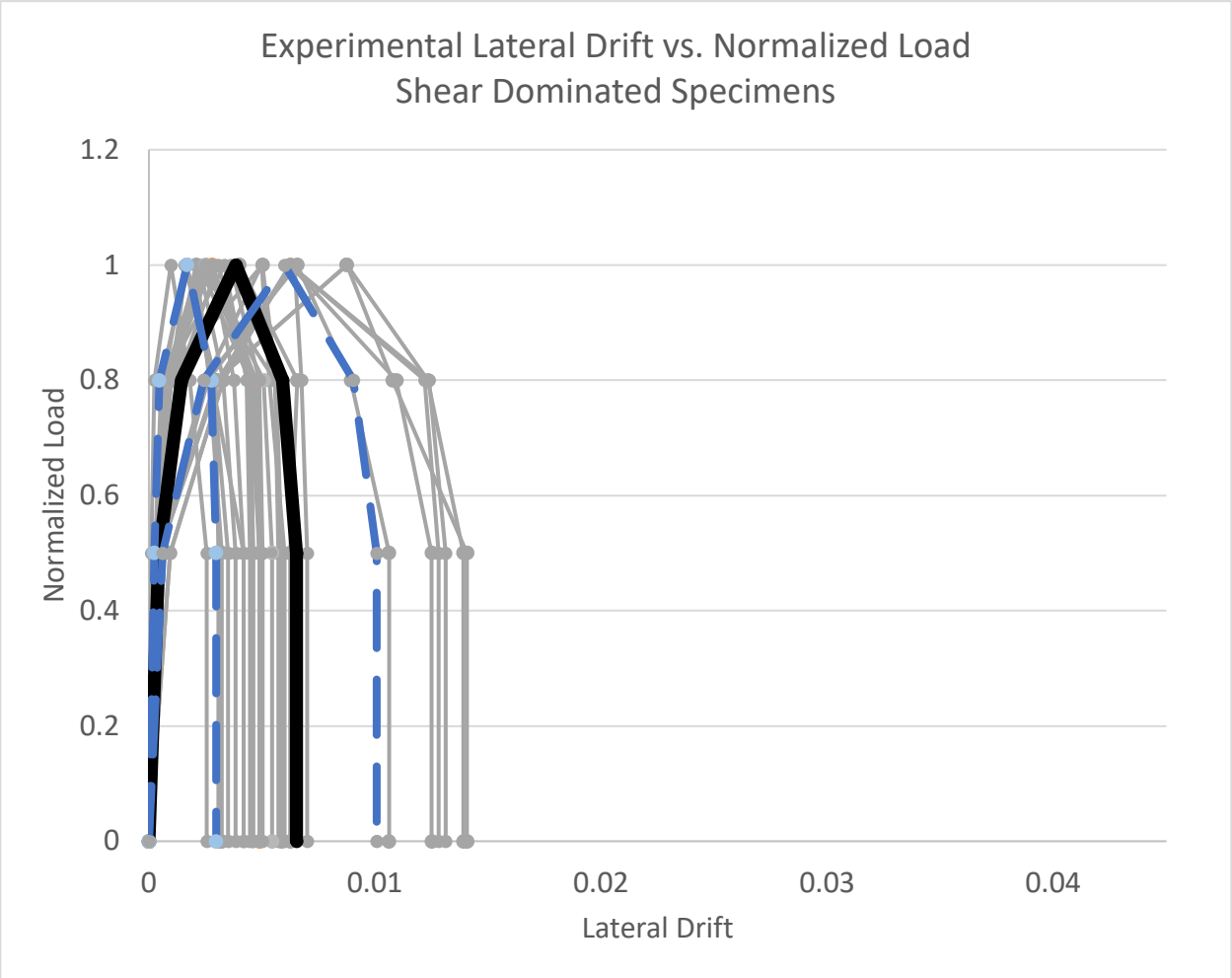

Figure 2.14) Experimental lateral drift ratio vs. peak normalized load of shear dominated specimens considered in the database: Drift ratios at failure range from 0.25% to 1.5%.

Looking at the specimens that failed due to a shear controlled diagonal tension failure, we can observe the similar observation made from the flexure specimens, which is that the experimental lateral drift ratios recorded in the Canadian experiments were not aligned with the values proposed by the American NIST framework. According to the recommended backbone curves for shear dominated specimens from NIST, a limit for drift levels of 2 percent are expected to occur for shear-controlled specimens. From the Canadian experimental data plotted in Figure 2.14 above, we can see that the experimental performance was well below this provided range. The highest recorded level of drift was record as around 1.5 percent, with the mean value for all shear specimens exceeding 0.7 percent, a value much lower than what is proposed by the NIST backbone envelope. In addition, a plateau of response was predicted to occur by the NIST in accordance with the prescribed backbone envelopes between drift levels of 1 to 2 percent. This

behaviour was not at all observed in any of the shear-controlled specimens from the Canadian literature, further highlighting the inapplicability of the NIST backbone response curve for specimens built in accordance with the Canadian design approach.

The NIST, nor ASCE, seismic assessment frameworks provide standard backbone envelop curves for reinforced masonry walls with a shear-flexure mixed response, however, Figure 2.15 below illustrates the normalized curves that have been assembled from the Canadian experimental data. From this curve, we can see that the response of such specimens indeed follows a profile that comprised a contribution of both a brittle shear-controlled response and a ductile flexure response.

	$\theta 0.5_{u\ +ve\ Pre}$	$\theta 0.8_{u\ +ve\ Pre}$	θ_{Peak}	$\theta 0.8_{u\ +ve\ Post}$	$\theta 0.5_{u\ +ve\ Post}$
Mean	0.0004	0.0014	0.004	0.006	0.0065
Standard Deviation	0.0002	0.001	0.002	0.003	0.004
Mean - St.Dev	0.0002	0.0005	0.002	0.003	0.03
Mean + St.Dev	0.0006	0.002	0.006	0.009	0.01

Table 2.3) Mean and standard deviation values for the milestone points of the shear dominated specimens

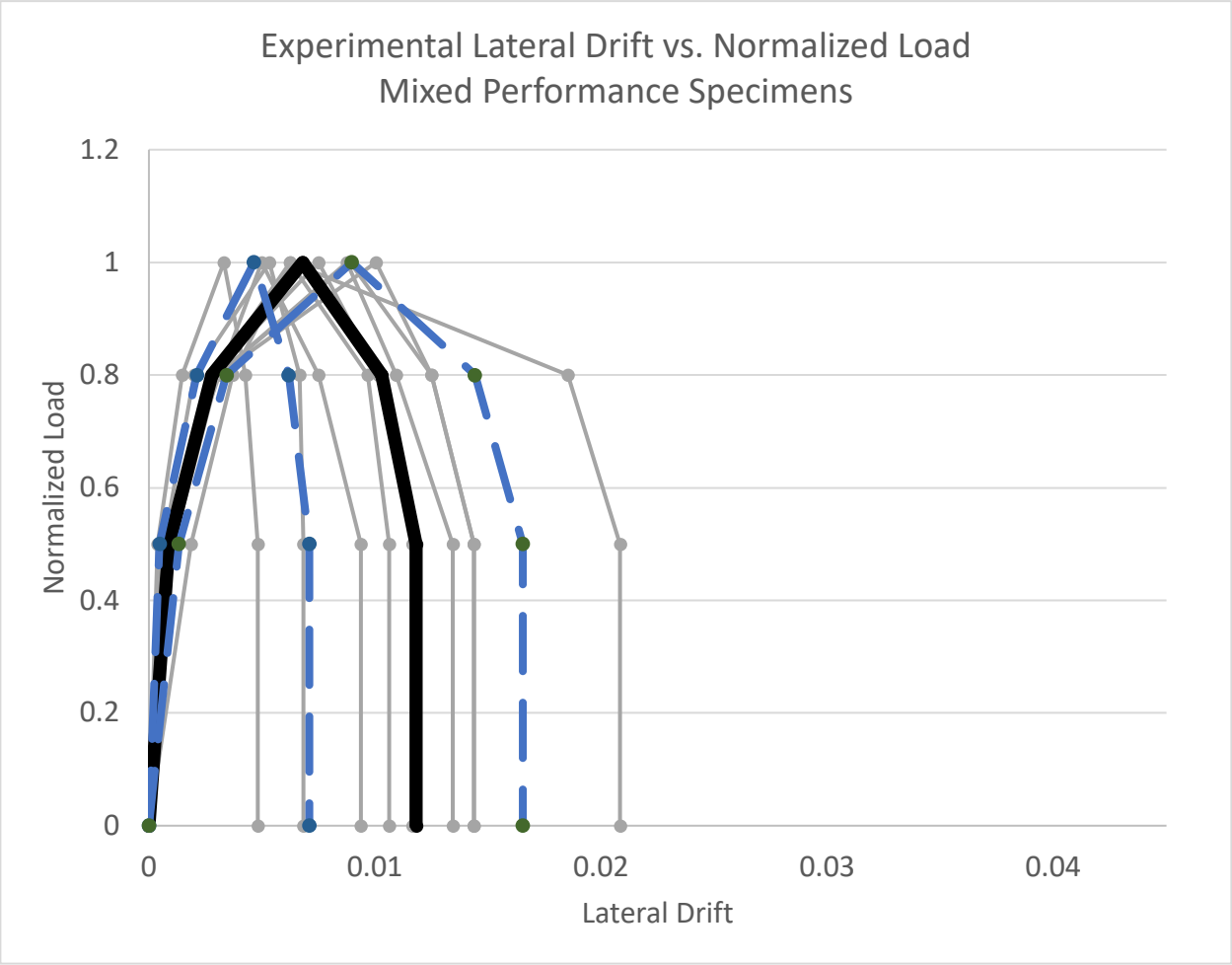

Figure 2.15 Experimental lateral drift ratio vs. peak normalized load of mixed behaviour specimens considered in the database. Drift ratios at failure range from 0.4% to 2.05%.

	$\theta 0.5_{u\ +ve\ Pre}$	$\theta 0.8_{u\ +ve\ Pre}$	θ_{Peak}	$\theta 0.8_{u\ +ve\ Post}$	$\theta 0.5_{u\ +ve\ Post}$
Mean	0.0009	0.003	0.007	0.010	0.012
Standard Deviation	0.0004	0.0007	0.002	0.004	0.005
Mean - St.Dev	0.0005	0.002	0.005	0.006	0.007
Mean + St.Dev	0.0013	0.003	0.009	0.0014	0.017

Table 2.4) Mean and standard deviation values for the milestone points of the shear-flexure mixed performance specimens

The following sets of curves display the experimentally response of the wall in regards to the recorded lateral drift ratio as the loading cycles progressed until eventual failure of the specimen, when observing the curves relative to the flexure dominated specimens, the linear slope of the ascending branch of response is visible until the point of yielding similar to what is presented in the given NIST curve in the left graph of Figure 2.7. When comparing the response of the flexure dominated walls with that of the shear dominated ones, it becomes clear that significant ductility was achieved for the flexure specimens given that substantially larger drift ratios were reported during these tests.

For cantilever walls with lateral loads applied at the top of the specimen, the maximum load capacity is defined as $Q_{max} = M_{max} * H_e$ (2.6). From these diagrams shown in Figure 2.11 below, the resulting flexural deformations (θ) and shear distortion (γ) that results from the applied lateral loading is illustrated on the wall. The fundamental theories used in the derivation of the prescribed backbone envelopes for the flexure dominated walls is based on flexural theory, which assumes that the total drift capacity of a reinforced masonry wall can be computed through the considerations of these flexural and shear deformations:

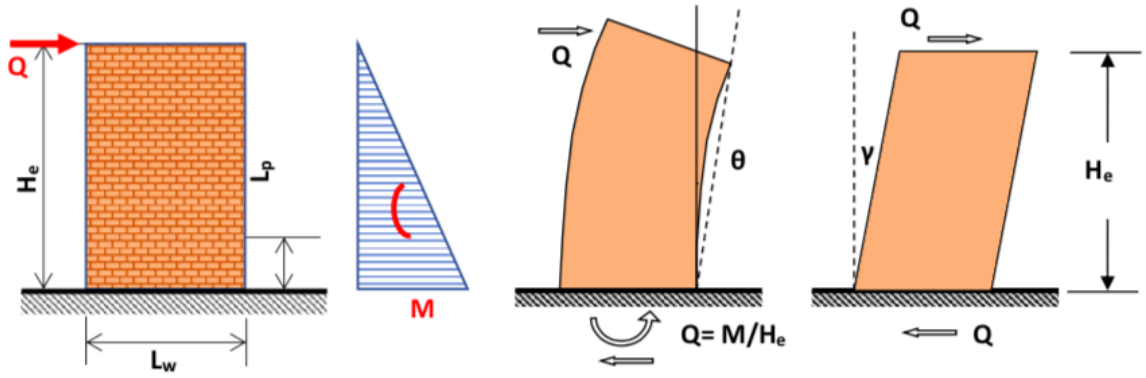

Figure 2.16) Cantilever model, moment diagram and drift ratio contributions from flexural curvature (θ) and shear distortion (γ) of a typical reinforced masonry wall specimen tested under a case 1 type actuator arrangement (Adapted from Pantazopoulou 2023)

From this model, the individual terms can be computed through the following mathematical expressions:

$\theta_{m\text{-}elast} = \frac{1}{3} * \phi_m * H_e = \frac{M_{max}}{3E_m I_e} * H_e^2$ (2.18)

$\theta_{m\text{-}plast} = \phi_{plas} * L_p$ (2.19)

Therefore, the total flexural contribution to the curvature is the following:

$\theta_{m\text{-}flex} = \theta_{m\text{-}elast} * \theta_{m\text{-}plast}$ (2.20)

$\theta_{m\text{-}flex} = (\frac{1}{3} * \phi_m * H_e = \frac{M_{max}}{3E_m I_e} * H_e^2) * (\phi_{plas} * L_p)$ (2.21)

The shear contribution to the wall curvature is computed through:

$\theta_{m\text{-}shear} = \frac{Q_{max}}{0.2 * A_v * G_m}$ (2.22)

Where Q_{max} is the peak lateral experimental load, which can also be calculated through:

$Q_{max} = \frac{M_{max}}{H_e}$ (2.23)

Combining these relations all together, the total curvature of the wall at any of the milestone points can be computed through the following arithmetic:

$\theta_m = \theta_{m\text{-}flex} + \theta_{m\text{-}shear}$ (2.24)

$\theta_m = (\frac{1}{3} * \phi_m * H_e = \frac{M_{max}}{3E_m I_e} * H_e^2) * (\phi_{plas} * L_p) + \frac{Q_{max}}{0.2 * A_v * G_m}$ (2.25)

Elastic:

$\Delta_{flex,\ elast} = \phi_{m,\ el} * \frac{He^2}{3} = \frac{Mmax}{3EmIe} * H_e^2$ (2.26)

$\theta_{flex,\ elast} = \frac{1}{3} * \phi_{m,\ el} * H_e = \frac{Mmax}{3EmIe} * H_e^2$ (2.27)

Where:

H_e = Effective height (shear span) of specimen (mm)

$\phi_{m,\ el}$ = Curvature at peak, obtained through relationship of axial load ratio (β) as a function of reinforcement index (α)

β = Axial Load Ratio = $\frac{P}{f'w * An}$ (2.28)

α = Reinforcement index = $\frac{f_y}{f'_w} \cdot \rho_v$ (2.29)

M_{max} = Peak maximum moment (Nmm)

E_m = Modulus of elasticity of masonry = 850 * f'$_w$ (MPa) (2.30)

I_e = Effective (uncracked) moment of inertia = $\frac{t * Lw^3}{12}$ (mm^4) (2.31)

Plastic:

$\Delta_{flex,\ plast} = \phi_{plas} * L_p * (H_e - 0.5L_p) = \theta_{flex,\ plast} * (H_e - 0.5L_p)$ (2.32)

$\theta_{flex,\ plast} = \phi_{plas} * L_p$ (2.33)

ϕ_{plas} - The plastic component of curvature in the plastic hinge zone

$\phi_{plas} = \phi_m - \frac{Mmax}{3EmIe}$ (2.34)

L_p - Effective plastic hinge length (ksi)

$L_p = 0.04H_e + 0.1L_w + L_{sp} \geq 3 * L_{sp}$ (*all units in ksi and inches)* (2.35)

$L_{sp} = 0.15 * f_{ye} * D_b$ (2.36)

f_{ye} - Expected yield strain of bars (ksi)

D_b - Diameter of vertical longitudinal bars (in)

For the application of these equations, the NIST guidelines provide standardized values relating to the curvature (ϕ) and maximum moment (M_{max}) tabulated against coefficients for the axial compression ratio ($\beta = \frac{P}{f'w * An}$) (2.11) and the available reinforcement index ($\alpha = \frac{f_y}{f'_w} \cdot \rho_v$) (2.12). In these coefficients, P corresponds to the axial compressive load acting on the wall, A_n is the net area of the wall and ρ_v is the steel vertical reinforcement ratio.

Through evaluation of these coefficients, the user is able to obtain the milestone points that define the moment-curvature relationship of the reinforced masonry wall in accordance with NIST guidelines. It is important to note that α and β coefficients are reported in set increments of 5 percent and 0.05 respectively, and so for an arbitrary set of values between these intervals, linear interpolation is required to interpolate or extrapolate the curvature or moment values. Equations for the function of the lines presented in these NIST figures have been derived to make this procedure easier to code in spreadsheet calculations and will be presented in later sections of this thesis. The following figures depict the provided NIST values in chart format, where values are presented as nondimensionalized values as the product of curvature multiplied by the wall length (ϕ_{max}, ϕ_{75}, ϕ_c), and the maximum moment represented by $\frac{Mmax}{f'w * An * Lw}$ (2.20).

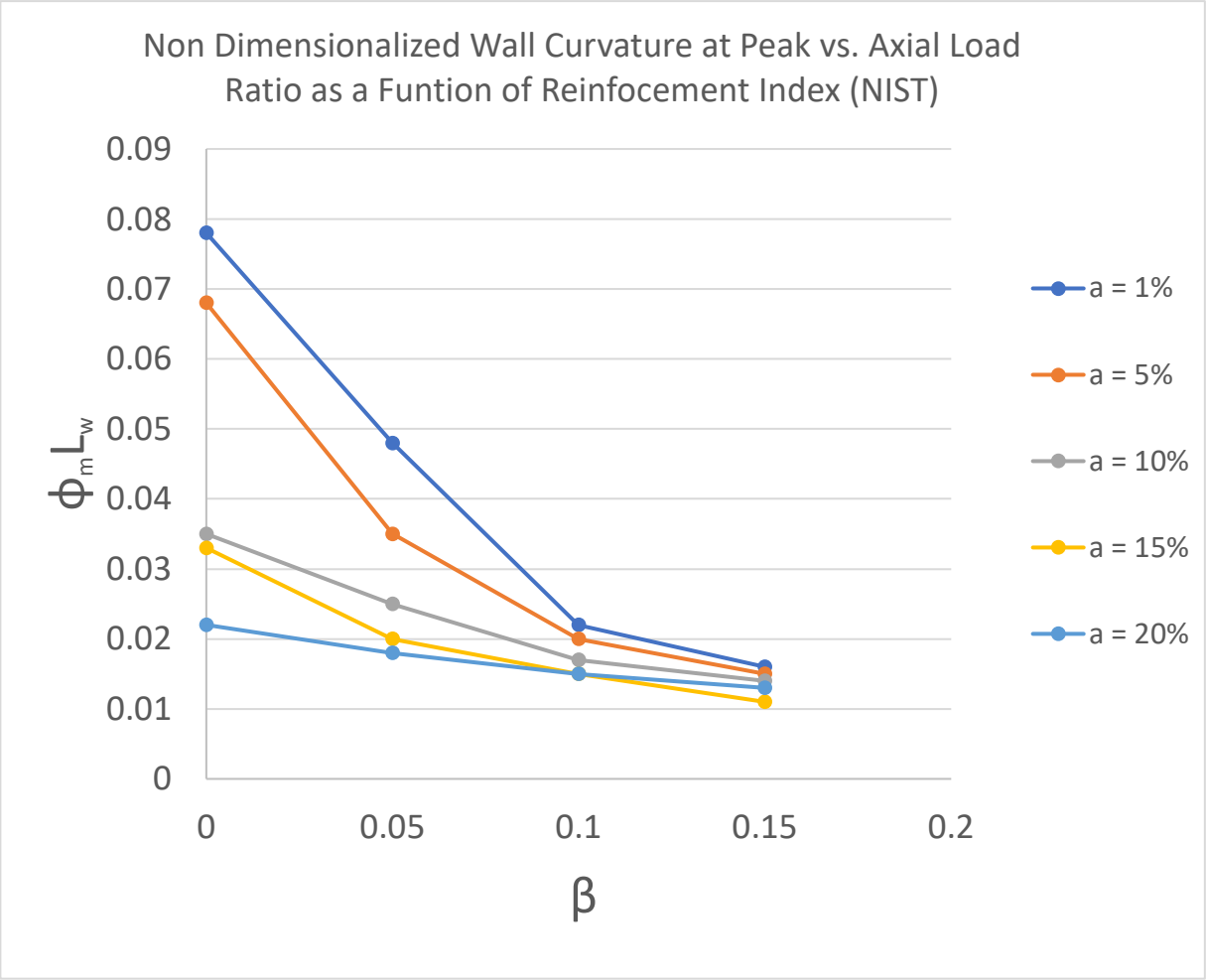

Figure 2.17) NIST standard values for the non-dimensionalized curvature at peak strength plotted against the axial compression ratio ($\beta = \frac{P}{f'_w \cdot A_n}$) and the available reinforcement index ($a = \frac{f_y}{f'_w} \cdot \rho_v$)

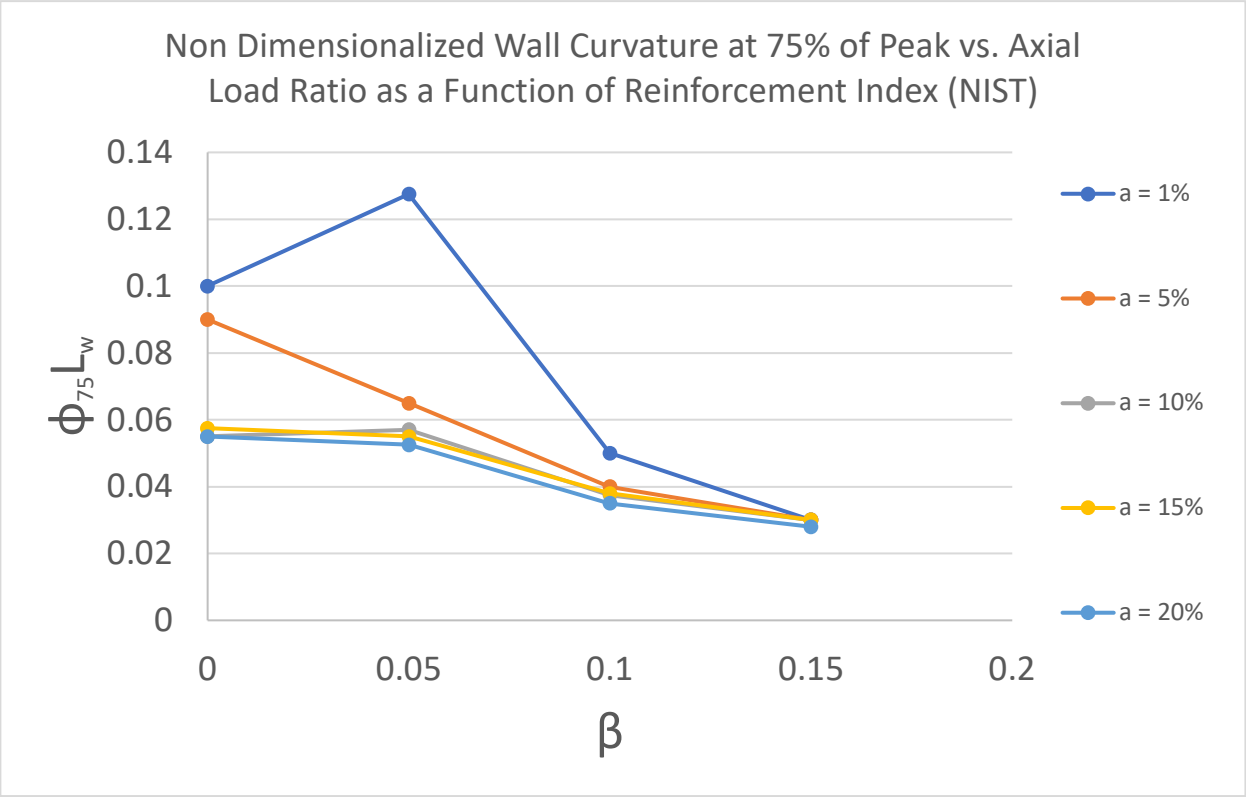

Figure 2.18) NIST standard values for the non-dimensionalized curvature at 75 percent of peak strength plotted against the axial compression ratio ($\beta = \frac{P}{f'_w \cdot A_n}$) and the available reinforcement index ($a = \frac{f_y}{f'_w} \cdot \rho_v$)

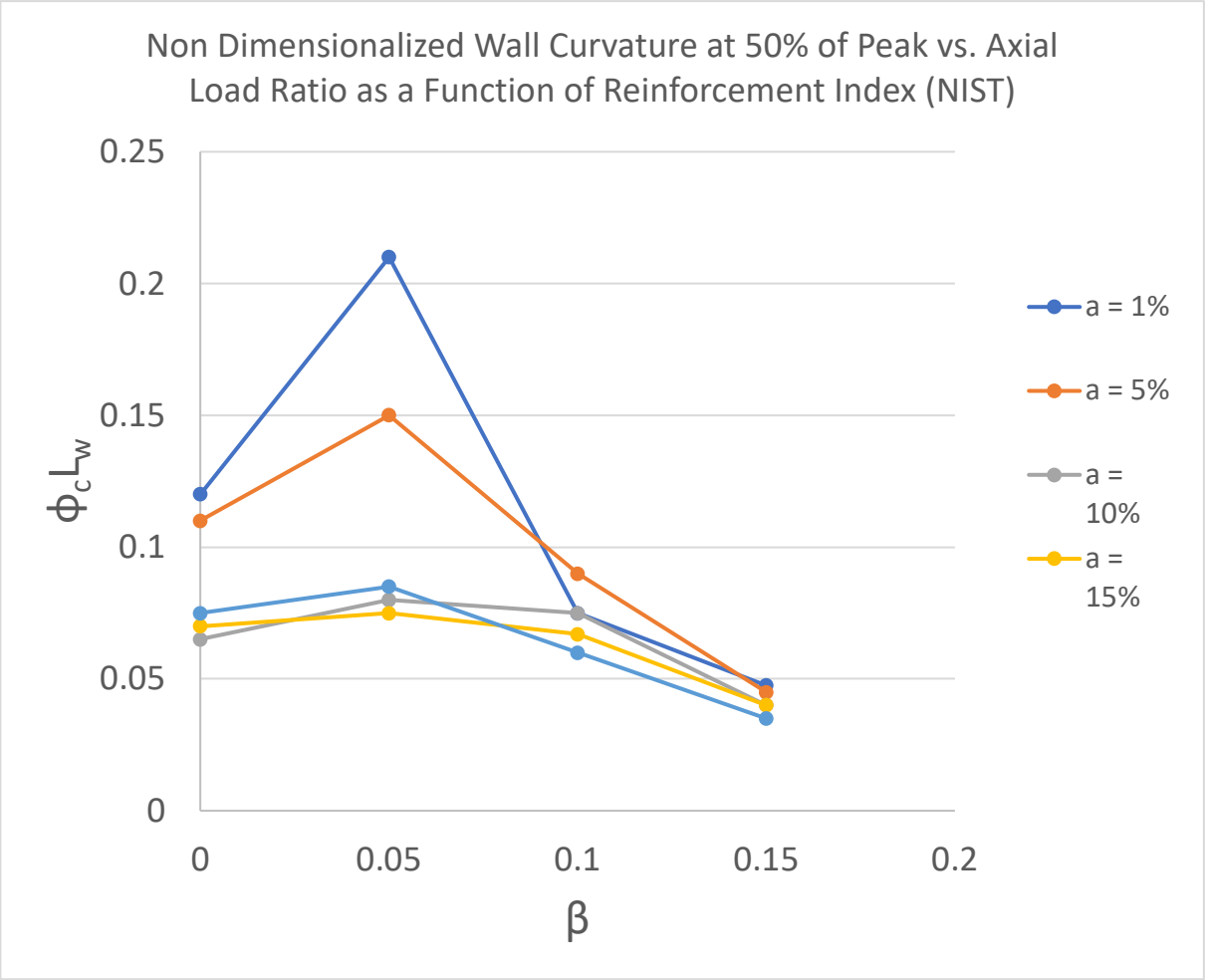

Figure 2.19) NIST standard values for the non-dimensionalized curvature at a residual crushing strength equal to 50 percent of peak strength plotted against the axial compression ratio ($\beta = \frac{P}{f'_w \cdot A_n}$) and the available reinforcement index ($a = \frac{f_y}{f'_w} \cdot \rho_v$)

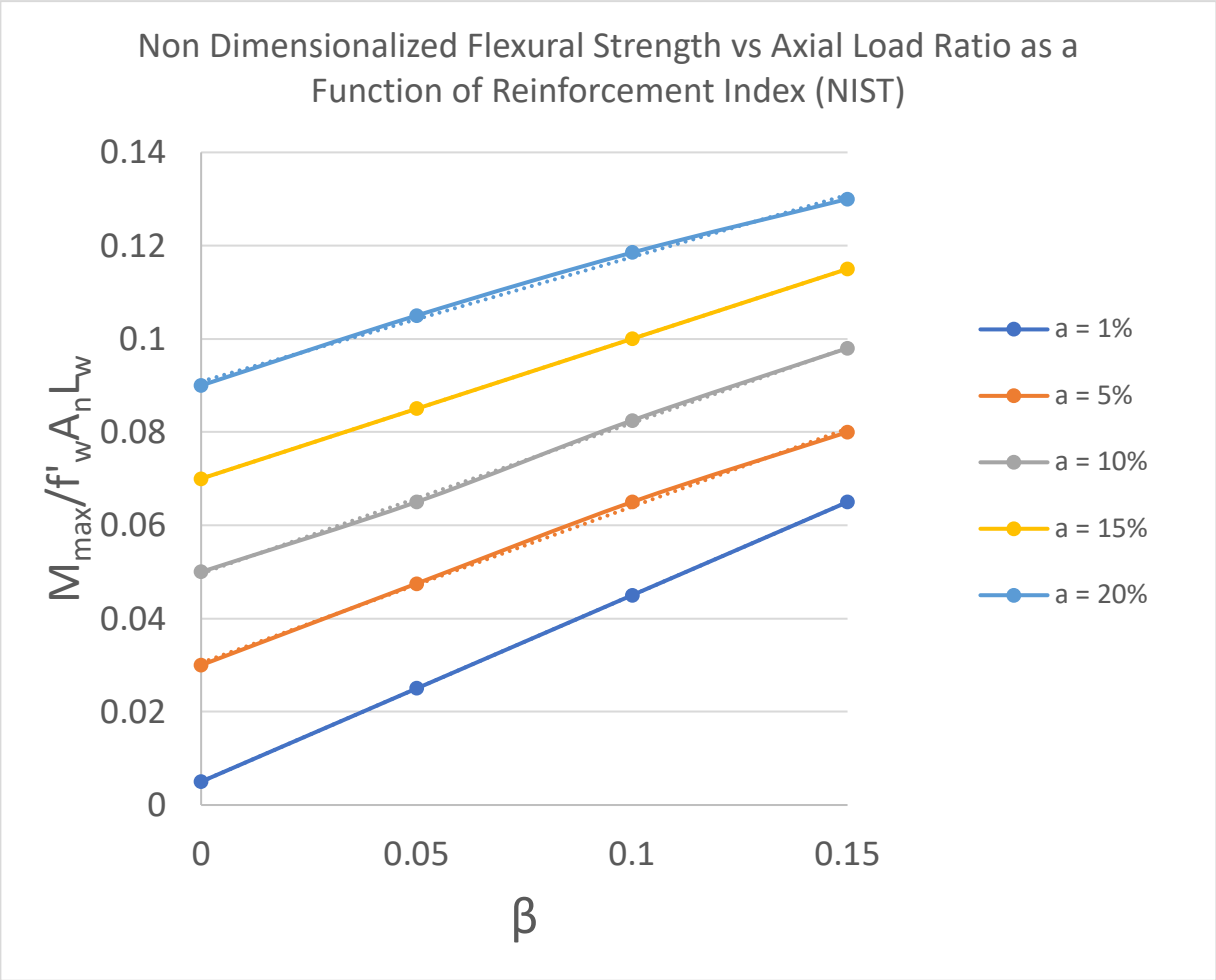

Figure 2.20) NIST standard values for the non-dimensionalized flexural strength of a reinforced masonry specimen plotted against the axial compression ratio ($\beta = \frac{P}{f'_w \cdot A_n}$) and the available reinforcement index ($a = \frac{fy}{f'_w} * \rho v$)

For shear dominated walls, the total shear resistance for a reinforced masonry wall considers a contribution owing from the masonry (V_{nm}) and a contribution owing to the transverse steel reinforcement (V_{ns}). The shear strength, which corresponds to diagonal tension failure, is defined as the peak coordinate on the NIST provided backbone curve, and computed through the expressions shown below:

$$Q_{max} = V_{nm} + V_{ns} \quad (2.21)$$

$$V_{nm} = (0.33 - 0.145 * \frac{He}{Le}) * A_n * \sqrt{f'_w} + (0.25*P) \quad (2.22)$$

$$V_{ns} = 0.5 * \frac{Av}{s} * f_y * d_v \quad (2.23)$$

These equations, as well as all other NIST provided figures and expressions, have been programmed into the database and assessed using the Canadian experimental data gathered from the literature in order to determine if the response they predict accurately represents what was obtained through real physical testing of specimens. Similarly, the alternative American assessment framework presented in the ASCE/SEI 41-23 document, was also programmed into the database and extended onto Canadian experimental data in order to validate the convergence of results between these two alternative procedures.

2.3.3 Analysis Methods in ASCE/SEI 41-23

ASCE/SEI 41-23, otherwise known as the framework for "Seismic Evaluation and Retrofit of Existing Buildings" is an American based guideline used for the evaluation and retrofit of existing structures for improved seismic performance. These guidelines present a variety of analysis methods for various structural systems and materials and present analytical expressions required in the assessment of seismic response and resistance capacity. For the purposes of this thesis, Chapter 11, which pertains to structural masonry, was considered.

In these recommended standards, several different analysis methods are discussed including the Linear Dynamic Procedure (LDP) and the Nonlinear Static Procedure (NSP), which aim to provide engineers tools needed for the seismic analysis procedure. Although the exact specifications of each of these methods lies beyond the scope of this thesis, it is important to identify the response curve linearization method followed in the NSP procedure.

The response curve of a structure can be computed by applying lateral loads to the building model representative to earthquake inertia forces. The concept of a response curve is a crucial component of the work presented in this thesis, and plays a pivotal role in the evaluation of the seismic performance of a structure. Understanding and utilising response curves are key in the evaluation of a structure's seismic performance as it describes the behaviour throughout varying levels of loading.

For common materials such as concrete and steel, standard response curves are preprogramed into the standard structural engineering software and, for most applications, do not require any input from the user. For reinforced masonry on the other hand, the load displacement response is much more ambiguous and varies from specimen to specimen based on the exact specifications of the design parameters and loading conditions. Through the use of the provided expressions by the NIST and the ASCE/SEI-41 Guidelines the individual members backbone

curves that relate strength with deformation are constructed and assigned to the corresponding plastic hinges of the modelled components. an average response envelope for reinforced masonry structure will be determined which will be a convenient reference for future research conducted on RM specimens. From here, the aim will be to obtain the necessary data that could be used to derive such a backbone response envelope that was made with specific reference with reference to Canadian experimental data, something that has yet to be published in any literature.

2.3.3.1 ASCE-41 Backbone Envelopes

The approaches prescribed in the ASCE/SEI 41-23 provisions pertaining to the structural assessment of masonry is similar in nature to what is recommended by NIST as it also provides the coordinates of milestone points for the member backbone (resistance) envelopes in tabular format in accordance with several design parameters. What sets these provisions apart from the corresponding NIST approach is the recommendation of a predefined generic backbone curve. These curves may be adapted to both unreinforced and reinforced masonry structures and relate the lateral load to drift ratio of specimens based on their governing mode of failure.

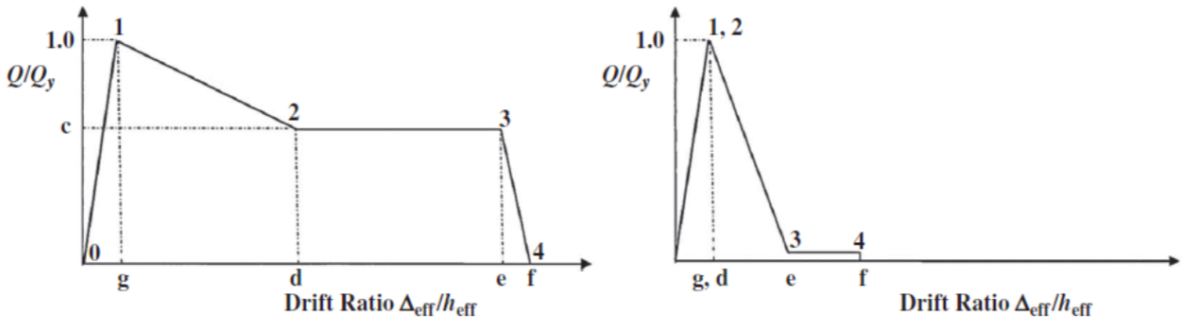

Figure 2.21) ASCE-41 recommended backbone curves for any type of masonry element based on whether they are dominated by flexural failure (left) or by shear failure (right)

Present on these curves are milestone points referred to as points g, d, e and f. To streamline the procedure for the application of these curves, the ASCE provides tabular values for each of these points based on parameters such as specimen behaviour, applied axial compressive stress, aspect ratio and effective reinforcement ratio. For any given wall specimen, deformation limits are provided in the form of acceptable drift ratio criterion for varying levels of damage based on the provided combination of these design parameters. Damage to a structural element is classified into

the following three distinct categories that relate the extent of damage to the risk of collapse of the structure.

Type	IO - Immediate Occupancy	LS - Life Safety	CP - Collapse Prevention
Primary Elements	Minor cracking No out-of-plane offsets	Major cracking Isolated masonry crushing	Extensive cracking Damage to opening and end regions
Secondary Elements	Minor cracking No out-of-plane offsets	Masonry crushing Damage to opening and end regions. Failure of non-structural elements connections	Glass panels shattered Non-structural elements no longer integrated onto superstructure
Drift	Minor to no non-structural damage owing to transient drift No permanent drift	Sufficient structural damage owing to transient drift Noticeable permanent drift	Extensive structural damage owing to transient drift Extensive permanent drift

Table 2.5) Structural performance levels of reinforced masonry structures according to ASCE/SEI-41 (2022)

In order to thoroughly illustrate the significance of parameters and deformation criteria governing the response of shear and flexure dominated walls, a series of plots have been developed for the coordinates of each set of points located on the standard backbone curves. In these figures, the constant red line indicates a shear dominated response, which has one constant value regardless of the aspect ratio. It is noteworthy that, with the exception of scenarios involving high aspect

ratios, low reinforcement ratios and negligible axial loads across all cases, the milestone points d and e tend to underestimate the deformation capacity of deformation-controlled walls, be they flexure or shear-dominated, in comparison to the brittle case of a force-controlled action.

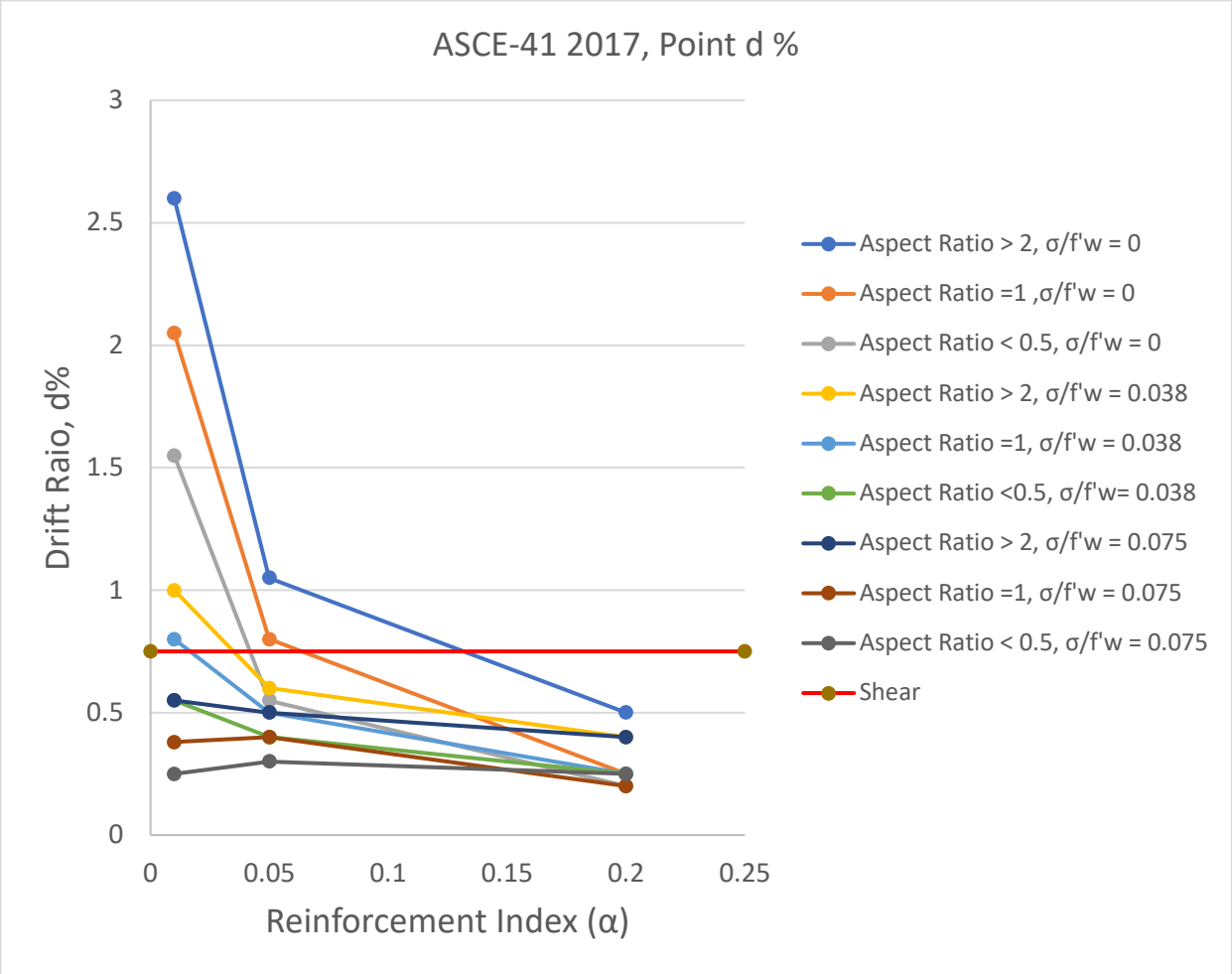

Figure 2.22) ASCE-41 2023 coordinates for point d for flexural controlled walls and shear-dominated behaviour (red line) as a function of the aspect ratio, ratio of applied axial stress to wall strength and reinforcement index ($a = \frac{f_y}{f'_w} \cdot \rho_v$)

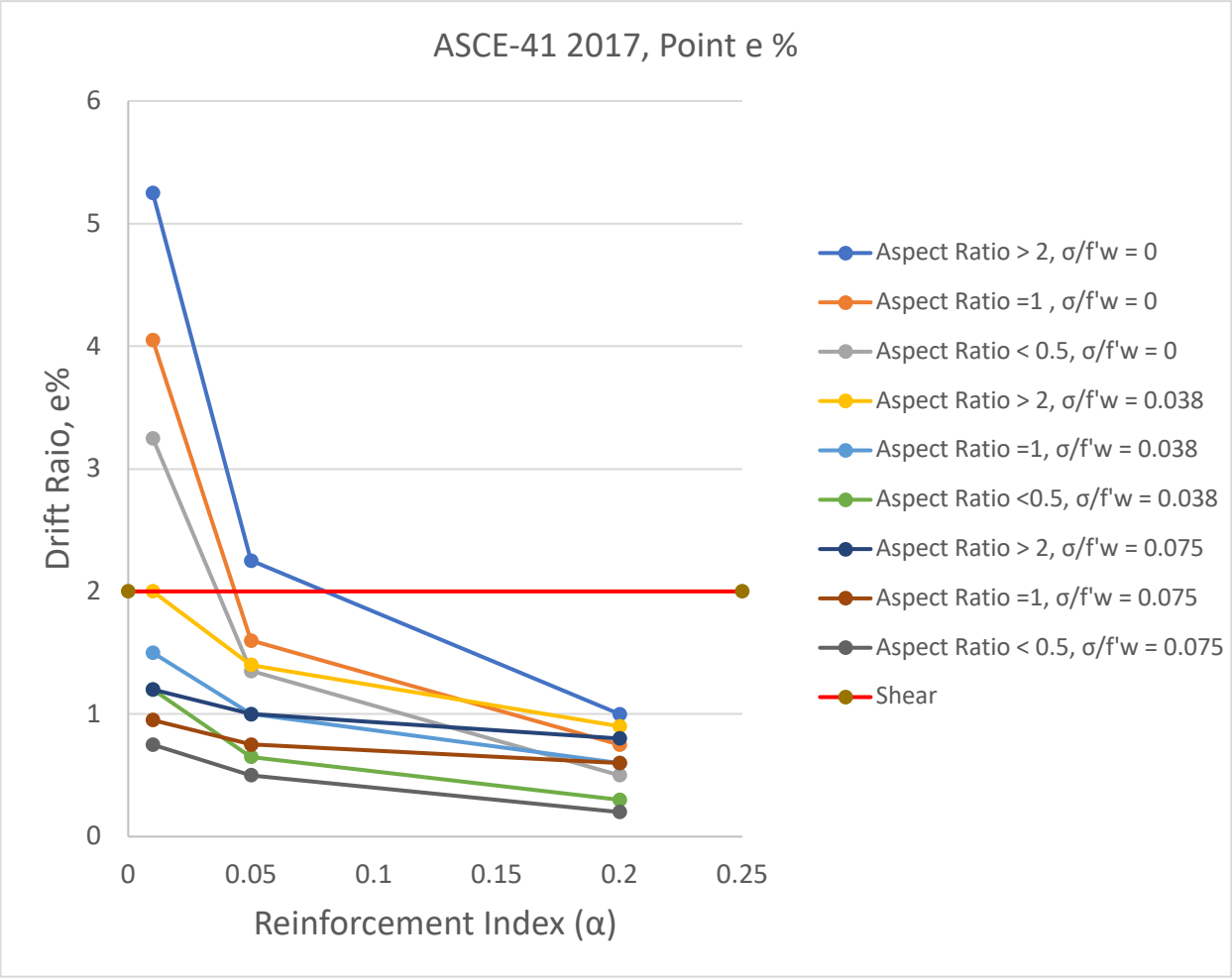

Figure 2.23) ASCE-41 2023 coordinates for point e for flexural controlled walls and shear-dominated behaviour (red line) as a function of the aspect ratio, ratio of applied axial stress to wall strength and reinforcement index ($a = \frac{f_y}{f'_w} \cdot \rho_v$)

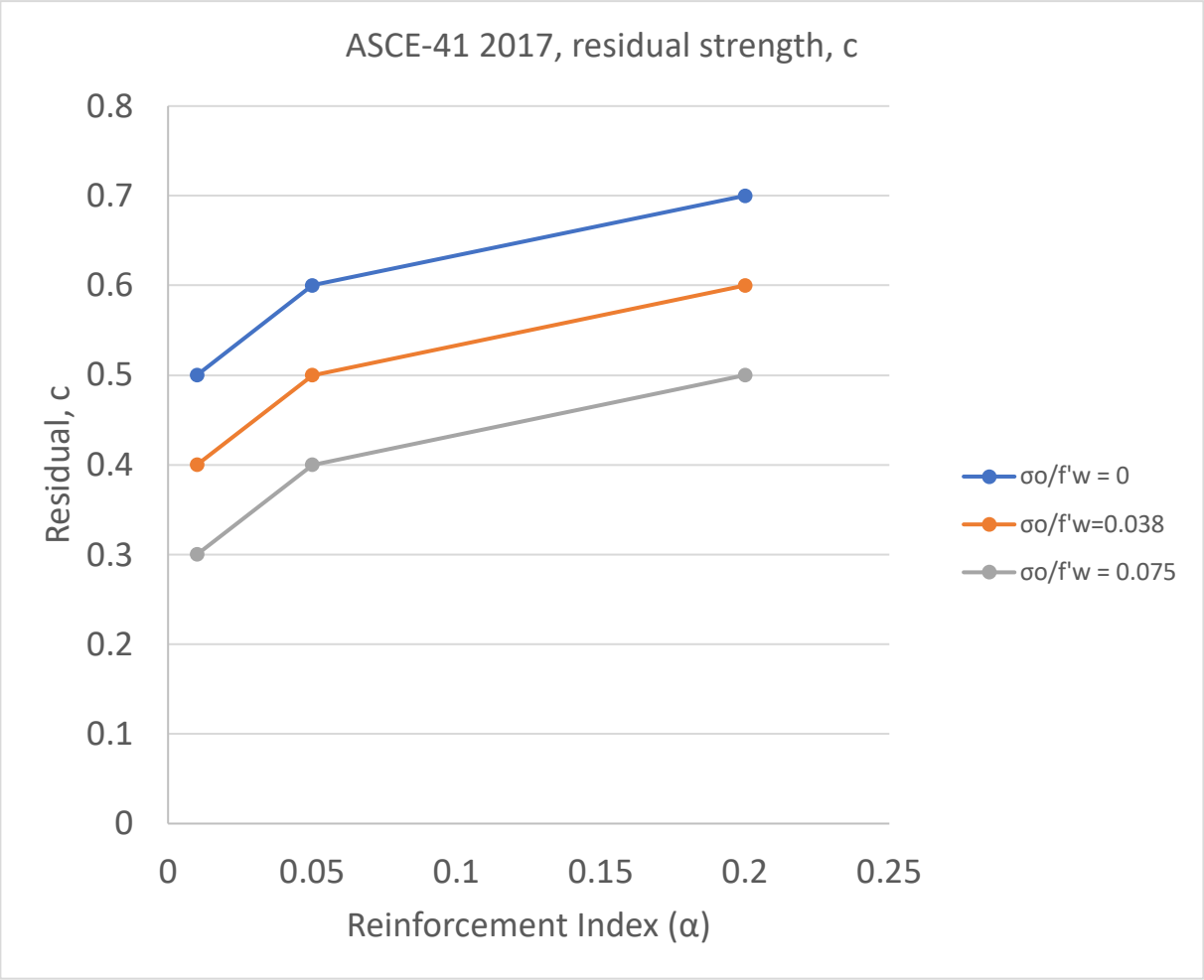

Figure 2.24) ASCE-41 2023 coordinates for point c for deformation-controlled walls as a function of the aspect ratio, ratio of applied axial stress to wall strength and reinforcement index ($a = \frac{f_y}{f'_w} \cdot \rho_v$)

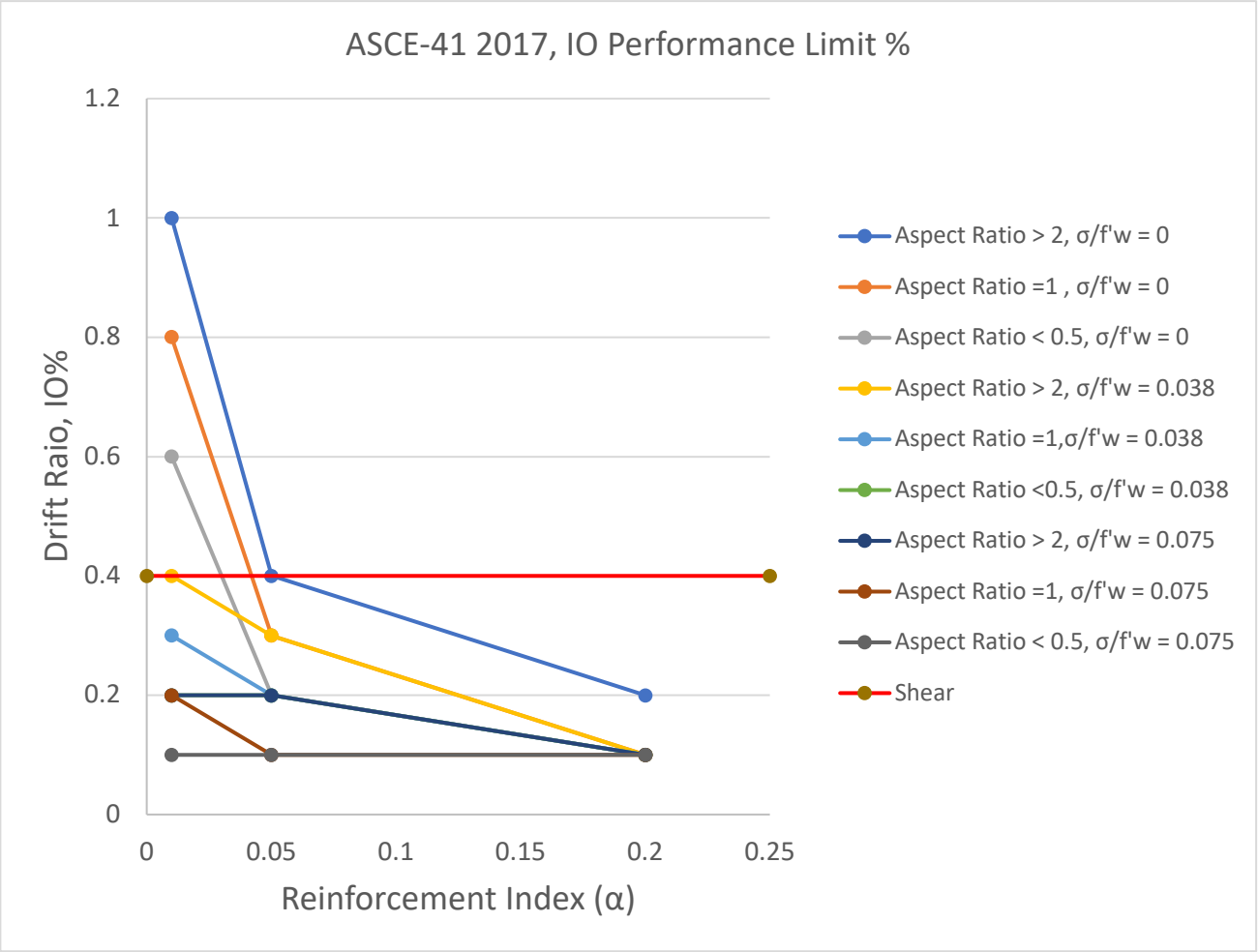

Figure 2.25) Sensitivity performance limit of the ASCE-41 2023 for Immediate Occupancy (IO) damage state

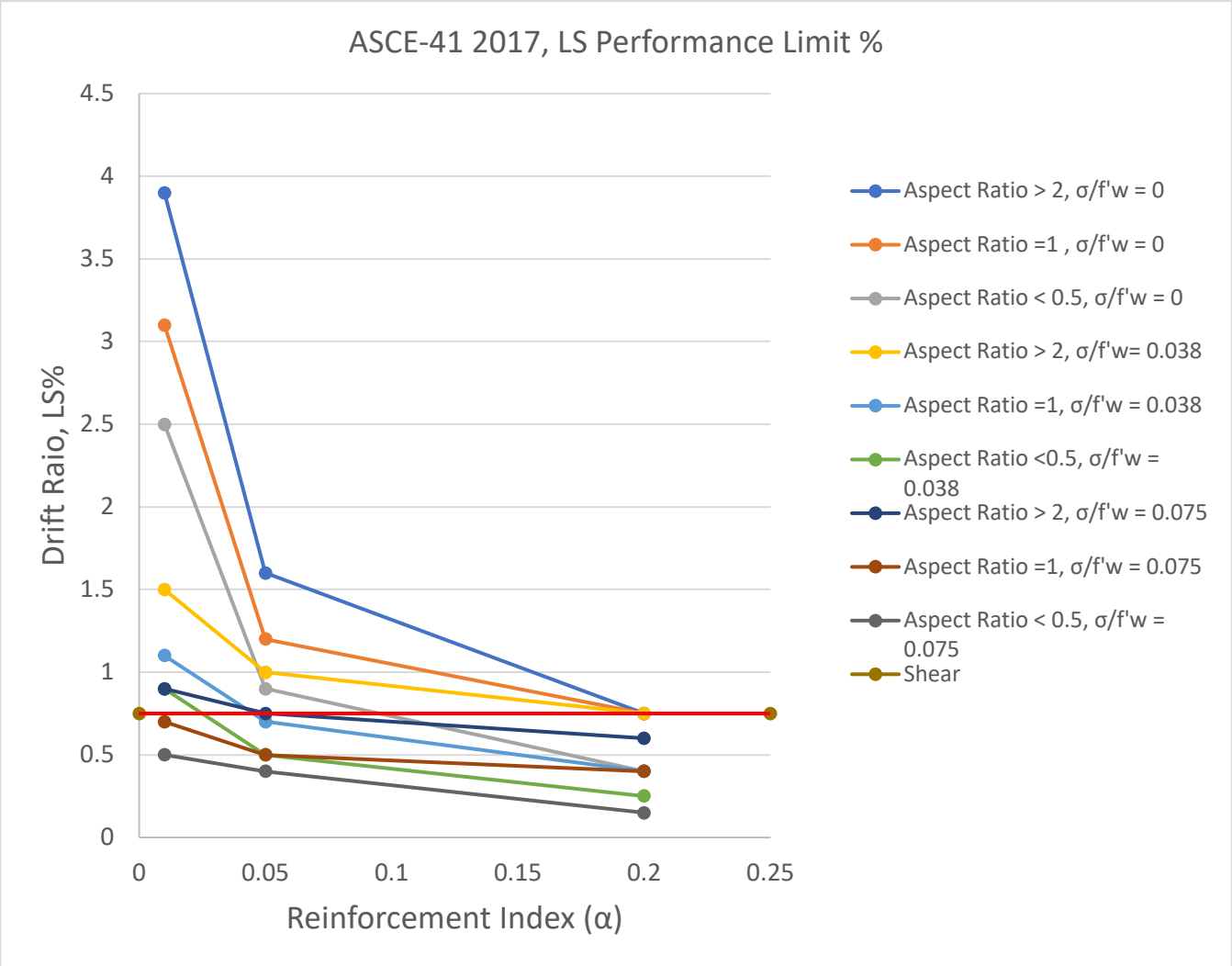

Figure 2.26) Sensitivity performance limit of the ASCE-41 2017 for Life Safety (LS) damage state

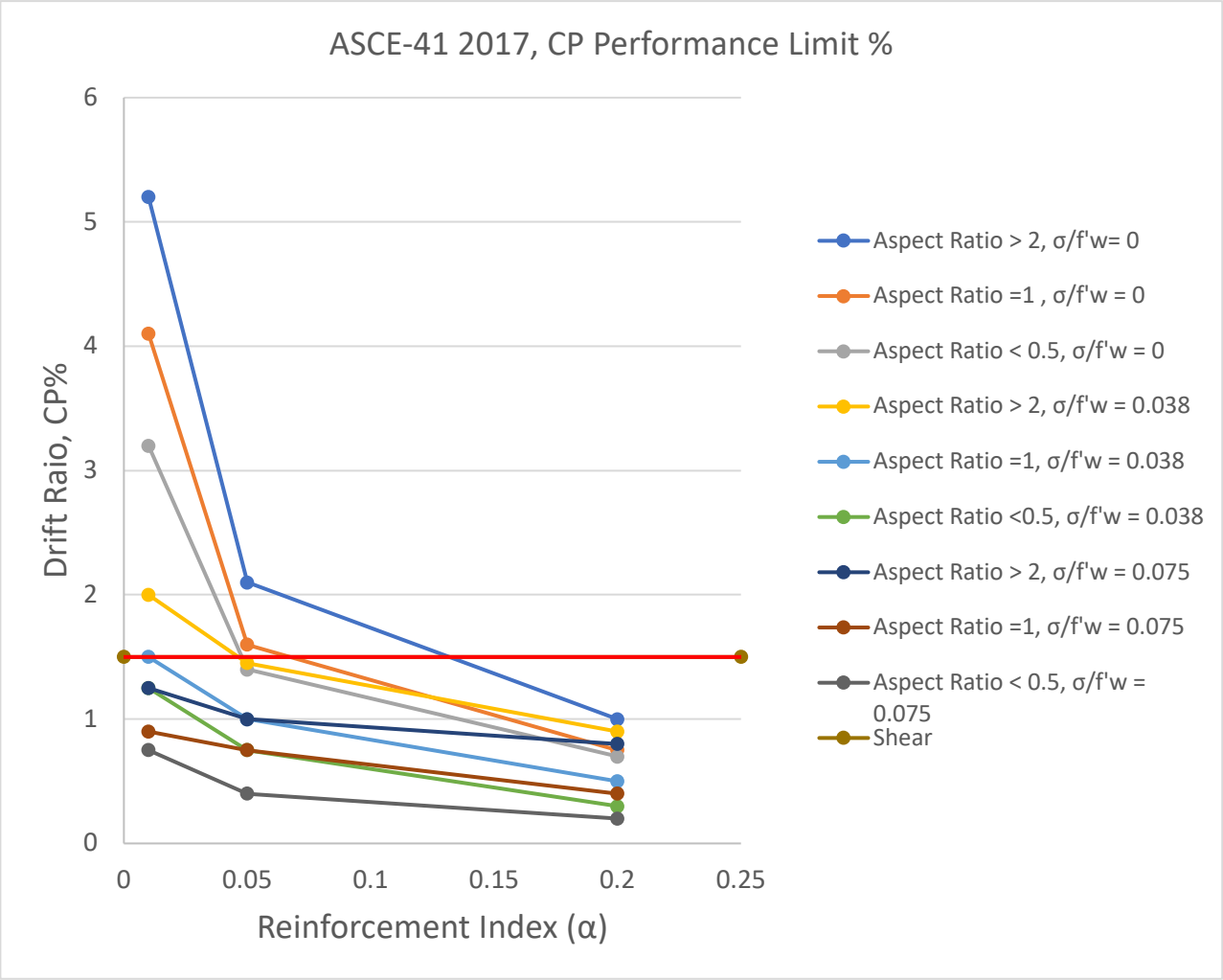

Figure 2.27) Sensitivity performance limit of the ASCE-41 2017 for Collapse Prevention (CP) damage state

2.4 Masonry Design Standards

2.4.1 CSA S304-24

The design and construction of masonry walls in Canada must be done with compliance of the CSA S304-14 Design of Masonry Structures, a guideline which provides guidance surrounding the various elements of design. With a prevalence in the Canadian engineering field since 1977, the first iteration of the code was developed in alongside with the British Standard (CP111). Since then, the standard has been continuously developed through 10-year cycles of revision to consider recent advancements within the Canadian practice, the evolution of similar codes in the USA and Europe, and the emerging methods and facility of analysis supported by computer software. This CSA provision provides information on a vast range of topics such as masonry structure design

requirements, structural analysis methods, reinforcement requirements and details, and special provisions for seismic design. Upon review of these seismic provisions, it is noted that no provisions are made regarding the required drift capacities of structures needed in order to materialize the design strengths.

As it stands, Canada currently does not have an explicit set of standards and guidelines for the assessment of masonry structures. In this area, Canadian practitioners usually rely on guidelines published by sister organisations such as the American Society of Civil Engineers (ASCE) and the National Institute of Standards and Technology (NIST).

2.4.2 TMS 402-22

The TMS 402-22, which stands for The Masonry Society, is an American developed design standard referred to as the "Building Code Requirements for Masonry Structure". It too has evolved on a similar 10-year cycle of continuous revision and played a role in the advancement of the corresponding Canadian standard, which had developed their companion load factors in based on alignment of values provided in the TMS 402. This standard provides requirement guidelines pertaining to the design and construction of masonry structures in areas such as materials, quality assurance, testing procedures, and most importantly for the context of this work, seismic design provisions. Although developed in the American context, this standard's principles and methodologies may offer valuable insights and benchmarks for assessing the performance of masonry structures within the Canadian context. For the purposes of this thesis, this American design standard will be investigated and programmed into the database in order to assess the accuracy of the outlined equations through comparison of the Canadian experimental data gathered through the literature. Successful convergence of results between strength estimates obtained through the TMS 402 equations and the experimental data will provide a justification towards the means of extending the NIST (GCR 17-917-45) and ASCE/SEI 41-23 seismic assessment provisions to the Canadian practice.

2.4.3 CSA S304 vs. TMS 402

When comparing the Canadian and American standard design provisions for reinforced masonry structures, several key differences surrounding the design and assessment procedures come to light. To begin, the determination of the specified compressive strength of the masonry (f'_w) differs between chosen approaches (unit strength and assembly strength) as well as mean

values used by the designers of walls published in literature. As per CSA S304 recommendations, the modulus of elasticity is obtained by multiplying the specified compressive strength of the masonry (f'_w) by a value of 850 and is not to exceed a value larger than 20 GPa. On the contrary, TMS 402 provisions recommend the modulus of elasticity be determined through the use of a different coefficient multiplied by the compressive strength of the masonry, where a value of 700 is used for clay bricks and 900 for concrete blocks. The disparities of the magnitude of this multiplier has been a key research area in the field and has been investigated by research teams around the globe, such as from École Polytechnique. Research suggests that the values presented in both CSA and TMS frameworks, which range from 700 to 900, are gross overestimates of the true magnitude and tend to be over optimistic, especially for older structures. A reduction for this value is currently being investigated for recommendation as it would yield a more conservative stiffness estimate, which would eliminate the possibility for overestimation of the seismic lateral load resistance of structures.

In addition to the apparent differences in the modulus of elasticity determination of the masonry (E_m), the useable maximum compressive strain (ε_{mu}) at the extreme compressive strain is set to 0.003 in the CSA S304 provisions, whereas the TMS-402 provisions limit this value to 0.0025. Differences between these approaches are largely due to differences present in standard building practices and estimated environmental risk which play a critical role in extreme loading events that the structure will experience. For example, although it does exist, the risk of earthquakes and hurricanes is not as severe in the Canadian context as compared to an American context. Despite this, the procedures for defining the structural systems for the various seismic design categories as well as response modification factors are largely comparable between the two approaches. In addition, the definition of the seismic loads and site classifications are directly akin to each other. One important difference between the two is that the American load combinations for seismic forces considers a 20 percent larger weighting of seismic forces in the load combinations, essentially meaning that for a given response acceleration, the base shear that is calculated from the American codes will be more severe than those obtained from their Canadian counterparts. In a sense, this means that American structures undergo a more rigorous design as they considered with more severe loading which in turn demands more dependable structural design to withstand such loading. The Canadian approach does however use a lower stiffness estimation which predicts larger deflections and a rarer seismic event than the U.S. Codes (2%

probability of exceedance in 50 years vs. 10% probability of exceedance in 50 years), requiring additional consideration in the structural design that helps level out the gap from the lower seismic design forces and help put it on par with the American design.

2.5 Induced Seismicity

In recent years, regions of otherwise stable Canada have been subject to abnormal levels of seismic activity, which has been linked to the use of hydraulic fracturing procedures for oil and natural gas extraction procedures. What was recently thought of as a harmless procedure that involved the injection of high-pressure fluids into open rock fractures in the earths crust, has now become a well-researched and investigated topic, as the influence that this procedure has on triggering severe earthquake events has been found to not be negligible as it once was predicted. Numerous earthquakes have been recorded in regions not typically known to experience seismic activities, with some of these reaching magnitudes 4.0 or higher and were directly attributed as induced seismic events. Atkinson (2020) describes the relationship between the volume and flow rate of the injection of pressurized fluids and the likelihood of triggering a seismic event, where higher amounts of fluid induced more frequent and severe seismic activity. In addition, this work emphasises the fact that these induced seismic events tend to occur at much shallower depths, allowing for a better indicator that is able to highlight differences between natural and manmade seismic activity. As a result of these shallower depths, the proximity to infrastructure also decreases and places them at a greater risk of damage, where a lower magnitude induced earthquake could result in damage levels similar to a more intense natural event occurring at a deeper depth.

Chapter 3

Assembly of Database

3.0 Introduction

This chapter discusses the procedure for assembly of the experimental database developed in Microsoft Excel and the various forms of data collected from physical tests conducted on reinforced masonry wall specimens within Canada. Throughout the chapter, the methodology followed in the development of the database is described, including the information recorded from the tests, as well as a discussion of the importance attributed to each parameter of interest.

3.1 Background

The intent of a database such as this is to acquire the statistical confidence needed to overcome the uncertainties surrounding the mechanistic properties of masonry as a material, which can be used to validate the applicability of the U.S. seismic evaluation standards being extended into Canadian practice. Through rigorous data vetting, the database was employed to bridge several uncertainty gaps present in the seismic assessment provisions for existing reinforced masonry structures in Canada. The database has been constructed considering an extensive range of tests for a wide range of specimen types which will serve as a crucial tool in addressing many of the open issues present in the current standard provisions.

For example, the equations provided in the recommended design frameworks do not address wall specimens that were constructed with specially detailed sections, such as flange or end-confined components, due to a lack of experimental data within the literature on such configurations. In addition, the analytical design equations refer to fully grouted walls, however, reinforced masonry walls can typically be only partially grouted according with the Canadian construction practice - specifically in the regions that contain reinforcement. To address this, the equations required a standardised reduction coefficient of 0.75 for the shear strength of partially grouted walls, however, this standard value does not consider the variation of partial grouting between specimens with different reinforcement layouts, and so is only a rough approximation. As a result, structures in the field with different partial grouting configurations will present analytical inaccuracies since the empirical expressions may not be able to accurately estimate its performance in terms of strength and drift capacities on account of these disparities. This is a severe design issue as discrepancies between predicted and actual structural performance can result in under designed structures that will not be able to effectively accommodate the anticipated seismic demands. Issues such as these are addressed in the database as experimental data collected from

tests of specimens of all forms of configurations and design details were considered in the test matrix, which allowed for a more thorough picture of response associated with the various forms of reinforced masonry construction that are found throughout Canada. In addition, the completed database will serve to act as a point of reference for proof testing the applicability of the American modelling procedures and analytical expressions by examining the influence from crucial modelling variables within a collective data source through comparisons on analytical U.S. values to those from the Canadian experimental endeavours.

3.2 Testing Procedures Used in Lateral Loading RM Wall Tests

Each experimental program considered in the database contained a number of wall specimens that were subjected to fully reversed displacement-controlled quasi-static cyclic loading (in both the positive push and negative pull directions) to simulate earthquake effects and were cycled far enough in strength degradation so as to obtain enough information on their post-peak behaviour. The specimens were tested solely in the lateral in-plane direction acting parallel to the direction of the wall, which is the primary direction of response that occurs during an earthquake. Although the out-of-plane direction is a crucial form of response for a reinforced masonry wall, it generally involves separate failure modes, such as overturning and buckling failure. To this end, the strength of a reinforced masonry wall in the out-of-plane direction is marginal, and its contribution to the main structural system is much less critical in this plane. In order to facilitate the in-plane loading conditions, specimens were tested through the use of applied lateral displacements at the top of wall through double-acting horizontal, as well as vertical (for some tests), hydraulic actuators. The presence of vertical actuators was required to induce axial compressive loads, and played a crucial role in the data assessment procedures. Displacements were recorded at predetermined locations along the wall heights through a variety of different methods such as dial gauges, potentiometers, strain gauges etc. All wall specimens were constructed on reinforced concrete foundations and connected to strong flooring, so as to provide a fixed boundary condition at the bases of the walls, thereby allowing specimens to perform as fixed vertical cantilevers.

3.3 Loading Protocols

The tests considered in the databased were conducted through the application of cyclic lateral displacements that were applied to the walls through the use of hydraulic actuators which were typically fastened to a rigidly stiff steel loading beam connected to the vertical reinforcing bars at the top of the wall. The loading procedure found in the tests varied slightly in the form of the location of the actuator arrangement which was tailored to simulate specified conditions of a real-life wall in different settings. The most common way contained only one horizontal actuator that coincided with the top level of the wall so as to create a zero-moment condition at the top of the wall. A few test setups saw the implementation of additional vertical actuators in order to introduce axial compression forces. This had an impact on the location of the zero-moment condition for a few specimens which, in turn, decreased the shear span of the wall. Loading beams were designed to imitate the response expected from earthquake loads being transferred to shear walls through a rigid diaphragm, resulting in a uniformly distributed lateral load at the wall top as opposed to concentrated loads at the corner regions near the top of the walls. Displacement potentiometers were positioned along the wall to record displacements relative to the rigid structural floor/foundation in vertical, horizontal and diagonal directions. Strain gauges were also attached to steel reinforcing bars which recorded local strains during the loading procedures. Bracing systems were also implemented in order to negate any unwanted out-of-plane displacements.

3.4 Experimental Setup

The experimental arrangement of actuators varied between the specimens present in the test matrix with slight variance in the position, arrangement, direction and number of actuators. Different actuator arrangements were favoured by the researchers in order to achieve different loading configurations. For example, in the case of specimens tested with an absence of axial compressive forces, a single horizontal actuator was sufficient in applying lateral loads at the top of the wall. A total of three distinct actuator arrangements were encountered in the considered literature:

3.4.1 Case 1 Arrangement

The most common test setup found in the literature comprised a single horizontal actuator aligned with the wall's centreline and positioned with the top of the wall in order to create a zero-moment condition at the top of the wall. The actuator was used to induce cyclic lateral displacements onto the specimen representative of the effects caused by seismic forces. This loading condition creates a linear moment distribution and ensured that the shear span of the specimen was equal to the entire height of the wall. The actuator was attached to a rigid steel beam fixed to the vertical reinforcement at the top of the wall which allowed for a uniform transfer of lateral loads onto the specimen. Specimens were fixed to a rigid concrete foundation and restraints were set in place to limit any unwanted out-of-plane displacements.

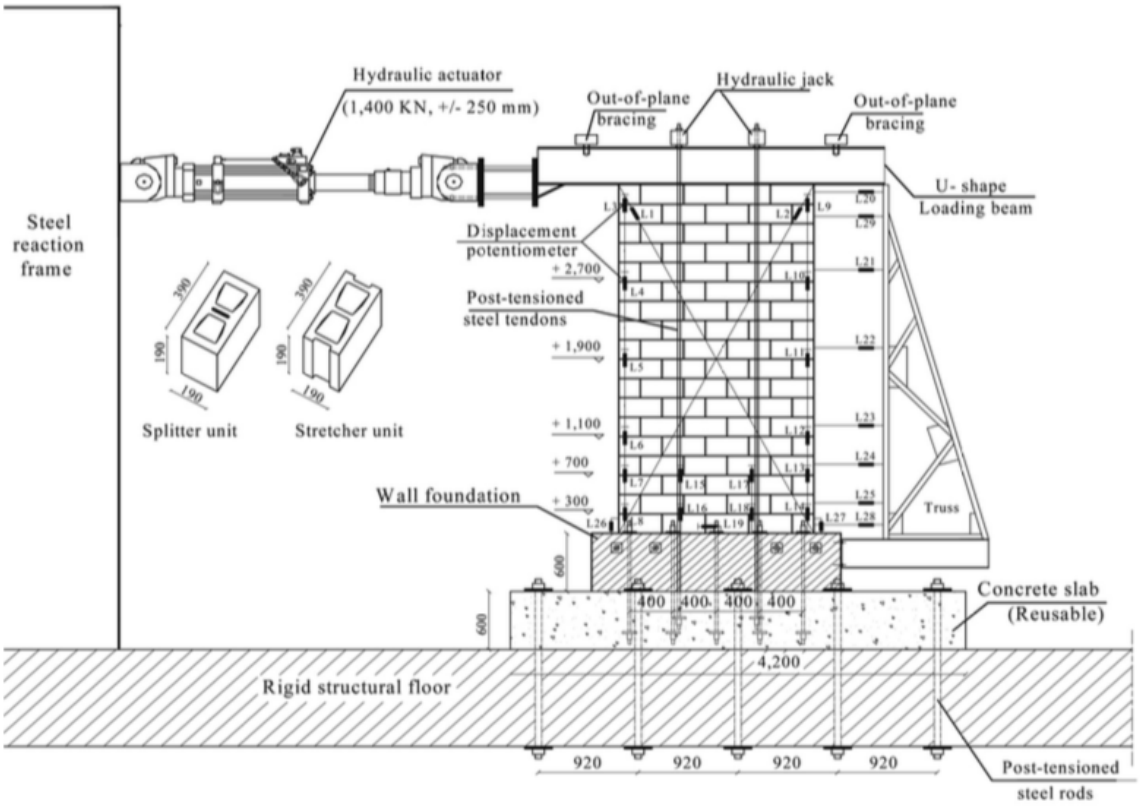

Figure 3.1) Example of a case 1 actuator setup used during testing. This figure, adapted from Shedid (2009), displays a single horizontal actuator located at the top of the wall

3.4.2 Case 2 Arrangement

This test case is a modified version of an arrangement developed by the ESECMaSE (Enhanced Safety and Efficient Construction of Masonry Structures in Europe) specifically for reinforced masonry walls, and was meant to simulate the boundary conditions of a middle story shear wall subjected to lateral loading. The arrangement incorporated an additional two vertical actuators in addition to the standard horizontal one. The vertical actuators were introduced into the test setup in order to apply axial compressive forces and maintain constant axial stress on the specimen, and the horizontal actuator served the standard purpose of inducing cyclic lateral displacements representative of seismic load effects. Specimens tested through this actuator arrangement required special consideration for the extrapolation of the shear span since the additional moment resulting from the above stories alters the moment distribution profile along the height of the wall. The actuators were attached to the rigid steel beam in the same manner as the other cases and out-of-plane restraints and fixed foundation supports are also present.

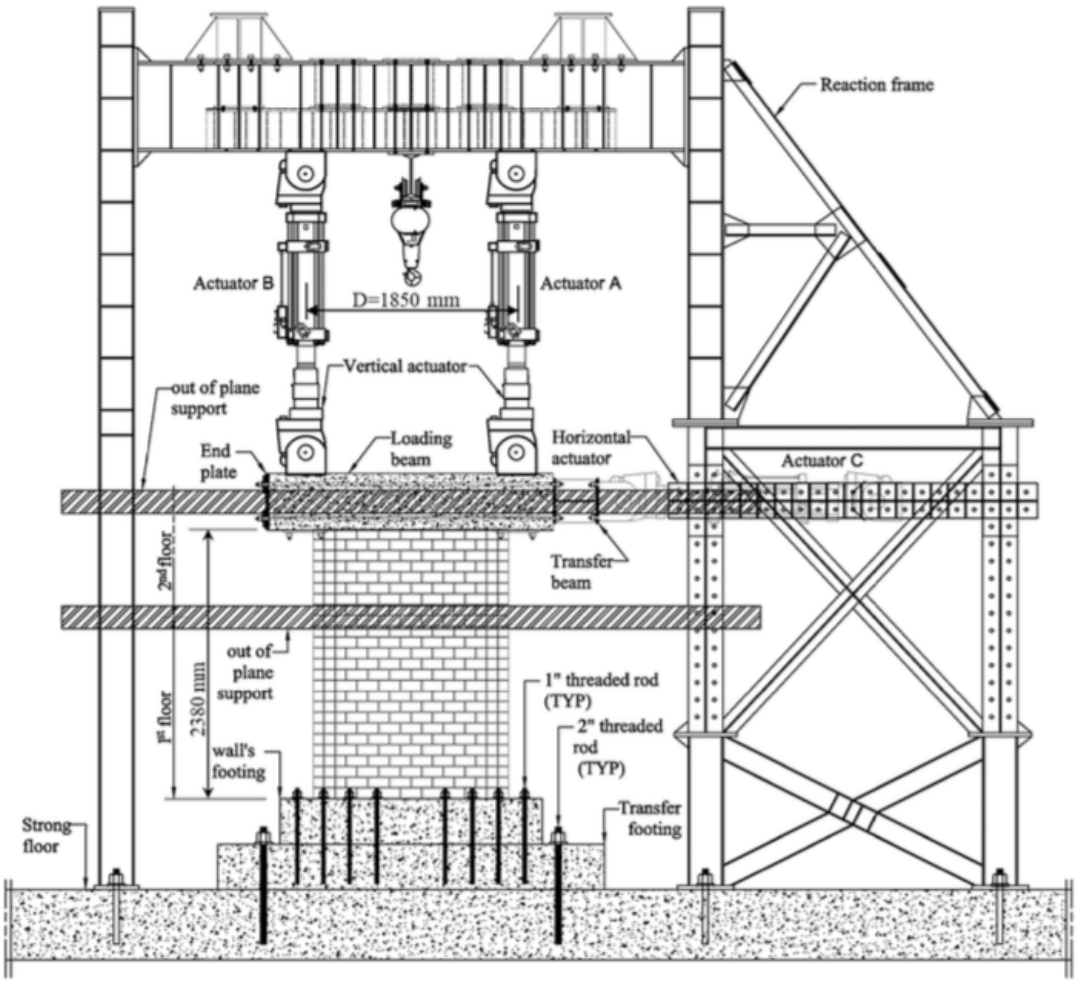

Figure 3.2) Example of a case 2 test setup used during testing. This figure, adapted from Albutainy (2021), shows the two vertical actuators required for the application of axial load in addition to the standard horizontal actuator.

3.4.3 Case 3 Arrangement

For one of the tests considered from the literature, a third unique test custom designed by researchers at the University of British Columbia arrangement was employed. This arrangement contained three actuators, these being one horizontal and an additional two vertically inclined actuators. These inclined actuators induced varied loads which simulated the effect of a nonzero moment at the top of the specimen as it occurs in a wall in a multi-storey building.

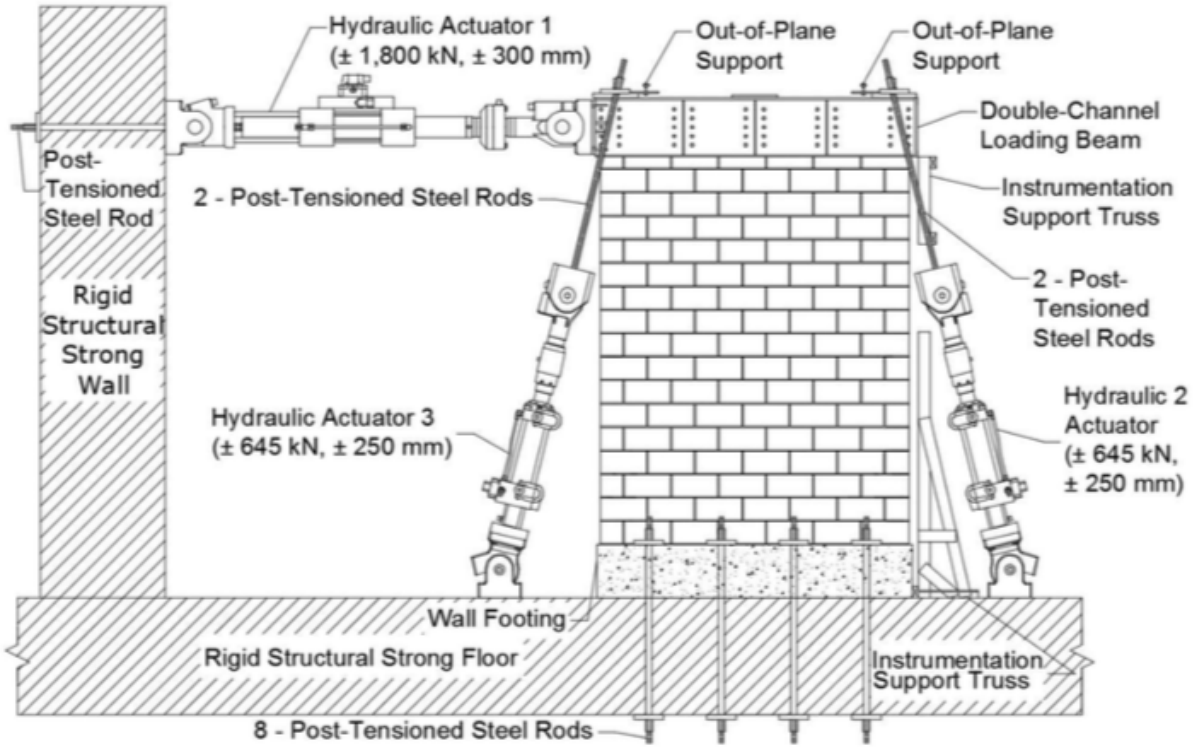

Figure 3.3) Example of a case 3 test setup used during testing. This figure, adapted from Robazza (2015), shows the two inclined actuators in addition to the standard horizontal actuator.

3.5 Data Collection

The constructed database contained experimental test data comprising over 70 concrete block reinforced masonry walls tested under in-plane cyclic lateral loading. In order for the database to be effective, a comprehensive record of the design details, reinforcement configurations, loading procedures, and load-displacement performances from all the considered specimens were considered in the assembly procedure. This broad collection of data did not only enhance the accuracy of analysis procedures, but also shed light into the variability present in the design of masonry walls. Analytical expressions and computational models were prepared for a range of parameters representative to those commonly encountered in real-world Canadian construction applications.

3.5.1 Database Parameters

The following section displays the excel cells recorded in the database for a typical wall specimen:

ID #	Paper Title	Specimen	Grouting	Grout Strength (Mpa)	Scale	Block Used
1	Drysdale, R. G, et al. "Characteristics of Rectangular, Flanged, and End-Confined Reinforced Concrete Masonry Shear Walls for Seismic Design." Journal Of Structural Engineering, 2010.	W4	Fully Grouted	21	Half Scale	Two-cell 20 cm hollow concrete

Figure 3.4) Information relating to general details of the reinforced masonry specimens recorded in the database

ID # - An internal reference number given to each paper examined in the database to allow for easy lookup and refence in the list of considered literature

Paper Title – Cited reference of the paper

Specimen – ID given to each specimen by the researchers when conducting their tests, where many papers constructed and tested several different specimens

Grouting – Details regarding the arrangement of grout in the construction of the specimen, where walls were either fully or partially grouted in select cells only

Grout Strength – Average cylinder compressive strength of the grout used in the construction of the specimen (MPa)

Scale – Calibration of size of the constructed specimen, where some walls were built to a smaller scale than reality in order to make construction and testing procedures easier

Block Used – Details regarding the blocks used in the construction of the wall specimen

tw (mm)	f'_c Block (Mpa)	f'_c Mortar (Mpa)	f'w wall (Mpa)	f_y Vertical (Mpa)	f_y Horizontal (Mpa)
90	27.2	21.8	16.4	495	534

Figure 3.5) Information relating to strengths of the materials used in the construction of the reinforced masonry specimens recorded in the database

t_w - Thickness of the blocks used in the construction of the wall specimens (mm)

f'_c Block – Average block compressive strength based on the net area (MPa)

f'_c Mortar – Average compressive strength of mortar cubes (MPa)

f'_w Wall – Average compressive strength of the entire reinforced masonry wall specimen (MPa)

f_y Vertical – Yield strength of the vertical reinforcement bars (MPa)

f_y Horizontal – Yield strength of the horizontal reinforcement bars (MPa)

H_e (mm)	H_w (mm)	L_w (mm)	Aspect Ratio	A_n (mm^2)
2660	2660	1802	1.48	162180.00

Figure 3.6) Information relating to dimensions of the constructed reinforced masonry specimens recorded in the database

H_e – Effective height, which is equal to the shear span, of the specimen. That is, the distance between the point of maximum moment to the point of zero moment (mm)

H_w – Height of the constructed wall specimen (mm)

L_w – Length of the constructed wall specimen (mm)

Aspect Ratio – Ratio between the height and length dimension of the wall specimen

A_n – Net cross-sectional area of the wall specimen (mm^2)

Vert Reinf A_v (mm^2)	# of Vert. Bars	ρ_v (%)	$\rho_v * f_{yv}/f'_w$	Spacing V (mm) -
1900	19	1.17	0.35314024	92.5

Figure 3.7) Information relating to arrangement of the vertical (longitudinal) reinforcement used in the construction of the reinforced masonry specimens recorded in the database

Vert Reinf A_v – Total area of all the vertical (longitudinal) reinforcement bars used in the construction of the wall (mm^2)

# of Vert. Bars – Number of vertical bars used in the construction of the wall

ρ_v – Vertical (longitudinal) reinforcement ratio (%), which is related to the amount of steel reinforcement used in the wall relative to its cross-sectional area

$\rho_v * f_{yv}/f'_w$ – Vertical (longitudinal) reinforcement ratio normalized with the strength of the wall

s_s – Spacing of the vertical (longitudinal) reinforcement bars in the horizontal direction (mm)

A_H per bar (mm^2)	Total Horiz Reinf A (mm^2)	# of Horiz. Bars	ρ_{Horiz} (%)	Spacing H (mm) -
129	1032	8	0.6	332.5

Figure 3.8) Information relating to arrangement of the horizontal (transverse) reinforcement used in the construction of the reinforced masonry specimens recorded in the database

A_H per bar – Cross sectional area of each horizontal reinforcement bar used (mm^2)

Total Horiz Reinf A - Total area of all the horizontal (transverse) reinforcement bars used in the construction of the wall (mm^2)

# of Horiz. Bars – Number of horizontal bars used in the construction of the wall

ρ_{Horiz} - Horizontal (transverse) reinforcement ratio (%), which is related to the amount of steel reinforcement used in the wall relative to its cross-sectional area

Spacing H – Spacing of the horizontal (transverse) reinforcement bars in the vertical direction (mm)

Boundary Element	BE h (longitudinal)	BE t (mm)	BE Bar Size	BE # of bars	Bar Area	$A_{s,BE}$ (per boundary element)
None	-	-	-	0	0	0

Figure 3.9) Information relating to the details of boundary elements used in the construction of the reinforced masonry specimens recorded in the database

Boundary Element – Details of the boundary element arrangement, which was set to none for this specimen in the absence of one

BE h (longitudinal) – Longitudinal dimension of the boundary element (mm)

BE t (mm) – Thickness of the boundary element (mm)

BE Bar Size – Bar designation of the vertical bars placed within the boundary element

BE # of bars – Number of vertical bars placed within the boundary element

Bar Area – Cross-sectional area per vertical reinforcement bar used in the boundary element (mm^2)

$A_{s,BE}$ – Total cross-sectional area of all the vertical reinforcement bars (mm^2)

Axial Stress (Mpa)	N (N)	$N/ A_n*f'_w$
1.05	170289	0.064024

Figure 3.10) Information relating to the details of the applied axial stress used in the testing of the reinforced masonry specimens recorded in the database

Axial Stress – Specified axial compressive strength applied to the specimens during the testing procedure (MPa)

N – Applied axial stress converted into a point load by multiplying the stress by the net cross-sectional area of the wall (N)

$N/ A_n*f'_w$ –Dimensionless normalized axial load ratio with the net area of the wall and the specified compressive strength

Qpeak +ve (kN)	θpeak +ve	Qpeak -ve (kN)	θpeak -ve
265	0.005263158	-267	-0.004699248

Figure 3.11) Information relating to the peak experimental performance in the positive push (denoted in green) and negative pull (denoted in orange) of the reinforced masonry specimens recorded in the database

$Q_{peak\ +ve}$ – Peak experimental load recorded in the experiment of the tested wall specimen in the positive push direction (kN)

$\theta_{peak\ +ve}$ – Drift ratio corresponding to the peak experimental load in the positive push direction, which is defined as the corresponding lateral displacement at this achieved load divided by the height of the specimen

$Q_{peak\ -ve}$ – Peak experimental load recorded in the experiment of the tested wall specimen in the negative direction (kN)

$\theta_{peak\ -ve}$ – Drift ratio corresponding to the peak experimental load in the negative pull direction, which is defined as the corresponding lateral displacement at this achieved load divided by the height of the specimen

Q0.8u +ve (kN) Pre	θ0.8u +ve Pre	Q0.8u +ve (kN) Post	θ0.8u +ve Post
212	0.001353383	212	0.009398496

Figure 3.12) Information relating to the ultimate (80 percent of peak) experimental performance in the positive push direction of the reinforced masonry wall specimens recorded in the database

$Q_{0.8u\ -ve}$ (kN) Pre	$\theta_{0.8u}$ -ve Pre	$Q_{0.8u\ -ve}$ (kN) Post	$\theta_{0.8u}$ -ve Post
-213.6	-0.001278195	-213.6	-0.012781955

Figure 3.13) Information relating to the ultimate (80 percent of peak) experimental performance in the negative pull direction of the reinforced masonry wall specimens recorded in the database

$Q_{0.8u+ve,\ -ve}$ Pre – Ultimate experimental load recorded in the pre-peak ascending branch of the response recorded during the experiment of the tested wall specimen in the positive push direction (green) and negative pull direction (orange) (kN)

$\theta_{0.8u+ve,\ -ve}$ Pre – Drift ratio corresponding to the ultimate experimental load recorded in the pre-peak ascending branch of the response recorded during the experiment of the tested wall specimen in the positive push direction (green) and negative pull direction (orange), which is defined as the corresponding lateral displacement at this achieved load divided by the height of the specimen

$Q_{0.8u+ve,\ -ve}$ Post – Ultimate experimental load recorded in the post-peak descending branch of the response recorded during the experiment of the tested wall specimen in the positive push direction (green) and negative pull direction (orange) (kN)

$\theta_{0.8u+ve,\ -ve}$ Post – Drift ratio corresponding to the ultimate experimental load recorded in the post-peak descending branch of the response recorded during the experiment of the tested wall specimen in the positive push direction (green) and negative pull direction (orange), which is defined as the corresponding lateral displacement at this achieved load divided by the height of the specimen

Q0.5u +ve (kN) Pre	θ0.5u +ve Pre	Q0.5u +ve (kN) Post	θ0.5u +ve Post
132.5	0.00037594	132.5	0.012030075

Figure 3.14) Information relating to the residual crushing strength (located at 50 percent of peak strength) of experimental performance in the positive push direction of the reinforced masonry wall specimens recorded in the database

Q0.5u -ve (kN) Pre	θ0.5u -ve Pre	Q0.5u -ve (kN) Post	θ0.5u ve Post	Failure from paper
-133.5	-0.00075188	-133.5	-0.016917293	Flexure

Figure 3.15) Information relating to the residual crushing strength (located at 50 percent of peak strength) of experimental performance in the positive push direction of the reinforced masonry wall specimens recorded in the database

$Q_{0.5u+ve,\ -ve}$ Pre – Residual crushing strength experimental load recorded in the pre-peak ascending branch of the response recorded during the experiment of the tested wall specimen in the positive push direction (green) and negative pull direction (orange) (kN)

$\theta_{0.5u+ve,\ -ve}$ Pre – Drift ratio corresponding to the residual crushing strength experimental load recorded in the pre-peak ascending branch of the response recorded during the experiment of the tested wall specimen in the positive push direction (green) and negative pull direction (orange), which is defined as the corresponding lateral displacement at this achieved load divided by the height of the specimen

$Q_{0.5u+ve,\ -ve}$ Post – Residual crushing strength experimental load recorded in the post-peak descending branch of the response recorded during the experiment of the tested wall specimen in the positive push direction (green) and negative pull direction (orange) (kN)

$\theta_{0.5u+ve,\ -ve}$ Post – Drift ratio corresponding to the residual crushing strength experimental load recorded in the post-peak descending branch of the response recorded during the experiment of

the tested wall specimen in the positive push direction (green) and negative pull direction (orange), which is defined as the corresponding lateral displacement at this achieved load divided by the height of the specimen

3.5.2 Milestone Points

Reported in the literature of the examined papers in the database were the recorded force-displacement (or drift ratio) response hysteretic curves, which presented the deformation of the wall as a function of the increasing lateral load that was applied during the test. These load and displacement/drift values were recorded at several distinct points of the test that were specifically chosen in order to obtain an accurate picture of the response that occurred during the testing, These distinct points are referred to herein as the milestone points of response, and are located at the peak experimental load, the point of yielding/ultimate strength (equal to 80 percent of the peak load) and at a residual crushing strength (equal to 50 percent of the peak load) in both the positive push and negative pull directions. As visible in the hysteretic curve shown below, the wall response is nearly elastic up until the point of yielding, which was assumed to occur at a location equal to 80 percent of the peak strength. This assumption was required as the exact point of yielding was not directly reported in all experiments, however in the few experiments that did report the exact location of yielding, the values were in close agreement with this 80 percent of peak estimate, which validated the assumption.

An example of one such force-displacement response hysteretic curves that was reported in the literature has been shown in the figure below, in which the lateral displacement of the wall due to the increasing lateral force being applied to the wall in increasing cycles is reported.

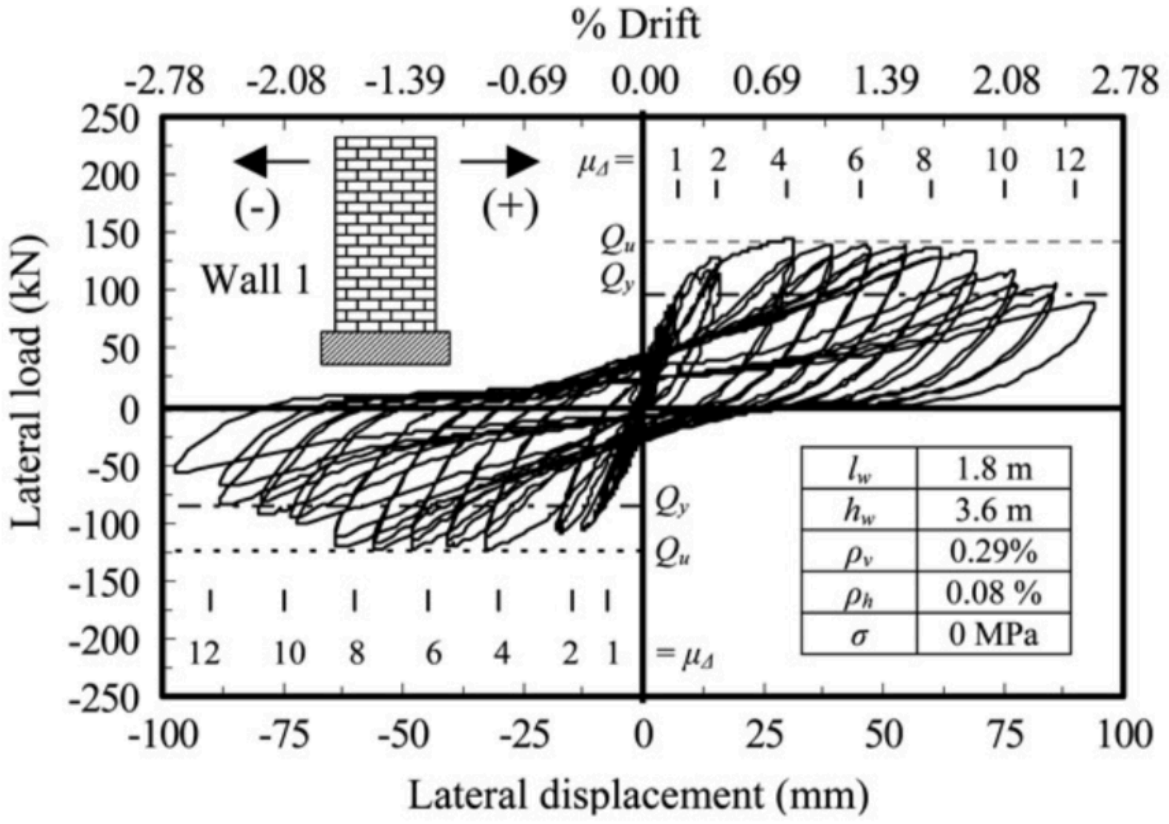

Figure 3.16) Hysteretic lateral load-displacement output of a typical test considered in the literature, figure adapted from Shedid (2009)

The nature of a hysteretic curve such as the one shown above is to depict the cyclic response of the specimen that occurred during the repeated push and pull loadings that were applied to the specimen. From these diagrams, the displacement (as well as the drift) can be read on the horizontal axis for any level of loading that was applied to the wall, which can be read on the y-axis. The area within the hysteretic loops illustrates the amount of energy dissipation that occurs throughout the specimen as a result of plastic deformations, where larger areas within the loops are optimal in seismic performance as it represents large energy dissipation. The successfully dissipation of energy is a favoured characteristic of a structure as it results in a reduction of seismic forces that are transferred to the structure as well as allow for significant amounts of displacement with little reduction to strength. Additionally, pinching of loops in these curves is a behaviour that occurs as a result of cracking, where locations of pinching result in a reduction to the load carrying capacity of the specimen.

Since these loops report the response of the structure from various loading cycles, the average response envelope was drawn so as to establish the maximum values at each level of displacement that was reported from the repeating loading cycles. Once this response envelope was defined, the average values of response were recorded at the established key milestone points. The experimental stiffness of the linear-elastic portion of response was computed as the slope of the ascending branch of all wall specimens in the database and was compared with the analytical values obtained through empirical relationships defined by ASCE/SEI 41-22, as explained in the following chapters of this thesis. The figure below illustrates the location of the milestone points on the average response envelope of the hysteretic curves in the positive push direction. In this figure, the red data point illustrates the peak response, the purple point illustrates the point of yielding, the cyan point corresponds to the ultimate deformation capacity of the component and the blue point illustrates the residual crushing strength at 50 percent of peak strength in the post peak branch. In addition, an orange point is seen at this location on the pre-peak ascending branch to provide additional information on the recorded response in the lower portion of the envelope. This response envelope depicts the lateral displacement in the form of a drift ratio (θ), which was computed by dividing the recorded displacement by the shear span (H_e) of the wall.

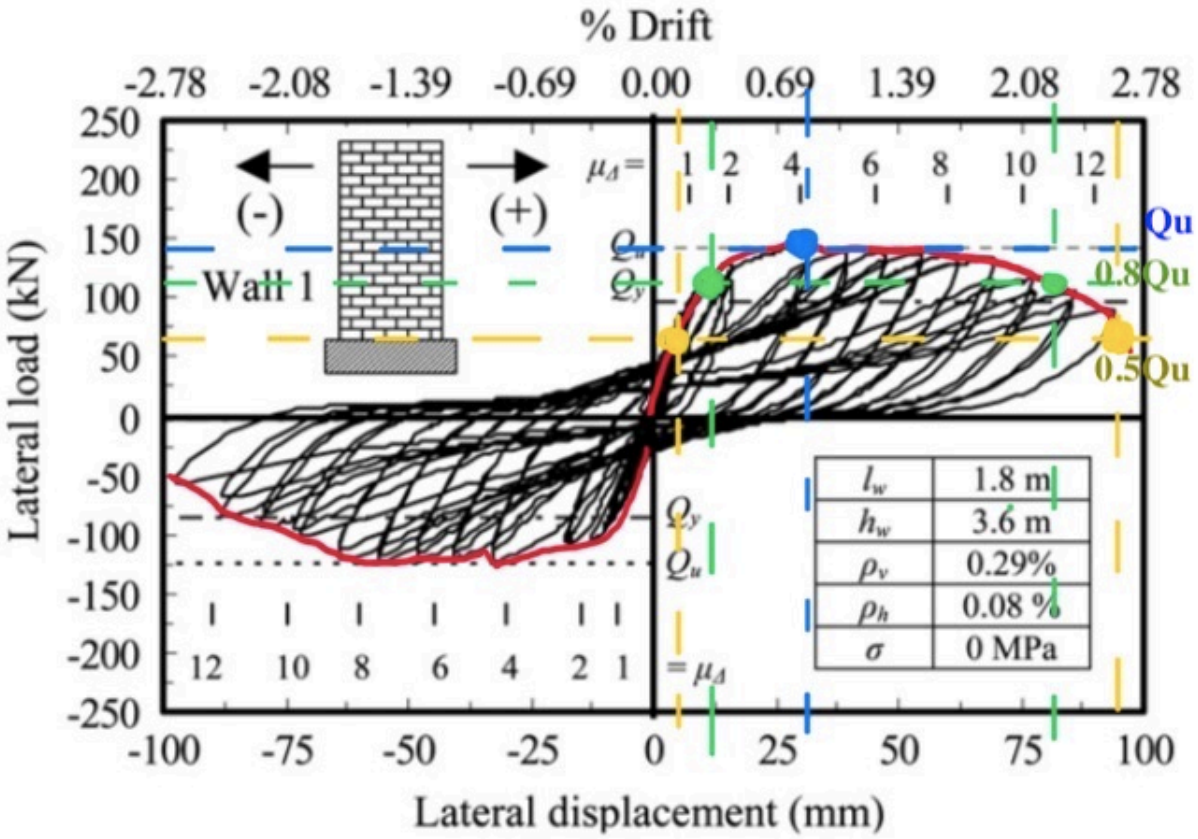

Figure 3.17) Annotated hysteretic lateral load-displacement output of a typical test considered in the literature, figure adapted from Shedid (2009

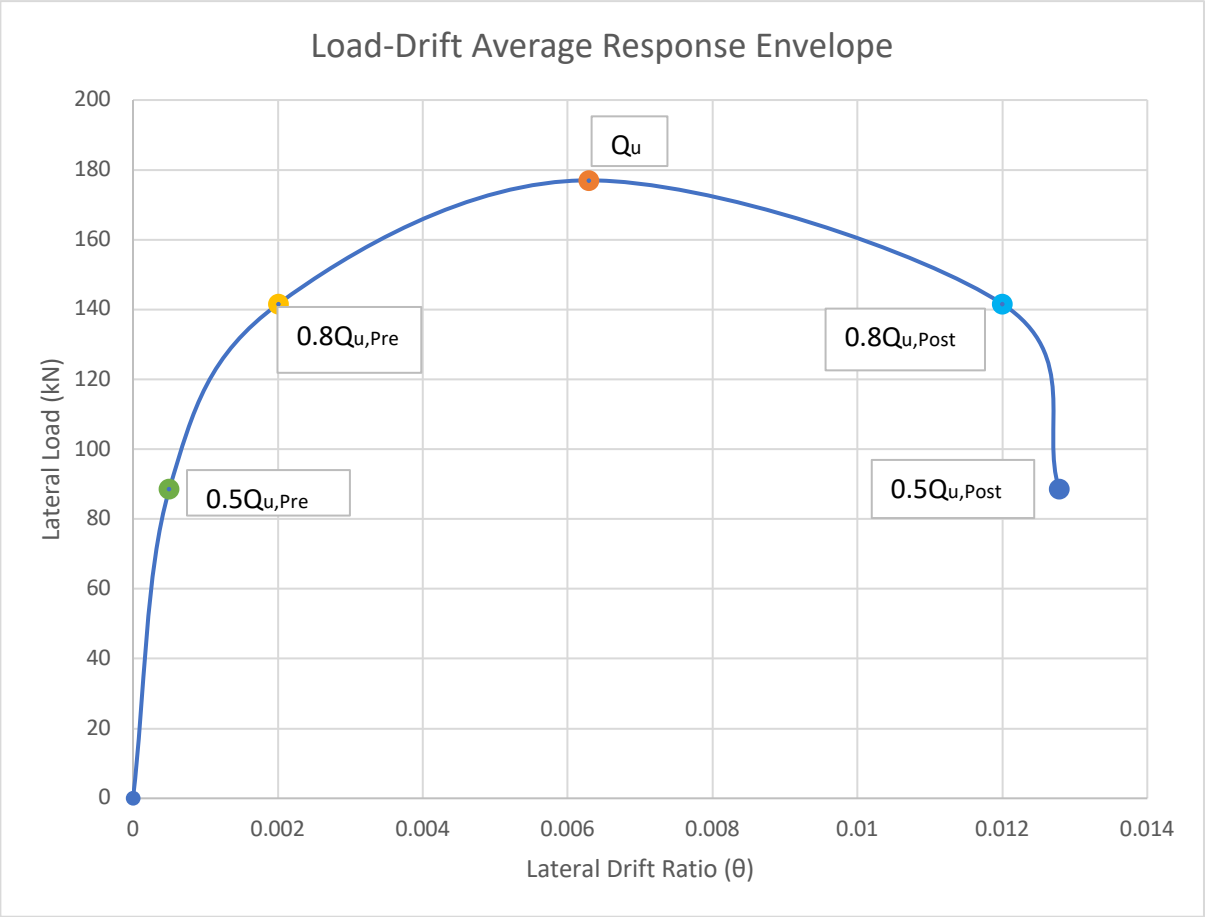

Figure 3.18) Annotated recreation of positive average hysteric response envelope with milestone point definition, data adapted from Shedid (2010)

3.6 Design parameters

In the following section the distribution of values for each variable of design that was encountered in the test matrix considered in the database is provided. Given the large distribution of values for several key design parameters, a crucial component of the database analysis was to investigate the influence each criterion of design has on the structural performance of the specimen so as to validate their significance and role in the assessment frameworks. According to the prescribed ASCE-SEI 41 approach, the three primary variables that impact the lateral drift capacity of a reinforced masonry wall are the aspect ratio, longitudinal reinforcement ratio and the normalised axial stress. All of three of these parameters, as well as several other insightful design parameters, were recorded in the database and were analysed to assess their influence they play on the overall behaviour of the specimen. The results and findings of this evaluation are given below.

3.6.1 Specimen Scale

A significant construction detail regarding the design of these specimens was the fact that they were all constructed as single wythe walls. This is a common construction method followed in practice, especially for low to mid rise buildings, where the structural loads can be adequately supported by a single row of masonry blocks. What did vary between tests, however, was the scale of constructed specimens. As shown in the figure below, less than half of the specimens were constructed at half scale, which meant that all dimensions of the specimen were reduced to 50 percent of its full scale counterpart. This form of construction allowed for an easier construction processes, and produced specimens that could be tested in the available lab facilities (limitations in this regard were space and capacity of the loading actuators). Careful consideration is required when generalizing from the response of scaled specimens since although material properties such as stress and strain remain constant in their scaled models, mechanical properties relating to the strength and stiffness of the specimen might not scale directly.

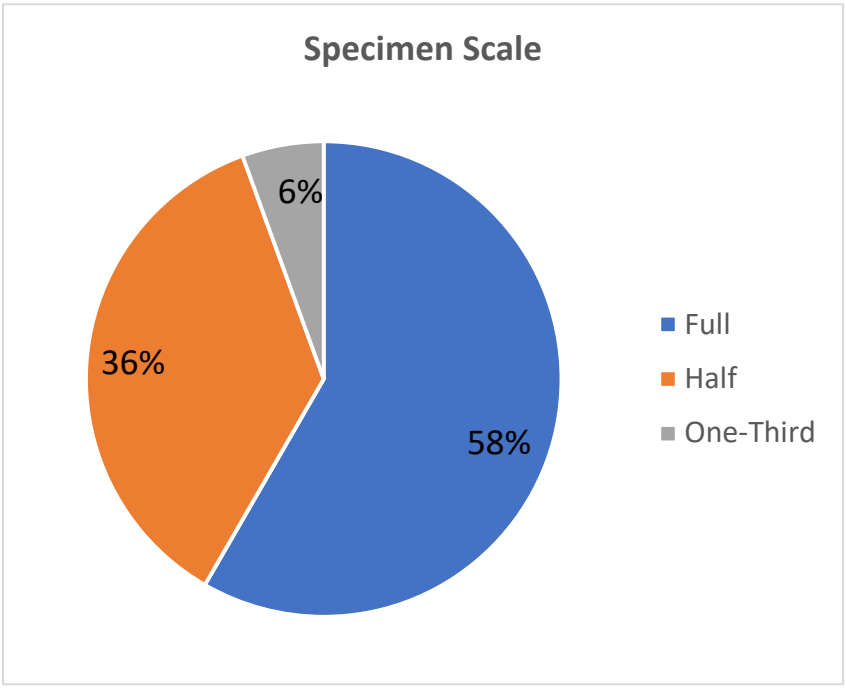

Figure 3.19) Schematic showcasing the distribution of construction scale used for the considered specimens in the database

3.6.2 Aspect Ratio

The aspect ratio of the walls, which is defined as the ratio of the height to length dimensions of the specimen, plays an important role in the structural behaviour and performance of the specimen. It is important to note that the effective height of a wall specimen is not necessarily equal to the height of the physical test specimen, but rather is the vertical distance between the point of maximum moment to the point of zero moment of the specimen (in continuous walls this is the point of inflection at the mid-height). The effective height is a recurring variable in many of the design standard equations.

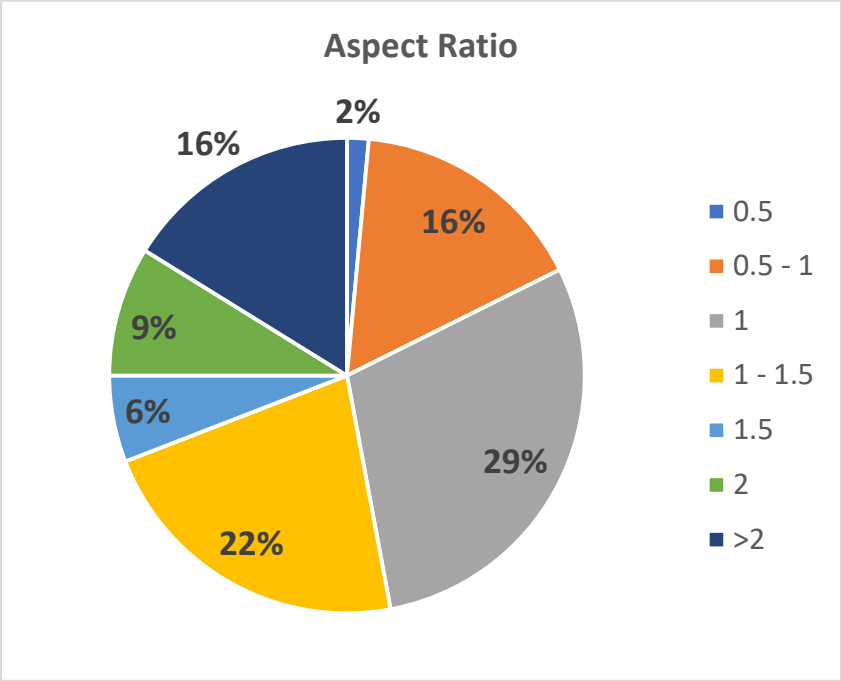

Figure 3.20) Schematic depicting the aspect ratio of wall specimens found in the test matrix of the database

From Figure 3.20 above, it is observed that the majority of the specimens were squat walls with aspect ratio values less than 1.5, with some specimens within the higher value ranges. The range of values will provide valuable testing on the limits of validity of code equations for this variable.

3.6.3 Material Properties

The wall specimens gathered from the literature were constructed with unique design details that met the requirements of CSA S304-24, the Canadian design standard for masonry

structures, but generally followed typical details of those found in typical mid to low rise masonry construction. Material properties such as the compressive strength of the grout (f'_c grout) and mortar (f'_c mortar) as well as the compressive strength of concrete blocks (f'_c block) used in the construction were reported in each experiment and calculated through respective compression testing.

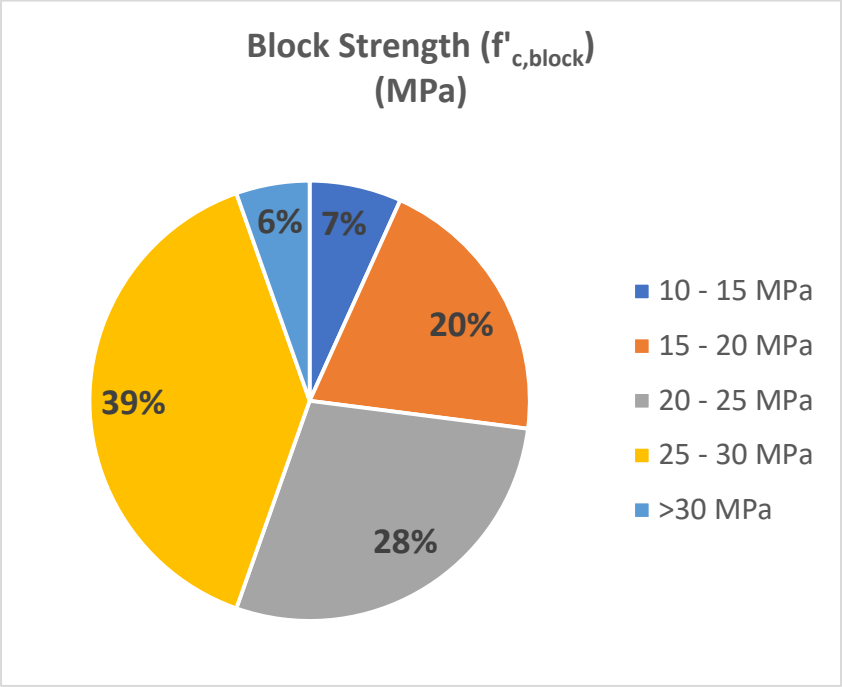

Figure 3.21) Schematic representation of compressive strengths encountered in the test matrix for concrete blocks (f'c,block)

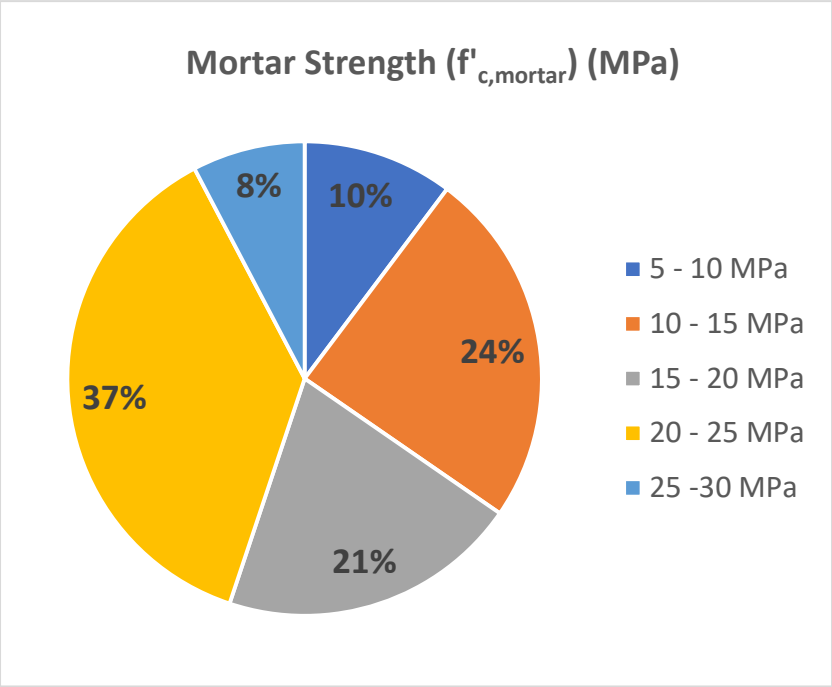

Figure 3.22) Schematic representation of compressive strengths encountered in the test matrix for mortar used in the construction of the wall specimens (f'c mortar)

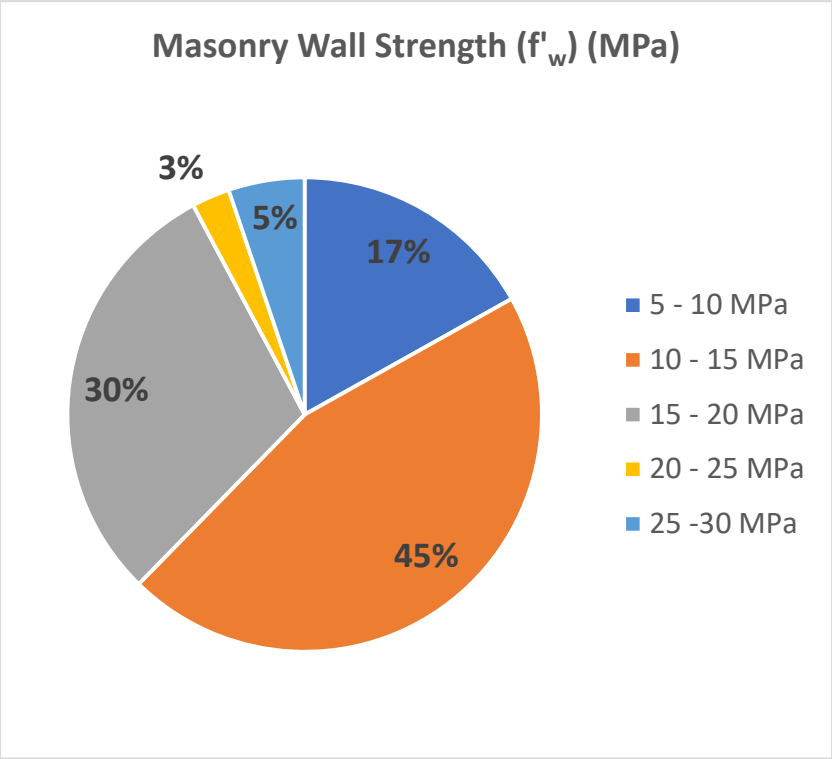

Figure 3.23) Schematic representation of compressive strengths encountered in the test matrix for masonry wallette units (f'w)

From the above figures, we notice that the masonry wall compressive strength (f'w) is not necessarily the average value obtained between the concrete block and masonry prism, but in fact, tends to be lower than both of these values. The compressive strength of the concrete blocks used for the construction of most specimens was in the range of 20 - 30 MPa (represented by the light blue and yellow regions in figures above), and the mortar compressive strength was slightly lower, around 15 - 25 MPa (represented in grey and yellow regions in figures above). This is largely due to the fact that the mechanical behaviour of a masonry wall is influenced not only by the strength of its constituent materials, but also the interactions occurring at the interfaces between them. The arrangement of blocks can cause complex stress distributions and loading conditions to occur within the wall which can be difficult to estimate and predict in analysis. This irregular nature of masonry is one of its greatest challenges and must be acknowledged during assessment procedures.

The evaluation of the compressive strength of a masonry wall (f'w) is not as straightforward as it is for a typical concrete section, which is treated as a homogeneous and isotropic material at least up to the onset of cracking. To overcome this, the masonry wall must be tested as a composite unit, which is achieved through compressive crushing tests conducted on

representative small-scale samples of the wall. These samples are referred to as wallettes, and serve to capture the interaction occurring between the individual blocks and mortar joints during testing.

An important consideration to keep in mind for the present study is that the compressive strength of the masonry wall (f'w) will not necessarily be the governing strength parameter of the specimen during lateral loading. Rather, the majority of the specimens will have their strength governed by the strength of bond between the mortar joints and blocks which run parallel to the direction of the simulated seismic forces.

3.6.4 Reinforcement Details

The database encompassed a diverse range of reinforcement details in the test matrix, which consisted of varying amounts of vertical and horizontal steel reinforcement bars of different strengths. The configuration and placement of reinforcement within masonry walls is often chosen by designers based on loading conditions, structural layout and design considerations. It is important to note that conclusions made from Maleki (2009) found that the overall response of a reinforced masonry wall is not sensitive to the pattern of reinforcement used, but is sensitive to changes in the dimensions of the specimen though the aspect ratio.

From the figure below, we can see the variation and distribution of yield strengths encountered in the test specimens. A commonly encountered bar strength for both vertical and horizontal bars was around the 425 to 450 MPa range. For the horizontal reinforcements, there were quite a few specimens that utilised bars with a yield strength greater than 550 MPa, with one specimen from Drysdale (2008) using deformed wires with an exceptionally high yield strength of 743.7 MPa.

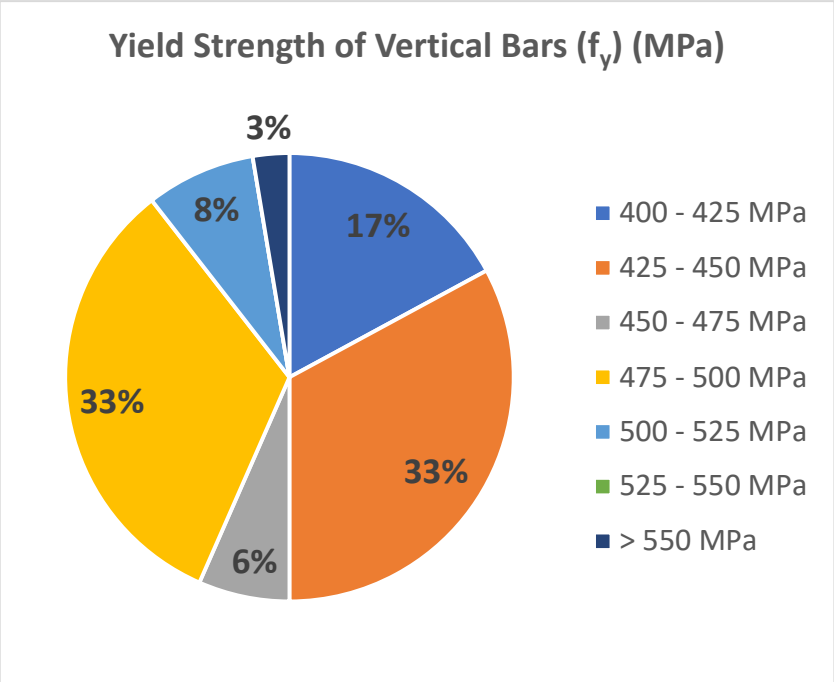

Figure 3.24) Schematic showing the distribution of vertical rebar strengths used in the construction of the wall specimens considered in the database

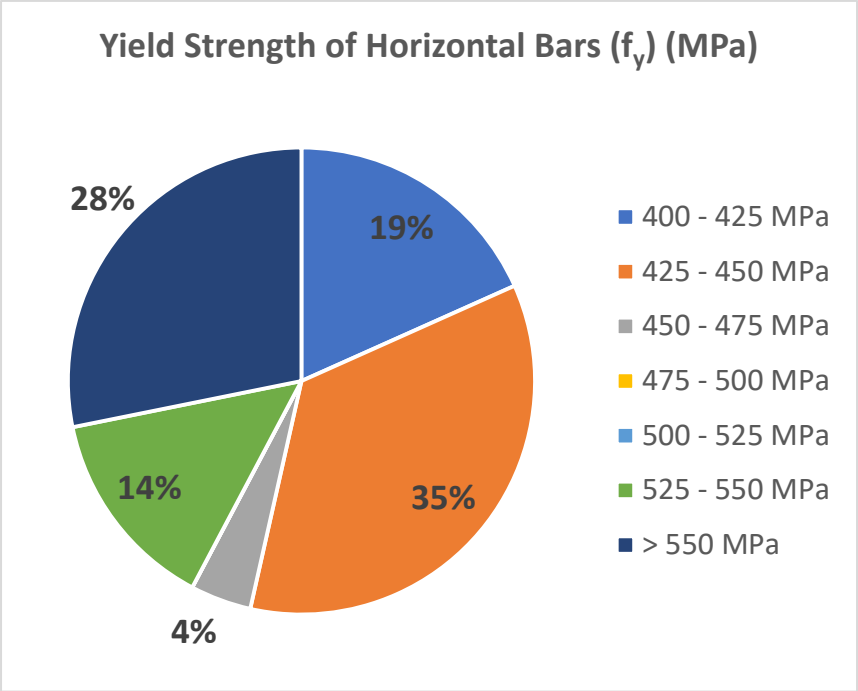

Figure 3.25) Schematic showing the distribution of horizontal rebar strengths used in the construction of the wall specimens considered in the database

Having this large range of strength values incorporated into the database will allow for investigation into the shear performance of the specimens, which will be discussed further in the data analysis section present in the Fourth Chapter of this thesis. Given the complexities associated with the geometry and failure modes of reinforced masonry walls, correct shear strength prediction of specimens is currently open to investigation as the code prescribed empirical equations could be inaccurately estimating the response. The roots for these inaccuracies could be stemming from a variety of sources such as the compressive strength of the masonry wall (f'w) being used in performance equations for specimens tested through lateral loading, given the fact established earlier that the compressive strength of the wall will not control the failure mode during lateral load testing.

Additionally, the equations for the masonry contribution of shear strength contain slight variations between the Canadian and American design standards which is an irregularity that points to the extent of the discord between the two guidelines. By programming all of the design and assessment equations from both the Canadian and American provisions within the database the validity and accuracy of the frameworks will be assessed. Differences between experimental data and the results obtained through the recommended theoretical expressions, will be an indication of inaccuracy between the approaches.

In addition to the strengths of the reinforcement used in the construction of the specimens, there was also a large variation in the amount of reinforcement used which has been presented in terms of the reinforcement ratio. Denoted by ρ, the reinforcement ratio has a significant role on the structural performance and behavior mode of a reinforced masonry specimen. Defined as the ratio between the total area of steel reinforcement to the gross cross-sectional area of the wall ($\rho = \frac{A\_steel}{A\_wall}$), there was a significant spread in values across the test matrix of the database. In terms of the vertical reinforcement ratios, there was a majority of specimens the were constructed with reinforcement ratios less than 0.25 percent, with the majority of specimens within the range of 0.16 to 0.19 percent. It is noted that these amounts are very low when considering flexural theory.

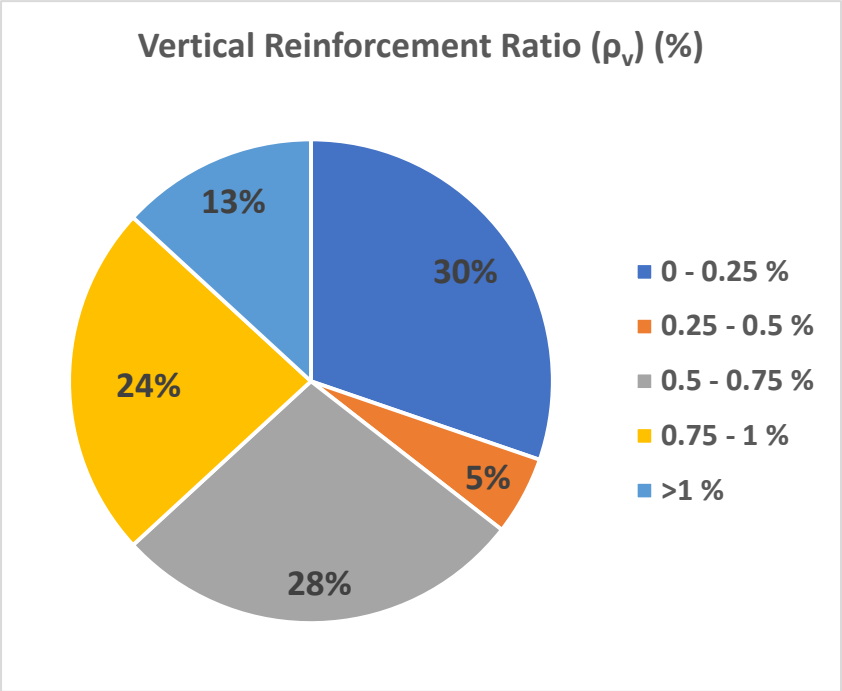

Figure 3.26) Visual representation of the distribution of vertical reinforcement ratio from the wall specimens considered in the database

Prior to analysing the influence that varying reinforcement ratios had on the wall performance it is important to first introduce the conceptual theory of what results are expected to occur based on the level of reinforcement ratio so that trends in the experimental data may be validated. For specimens constructed with large amounts of vertical reinforcement ratios, increased flexural strength is expected since the reinforcement is able to effectively resist larger amounts of tensile stresses and delay the onset of cracking.

In a similar manner, adequate amounts of horizontal reinforcement within a reinforced masonry wall should be able to provide significant amounts of shear resistance, which will be accompanied by a resistance against potential sliding modes of failure or diagonal cracking under lateral loads. From the figure below, we can see that the majority of wall specimens were constructed with horizontal reinforcement ratios in that same range of less than 0.25 percent, with the average value being around 0.1 percent, a value much lower than the average of vertical reinforcement ratio. Given that some specimens greatly exceeded the values in this range and reached as high as above 1 percent, we can anticipate that specimens constructed with horizontal reinforcement ratios of less than 0.1 percent to be prone to shear failures due to the lack of shear resistance.

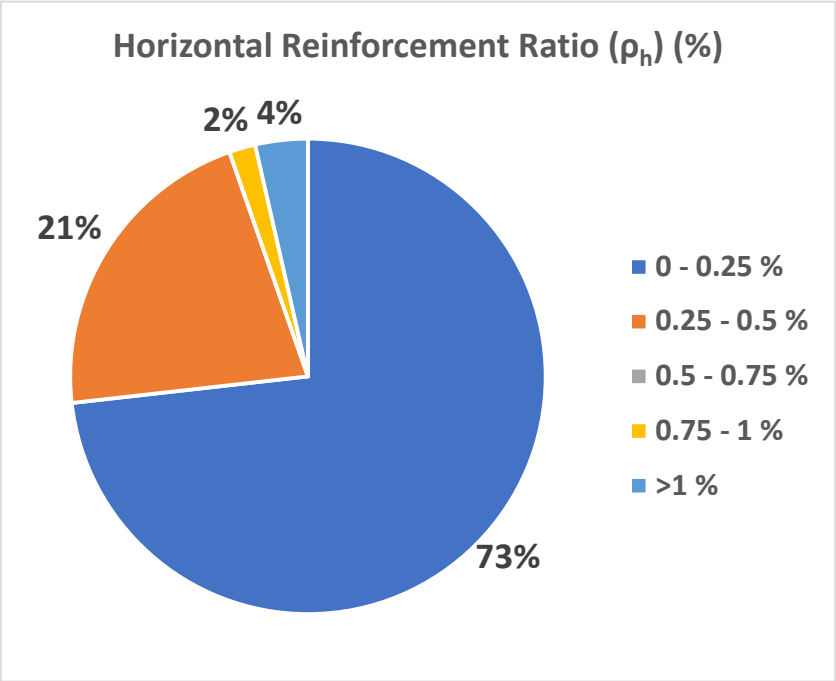

Figure 3.27) Visual representation of the distribution of horizontal reinforcement ratio from the wall specimens considered in the database

3.3.5 Applied Axial Stress

The presence of an applied axial stress, represented in the experiments through a compressive load induced during testing through vertical actuators affects the behaviour of masonry walls in terms of the onset of governing failure modes. High axial stress values are able to improve the lateral in-plane performance, as well as shear strength of the masonry specimens, due to the added compressive forces that work to prevent sliding of the blocks along the mortar joints or at the wall base.

In a similar fashion to what was done for the reinforcement ratio, it is crucial to first establish a basis for the influence that an axial load can have on the behaviour of a test specimen. Out of the specimens gathered from the literature, a variety of levels of applied axial compressive stresses have been considered in the test matrix of the database which will prove useful in providing a more in-depth understanding of how masonry walls perform under these different stress levels. An additional consideration was the axial stress ratio, which was computed by dividing the applied axial stress by the compressive strength of the masonry wall. For specimens with low axial stress ratios, a purely flexural behaviour can be expected from the specimen which

is the reason for a relatively small compression zone depth in comparison to the wall dimensions. Under low levels of axial stress, the masonry wall is more susceptible to sliding and the formation of separation cracks along the mortar joints due to the absence of adequate compressive force to keep the masonry blocks bearing on each other. Therefore, it is expected that the specimens that were tested with moderate axial stress levels should have the greatest ductility performance, which may be attributed to larger levels of lateral drift capacities, in comparison to similar specimens with no overburden axial stress.

From Figure 3.28 below, it is shown that there was a significant amount of variation in the levels of axial stress in the test specimens, with the majority of walls being tested with either no axial stress or an axial stress of less than 1 MPa. These specimens will prove to be advantageous in the database analysis as they will serve as a point of comparison with specimens that were tested with significant axial stress levels and compared in terms of experimental lateral drift capacities.

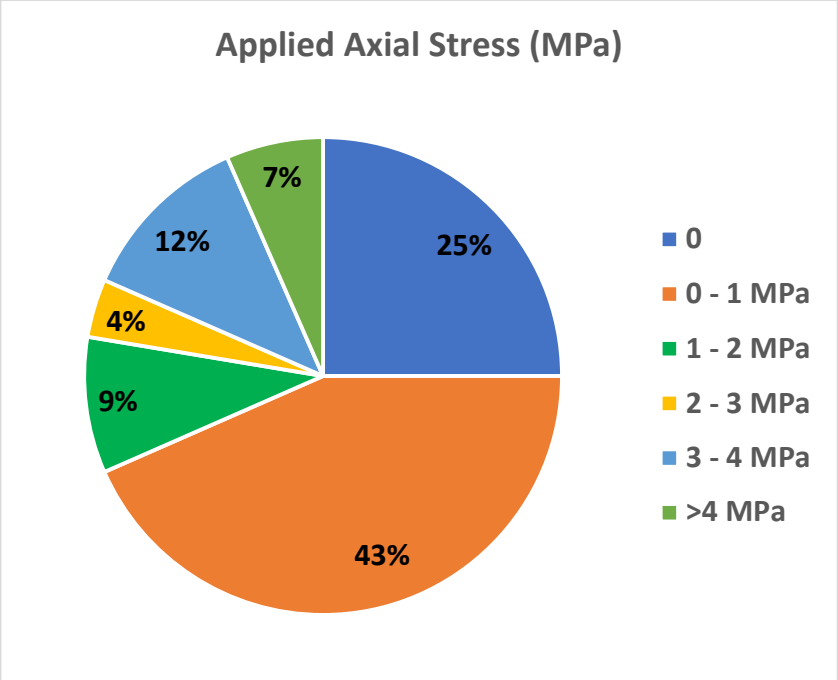

Figure 3.28) Graphical representation of the varying levels of applied axial stress on specimens considered in the database

3.6.6 Boundary Elements

A commonly encountered building technique employed in masonry as well as in reinforced concrete wall construction is the incorporation of structurally connected boundary elements to the end regions of the wall. They are typically thickened sections in comparison to the web dimensions of the wall and are specially reinforced. The inclusion of these elements is a more recent advancement in the field and, as a result, their precise contributions to the seismic performance of reinforced masonry walls has not fully been quantified. Based on current studies however, the inclusion of these elements has been found to provide out-of-plane stability, exhibit enhanced curvature capacity, limit damage to the wall in these regions and allow for an increase in displacement ductility as well as drift capacity. In addition, the contribution that stems from the high reinforcement concentration in these regions promotes an optimal arrangement of flexural cracks and an increase in the height of the plastic hinge region. As a result, boundary elements are commonly employed on structures at risk of seismic activity as the additional ductility allows the specimen to sustain large inelastic deformations with little strength reduction, making them a potential Seismic Force Resisting System (SFRS).

Out of the 70 specimens gathered in the database, a total of 16 specimens were constructed with boundary elements. The design matrix of these elements had a range of geometries such as perpendicular flanges, pilaster units, and two C-shaped or stretcher blocks, and reinforcement details ranging from typical vertical bars in the cells, to specialised 3 mm spiral reinforcement bars. The dimensions of each boundary element as well as details regarding the reinforcement layout were tabulated for each specimen and considered in the data analysis, particularly in the determination of flexural strength and drift capacity since the confinement in the extreme compression zone provided by the transverse reinforcement in the boundary's delays crushing in compression.

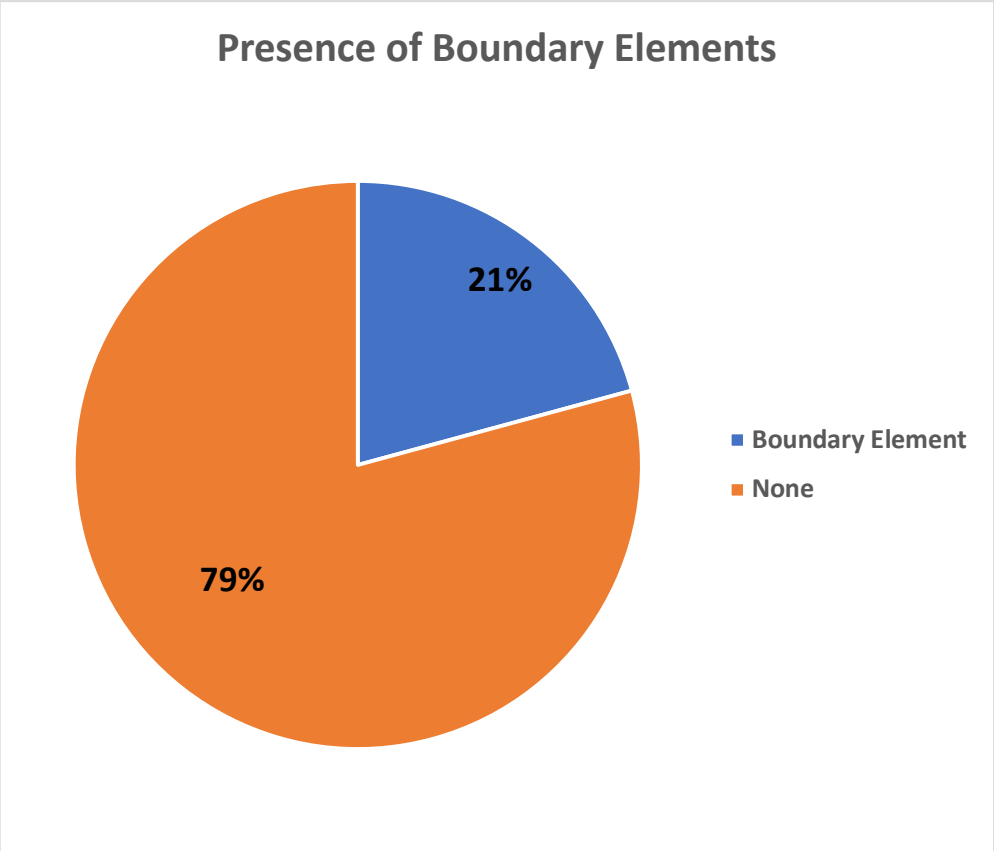

Figure 3.29) Schematic representation of boundary element distribution present within considered specimens of the database

One consideration that needed to be accounted for was the reduction in the size of the compression zone as a result of the change of stress distribution from the presence of these elements. The effective depth was computed as the distance from the extreme tension fibre to the centroid of the tensile reinforcement, which for the majority of specimens, was equal to the midpoint of the boundary element subtracted from the total length of the wall. The depth of the compression zone (c) will be a recurring parameter of interest for this work due to its contribution in the shear strength equations. Furthermore, there are currently irregularities between the masonry components of the shear strength estimation equations. An alternative equation for this contribution has been proposed in the design codes, which has been derived from reinforced concrete beams, equal to $V_m = 0.4 \cdot \sqrt{f'_w} \cdot c \cdot t$, Whether or not this is a realistic assumption to make, or if it overestimates results, will be determined through the application of the database.

3.6.7 Failure Mode

In addition, the reported failure mode of the test specimens was recorded within the database and compared against the theoretically determine failure mode based on shear and flexural strength expressions provided in the Canadian masonry standards (CSA S304-24 and based off of basic structural analysis and first principles. Once the flexural and shear strengths of each specimen were computed through the empirical expressions, it was found that the analytically determined governing mode of failure for a few of the specimens differed from the actual failure mode observed in the experimental testing process. That is, some specimens that were observed in the test to have failed in flexure actually reported a governing shear failure based on the analytical values obtained by the empirical expressions provided in the code (and vice-versa). This discrepancy is shown in the following figure set below, which depicts the percentages of the reported failure modes based on experimental and analytical performances, in which slight deviations in the total percentages of each failure mode can be observed.

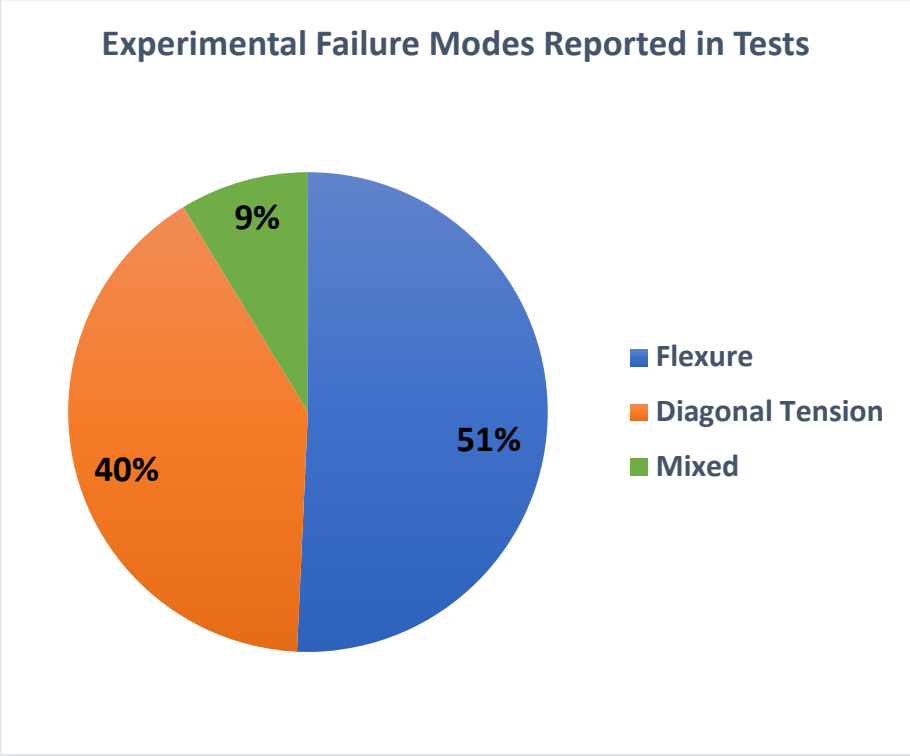

Figure 3.30) Failure mode reported in gathered test papers that was based on observed performance during experimental test

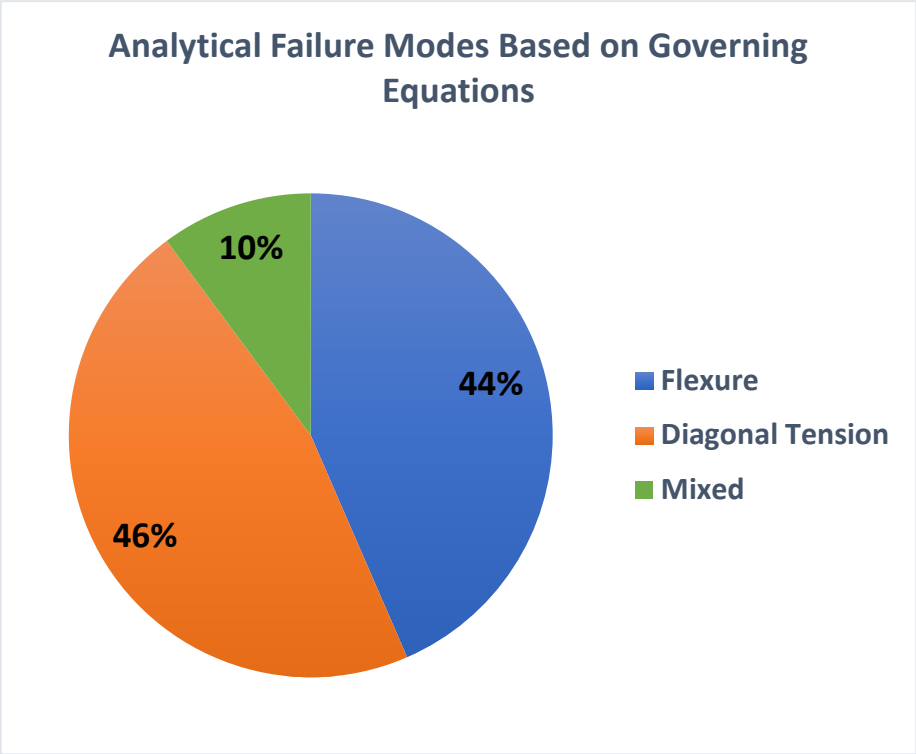

Figure 3.31) Failure mode based on calculated analytical performances based on the governing empirical shear and flexure expressions as per CSA S304-24 provisions

Upon examination of the recorded flexural failures, a total of 35 specimens (51% of the total specimens) reported this mode according to the experimental test data, and only 30 specimens (44% of the specimens) reported this mode of failure as a result of having a flexural strength that was exceeded by its shear strength capacity, implying that a flexural failure was imminent. Similarly, 28 specimens (40% of the test matrix) exhibited a shear failure during the experiment, yet 32 specimens (46% of the test matrix) exhibited a shear failure based on analytical values, which resulted when the governing shear strength was exceeded by the flexural strength of the specimen. For mixed behaviour specimens, there was much less observed deviation between the experimental and analytical results. The discrepancy in mixed failure modes is not as critical as it is for flexural and shear behaviour as a mixed mode is classified by performance that possess no more than 5 percent similarity in values between their analytical flexural and shear strengths calculations. Therefore, data points that switched between flexural/shear to a mixed failure are less severe inconsistencies in failure mode since their behaviour was classified as a mixture of their original failure mode.

3.7 Papers Collected in the Database

3.7.1 Drysdale, R. G, et al. "Characteristics of Rectangular, Flanged, and End-Confined Reinforced Concrete Masonry Shear Walls for Seismic Design." Journal Of Structural Engineering, 2010.

This paper contains results of an experimental study conducted at McMaster University in Ontario, Canada aimed to evaluate energy dissipation characteristics, ductility and stiffness degradation of end-confined walls designed to fail in flexure. The test matrix consisted of seven two- and three-story shear walls with concrete story slabs. The boundary element formation of the walls was as followed:

Phase 1 W1 & Phase 2 W4 - None

Phase 1 W2 & Phase 2 W5 - Flange

Phase 1 W3 & Phase 2 W6 - Two block boundary element

Phase 2 W7 - Pilaster unit (3mm spiral reinforcement)

The lateral load was applied to the walls using a single hydraulic actuator positioned to keep a zero-moment condition at the top of the wall, causing the shear span to be equal to the whole height of the wall. This loading case was quite common throughout the collected papers and will be referred to as the default case 1 type arrangement.

3.7.2 ***Drysdale, R. G., et al. "Behaviour of Partially Grouted Reinforced Masonry Shear Walls-Experimental Study." 11th Canadian Masonry Symposium, 2009***

This experimental study was conducted at McMaster University in Ontario, Canada which aimed to gather information required to evaluate the performance of partially grouted reinforced concrete block shear walls under in-plane loading. A total of five wall specimens were created with half-scale model units of a 20 cm hollow concrete block and had closely comparable ultimate load carrying capacities of those predicted from the Canadian masonry standard. The main emphasis of the tests was to examine the impact the spacing of reinforcement and aspect ratio have on the behaviour of the walls. The test setup followed the default case 1 of a single horizontal actuator at the top of the wall which ensured no moment at the top of the wall. Loading cycles were completed twice and continued until the specimens had all degraded to over 50% of the ultimate strength so as to obtain adequate post-peak information. The test results concluded with a shear dominated failure for the first four specimens (with aspect ratio less than 1) and a mixed shear-flexure failure for the fifth specimen. (having a larger aspect ratio of 1.5). This experimental

investigation concluded that the behaviour of the wall specimens was not sensitive to changes in the reinforcement pattern, but it was sensitive to changes in the aspect ratio of the walls.

3.7.3 Shedid, Marwan T, et al. "Behaviour of Fully Grouted Reinforced Masonry Shear Walls Failing in Flexure: Analysis." Engineering Structures, 9 Mar. 2009.

The following experimental program was carried out by the civil engineering department at McMaster University in Ontario, Canada, which contained tests conducted on six partially grouted, half scale reinforced concrete masonry shear walls focused on evaluating the ductility and energy dissipation characteristics of flexure walls. The main focus of the research endeavour was to record the ductility levels of the walls and evaluate the impact that flexure and shear deformations have on the total lateral displacement of the wall. The test setup of the experiments followed the default first case of a single horizontal actuator at the top of the wall which ensured no moments were induced and the shear span remained the total height of the wall. All six of the tested specimens were loaded until 50% degradation of maximum capacity and experienced a flexural mode failure.

3.7.4 Galal, Khled, et al. "Effect of reinforcement anchorage end detail and spacing on seismic performance of masonry shear wall." Department of Building, Civil and Environmental, Concordia University, 22 Dec. 2017.

The specimens collected from this paper were constructed and tested by the Department of Building, Civil and Environmental Engineering at Concordia University in Quebec, Canada. The paper investigated the in-plane seismic performance of fully grouted reinforced masonry shear walls dominated by shear-flexure failure through the assessment of five single-story full-scale walls subjected to in-plane axial compressive stresses and cyclic lateral excitations. The parameters of interest from the specimens were the spacing of vertical and horizontal reinforcement as well as the end detailing of the horizontal reinforcement. Three unique end details were evaluated, these being: straight, 180-degree standard hook and 90-degree hook. The walls were tested through a case 2 configuration which consisted of two vertical actuators which applied the axial compressive forces and one horizontal actuator at the top of the wall to introduce the representative seismic displacements. The specimens all experienced a shear-flexural failure and the test concluded that each of the different reinforcement end details had different levels of efficiency. The 180-degree standard hook was found to have comparable strength to the 90-degree

hook, however was more ductile. Both specimens outperformed the specimen constructed with straight horizontal bars in terms of both strength and displacement ductility.

3.7.5 El-Dakhakhni, Wael, et al. "Seismic Performance Parameter Quantification of Shear-Critical Reinforced Concrete Masonry Squat Walls." Journal of Structural Engineering, ASCE, June 2013.

This paper contains a study performed at McMaster University in Ontario, Canada that investigated eight squat reinforced masonry walls under quasi-static reversed cyclic loading to quantify shear strength capacities, drift-damage relationships and lateral stiffness degradation. The fully grouted wall specimens were constructed at full scale and were detailed with parameters representative to those commonly encountered in low-rise reinforced masonry structures. Specimens were specifically designed with high flexural reinforcement ratios to ensure shear mechanism developments before any yielding of the flexural reinforcement so any ductility in the specimen can be directly related to a shear mechanism. The walls were tested under reversed quasi-static displacement-controlled loading through the use of a single actuator placed in a case 1 arrangement and experienced shear failure. Despite being designed with the intent of experiencing shear failure with a flexural plastic hinge mechanism, the specimens all demonstrated a ductile behaviour. The development of shear ductility is favoured in reality for low-rise reinforced masonry squat walls as an alternative way to dissipate earthquake energy instead of plastic hinge mechanisms.

3.7.6 Rizaee, Samira et al. "The effect of the amount, distribution, and end anchorage conditions of bond beam reinforcement on the behaviour of concrete masonry shear walls." Canadian Science Publishing, November 2020.

The Schulich School of Engineering in Alberta, Canada investigated the behaviour of partially grouted concrete masonry shear walls with fixed boundary conditions through the testing of seven groups of two shear walls (resulting in a total of fourteen tested wall specimens). Combinations of three horizontal reinforcement ratios (0.12%, 0.06% and 0.03%) and four end anchorage conditions (straight, 90 degrees, 180 degrees and shear studs) were used. Specimens had an aspect ratio of 1.0 which was chosen in order to anticipate diagonal shear failures for the specimens. The experiments utilised a case 2 test arrangement, however, the vertical actuators were not able to apply the tensile forces required to maintain the mid height zero moment condition

for large horizontal push loads so the location of zero moment was changed to 415mm below the top of the wall for some specimens.

3.7.7 Khaled, Galal et al. "Effect of shear span to depth ratio on seismic performance of reinforced masonry shear walls." Resilient Infrastructure, June 1-4 2016.

This paper presents a Canadian study carried out in Concordia University to investigate the impact of shear span to depth ratio (M/Vdv) on seismic performance through testing of two full-scale, fully grouted rectangular reinforced masonry shear walls governed by diagonal shear failure. The test specimens were identical in design with an aspect ratio of 0.89 and containing both vertical and horizontal reinforcements, however, one of the specimens was subjected to a top moment in order to increase the shear span to depth ratio as well as the overall height-to-length ratio of the specimen so a comparison could be made. The test setup used was that of case two, having one horizontal actuator to apply the in-plane cyclic excitations, and two vertical actuators to apply the axial compressive stress (equal to 1.0 MPa) and a top moment on one of the specimens (equal to 0.9V, where V is the lateral load from the horizontal actuator).

3.7.8 Banting et al. "Seismic performance quantification of reinforced masonry structural walls with boundary elements". Department of Civil Engineering, June 6 2014

In this paper, data regarding tests conducted on five half-scale walls with boundary elements was collected for the database. The walls were tested with a constant applied compressive stress of 0.89 MPa across all specimens. Walls were tested and loaded through a case 1 actuator arrangement. For all the specimens, the dominant form of behaviour was flexure, however, it was noted that some specimens exhibited larger shear deformations as a result of differing lengths of wall and boundary elements.

3.8.9 Albutainy, Mohammed, et al. "Experimental investigation of reinforced concrete masonry shear walls with C-shaped masonry units boundary elements." Structures, September 20 2021

This paper presents research conducted at Concordia University in Quebec, Canada that aimed to quantify the effect of influential parameters on the seismic performance of reinforced masonry walls with boundary elements. Two half-scale specimens were designed to experience flexural failure and were tested under a reverse cyclic top moment as well as lateral loading. A case 2 loading setup was required for the experiments as the vertical actuators were essential in creating the top moment, which was designed to specifically mimic the loading conditions on the plastic hinge zone of a 12-story tall masonry structure. The results of the study provided insight

on the applicability of C-shaped masonry boundary elements to improve strength and ductility of lateral force resisting systems.

3.7.10 "Seif EIDin, Hany; Galal, Khaled. "In-Plane Seismic Performance of Fully Grouted Reinforced Masonry Shear Walls." Journal of Structural Engineering, November 18 2016."

This paper, presented by researchers at Concordia University in Quebec, Canada, investigates the performance of fully grouted reinforced masonry shear walls designed for shear failure. Experiments were carried out to assess the response of four single-story walls under in-plane axial compressive stresses as well as lateral excitations and a top moment. A case 2 actuator was utilised for the experiment as vertical actuators were required to instil the top moment and compressive forces. All of the tested specimens exhibited a shear failure.

3.7.11 Aly, Nader, et al. "Experimental Investigation of Axial Load and Detailing Effects on the Inelastic Response of Reinforced-Concrete Masonry Structural Walls with Boundary Elements." Journal of Structural Engineering. June 24 2020

This paper, published by the department of Building, Civil and Environmental engineering at Concordia University in Quebec, Canada contains test data for three half-scale fully grouted reinforced masonry shear walls with boundary elements which were tested to determine if end zone detailing and confinement is able to reduce the impact of high axial loads. The walls were designed to meet the requirements of the CSA S304, the design standard for masonry structures in Canada, but also satisfied the American TMS 402/602 building code requirements. Walls were designed for flexural failure by ensuring the shear capacity was greater than the demand corresponding to the plastic hinge formation at the base of the wall. The specimens were tested through a case 2 arrangement as vertical actuators were required, in addition to the horizontal actuators, to apply a top moment and axial compressive load. The obtained results showed an increase in structural performance and ductile flexural failure of the specimens.

3.7.12 Brook, Robazza, et al. "A Study on the out-of-plane Stability of Ductile Reinforced Masonry Shear Walls Subjected to in-plane reversed Cyclic Loading." 12th North American Masonry Conference. May 17-20 2015

This study, published in the North American Masonry Conference but conducted by researchers in the University of British Columbia, presents results of five full-scale reinforced masonry shear walls with varying height-to-length ratios, amount and layout of reinforcement and test setups. The walls were tested through the use of a custom-built setup which incorporated either

one horizontal actuator and/or the inclusion of an additional two vertically inclined actuators. The first specimen included these additional actuators as a means to induce axial pre-compression and an overturning moment. All of the tested specimens exhibited a flexural response which was evident in the severe cracking that occurred in the horizontal bed joints.

3.7.13 Banting, Bennett, et al. "Force- and Displacement-Based Seismic Performance Parameters for Reinforced Masonry Structural Walls with Boundary Elements" Journal of Performance of Constructed Facilities. December 1 2012

This paper contains test results of four reinforced masonry wall specimens conducted at McMaster University in Ontario, Canada. The specimens were constructed with identical dimensions, however, varied in the presence of boundary elements and inter-story slabs, as well as axial load. Specimens were tested through a case 1 loading configuration which consisted of a single horizontal actuator located at the top of the wall. All of the tested specimens exhibited a flexural failure.

3.7.14 Siyam, A. Mustafa, et al. "Seismic Response Evaluation of Ductile Reinforced Concrete Block Structural Walls: Experimental Results and Force-Based Design Parameters" Journal of Performance of Constructed Facilities. December 29 2015

This paper, conducted by researchers at McMaster University in Ontario, Canada, presents results of six one-third scale, fully grouted reinforced concrete block masonry walls with different wall details in addition to the presence of inter-story slabs. The objective of the study was to observe and quantify the wall slab coupling effects. Specimens were tested through a case 1 configuration which utilises the use of a solo horizontal actuator at the top of the wall. The walls were designed to exhibit a ductile behaviour during loading and fail in a flexural manner, however, the varying cross-sectional configurations resulted in crack patterns representative of shear-flexural failure in two of the specimens.

Chapter 4

Analysis of the Wall Database:

Strength Estimates of RM Wall Specimens

4.0 Introduction

The analysis of reinforced masonry structures can be a quite cumbersome procedure on account of the complex geometry and interactions between the materials that make up the composite wall unit. This chapter delves into a detailed analysis of the flexural and shear strength estimates of the wall specimens contained in the experimental database assembled in Chapter 3. This chapter aims to present the procedures and findings of an analysis between design parameters and experimental performance, as well as a comparison between experimental and analytical values obtained through the database. Through the evaluation of the validity of the current framework procedures the seismic assessment framework for existing reinforced masonry structures will be vetted whereas points for improvement will be identified.

4.1 Analytical Calculations

It is well-established that the Canadian and US Masonry standards contain several differences in key parameters such as the estimation of the modulus of elasticity of masonry (E_m) and the definition of stiffness for deflection estimations. In addition, the existing masonry structures present critical differences in terms of standard construction practices, environmental considerations, and most importantly, varying seismic risk. Analytical expressions provided in the Canadian masonry design standard provisions (CSA-S304 24) were programmed within the database and used to determine the governing shear and flexural strengths of the walls, for comparison of these values with the experimentally recorded counterparts.

Calculation of the flexural and shear strength terms of the specimens is the starting point in the assessment exercise. Depending on the relative magnitude of the two strength values the governing mode of failure and anticipated ductility is defined, at least qualitatively. Flexural strength was calculated using first principles as per NIST (2017) assumptions, which assume that plane sections remain plane, thereby considering compatibility of deformations and pertinent constitutive reactions for the uniaxial stress strain response of masonry and the steel reinforcement. This analytical estimate of flexural strength was then compared to the peak experimental moment which was determined through the product of the peak experimental load multiplied by the height of the wall. ($M_u = Q_{Peak} * h_e$)

Shear strength was computed following the Canadian CSA S304 standard. In addition, attention was placed on the standard expressions of the NIST and ASCE Guidelines for comparison of analytical values between the code equations.

4.1.1 Flexural Strength Calculations

4.1.1.1 First Principles Flexural Moment

Following the calculation of the flexural moment based on first principles (M_{1R}) computed through Equation 2.14, these values were compared to the maximum moment that developed on the specimen during the experimental testing. Plots shown in Figures 4.1 and 4.2 compare the analytical (abscissa) and the experimental estimates (ordinate) where the difference is in the colour of the data points. In these plots, colour is used an indicator of the prevalent mode of failure, where blue denotes a flexural failure, red shear and green for a mixed shear-flexure failure. Therefore, when observing Figure 4.1 below, the points correspond to the experimentally reported mode of failure, whereas in Figure 4.2 they correspond to the mode that has been estimated based on the governing analytical expressions presented in Equation 2.17.

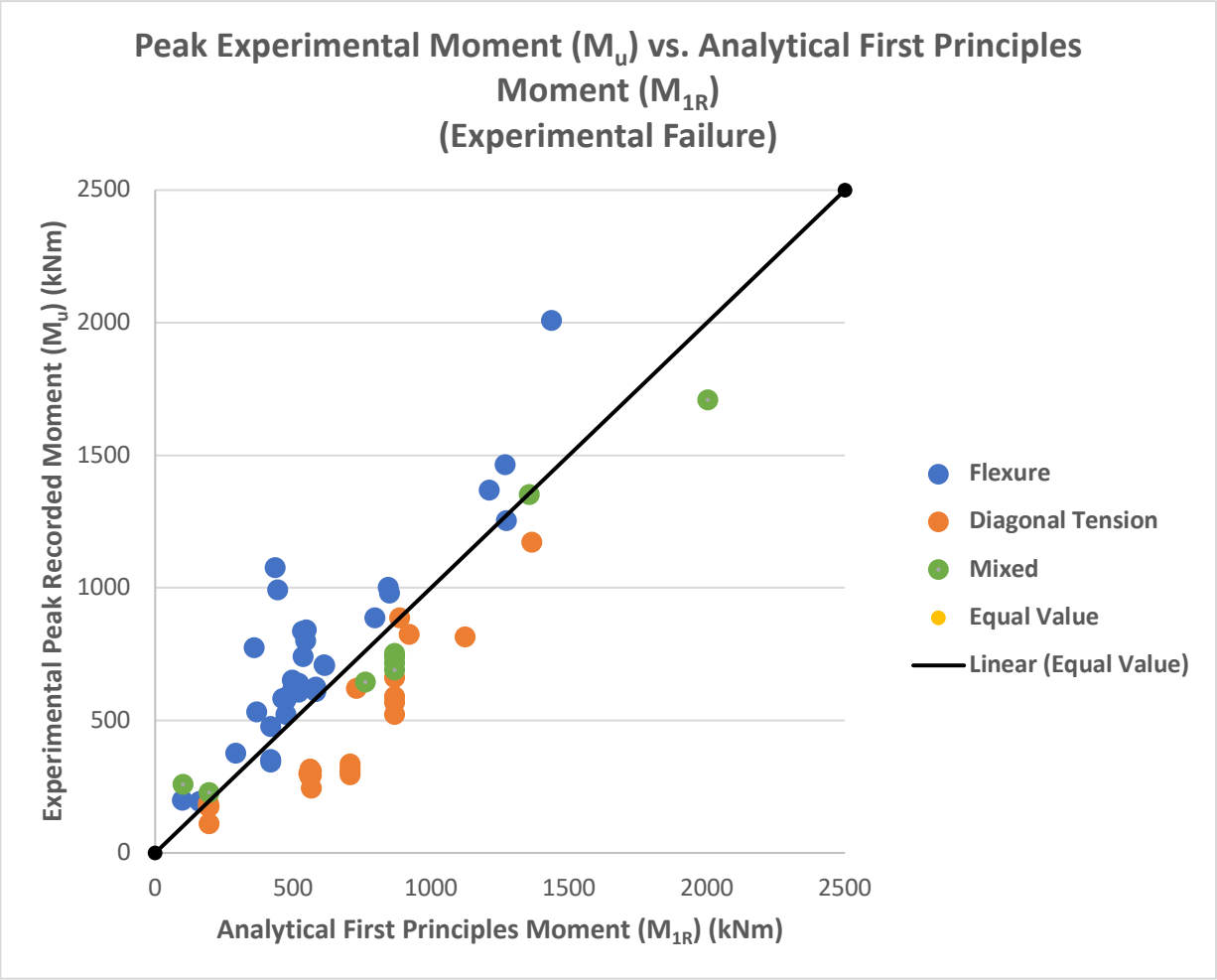

Figure 4.1) Comparison of first principles analytically derived flexural moment (M_{1R}) and experimentally recorded maximum moment (M_u), where failure modes have been classified based on experimental reporting

Observations from Figure 4.1 depicts a fairly good convergence between the estimates obtained from first principles equations and the experimental flexural moments since the blue points identifying flexural failure are clustered along the equal value line. It is important to note that the first principles equation tends to underestimate the moment for flexure-dominated specimens based on the experimental failure mode classification for the most part – but specimens in the low strength range were, in fact, overestimated (see points in the red ellipse). In contrast, shear-dominated specimens follow an opposite trend as all points tend to lie under the equal value line, indicating correctly that flexural mode of behaviour was stronger than the shear resistance, consistent with the experimental evidence.

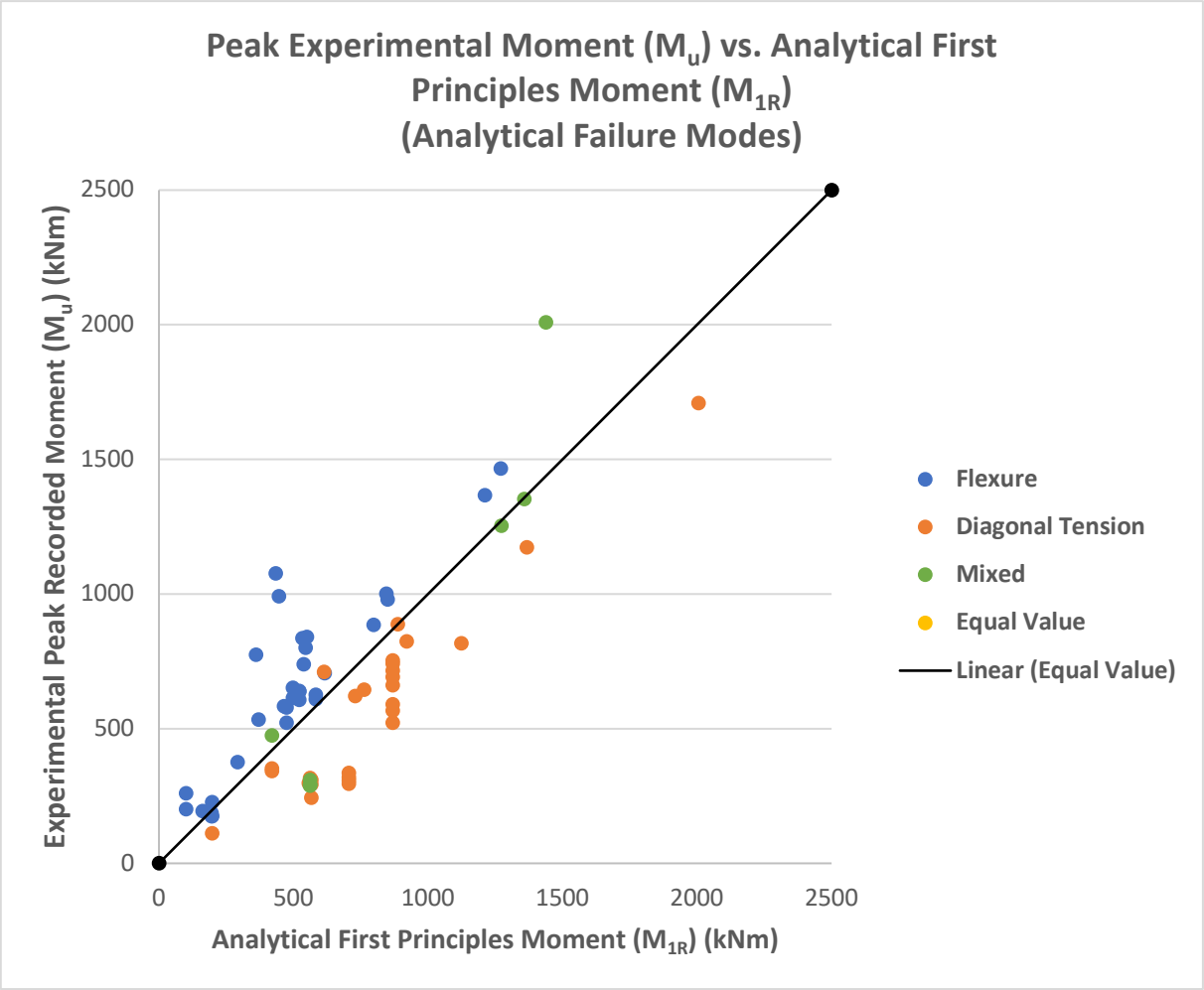

Figure 4.2) Comparison of first principles analytically derived flexural moment (M_{1R}) and experimentally recorded maximum moment (M_u), where failure modes have been classified based on analytical calculations

The results are similar when the failure mode is estimated analytical, which confirms that flexural strength estimations are dependable, and no apparent modification to the estimating expressions (2.13) are necessary. Outliers are the specimens with very high flexural strengths, which were shear-dominated specimens that were built and tested in the research conducted by El-Dakhakhni (2011). These walls were the larger size specimens in the database, with a height and length value of 3 m (aspect ratio of 1.0), and were tested without the presence of an applied axial load. A total of eight specimens that were tested in this study under quasi-static reversed cyclic loading to precisely quantify their shear strength and displacement ductility. The tested specimens were constructed with a range of values encompassing the typical low-rise reinforced masonry details such as the reinforcement ratio and aspect ratio. What did differ between the specimens

was the axial stress applied to the specimens during testing, where some specimens were tested without the presence of any axial load at all. In addition, the walls were specially detailed with additional flexural reinforcement ratios to ensure the walls failed due to shear well before any flexural reinforcement could occur, which was indeed the case of what occurred during the experimental testing. This agreed with the analytical values computed through equations (2.1, 2.6 and 2.7), which yielded an analytical shear failure to govern the response as well. Figure 4.3 below outlines the location of the reference specimen, Wall W-1, and the highest performing specimen, Wall W-8.

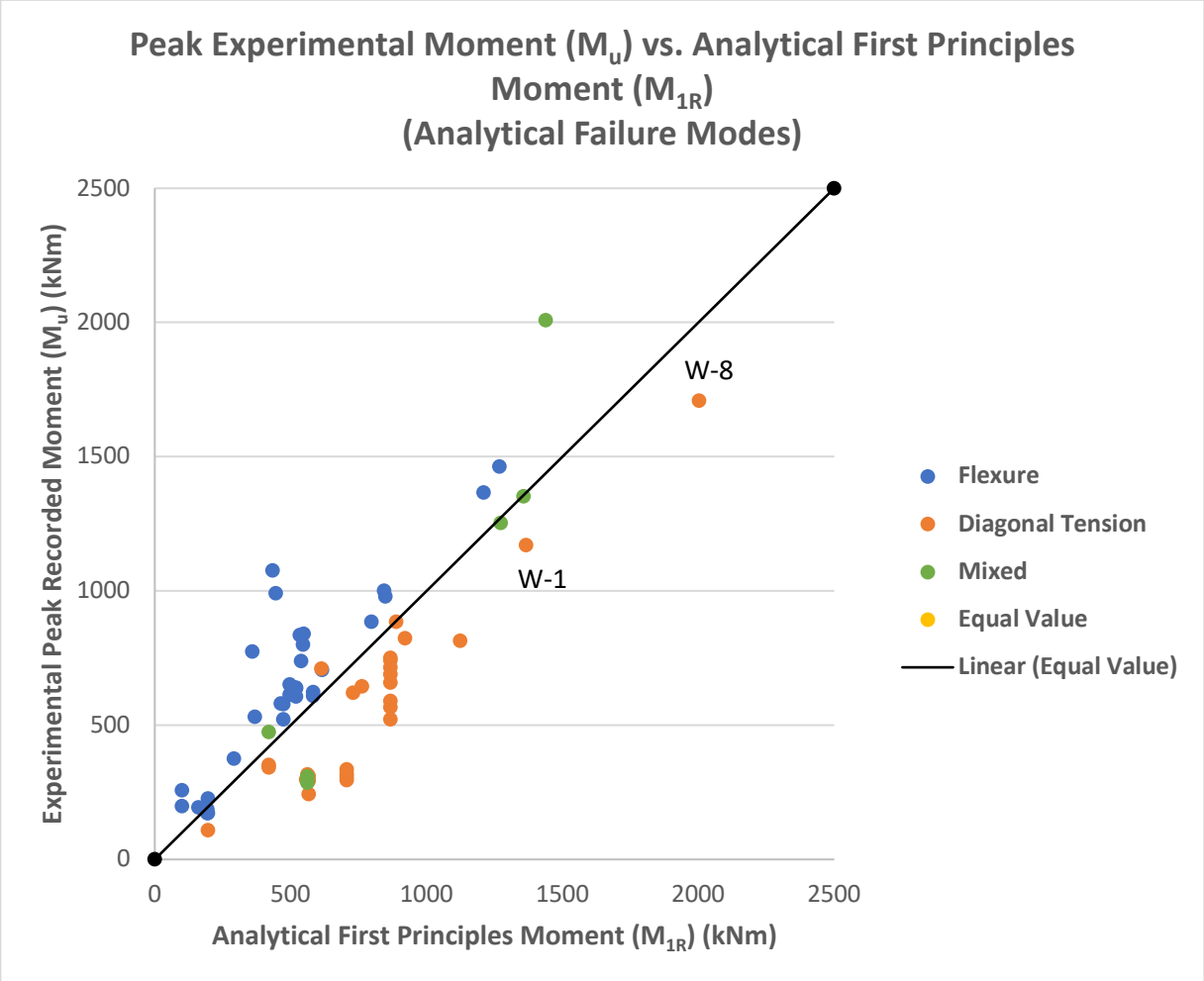

Figure 4.3) Comparison of first principles analytically derived flexural moment (M_{1R}) and experimentally recorded maximum moment (M_u) with data from El-Dakhakhni (2011) highlighted

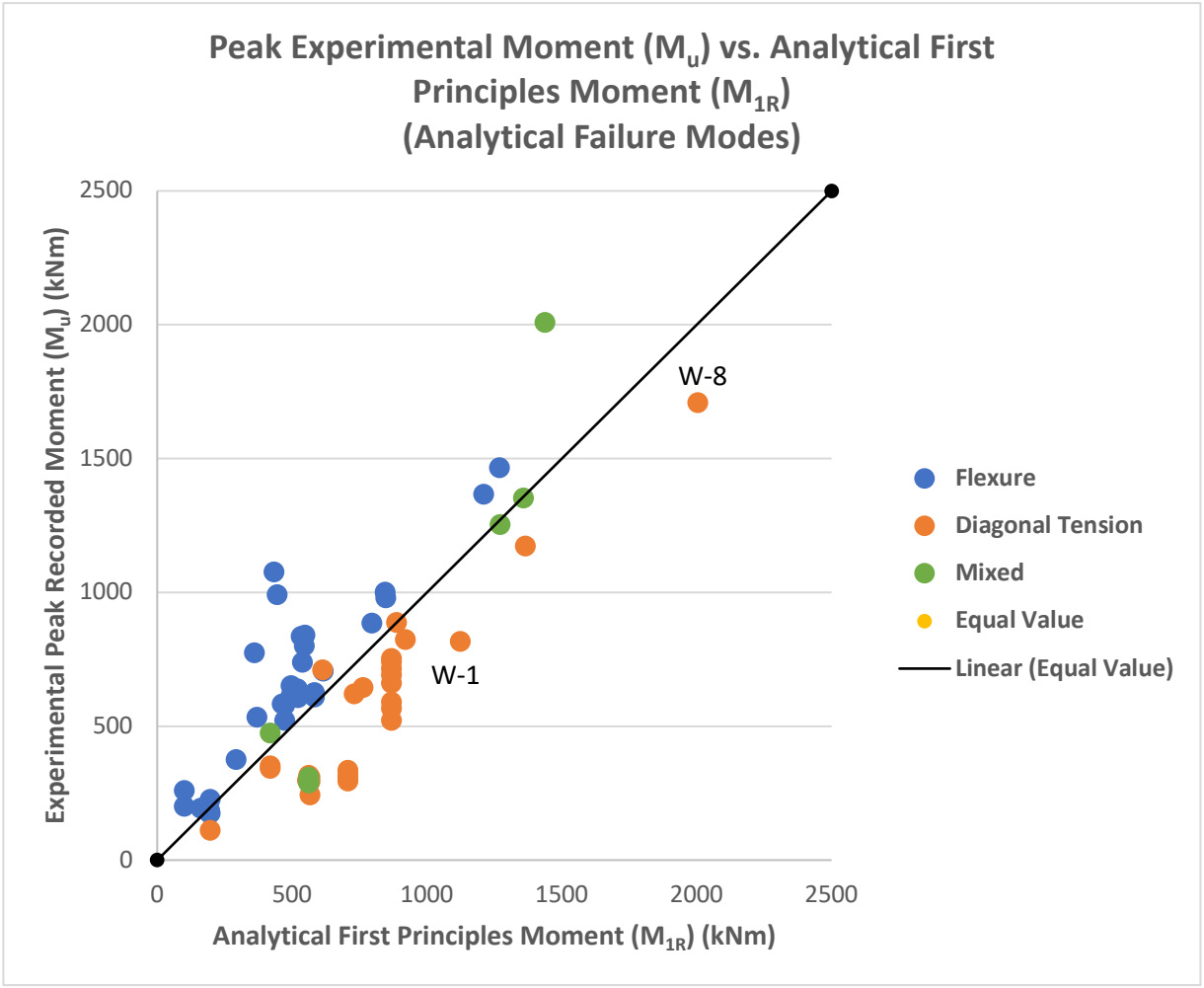

Figure 4.4) Comparison of first principles analytically derived flexural moment (M1R) and experimentally recorded maximum moment (Mu) with data from El-Dakhakhni (2011) labelled

Table 4.1 below depicts the design details of each wall specimen where it can be observed that the only differences between these two specimens were (a) the applied axial pressure of 1.0 MPa on W-1, whereas no axial load was acting on W-8; and (b) the lower specified masonry compressive strength of W-8. Despite having identical design and reinforcement details, as well as a lower material compressive strength, wall W-8 managed to outperform W-1 and achieved a higher strength corresponding to a peak load of 548 kN and a maximum moment of 1710 kNm. On the contrary, W-1 only managed to resist a peak load of 408 kN and 816 kNm, less than 50 percent of the capacity of W-8. The exact reason for such a disparity between results was observed for two walls built with nearly identical design details, yet the specimen that was built with a lower masonry strength and without any axial load was able to demonstrate twice as large of a moment capacity is a unique consideration to be made.

Parameter	W-1	W-8
f'_w	15.4 MPa	12.7 MPa
L_w	2.0 m	3.0 m
H_e	2.0 m	3.0 m
Aspect Ratio	1.0	1.0
$A_{vertical}$	300 mm^2	300 mm^2
$S_{vertical}$	800 mm^2	800 mm^2
ρ_v	0.79 %	0.79 %
$A_{horizontal}$	100 mm^2	100 mm^2
$S_{horizontal}$	800 mm^2	800 mm^2
ρ_h	0.079 %	0.070 %
Axial Stress	1.0 MPa	0
Q_{Peak}	408 kN	570 kN
M_{max}	816 kNm	1710 kNm

Table 4.1) Comparison of design parameters and peak load between wall specimens W-1 and W-8

4.1.1.2 NIST Definition of Flexural Strength

Additionally, the flexural strength of the wall specimens was computed through the programming of the NIST provisions into the database in which the maximum moment could be obtained for every specimen based on the relationship between the axial compression ratio ($\beta = \frac{P}{f'_w \cdot A_n}$) and the available reinforcement index ($\alpha = \frac{f_y}{f'_w} \cdot \rho_v$) in accordance with the figure below. The chart given in the provisions was programmed into the database so that the flexural strength could be computed for every specimen for a wide range of these coefficients, allowing for a comprehensive analysis of this approach. Trendline equations were computed for each reinforcement index corresponding to the nondimensionalized flexural strength, which have been presented in Table 4.2 and on Figure 4.4 below, to allow for a more detailed analysis of values in between and beyond the limited provided values.

Reinforcement Index (α)	Trendline Equation
α = 1 %	y = 0.267β + 0.0909
α = 5 %	y = 0.3β + 0.07
α = 10 %	y = 0.323β + 0.0497
α = 15 %	y = 0.335β + 0.0305
α = 20 %	y = 0.4β + 0.005

Table 4.2) Trendline equations of the NIST Charts defining the non-dimensionalized flexural strength relationships as a function of the axial compression ratio (β) for different ranges of reinforcement index (a)

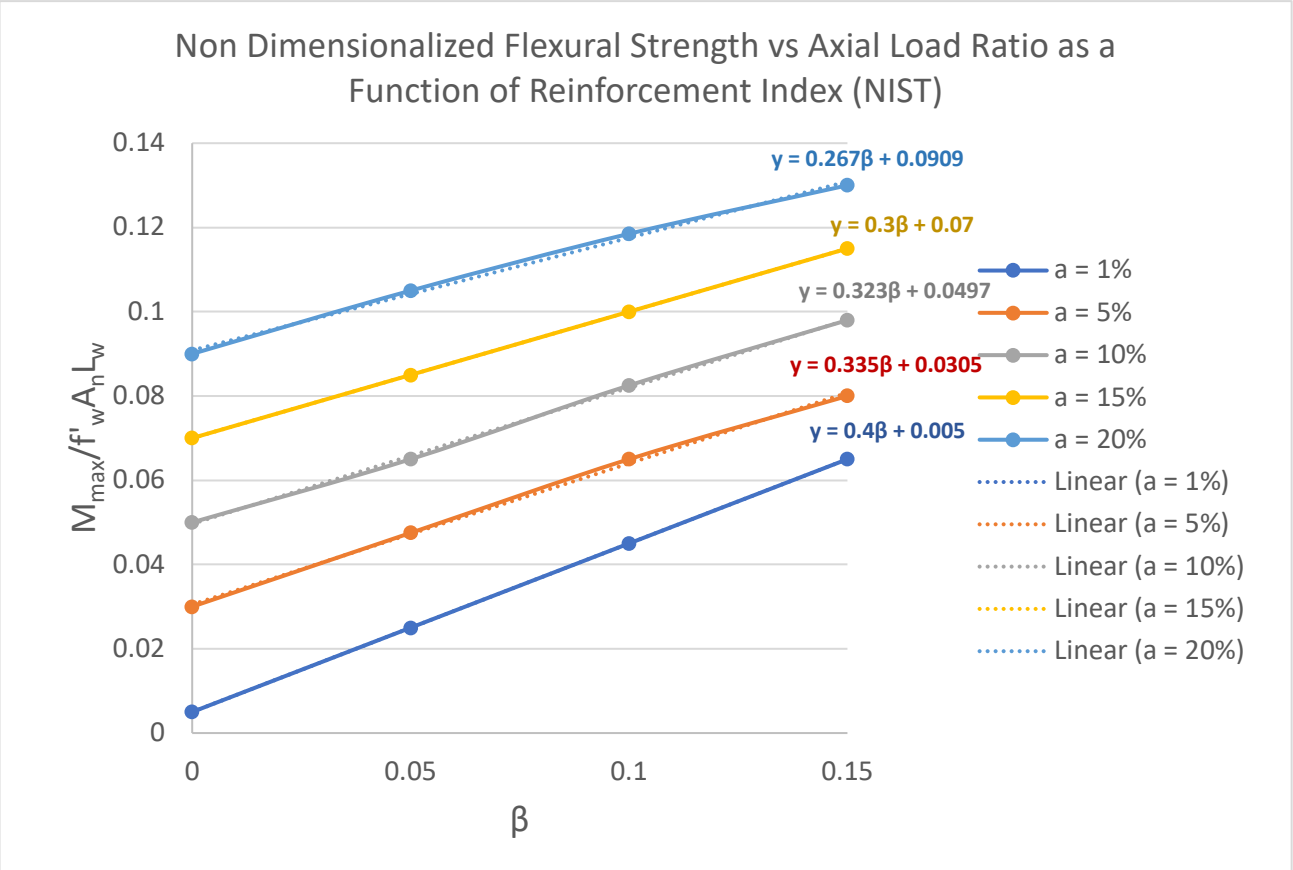

Figure 4.5) NIST standard values for the non-dimensionalized flexural strength of a reinforced masonry specimen plotted against the axial compression ratio ($\beta = \frac{P}{f'_w \cdot A_n}$) and the available reinforcement index ($a = \frac{f_y}{f'_w} \cdot \rho_v$) with trendline equations displayed

Once values for the nondimensionalized maximum moment $M_{max}/(f'_w \cdot A_n \cdot L_w)$ were calculated for each specimen, they were then divided by the aspect ratio in order to obtain the peak flexural load (Q_{flex}) of the specimen which should have close convergence to the peak experimental load if the NIST is predicting the response correctly.

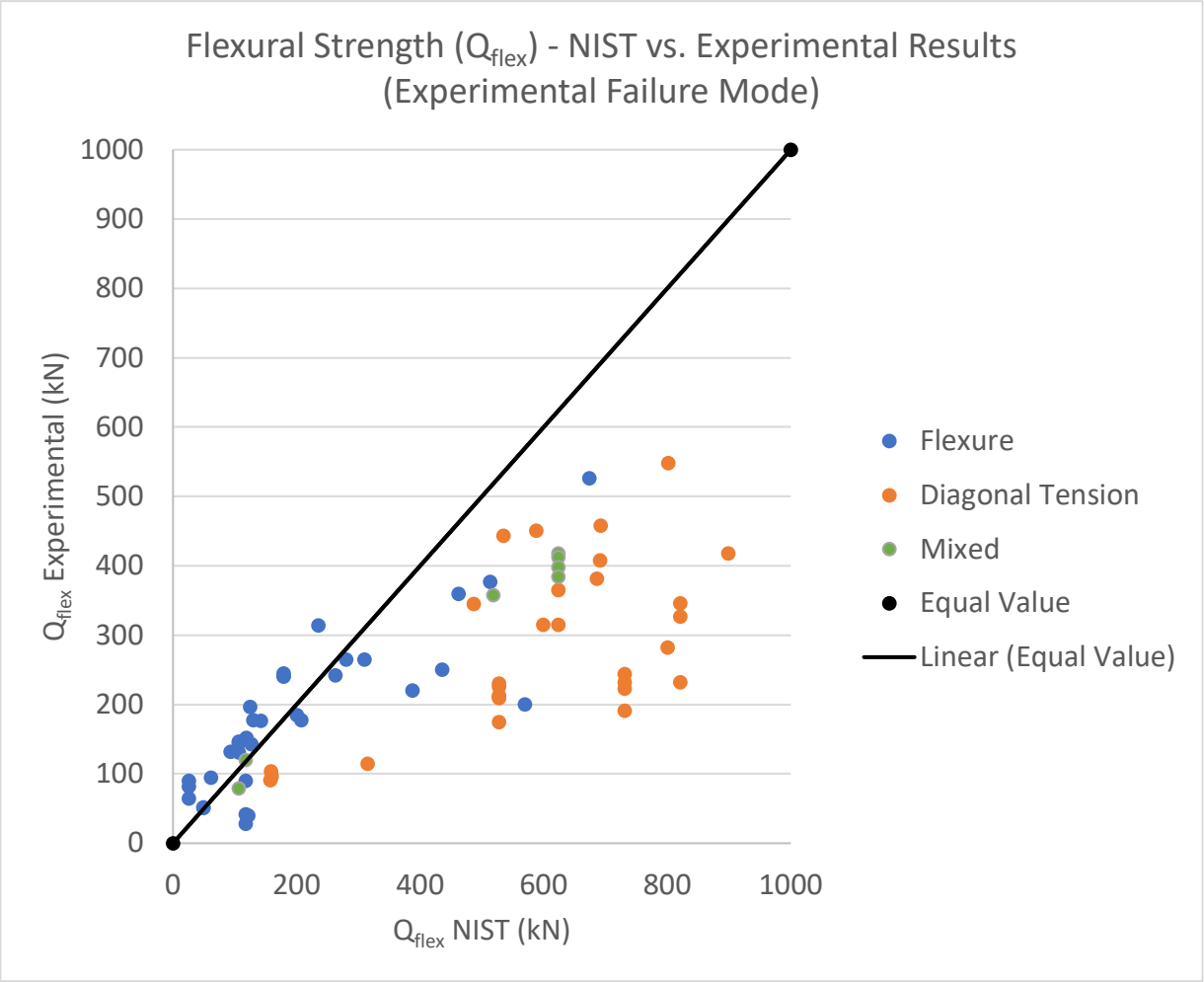

Figure 4.6) Peak lateral strength according to analytical NIST flexural strength calculations vs experimentally recorded values, with data points classified on failure mode based on experimental reporting

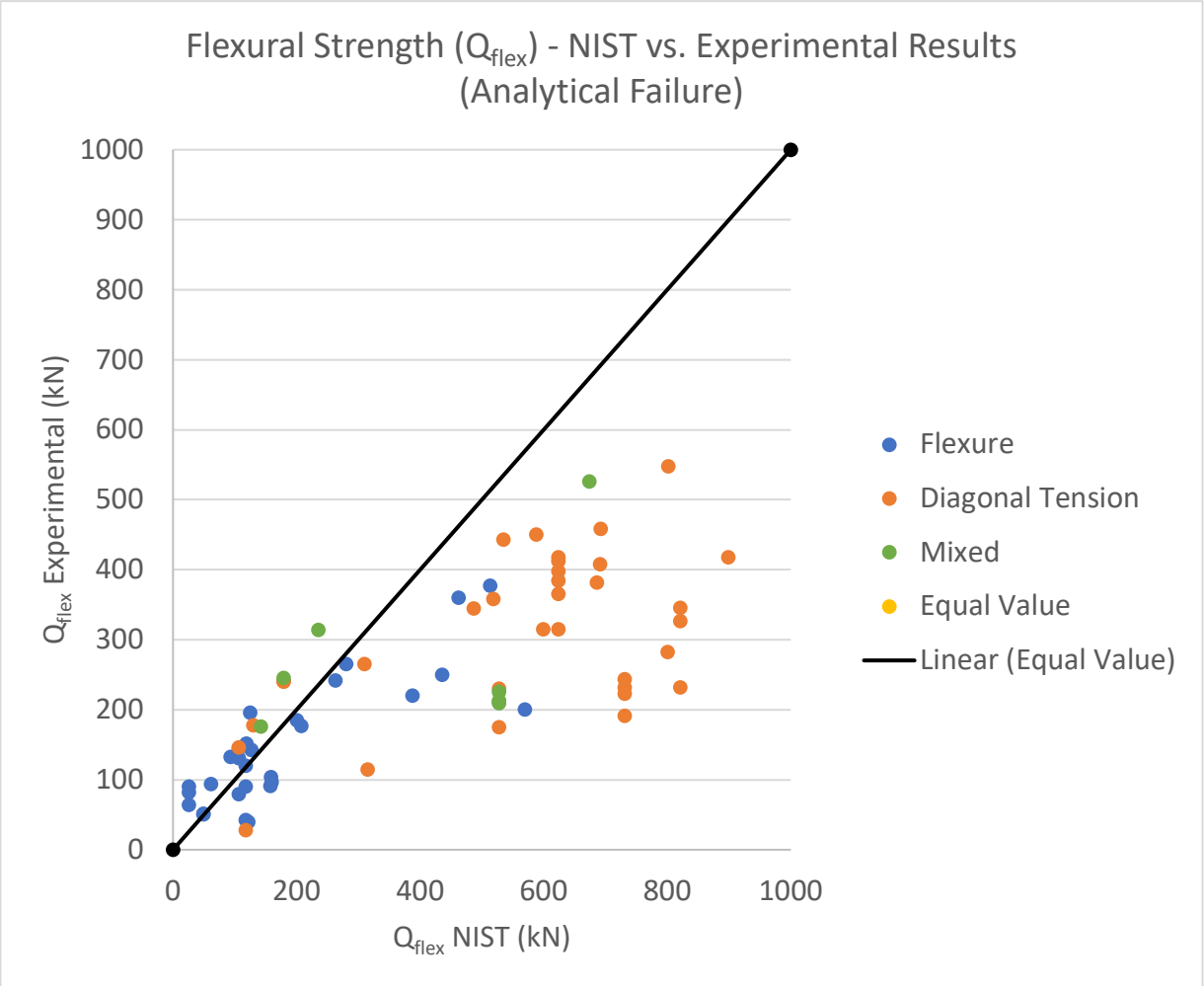

Figure 4.7) Peak lateral strength according to analytical NIST flexural strength calculations and experimentally recorded values, with data points classified on failure type based on the calculated governing analytical values

When comparing the set of figures shown above, a slight discrepancy in data point classification between the two plots is observed, illustrating the deviations in what failure mode the specimens were designed to fail in and what failure mode the Canadian analytical expressions have predicted to occur. It is important to note that although the discrepancies between the values of the reported failure mode and the analytically governing failure were quite small in some cases, it is still crucial to understand the reasoning behind the occurrence of these discrepancies. Additionally, it is seen that many of the flexural data points fail to follow close convergence with the 45-degree equal value trendline, and instead, tend to lie in the area underneath together with the shear-dominated specimens (which are expected to lie below the equal value line since they are not controlled by a flexure). For the flexural failures that fall below the equal value line, the

analytical estimates obtained from the NIST approach are unconservative. To further explore the results the strength of shear dominated specimens need be obtained from the governing shear strength equations. These were also programmed into the database as detailed below.

4.1.2 Shear Strength Calculations

The shear strength of a reinforced masonry specimen is governed by three main failure modes, these being sliding failure, the upper limit force established by the code which is believed to be a lower bound estimate of compressive crushing failure and the diagonal tension failure which is the mode based on which transverse reinforcement is designed for. Each of these failure modes are possible to occur in a given reinforced masonry wall specimen, however, the structural design details of the specimen will influence which failure mode will prevail. In theory, the failure mode that has been most under designed for, will govern the performance of the specimen. To facilitate this in the database, all three of these failure modes have been computed through extension of the analytical expressions for specimens considered in the database and the lowest value between them was taken as the governing mode of shear failure for the specimen according to Equation (2.17).

4.1.2.1 Experimental vs. Analytical Shear Strengths

During the evaluation of shear strength on the considered wall specimens in the database, an evaluation of the experimentally recorded peak strengths and those derived from the Canadian design equations (CSA S304-24) was essential for the evaluation of the empirical relationships prescribed in the code. Using the equations relating on the shear resistance of the specimens based on failure due to sliding and diagonal tension shear (Equations 2.1 and 2.7 respectively), these values were plotted against the peak strength values that were recorded during the experimental tests of walls that failed due to shear in Figure 4.8 below.

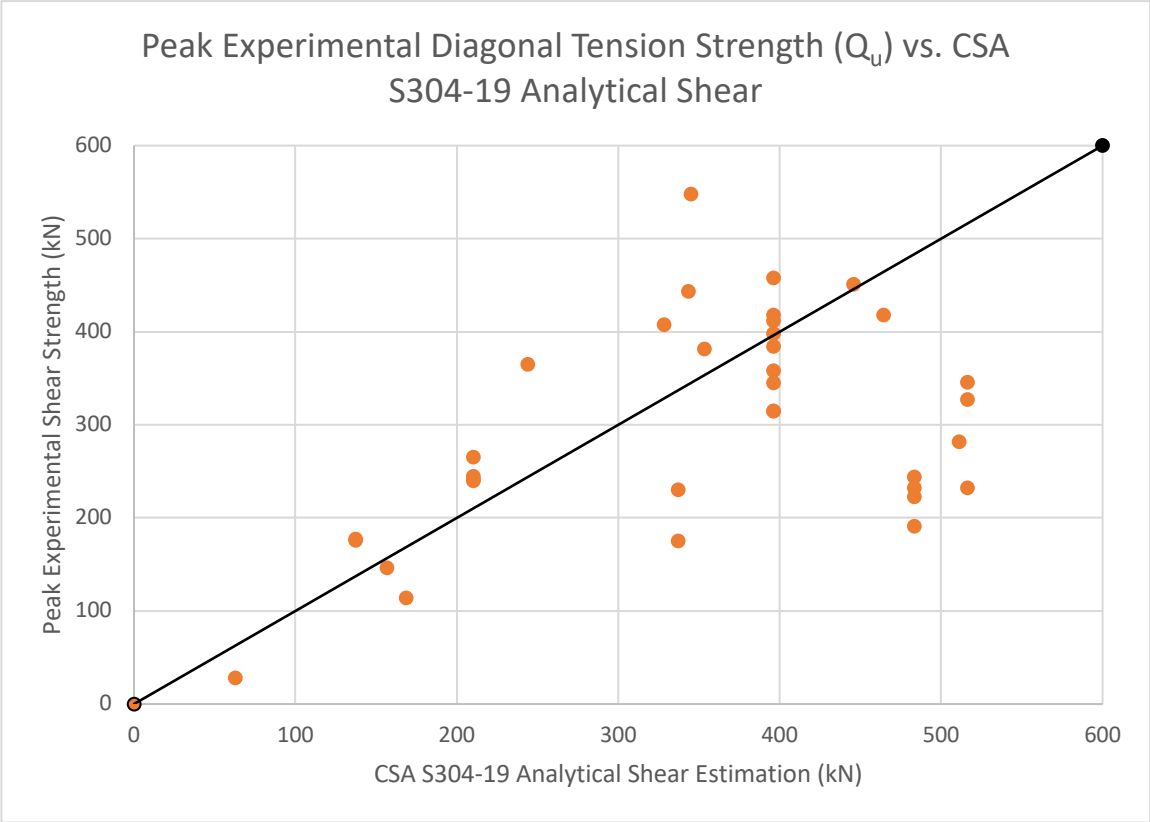

Figure 4.8) Peak experimentally recorded load for diagonal tension dominated specimens vs. analytically derived governing shear strength as per CSA S304-24 provisions

A key observation to be made is that the data is skewed below the equal value line, indicating a general trend that the CSA S304-24 analytically determined shear strength values overestimated the experimental values. This underscores that empirical relationships that have been calibrated to a limited set of data that might not always be applicable such as in applications that considerer parameters outside of the range for which they were derived.

Chapter 5

Analysis of the Database:

Drift Capacity of RM Walls

5.0 Introduction

The second part of analysis carried out using the database was related to the drift and deformation capacities of the wall specimens. Analytical estimates were computed through the NIST (GCR 17-917-45) and ASCE/SEI – 41 (2023) seismic assessment frameworks and compared with values recorded during the experimental testing. This chapter delves into the procedures followed in this comparison, as well as a discussion of results and findings.

5.1 Discussion of Results

The most fundamental form of analysis carried out by the database was an analysis of key parameters such as the aspect ratio of the wall, strengths of the materials used, the arrangement details of the reinforcement and applied axial stress. During the data vetting process specimens that were outliers in terms of analytical performance were identified, which led to in-depth investigation to determine if the design equations prescribed in the standards and guidelines were not successfully working for some specimens.

An example of considered test specimens that deviated from the mean values were those constructed in the tests conducted by Albutainy (2021) and Aly (2019). The tested specimens from these investigations were built with a height of 12.1 metres, a value that demonstrates a significant departure from the typical specimen heights encountered in the majority of considered tests that rarely passed a height of 3 metres. Although these specimens have a substantial deviation of height in comparison to the other specimens, the analytical expressions should still align with the experimentally recorded performance given that they are within the bounds of applicability for these equations. Therefore, it is cause for concern that the data from the analytical stiffness expressions did not predict a realistic approximation of the experimentally recorded stiffness for these specimens, and instead, was over four times as large. This inaccuracy in results underscores the outlined issues at hand surrounding several of the analytical expressions used in the analysis for reinforced masonry structures.

It is shown in the following sections that the discrepancy between experimental and theoretical values is not an isolated occurrence for specimens that were constructed with uncommon design parameters, but was also encountered in specimens constructed to typical design specifications found in the Canadian practice. This issue was also mentioned by the authors in several of the recorded papers in which limits and assumptions for many of the seismic provisions

and design and analysis of reinforced masonry shear walls prescribed in the CSA S304 were considered. This is backed by research published by Galal (2019), test results concluded that the current values for the maximum spacing of reinforcement required modifications to specify lower spacing limits that align closer with other foreign guidelines that provided results that better resembled their recorded experimental data, such as the Standards Association of New Zealand (NZS 4230). In addition, specimens constructed with spacing limits in agreement with these standards experienced increases to strength, ductility and energy dissipation capacities, which all worked to increase overall performance in seismic conditions and produced better convergence with experimental results. This study worked toward a common goal towards one of the key objectives of the current thesis, which is to provide recommendations for current empirical expressions and nonlinear assessment criteria that are being employed on existing reinforced masonry structures in Canada. These modifications will be critical in ensuring the resilience and safety of buildings in earthquake prone regions of Canada, as well as in areas more stable regions that have been exposed to extreme hydraulic fracturing (fracking) procedures over the years.

5.1.1 Measuring the Lateral Drift Ratio in the Tests

The lateral drift ratio of a wall specimen is referred to as the measurement of lateral displacement relative to its height. The lateral displacement of the wall specimens was recorded during the experiments at varying levels of loading during the fully reversed cyclic loading tests through the use of various instrumentation devices such as linear variable differential transformers (LVDTs).

Through the database the lateral drift ratio was investigated for the collection of the tests, to determine the resulting influence that different design parameters of the wall can play on the overall structural performance under lateral loading. This analysis aimed to identify patterns and correlations between the drift ratio and different failure modes, as data was plotted and classified based on the reported failure of the specimen. Drift ratios were plotted against several parameters at the point of yielding, which was assumed to occur at 80 percent of the peak load in the ascending branch of response, and at ultimate deformation capacity, which is taken by convention at 80 percent of peak on the post-peak descending branch of response. This investigation was carried out to provide insight into the validation of deformation criteria for RM walls.

5.1.1.1 The Effect of Aspect Ratio on Drift Magnitudes

The first parameter that was investigated in relation to the recorded experimental drift ratios was the aspect ratio of the specimen. Defined as the ratio between the height and length of the wall, several of the papers collected in the database, such as Majid (2008) concluded that the structural performance of a reinforced masonry wall experiences the largest sensitivity to changes in aspect ratio in comparison to any other design parameter. This is in close agreement with the ASCE-SEI 41 (2023) recommendations, which identifies the aspect ratio one of the three primary variables that affect the deformation capacity of a reinforced masonry structure, alongside the longitudinal reinforcement ratio and applied axial load.

When observing the plots of the aspect ratio against the experimental drift ratios in the set of figures below, data trends that describe the relationship between the dimensions of the specimen and lateral drift are identified. The groups of data points in these figures are clearly associated to different failure modes with not many outlying specimens. This indicates that the aspect ratio of a specimen has a strong influence on the failure mode of a specimen, and as a result, the magnitude of lateral drift.

The majority of tests that were reported to fail in shear in Figure 5.1 (20 specimens out of 29 total that failed in shear) were constructed with an aspect ratio equal to 1, and all of these specimens are grouped very closely together as a result of very similar reported drift ratios at peak strength. This is unique in comparison to the flexure dominated specimens which possessed a larger range of aspect ratio values that varied from values of 1 to over 3. There was only one squat wall with an aspect ratio of 0.5, reported to have failed in shear and had a much lower peak drift ratio in comparison to any other specimen in the database. Although the data is limited, it is expected that squat shear walls tend to experience a much more brittle behaviour accompanied by decreased lateral displacement and resulting deformations due to its increased stiffness that comes from its short unsupported length.

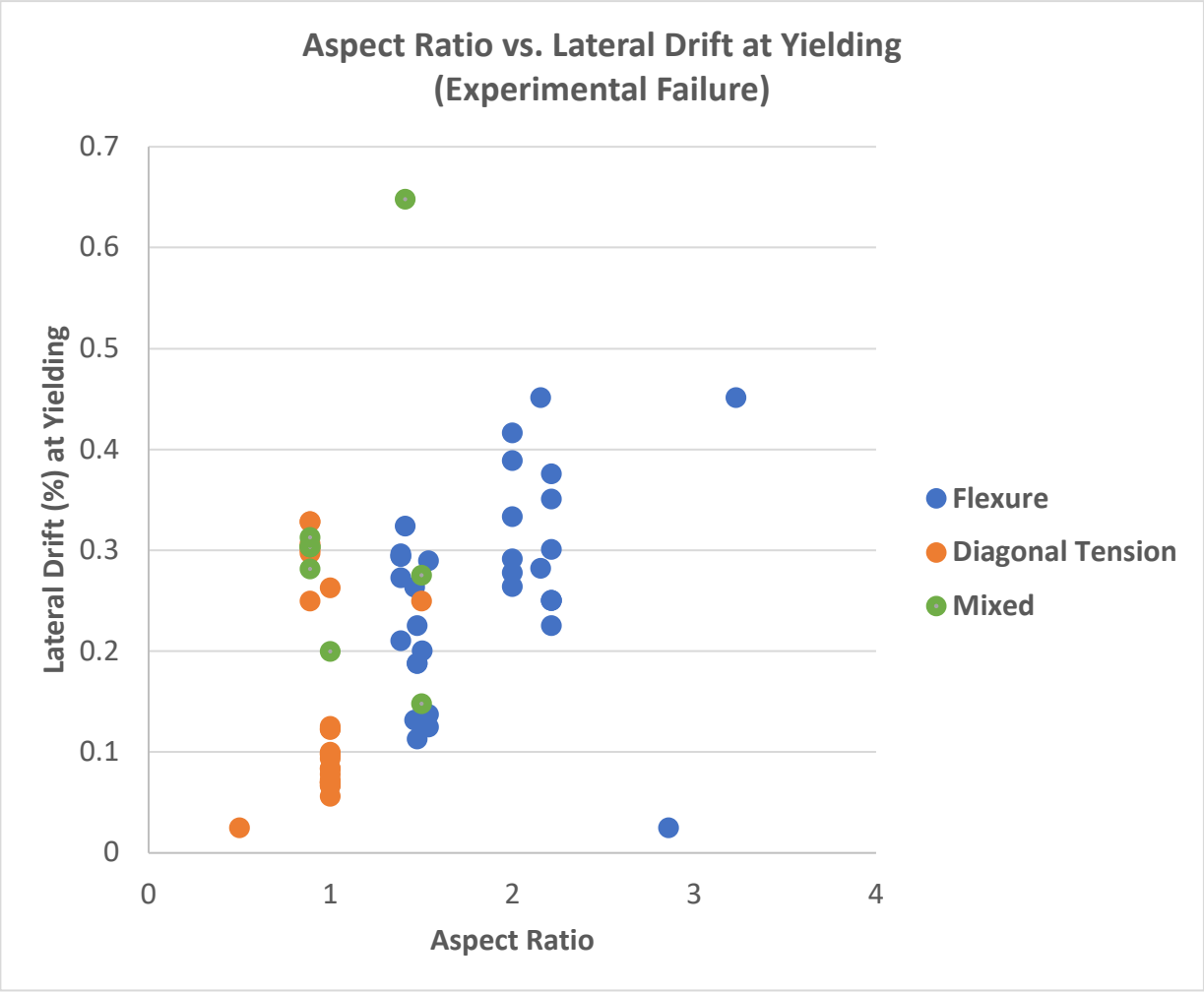

Figure 5.1) Experimental drift ratio at yielding (80% of peak ascending branch response) vs. aspect ratio of specimens, where failure modes have been classified based on experimental reporting

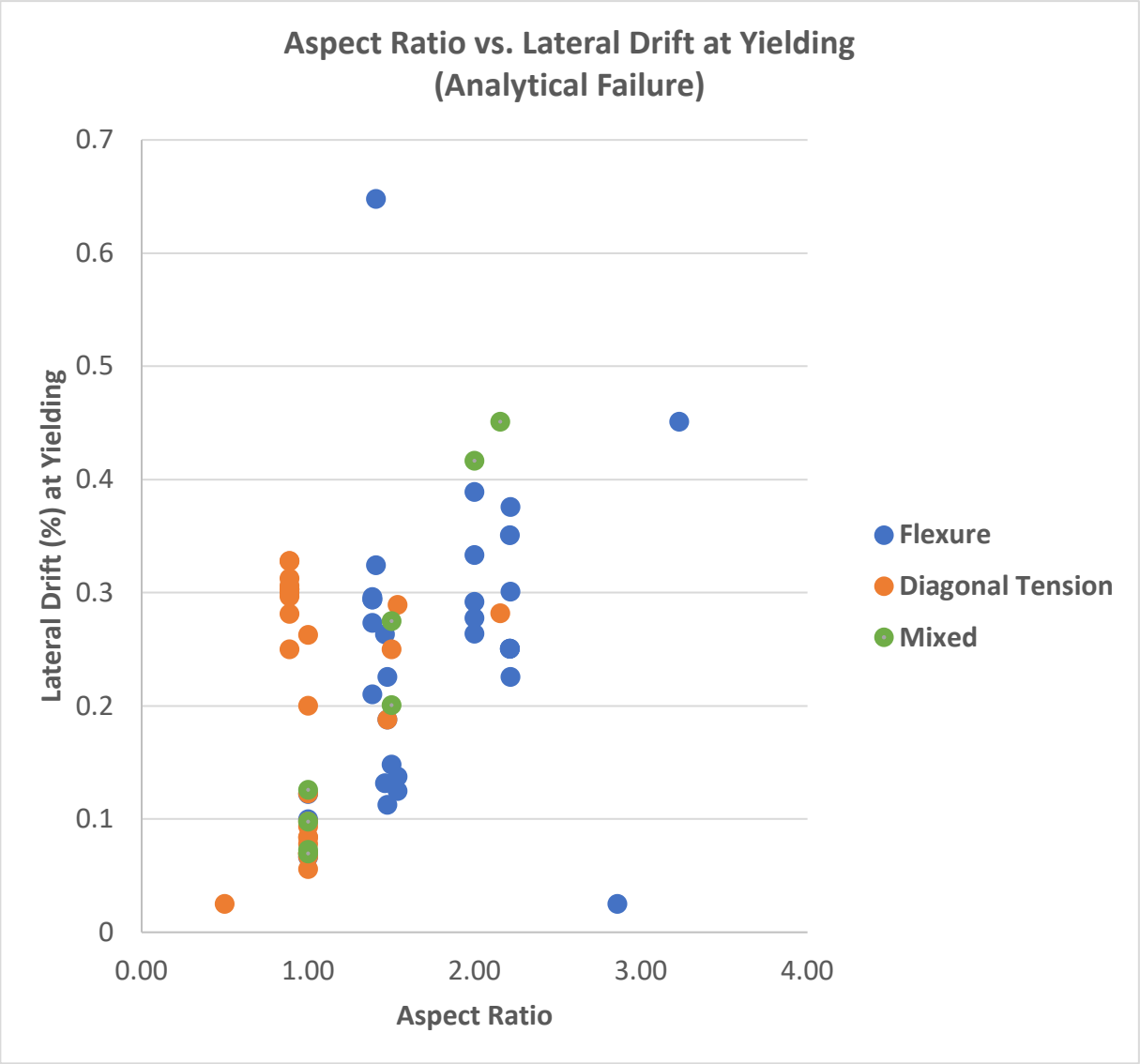

Figure 5.2) Experimental drift ratio at yielding vs. aspect ratio of specimens, where failure modes have been classified based on analytical reporting

Comparison between the two figures also highlights the inconsistencies between the recorded experimental failure modes and the analytically determined ones, where several of the data points change classification between the two figures. This occurred for specimens which reported a flexural failure during the experimental testing, yet the shear strength that was calculated using the analytical expressions yielded a value lower than its flexural strength. This might be due to underestimation of the transverse steel contribution by the CSA S304-2024, which was identified in the preceding chapter. If a specimen reports a shear strength that is lesser than its

flexural strength (and vice-versa), it should be expected to fail first in whichever mode it is weakest in. When this is not the case, it points to a flaw in the analytical expression used for determining the shear strength of the RM Wall.

When considering the flexural response of specimens with aspect ratios of around 3, it is noted that they exhibited significant amounts of lateral ductility and were able to achieve peak drifts of over 2 percent. Two of these highest-ranking specimens were tested in the same experimental investigation carried out by Aly (2019) which possessed several unique differentiations in the test procedures when compared to the other experiments in the test matrix. These specimens were constructed with unique boundary elements constructed out of non-conventional C-shaped masonry blocks. The use of these unique blocks allowed for more flexibility in the arrangement of transverse and vertical reinforcements, as well as a solid grout core to be formed inside the element. The specimens that were constructed in this manner reported a significant improvement in structural performance of the wall as a result of an increase in the ductility-related response modification factor (R_d), which provides a more optimal design through a reduction in seismic forces. This increase in R_d stems from the larger area of grout present in the confined end regions of the boundary elements which enhances the ductility capacity, which is evident when compared to other specimens in the database of similar dimensions and boundary elements built from conventional stretcher unit blocks.

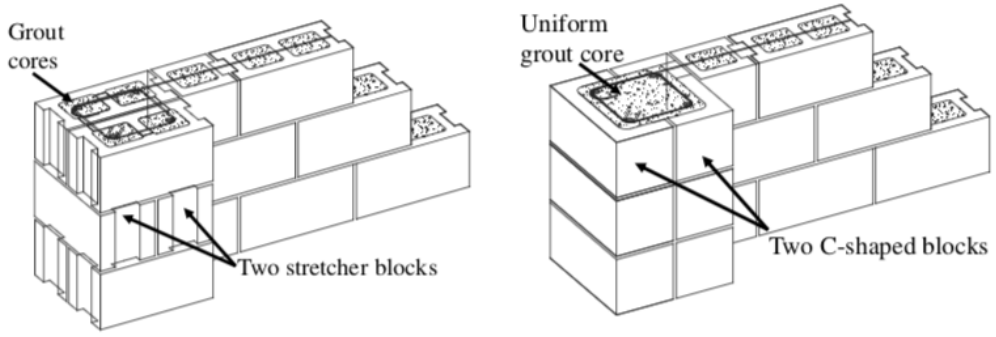

Figure 5.3) Side by side comparison of conventional stretch block (left) and unique C-shaped block boundary element construction

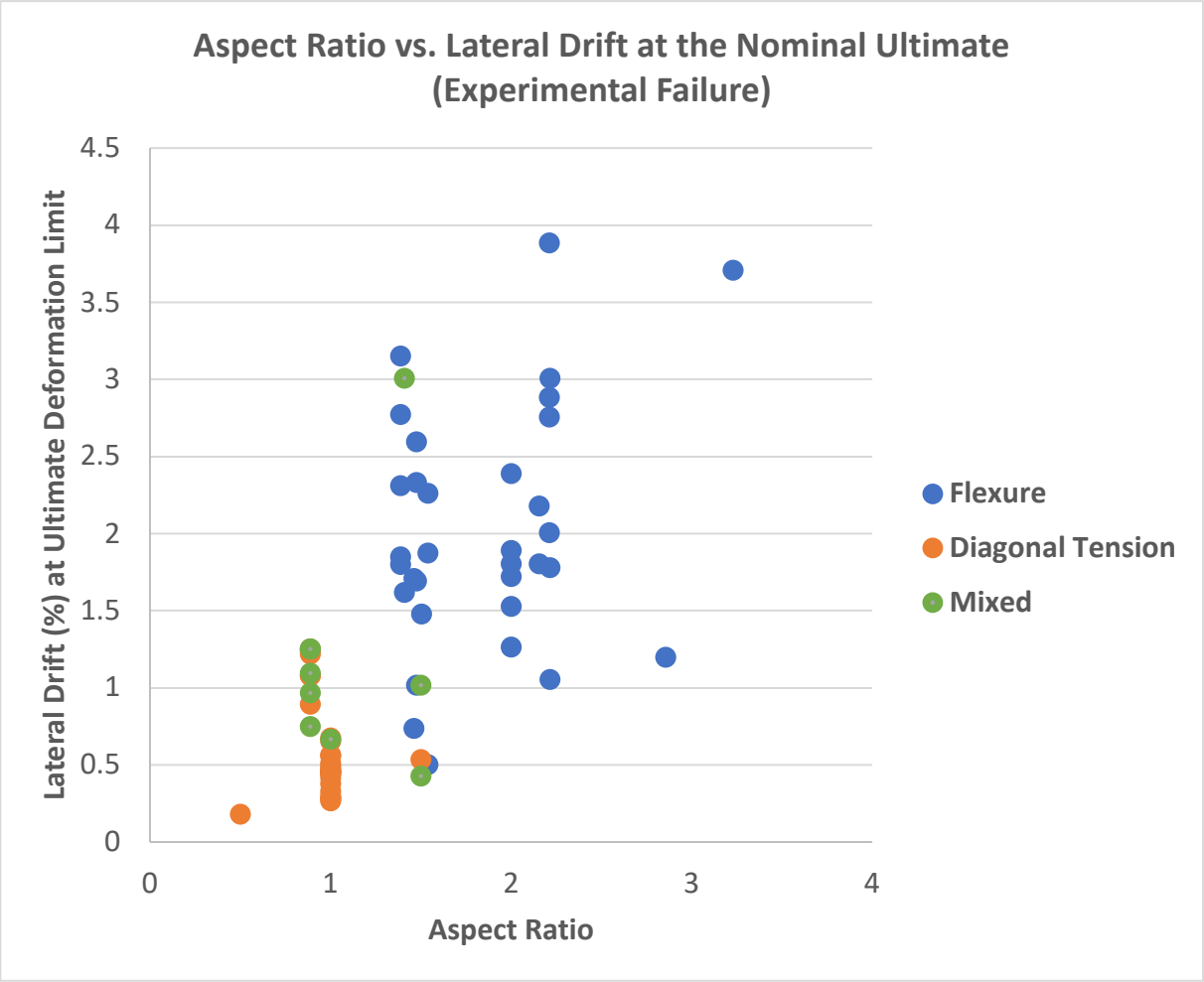

Figure 5.4) Experimental drift ratio at the nominal ultimate limit state (residual post peak strength equal to 80% of peak strength) vs. aspect ratio of specimens, where failure modes have been classified based on experimental reporting

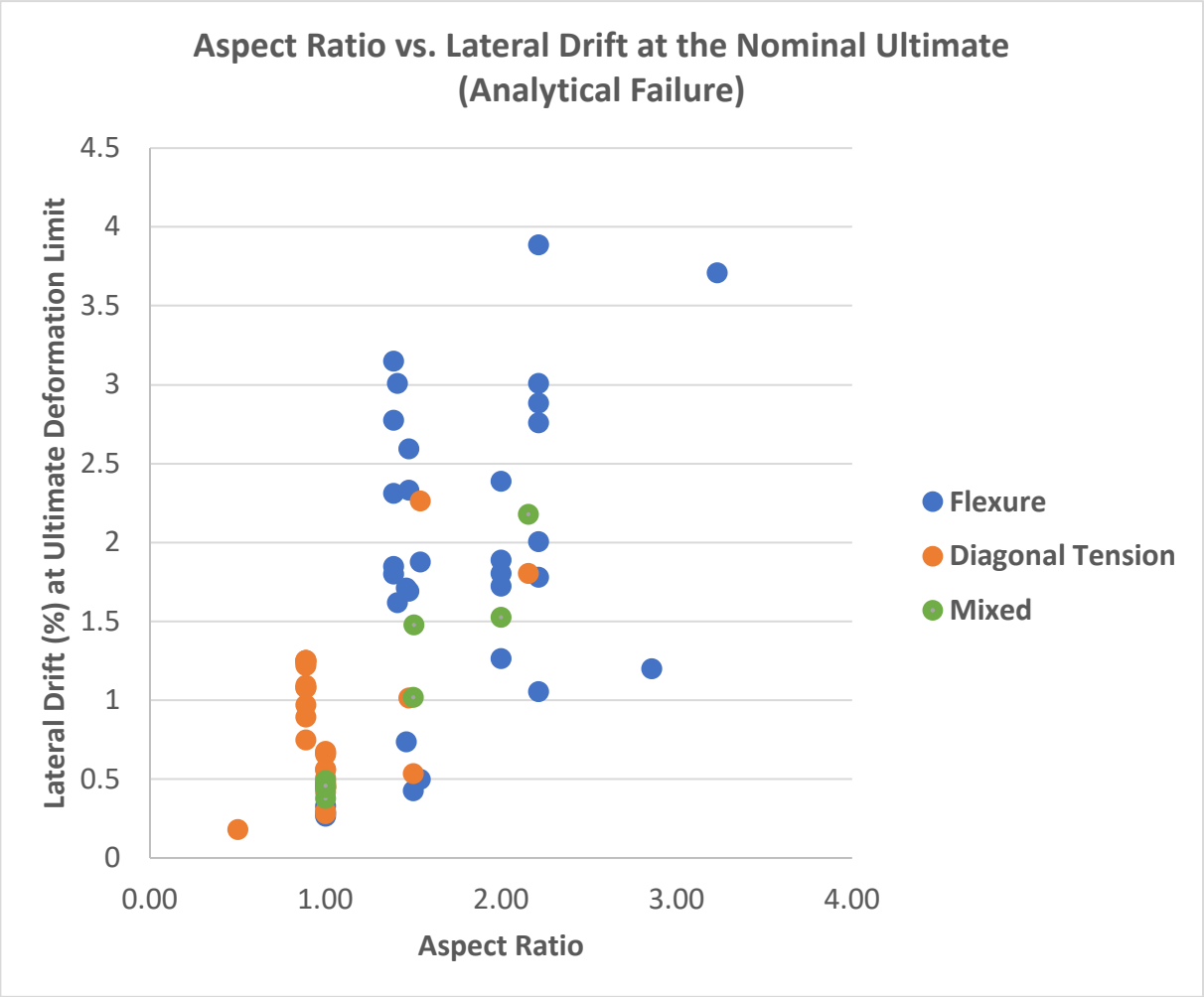

Figure 5.5) Experimental drift ratio at the nominal ultimate limit state vs. aspect ratio of specimens, where failure modes have been classified based on analytical reporting

5.1.1.2 Mechanical Reinforcement Ratio

The vertical reinforcement present in a reinforced masonry wall helps to mitigate sliding shear failures and therefore pinching of the hysteretic loops; thereby enhancing the energy dissipation capacity of the wall. Furthermore, increased amounts of vertical reinforcements provide and increase to the flexural moment strength, and therefore the lateral force demand in the wall, increasing the likelihood of diagonal tension failure to occur. The presence of vertical bars within the wall serve to keep the blocks confined through clamping, which increases the shear resistance by preventing the formation of diagonal cracks across the wall. In addition, the vertical bars tie together with the horizontal reinforcement that is placed along the bed joints or within

bond beam courses, where the combined action between the two reinforcements serve to provide enhanced overall strength for the wall.

The vertical reinforcement ratio, defined as the ratio between the cross-sectional area of the vertical bars to the net cross-sectional area of the wall's web, plays a dominant role on the lateral load resistance in flexure. For flexure, the typical way to organize the data is the use of the mechanical reinforcement ratio – i.e., the product of the geometric ratio of vertical reinforcement multiplied by the material strength ratio (the yield strength of the vertical bars divided by the uniaxial compressive strength of masonry). Examination of Figures 5.6 and 5.7, both of which depict the peak lateral drift ratio versus the mechanical reinforcement ratio shows that flexure dominated specimens (based on both experimental and analytical failure) tend to exhibit much higher lateral drifts in comparison with the shear dominated specimens. This data aligns with expected the behaviour of flexural failures, which typically exhibit ductile actions and enhanced deformation capacity, which can be quantified by the magnitude of lateral drift.

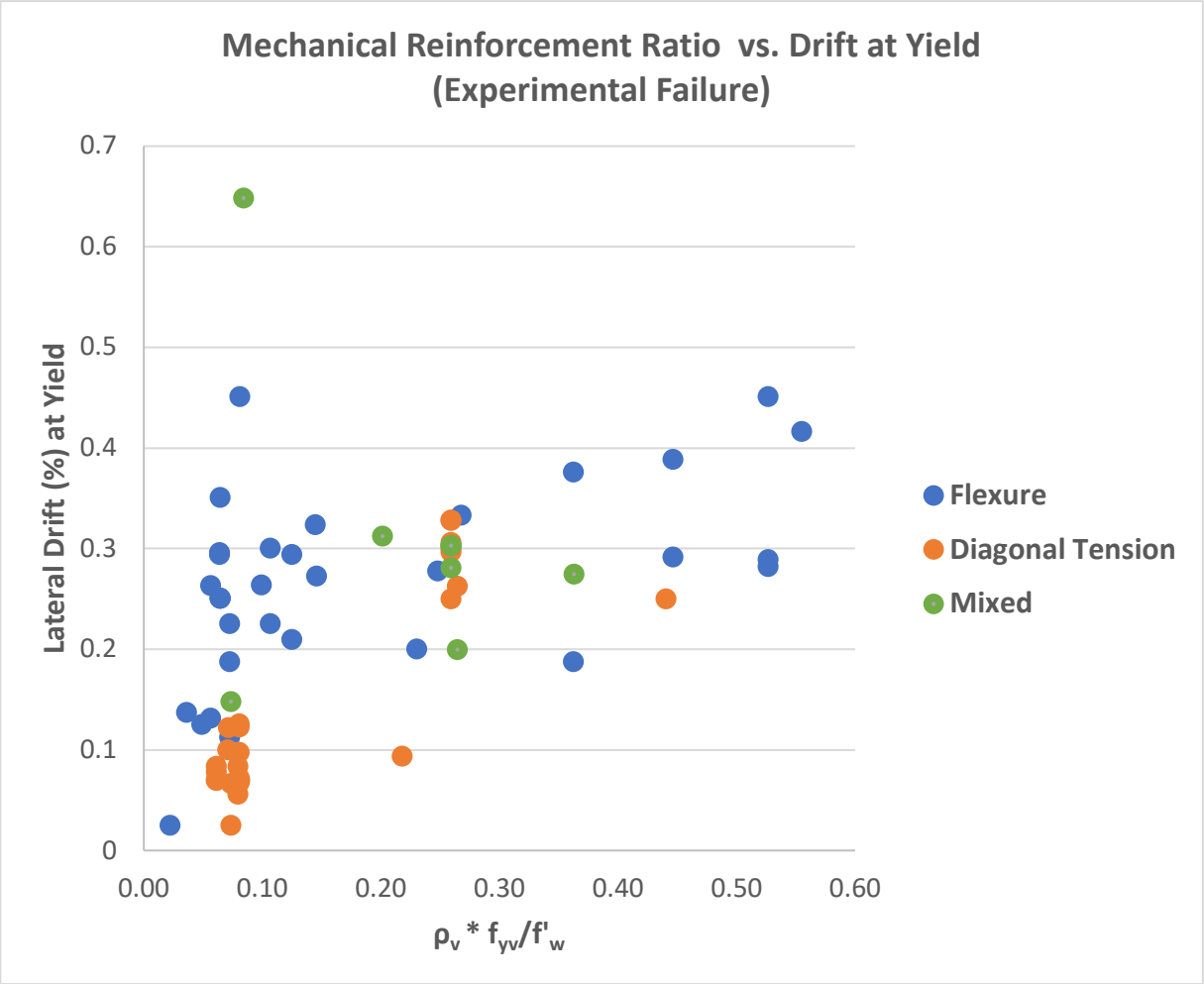

Figure 5.6) Experimental drift ratio at yielding vs. mechanical reinforcement ratio, where failure modes have been classified based on experimental reporting

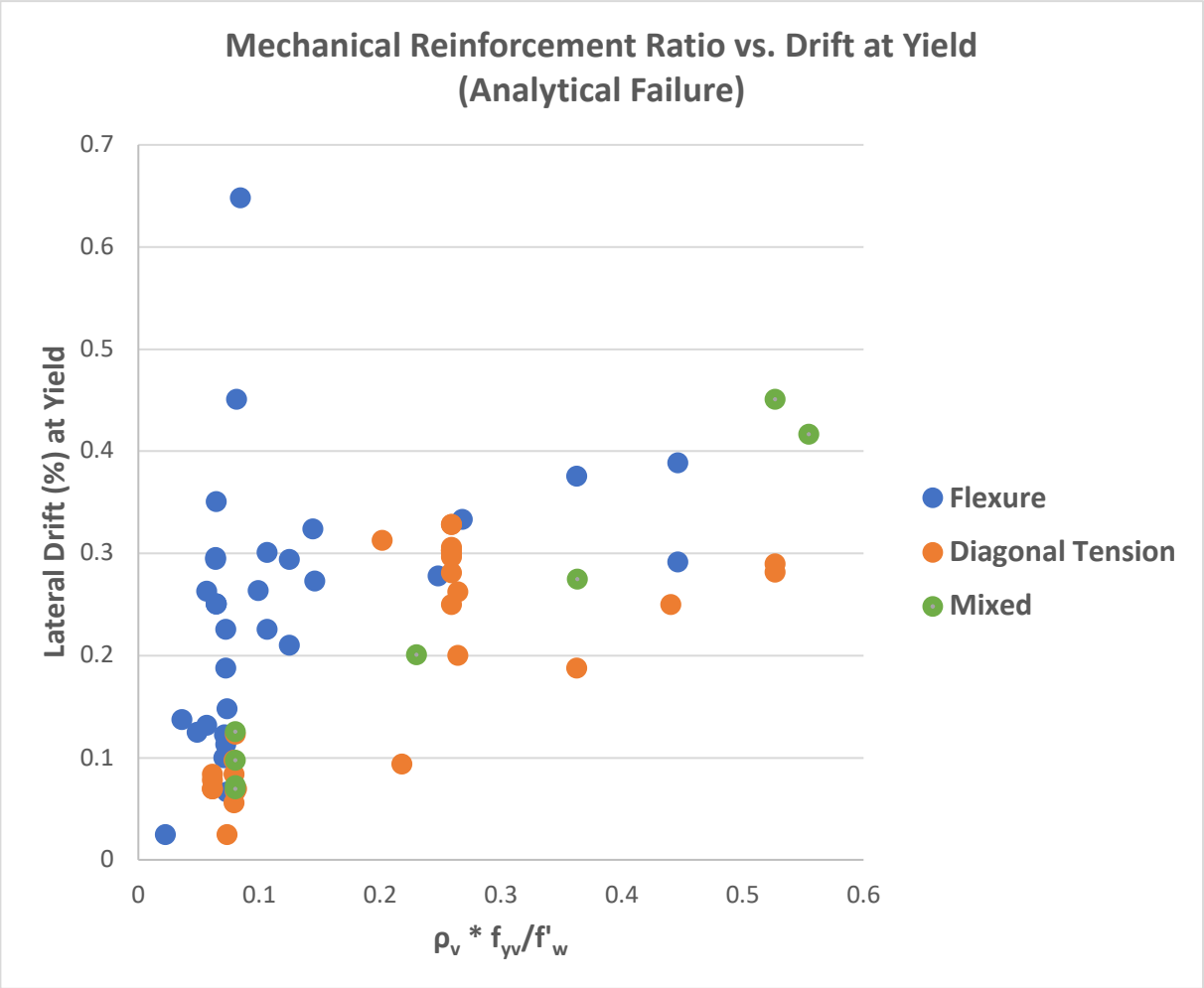

Figure 5.7) Experimental drift ratio at yielding vs. mechanical reinforcement ratio for vertical bars, where failure modes have been classified based on analytical reporting

There is a very strong concentration of experimentally defined shear failure specimens with reinforcement ratios of around 0.1 in Figure 5.6, with some of these specimens switching to flexure or mixed mode in Figure 5.7 in accordance with the analytical failure mode. This data clearly illustrates that the mechanical reinforcement ratio of a reinforced masonry wall specimen has a determining role on the ensuing failure mode during loading, a finding that is in agreement with NIST (GC 17-917-45). Specimens with higher amounts of mechanical reinforcement ratio, but still under the classification of being "under-reinforced", are expected to have much greater deformation capacity and will generally not fail as a result of a shear mechanism, but will rather fail in flexure. This is evident in Figure 5.6, where only a select few specimens with a vertical reinforcement ratio greater than 0.1 failed in shear, which could have been influenced by a

combination of other factors. (It is noted however that for mechanical reinforcement ratios $\rho_v f_{yv}/f'_w$>0.36 the response becomes brittle in flexure as the wall is considered over-reinforced (CSA A23.2 (2019)). In practice, flexural failure (if shear strength is suppressed) is optimal as it allows for more ductility which will be accompanied by warning signs that failure is imminent, allowing for retrofits to be carried out before total structural failure occurs.

When observing the mechanical ratio of vertical reinforcement versus the lateral drift at ultimate strength levels in Figures 5.8 and 5.9 below, similar data trends are noted between the flexural and shear specimens. That is, greater amounts of mechanical ratio of vertical reinforcement in relation to the gross cross-sectional area of the wall is able to yield larger drift capacities. In addition, the shear dominated specimens exhibit much lower drifts even at ultimate strength levels in comparison to flexural specimens as a result of the limited ductility that stems from the brittle nature of the performance of the specimens.

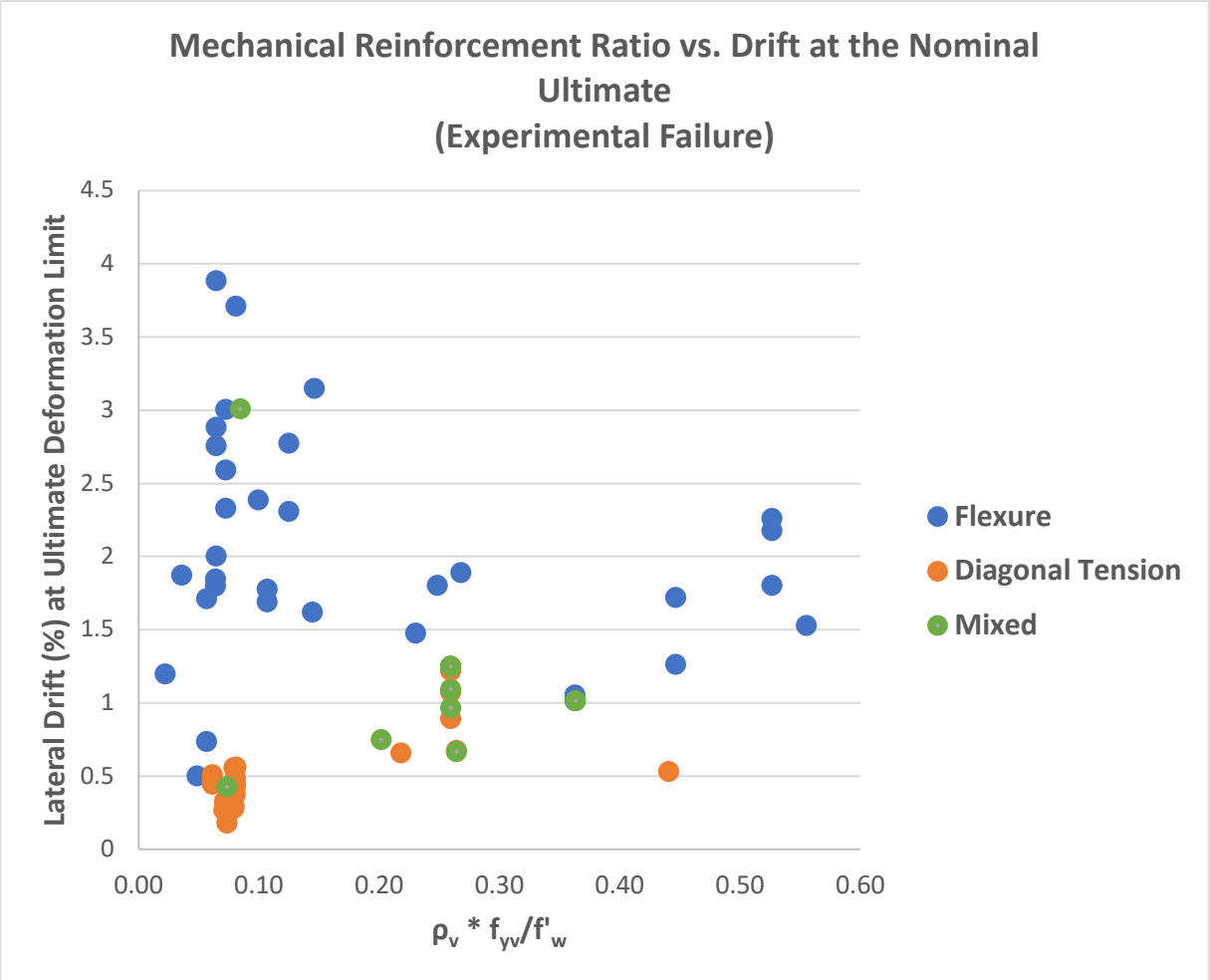

Figure 5.8) Experimental drift ratio at the nominal ultimate limit vs. mechanical ratio of vertical reinforcement, where failure modes have been classified based on experimental reporting

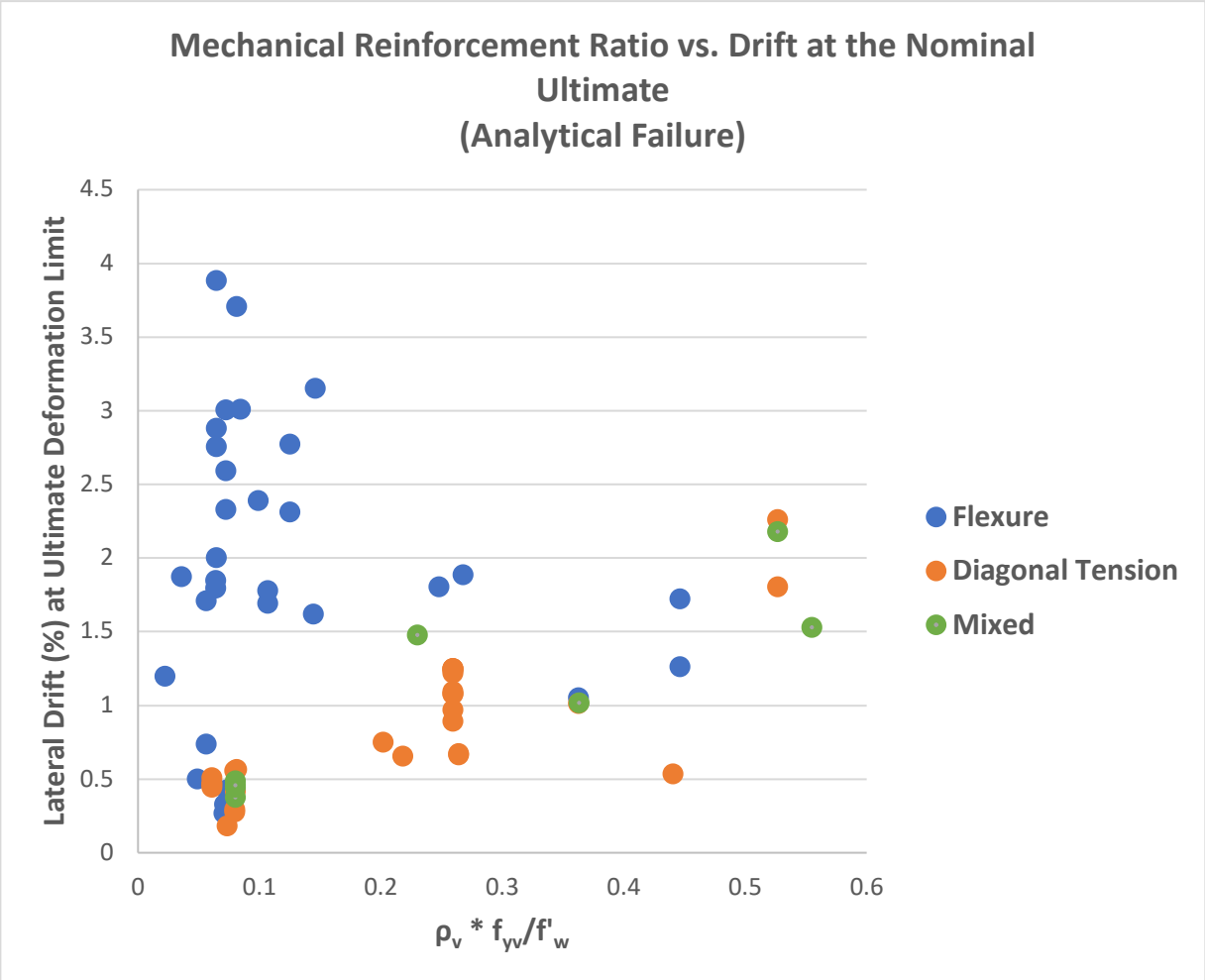

Figure 5.9) Experimental drift ratio at ultimate post peak strength vs. mechanical ratio of vertical reinforcement, where failure modes have been classified based on analytical reporting

5.1.1.3 Axial Load Ratio

The presence of an axial load on a reinforced masonry wall is able to significantly influence its behaviour as well as failure mechanism, especially when exposed to the lateral loading induced from a seismic event. In accordance with the CSA S304-24 equations for the factored shear resistance of the masonry components (V_m), a wall subjected to the combined action of vertical compression and lateral shear forces is prone to the development of a two-dimensional state of stress, which consists of a compressive stress (σ) and a shear stress (ν). The presence of this compressive strength allows for a delay in the onset and severity of cracking along the wall due to a reduction in the principle tensile stresses. As such, it should come with little surprise that the axial load ratio is among the three critical parameters listed by the NIST (GCR 19-917-45) that

impact the performance of a reinforced masonry component. To facilitate this assessment and quantify the influence it has on the specimen, the axial load ratio, which the ratio of the applied axial load divided by the axial load crushing load of the wall, has been plotted against peak and ultimate lateral drift ratios in the following sets of figures below.

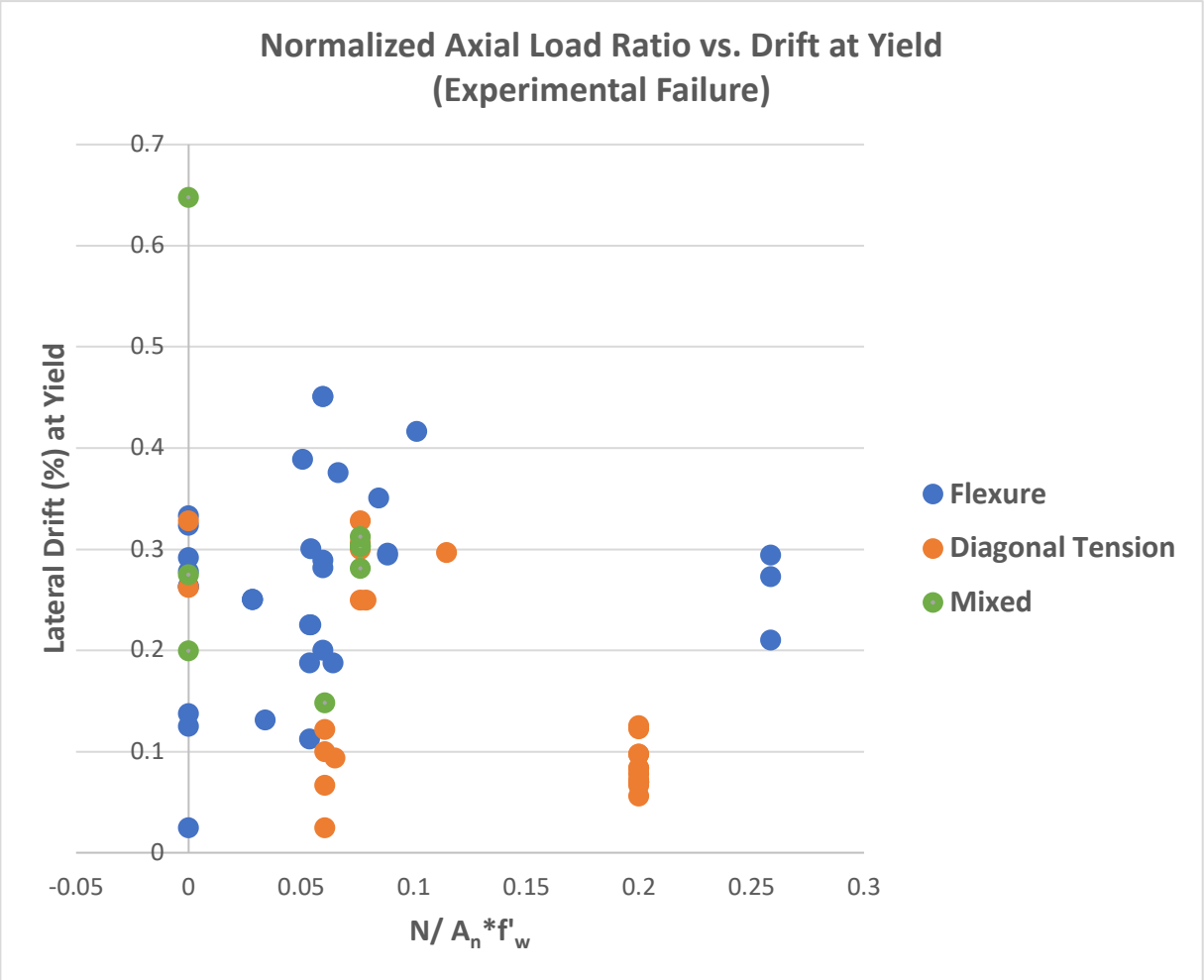

Figure 5.10) Experimental drift ratio at yielding vs. normalised axial load ratios, where failure modes have been classified based on experimental reporting

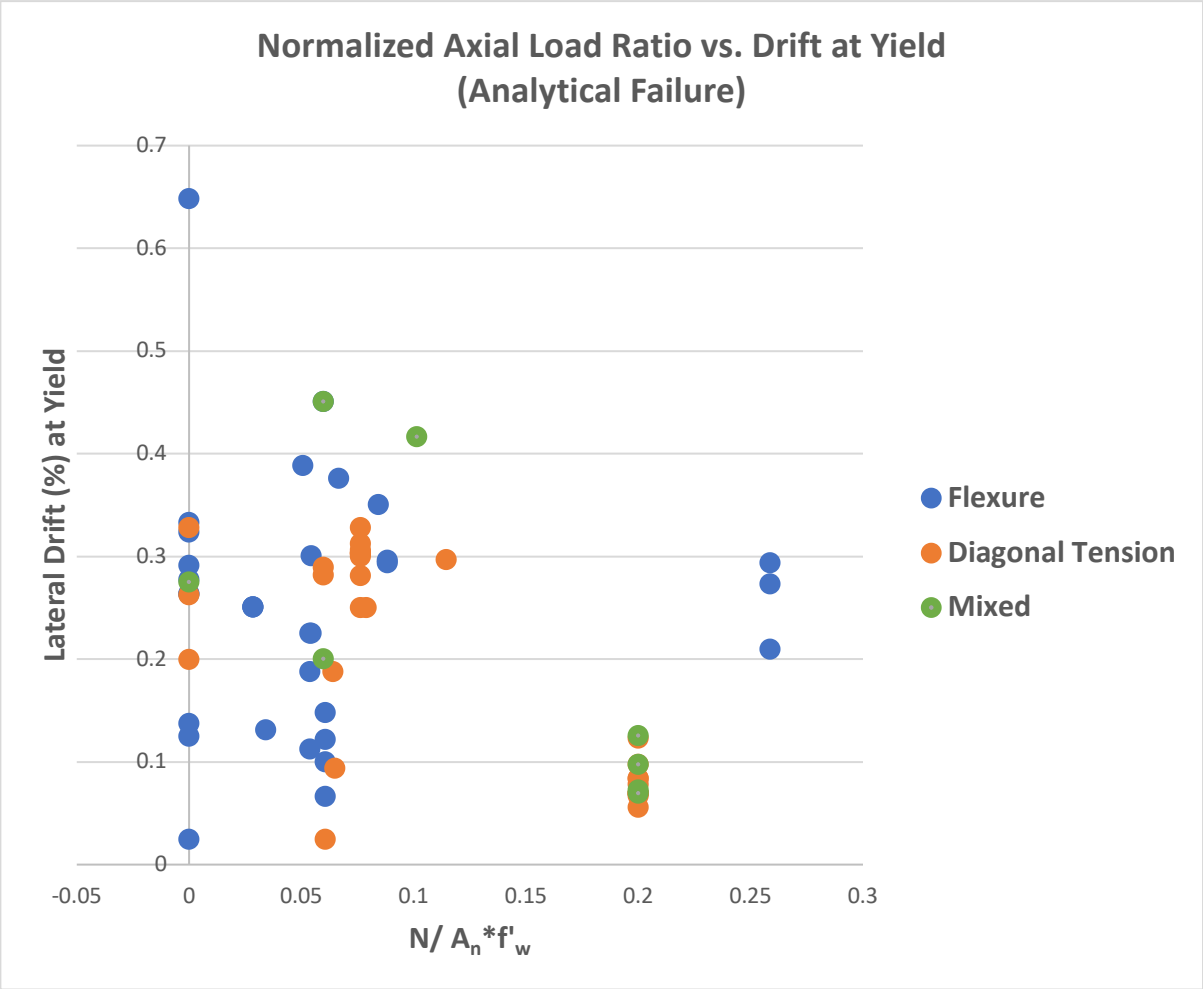

Figure 5.11) Experimental drift ratio at yielding vs. normalised axial load ratios, where failure modes have been classified based on analytical reporting

In this first set of figures above, we can see that the majority of specimens reached greater lateral drift values at lower magnitudes of axial load ratio. This data trend is in accordance with the true mechanical behaviour of reinforced masonry walls under axial loading, since these forces act in compression on the wall which, in turn, increases the stiffness of the wall. This increase in stiffness serves to enhance the walls compressive strength while also increasing the risk of a brittle mode of failure which is accompanied by low drift capacities. In addition, it is observed that specimens with high applied axial load ratios tend to fail in a brittle manner owing to shear dominated behaviour.

There were a few exceptions for this data trend, with specimens tested by Banting (2012) reaching quite high lateral drifts despite also being tested under large axial loads. This could have

been a result of other factors such as the specimens being constructed with an aspect ratio greater than 2, adequate amounts of reinforcement and reinforced inter-story slabs which acted as lacing thereby increasing significantly the shear resistance of the wall.

Figures 5.12 and 5.13 below are similar to the previous set of figures above, except they depict the experimental lateral drift ratios at the nominal ultimate limit of deformation capacity, plotted against the normalised axial stress. Visible in these figures are a few flexure-dominated specimens that despite having large applied axial stresses, were still able to have significant amounts of ductility. These were the same specimens that were constructed with boundary elements constructed with C-shaped masonry units in Aly (2019) which reported significant enhancements to ductility. This unique method of construction of the boundary element produced enhanced energy dissipation capacities.

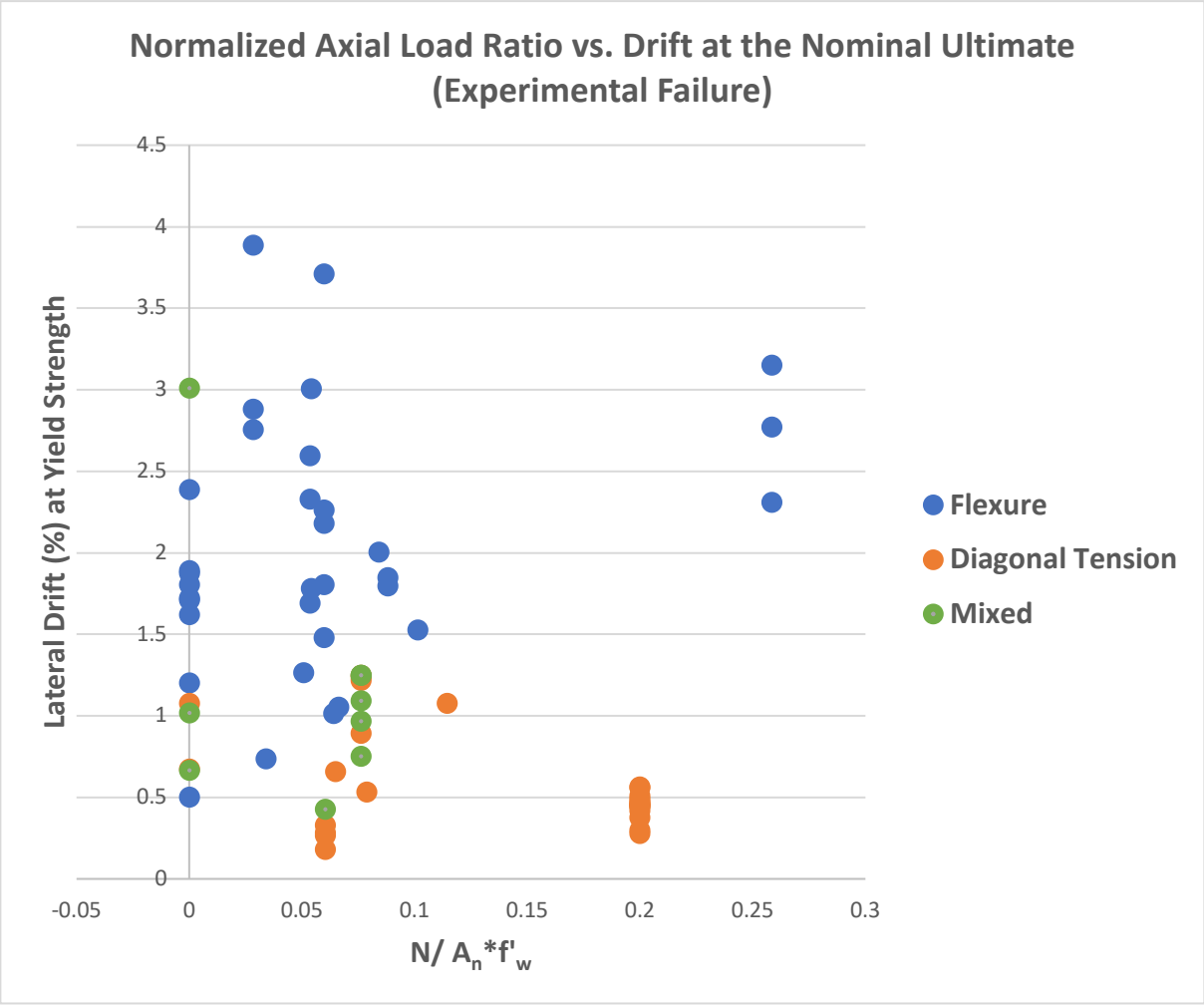

Figure 5.12) Experimental drift ratio at the nominal ultimate limit vs. normalised axial load ratios, where failure modes have been classified based on experimental reporting

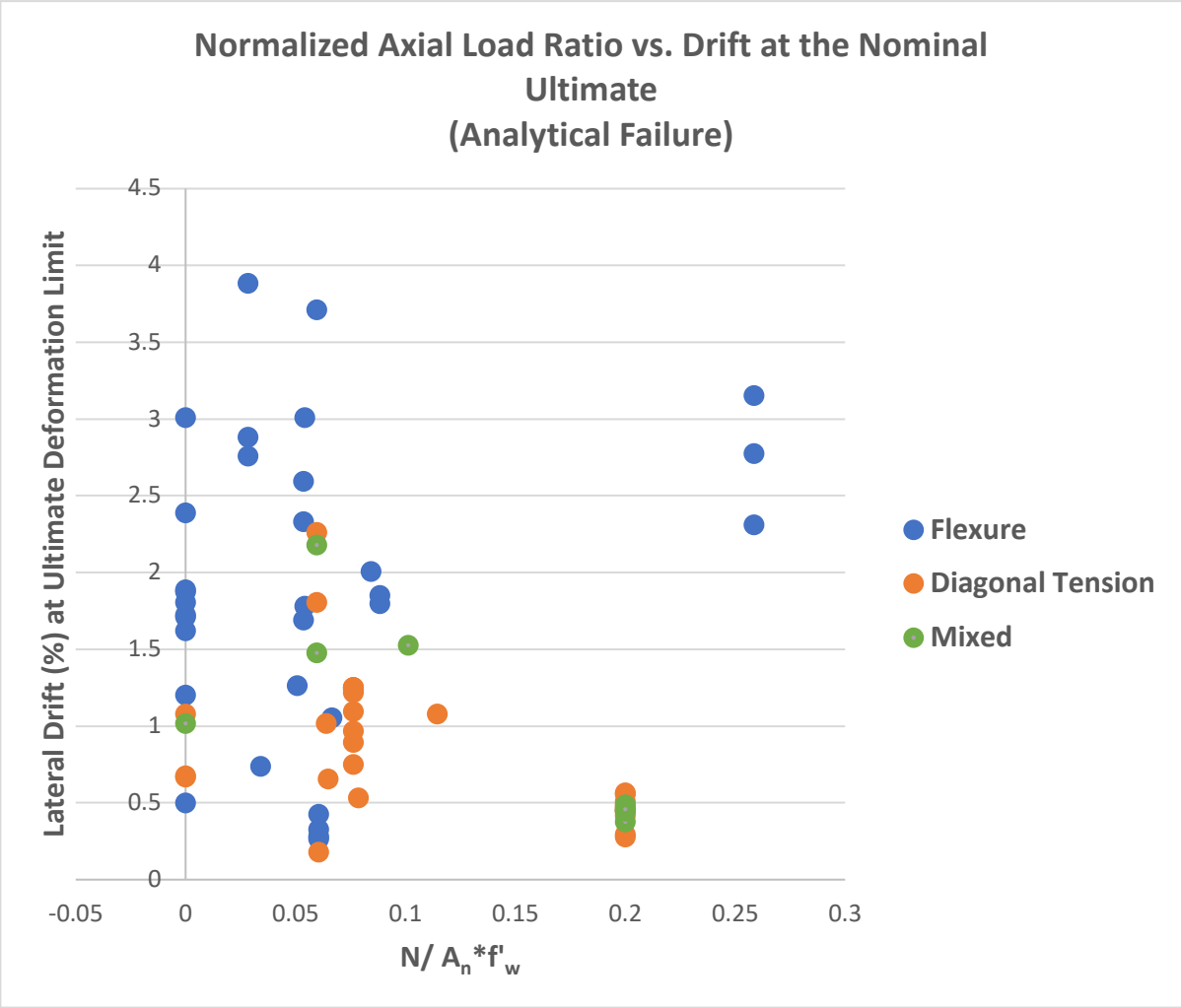

Figure 5.13) Experimental drift ratio at the nominal ultimate limit vs. normalised axial load ratios, where failure modes have been classified based on analytical reporting

5.2 Stiffness and Deformation Calculations

The stiffness of a structural element is the slope of the ascending branch in the linearized lateral load – displacement envelope, the information feeds into the calculations of fundamental dynamic properties of the structure (e.g. Natural Period) that determines the displacement demands under loads. In a structural analysis context, successful estimation of the stiffness of a member can be used to determine the load distribution, deflection and dynamic response that can be expected during its service life. The calculation of the stiffness requires information on the mechanical properties, the geometry and the boundary conditions of the element, all of which contain great variability in the context of a reinforced masonry structure. Therefore, the determination of the stiffness of a reinforced masonry wall can present some challenges due to the inherent

heterogeneous nature of not only the strength and arrangement of the masonry elements, but also the distribution of reinforcement, effect from cracking and the moment distribution along the height.

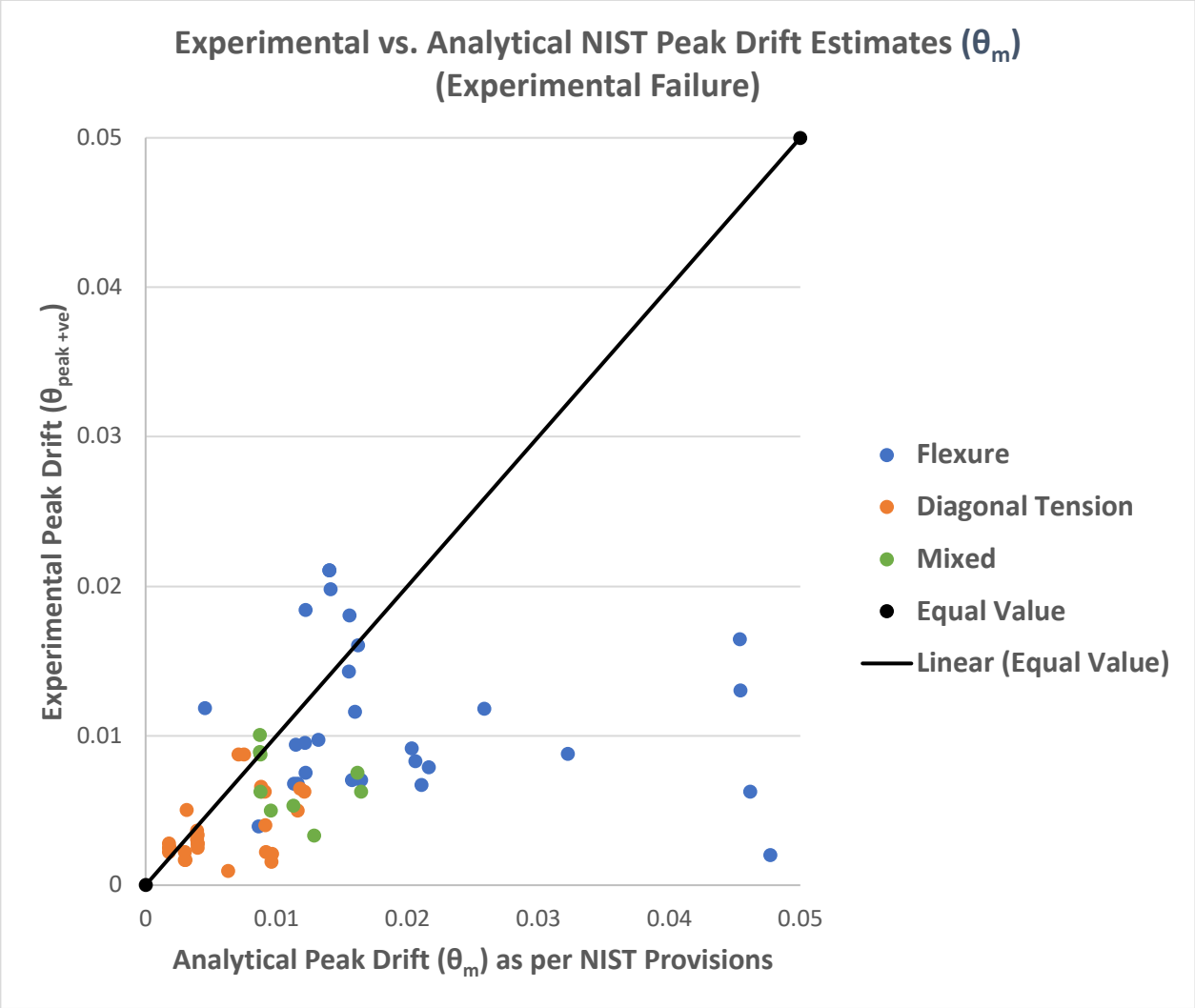

Figure 5.14) Graphical depiction of peak experimental lateral drifts vs. the corresponding values obtained from first principles, where failure modes have been classified based on experimental reporting

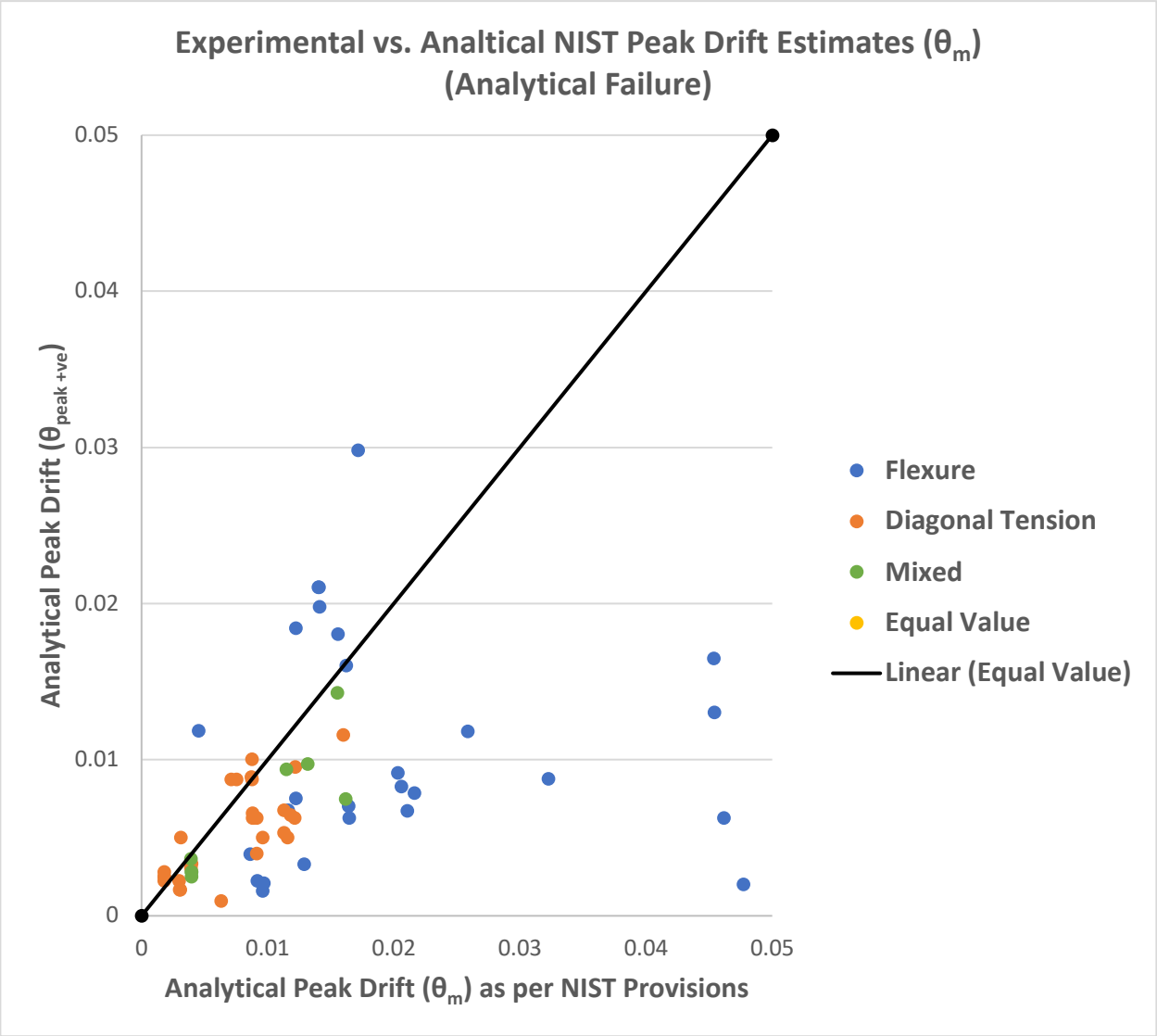

Figure 5.15) Graphical depiction of peak experimental lateral drifts vs. peak lateral drifts computed through NIST empirical relationships, where failure modes have been classified based on analytical reporting

Using fundamental structural analysis principles, the stiffness of the wall specimens was computed through an analytical expression that was derived from elastic beam theory. Assumption is that the wall section is cracked but remains elastic, as well as elastic contributions from flexure and shear deformations are considered in the response. The following expression is derived for the static model of a cantilever. It was programmed in the database and the convergence between the analytical value and the experimentally determined ones was evaluated; it is noted here that the experimentally derived stiffness of the walls was taken as the slope of the ascending branch of the

NIST backbone curve proposed for lateral loading of a cantilever wall.

$$K = \left(\frac{H_e^3}{3E_m \cdot I_e} + \frac{H_e}{0.35A_v \cdot G_m}\right)^{-1} \quad (5.1)$$

Where

K - The stiffness of the ascending branch of the backbone curve proposed by the NIST for lateral load (kN/m)

He - Effective height (shear span) of the reinforced masonry wall specimen (m)

E_m - Modulus of elasticity of the masonry, which is taken as 850 * f'w (MPa)

I_e - Moment of inertia, which is assumed to be taken from cracked section properties and to equal 50 percent of I_{gross} (mm^4)

I_{gross} - Moment of inertia based on gross properties = $\frac{t_w L_w^3}{12}$ (mm^4)

A_v - Effective shear area, taken as 80 percent of the net area (A_n) (mm^2)

G_m - Shear modulus of masonry, taken as 40 percent of the elastic modulus (E_m) (MPa)

From the set of figures below, it can be seen that the shear dominated specimens had much greater stiffness values than the flexural specimens in terms of both analytical and experimental contexts. This is an expected data trend as the increased stiffness of shear specimens is a clear demonstration of the brittle behaviour that was exhibited during the tests. Specimens that were shear dominated were either over-reinforced in flexure or carried very high axial loads – they were therefore more rigid in comparison to under-reinforced, flexure dominated specimens. In the plots shown below the stiffness of the walls was based on both cracked and uncracked properties. This was done to validate the assumption used in the theoretical stiffness estimation that the assumed properties do not exceed half the gross section properties, therefore to check if a cracked-section analysis should be performed to obtain a more accurate value of section properties.

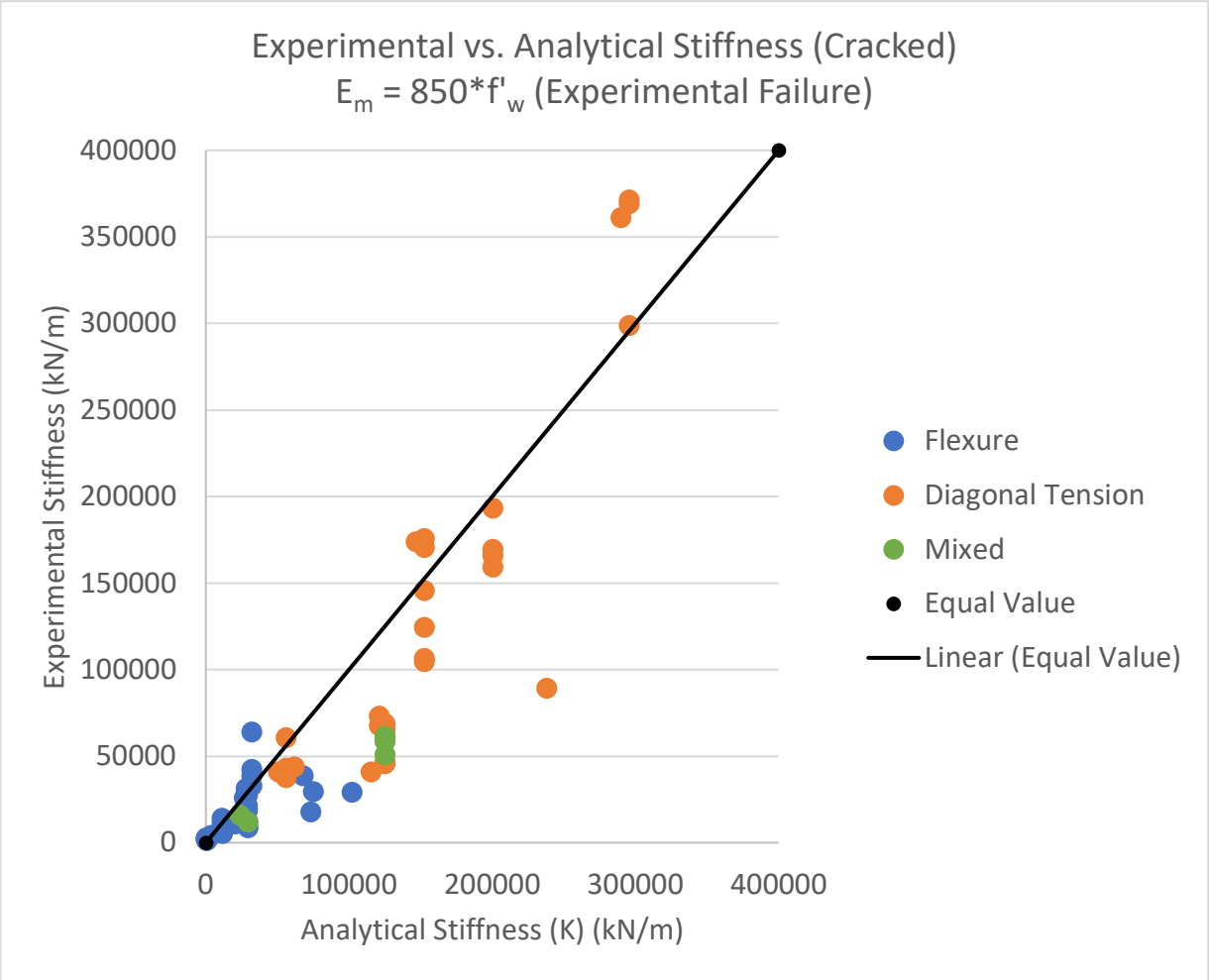

Figure 5.16) Graphical representation of experimental versus analytical stiffness values based on cracked properties which were used in analytical calculations, where failure modes have been classified based on experimental reporting

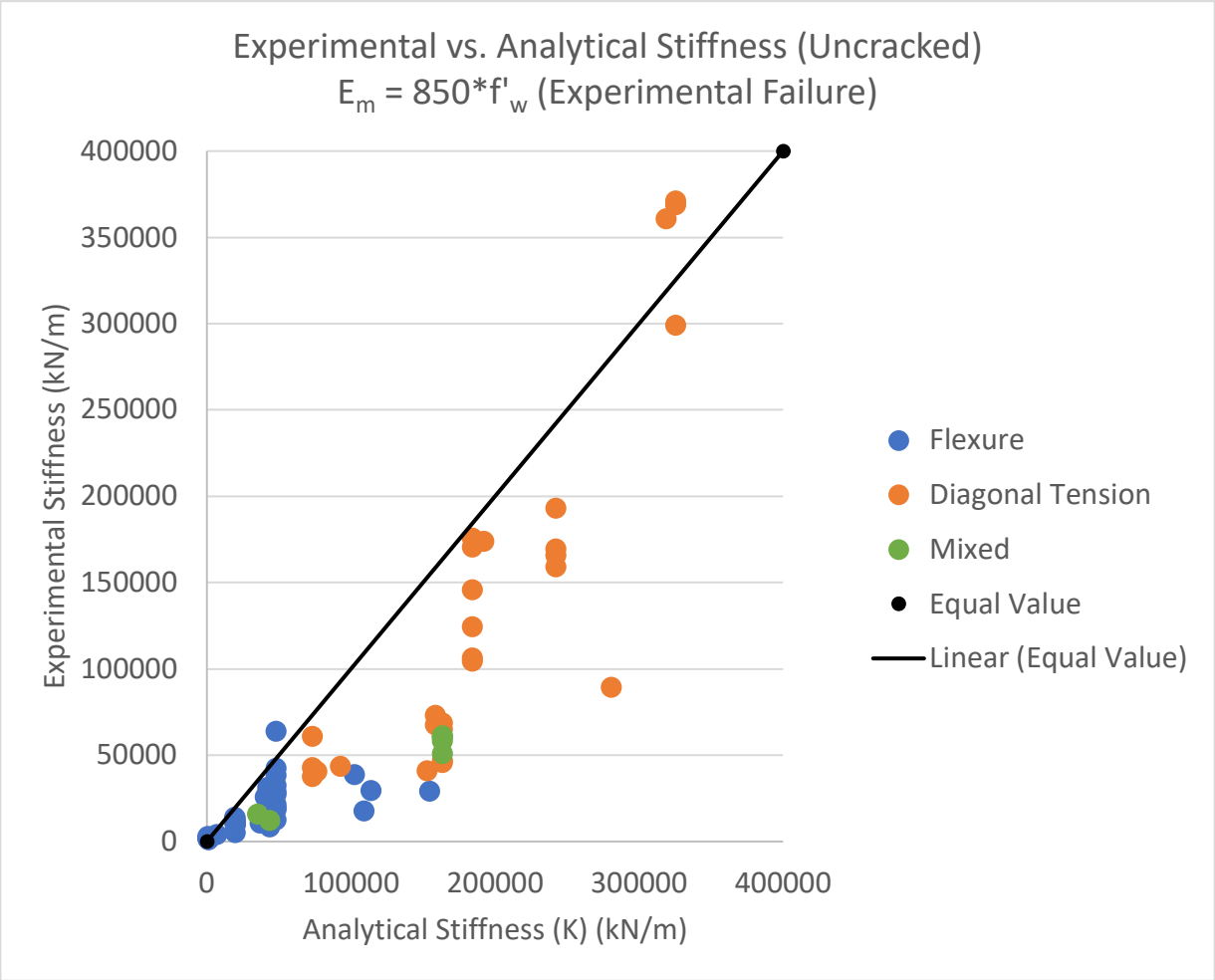

Figures 5.17) Graphical representation of experimental versus analytical stiffness values based on effective, uncracked properties where failure modes have been classified based on experimental reporting

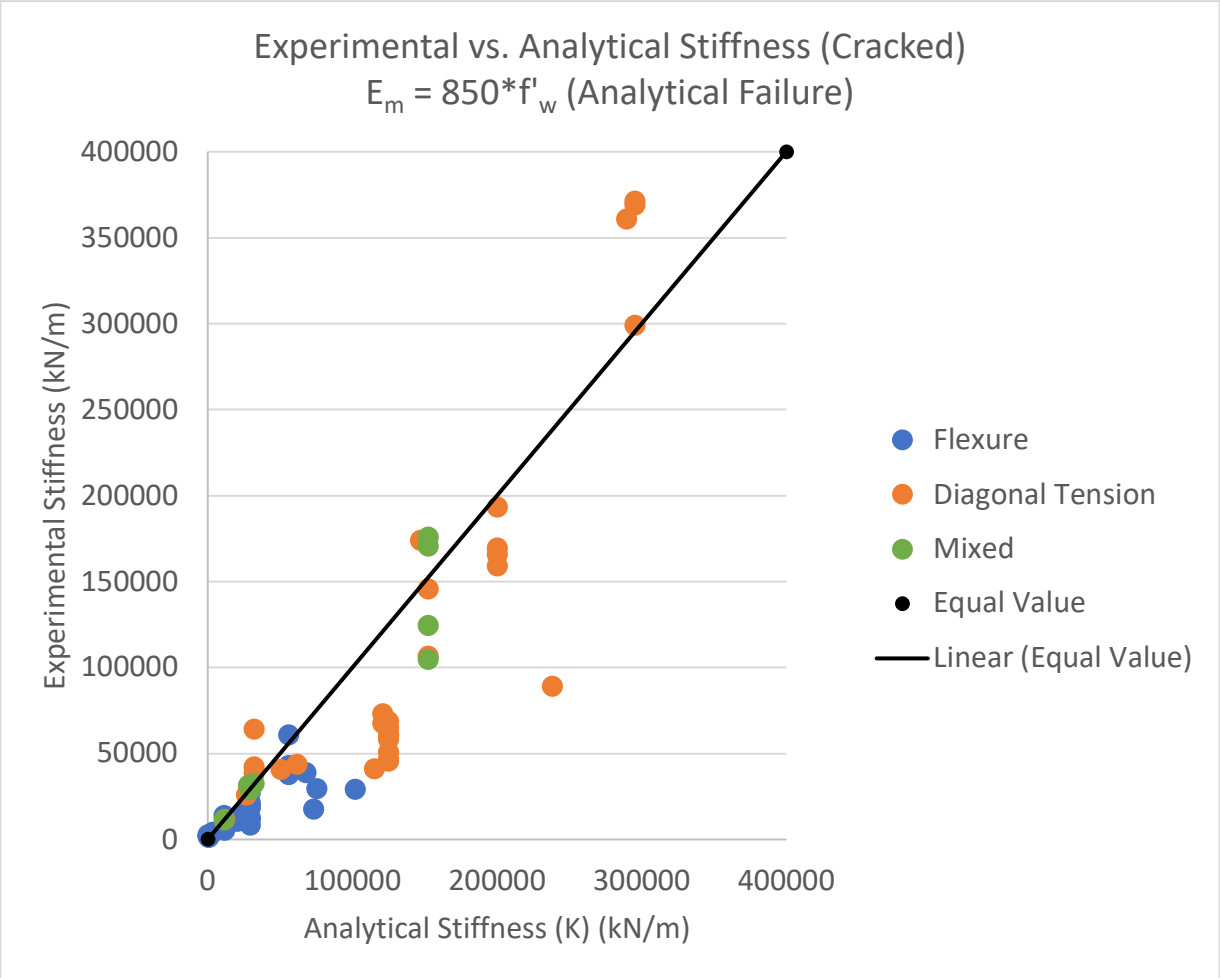

Figure 5.18) Graphical representation of experimental versus analytical stiffness values based on cracked properties were used in analytical calculations, where failure modes have been classified based on analytical reporting

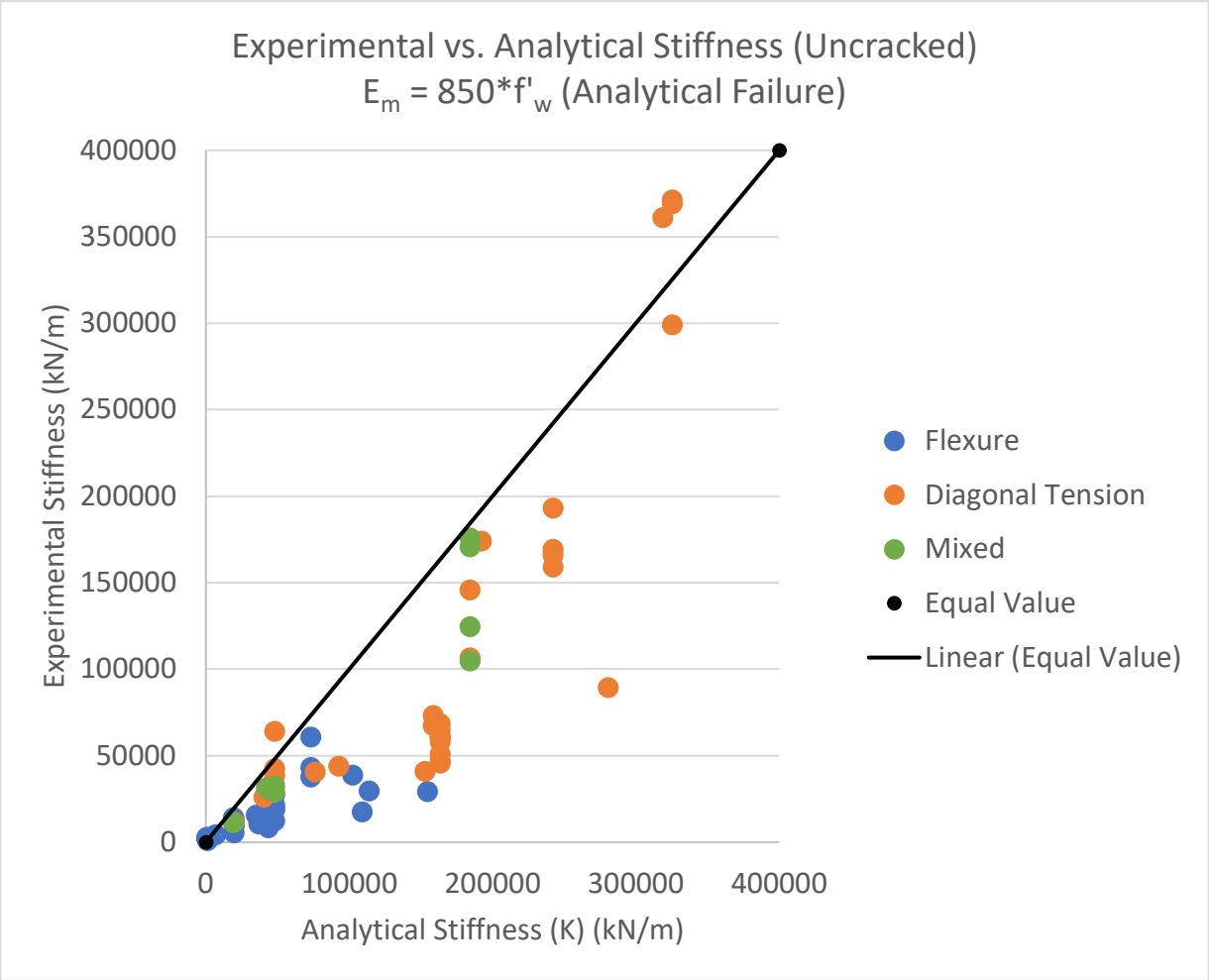

Figure 5.19) Graphical representation of experimental versus analytical stiffness values based on uncracked properties were used in analytical calculations, where failure modes have been classified based on analytical reporting

Comparison of these two sets of figures shows that the analytical stiffness value does demonstrate better convergence with experimental values when fully cracked section properties are assumed in the stiffness equation. That is, assuming a 50 percent reduction in the moment of inertia value (I_e for uncracked becomes $I_{cracked}$) leads to a better alignment between theoretical and observed values, validating the assumption present for these equations to use fully cracked values. This reduction in values accounts for the decrease in stiffness that results once cracking has occurred in the masonry along the wall, which represents a more realistic depiction of the true behaviour that occurs during testing.

The data present in these figures also depicts a trend that follows a linear profile to some degree, however, the majority of the values tend to lie beneath the equal value line of experimental

and analytical values. This signifies that the analytical stiffness values reported through the empirical relationship is overestimating the true stiffness of the specimen that was recorded during experimental testing, leading to unconservative results that are likely to underestimate the drift demands under seismic loads. This overestimation of stiffness is dangerous for design and assessment procedures since the actual deflections under loading will be much greater than what was predicted and cause rise to significant damage exceeding the acceptance criteria in the event of a seismic loading.

A key objective of the work conducted in this thesis was to not only validate a variety of assessment methods for reinforced masonry structures by comparing them to experimentally recorded results, but also to provide insight into the issues that exist in these frameworks as well as potential recommendations on how they might be improved. The systematic overestimation of the analytical estimate of the stiffness of reinforced masonry walls tested under lateral loading highlights that there are factors surrounding the true behaviour of the walls that are not currently being accounted for in the empirical estimates of the modulus and the effective stiffness. Particularly with regards to the modulus, it is plausible that the error is owing to that it is measured from compression tests where the axial load acts normal to the mortar joints of masonry, whereas under lateral loading the mortar joints are subjected to in-plane shear action. It is therefore essential to reconsider the expression for the masonry modulus E_m, provided in the CSA S304 2024.

5.2.1 Modified E_m Stiffness Calculation

The estimation of the modulus of elasticity of masonry (E_m) is based on the specified compressive strength of the masonry wall (f'_w) multiplied by a coefficient, denoted as α, with a value that varies between standards. The potential for inaccuracy in this calculation is twofold, with the first stemming from the compressive strength value of the masonry wall (f'_w). This value represents the maximum amount of stress that the wall can withstand under compressive loading, yet it still plays a crucial role in the estimation of the seismic performance and assessment of the structure. Under this form of lateral loading, the compressive strength of the masonry will not necessarily be the governing failure factor of response, and since the orientation of the load is parallel to the mortar joints, will depend on many other factors surrounding the properties of the mortar and the bond between the blocks.

The second element that can be contributing to the inaccuracy of the analytical expression is the α coefficient that is multiplied by the compressive strength of the masonry in the determination of the modulus of elasticity. The precise value of α is a debated topic in the field of reinforced masonry analysis and its validity has been an open investigation by researchers in the past. In accordance with the Canadian CSA S304 2014 code, the value of α is set to a standardised value of 850, whereas the American TMS 402 (2022) code recommends either 700 for walls built out of clay bricks, and 900 for concrete blocks. Since these values are empirical in nature, they are continuously being improved upon as more research data becomes available. Earlier versions of the TMS 402 (2022) prescribed a standardised value of 1000 for α, which was then proven by new data to not be appropriate for all types of masonry. As such, recommendations in the CSA S304 provisions have been investigated, and an alternative value of 450 for this α coefficient has been proposed by Pantazopoulou (2023) which has been shown to better align with experimental results.

With reference to this newly proposed α value of 450 used in the determination of the modulus of elasticity of the walls, the figure below depicts the relationship between the experimentally derived stiffness of the considered wall specimens, and the modified analytically determined values. From this figure, we can see that the results obtained from an α equal to 450 had an influence on the data by causing a shift in the majority of data points to the left as a result of lower analytical stiffness value. This shift allows the data to follow a closer approximation to the equal value line, with a few exceptions being the top outlying shear specimens. As such, this better approximation that results from the decreased α value indicates that it is indeed a valid recommendation to be made for the determination of the modulus of elasticity of masonry in the context of lateral loading.

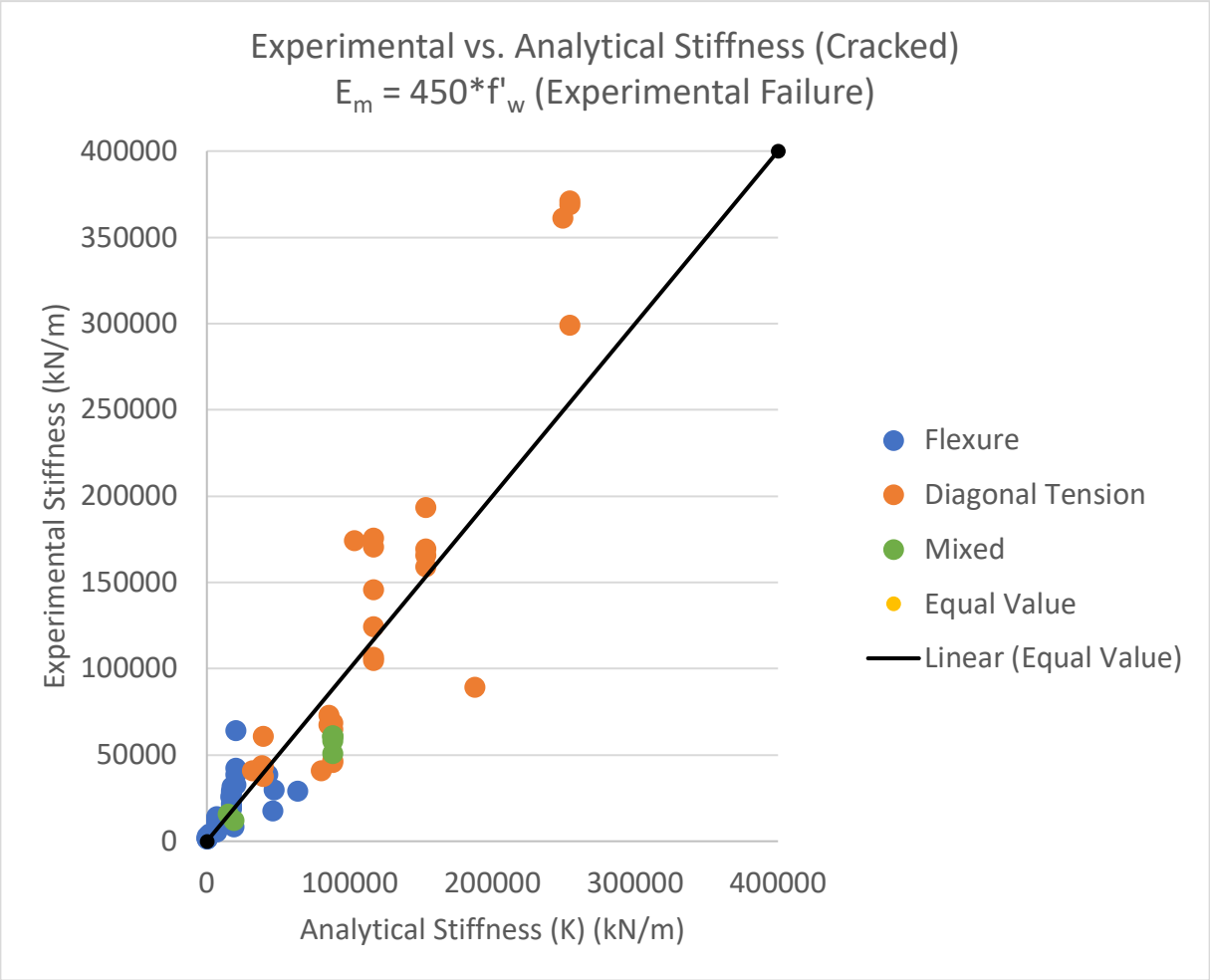

Figure 5.20) Graphical representation of experimental versus analytical stiffness values based off effective, uncracked properties with a modified modulus of elasticity ($E_m = 450 f'_w$), where failure modes have been classified based on experimental reporting*

Chapter 6

Finite Element Analysis Using ATENA

6.1 Introduction to Finite Element Analysis

This Chapter provides a discussion on the 3-dimensional Finite Element Analysis (FEA) of a reinforced masonry wall specimen considered in the database and analysed to compare the experimental behaviour recorded in the test with those obtained through FEA. Finite Element Analysis is an advanced numerical method used extensively in engineering analysis, primarily for the purpose of modelling the precisive structural behaviour of complex structures that would otherwise be far too tedious to solve through fundamental hand calculations (such as in the case of a reinforced masonry wall). The numerical procedure involves dividing the structure into a very large amount of small individual parts referred to as finite elements. These elements are connected to one another at points referred to as nodes. The software then works to assemble and solve stiffness matrices for each of these elements across the entire structure and solved for each individual element to approximate the real physical behaviour of the structure. The accuracy of these results can be fine-tuned based on the level of discretization chosen for the model. When the structure is divided into smaller parts, this process is referred to as “meshing”. A much finer mesh will have many more individual parts in comparison to a larger mesh size, which is able to provide more accurate results along the structure but requires much greater computational power.

For the purposes of this thesis, a finite element analysis conducted on GiD-ATENA 3D (Cervenka Consulting, 2023) was carried out on a reinforced masonry wall specimen that was presented in the database test matrix, built and tested in Maleki (2009). GiD was the graphical user interface program used to develop the model geometry and the analysis and post-processing was conducted on the ATENA Studio program. The follow sections will follow through the methodology used to carry out the analysis, staring with an introduction of the modelled specimen, the process and application for creating and running the finite element model of the wall, as well as a discussion of analytical results and their comparison to the experimentally recorded data.

6.2 Modelling Methodology

The follow sections will guide through the methodology used to carry out the finite element analysis on the ATENA software, staring with an introduction of the modelled specimen, the process and application for creating and running the finite element model of the wall, as well as a discussion of analytical results and their comparison to the experimentally recorded data. In addition, the results of a sensitivity analysis through the extension of the prepared model regarding

the influence of vertical (longitudinal) and horizontal (transverse) reinforcement ratios, as well as axial load, will be discussed.

6.2.1 Modelled Specimen

The test specimens presented in Maleki (2009) were partially grouted rectangular shear walls designed with the specific intent of investigating the impact that the aspect ratio and reinforcement spacing have on performance. In this study, a total of five specimens were built with constant length dimensions (equal to 1.8 m) and varied in height so as to obtain varying values of aspect ratios between the walls. For the purposes of this FEA, Wall 1 from the test matrix of the paper was considered since it had an aspect ratio of 1 and uniform spacing of vertical and horizontal reinforcing bars, making it an ideal reference case of a typical reinforced masonry wall specimen. In addition, it comprised design details, such as the amount and spacing of reinforcement in the longitudinal and transverse directions, that represented mean values found in the Canadian literature. Because of this, this specimen was chosen for the finite element analysis as it represented a typical Canadian reinforced masonry wall.

The wall was built on a rigid reinforced concrete base by a qualified mason at half scale in order to adhere to the limits of the actuator and laboratory capacities used in the test. The wall was built at half-scale, single wythe, partially grouted only in the cells that contained reinforcement and was assembled through 90 mm thick hollow concrete blocks connected via 5 mm thick mortar joints.Vertical reinforcement in the form of 10M rebar (Area = 100mm^2) and horizontal reinforcement in the form of D4 deformed wire (Area = 25.8 mm^2) were placed in end and middle sections of the wall, corresponding with typical partially grouted reinforced masonry shear wall bar spacings. This resulted in reinforcement ratios of approximately ρ_v = 0.19 % and ρ_h = 0.05 %. These were modelled in the software as 1D reinforcements and were assigned with their representative material properties as specified in the original test study. Figure 6.1 illustrates the composition of wall 1 that was modelled for the finite element analysis tested in Maleki (2009).

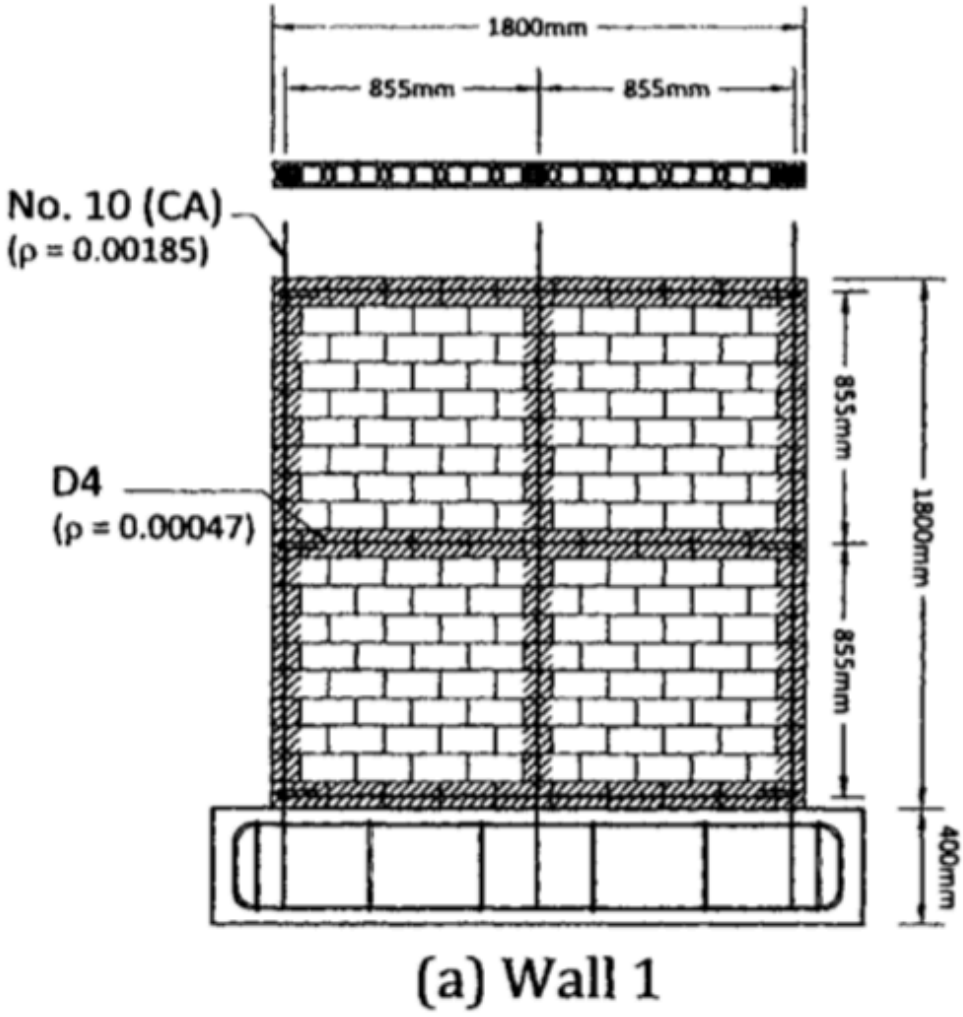

Figure 6.1) Visual representation of the considered tested wall specimen from Maleki (2009) that was modelled in the finite element analysis

6.2.2 Material Properties

Accurate representation of the material properties in the model was of paramount importance to represent the complexities that occur as a result of the composite interaction and nature of reinforced masonry construction. The model comprised of five constitutive materials being: concrete blocks, grout, mortar, steel reinforcement and air-filled voids. Each of these materials were individually defined based on either values directly reported in the literature, or were assumed based on recommended standards and guidelines, and were assigned to their representative elements in the model. Concrete, grout and mortar materials were assigned as

SOLID Elastic materials in the software, where the uniaxial compressive stress-strain response of concrete was modelled according to the Modified Hognestad parabola. Perfect bond was assumed for the steel reinforcement, which were defined in the software as a 1D reinforcement material.

When modelling the materials of the specimen, it was crucial to capture the compatibility between the individual blocks and the mortar joints to ensure that stresses were appropriately being transferred and distributed throughout the wall, which was achieved through proper modelling of common nodes between each element of the model Additionally, the air-filled voids of the concrete blocks were directly modelled as a volume with a material that comprised properties that were not to add any structural contributions to the model. The values selected for the material properties in the model were based on the reported value provided in the research whenever applicable, however, standards such as the CSA S304-24 and ASTM E111-04 (among others) were consulted for more specific properties of the concrete, mortar and grout. Within the GiD software, the following properties were assigned for each material:

6.2.2.1 Density (ρ)

The density of a material represents the ratio of mass per unit of volume of the material. The density of a material affects the experienced self-weight on the structure. Values for the materials were not directly reported in the test paper, and instead, were determined with reference to values reported in similar Canadian test studies and in accordance with CSA A165.1-24 "Concrete Masonry Units" provisions

$\rho_{mortar} = 2100\ \frac{kg}{m^3}$

$\rho_{block} = 2200\ \frac{kg}{m^3}$

$\rho_{grout} = 2300\ \frac{kg}{m^3}$

$\rho_{air} = 1.2\ \frac{kg}{m^3}$

$\rho_{steel} = 7850\ \frac{kg}{m^3}$

6.2.2.2 Onset of Crushing (F_{C0})

This material property represents the level of stress within the material at which significant failure or compressive crushing occurs, where a negative value was assigned based on the compression sign terminology in the software. This value is crucial for the assessing the loading

capacity of the masonry wall. Values for this property were not directly reported by the researchers, and so values were assumed based on recommendations from CSA S304-24 “Design of Masonry Structures”

$F_{C0,mortar}$ = -15 MPa

$F_{C0,block}$ = -12 MPa

$F_{C0,grout}$ = -15 MPa

$F_{C0,air}$ = -0.1 MPa

6.2.2.3 Fracture Energy (G_f)

The fracture energy of a material represents the amount of energy required in the material to fully propagate a crack in the material. Successful estimation of this parameter is crucial for the modelling of the post-cracking behaviour of the material, and since values were not directly reported in the test, values were instead assumed based on CSA A23.3-19 “Design of Concrete Structures” recommendations

$G_{f,mortar} = 30 \frac{N}{m}$

$G_{f,block} = 90 \frac{N}{m}$

$G_{f,grout} = 60 \frac{N}{m}$

$G_{f,air} = 0.01 \frac{N}{m}$

6.2.2.4 Modulus of Elasticity (E)

The modulus of elasticity (Young’s modulus) is defined as the ratio between stress and strain of the material in the elastic region of response. This parameter is used to represent the stiffness and deformation behaviour of the material, and values were assumed based on empirical expressions provided in the CSA S304-24 and CSA A23.1 for concrete materials were extended for the block and grout materials. In addition, ASTM E111-04 recommendations and experimental compressive test data of similar specimens built with type-S mortar in Banting (2012) were consulted for the mortar material properties.

E_{mortar} = 7000 MPa

E_{block} = 20 817 MPa

E_{grout} = 30 187 MPa

E_{air} = 0.1 MPa

E_{steel} = 200 000 MPa

6.2.2.5 Plastic Strain at Peak Compressive Stress (ϵ_{cp})

The value for the plastic strain at peak compressive stress corresponds to the level of strain in the material at which corresponds to the peak compressive stress, where compression is given a negative sign convention in the software. At this level of stress, the material undergoes recoverable elastic deformations, and permanent plastic deformations. Values for this property were assumed for the materials based on CSA S304-24 and ASTM C1314 recommendations.

$\epsilon_{cp,mortar}$ = -0.0025 MPa

$\epsilon_{cp,block}$ = -0.0015 MPa

$\epsilon_{cp,grout}$ = -0.0015 MPa

$\epsilon_{cp,air}$ = -0.0001 MPa

6.2.2.6 Critical Compressive Displacement (W_D)

The displacement that corresponds to the peak compressive strength at which the onset of crushing occurs. Beyond this point, the material experiences rapid decreases to its strength and is followed by a crushing failure. Values for this parameter were assumed based on CSA S304-24 recommendations.

$W_{D,mortar}$ = -0.3 mm

$W_{D,block}$ = -0.2 mm

$W_{D,grout}$ = -0.2 mm

$W_{D,air}$ = -0.01 mm

6.2.2.7 F_c Reduction

This term is assigned to materials to reduce the peak compressive strength (f_c) following the attainment of peak strength to model the decrease in capacity as failure occurs. This value was set to a constant 0.8 for all materials.

6.2.2.8 Aggregate Size

Represents the size of the aggregates used in the material model, which varies between each material and is not applicable for air. Values were assigned with reference to CSA A23.1 provisions and manufacturing data for type S mortar and representative block and grout samples of those used in the experiment.

Agg_{mortar} = 4.75 mm

Agg_{block} = 10 mm

Agg_{grout} = 10 mm

Agg_{air} = 0 mm

6.2.3 Macro Elements

In order to accurately model the connection between all the masonry components in the software, every individual component of the wall need to be properly connection to one another. To this end, every block was modelled as a macro element that comprised of individual nodes that were connected through lines to form a 2D surface, and then extruded into a third dimension. The first macro element defined in the model was the conventional concrete stretcher cinder block that was used in the construction of the wall, as shown in Figure 6.2 below.

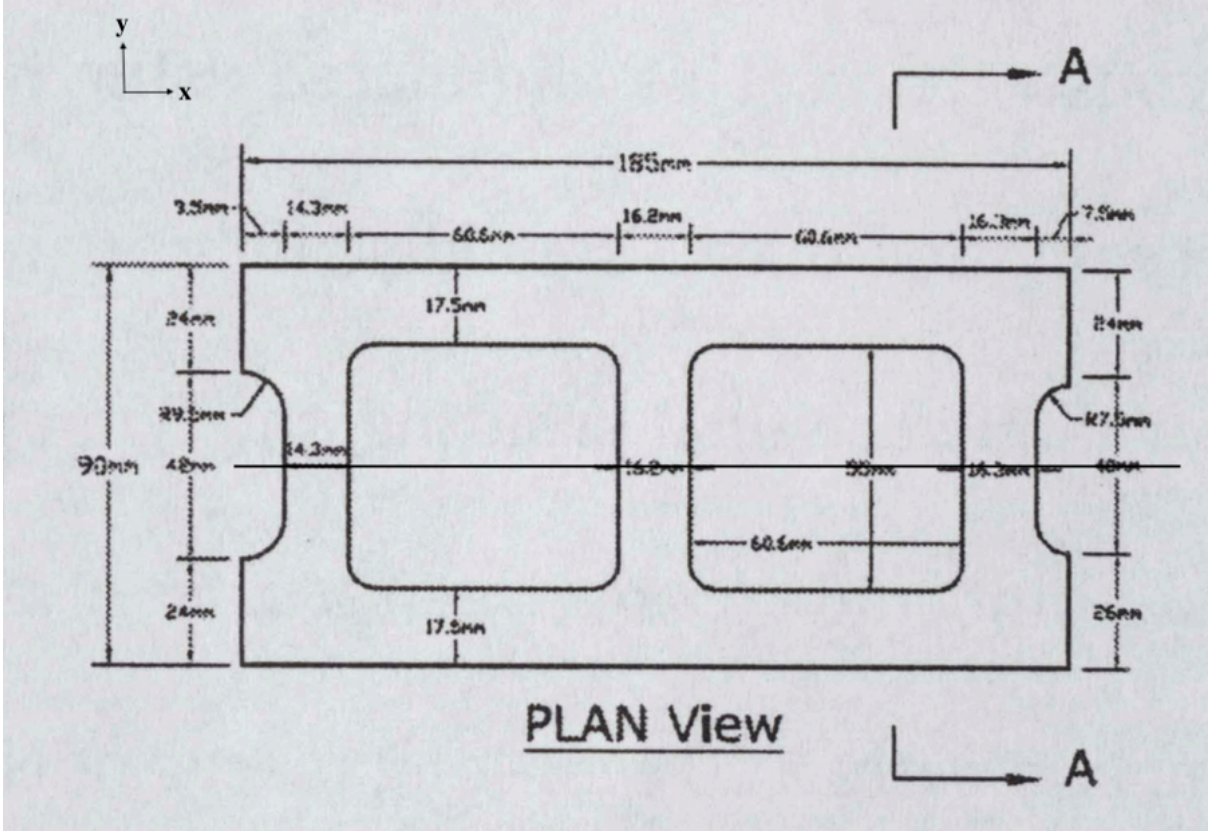

Figure 6.2) Plan view depicting the dimensions of a typical stretcher concrete masonry block used in the construction of the wall

The first step in the modelling procedure was to define nodes at the corner points of the plan view of a typical block in order construct a 2-dimensional plan view of the block. Individual nodes were connected through line elements and surfaces were defined on the closed boundaries that enclosed them. The final 2D block was then extruded into a 3D volume (shown in Figure 6.3), which was then copy and pasted numerous times until the specified height and length dimensions of the wall were achieved.

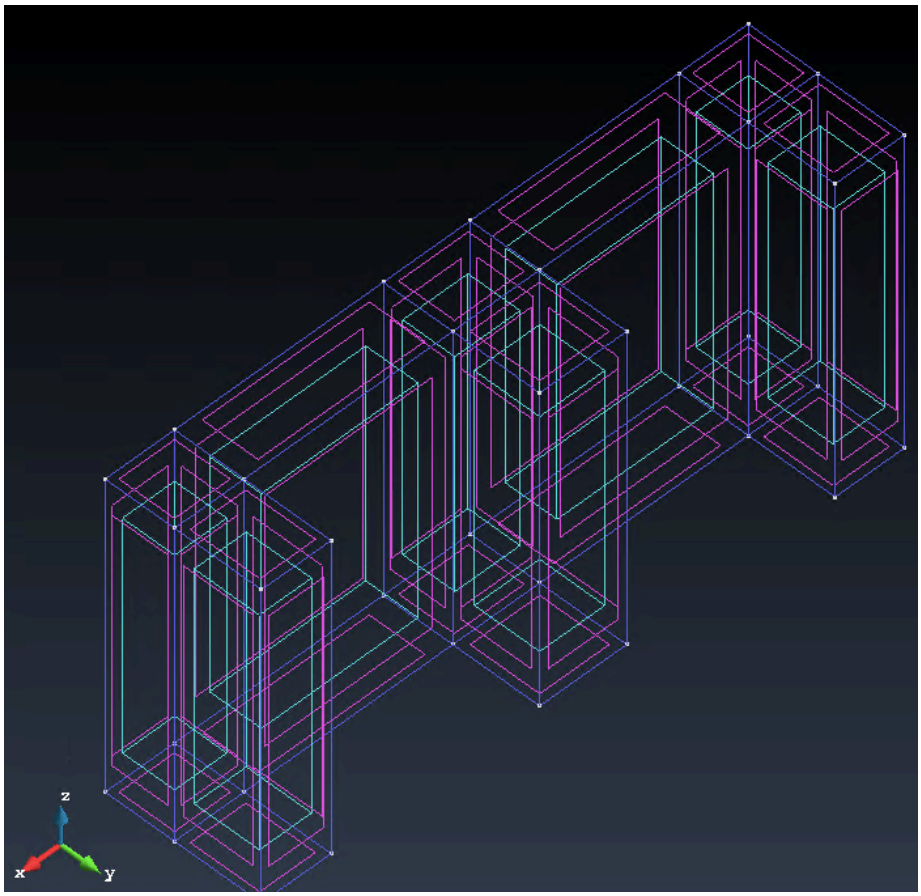

Figure 6.3) Modelled macro element of a typical masonry stretcher block that has been modelled along half of the symmetry plane

Modelling modifications were required on the block in the end zones of the wall and in regions that contained horizontal reinforcement to adhere to the specified dimensions and for the passage of reinforcement. These modifications required the modelling of a unique macro element to be made for the knockout masonry blocks, which were placed in the bottom, middle and top courses of the wall, and contained a grouted core. These units had the same dimensions as the

conventional blocks, except had their webs cut down to half their height, as seen in the model geometry of Figure 6.4 below.

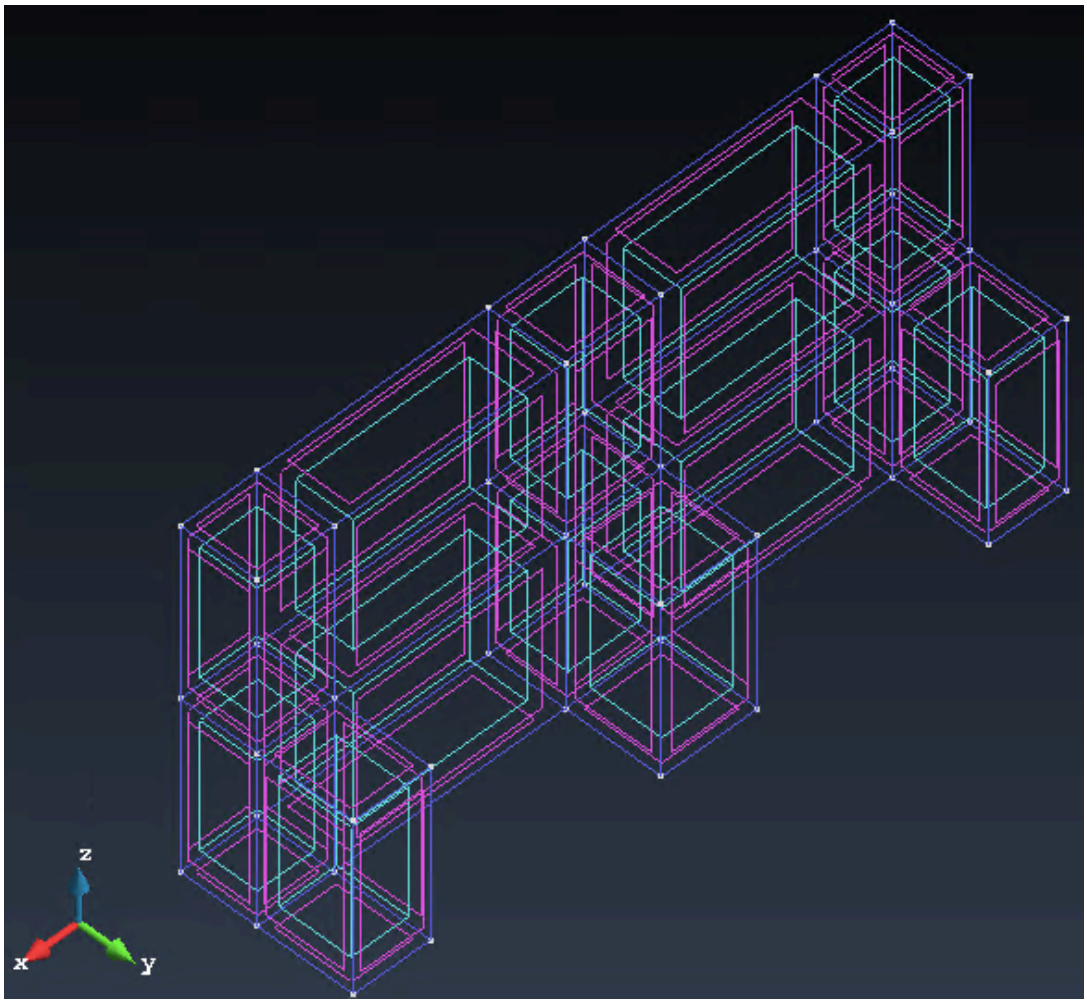

Figure 6.4) Modelled macro element of a knockout masonry block that has been modelled along half of the symmetry plane

Once the constitutive macro elements were completed, they were then copy and pasted in a repetitive manner similar to how a physical masonry wall is constructed until the entire specimen was completed. Blocks were connected though 5 mm mortar joints, which were defined in the model by extruding the top surface of the blocks and then assigned with the defined masonry material. By creating the model in this fashion, it eliminated the need for master slave surface conditions in these contact zones between the mortar and the blocks because the elements were

directly connected to one another since they were extruded from the same surfaces. Finally, the grout was defined in volumes modelled within the voids of the blocks and the reinforcement was placed in these regions. In addition, the steel loading plate at the top of the wall was modelled with loading plates on top to allow for the application of the that was simulated during the test. Combing all of this resulted in a final model that closely resembled the physical test specimen that was tested in the original experiment.

6.2.4 Boundary Conditions

Given the symmetric nature of the model in the y-direction, only half of the wall cross section was modelled in the GiD software in order to reduce the computational complexity of the assessment in ATENA Studio. This reduced the overall size of the model which allowed for a faster and more efficient computational analysis without reducing the accuracy of the results. In order to facilitate this assumption, boundary conditions were set along the out of plane (y-direction) symmetry plane on the model to restrict displacements in the y-direction. This placed a constraint at all the nodes along this plane, ensuring that they did not experience any displacements during the loading application, and effectively mirrored the other half of the wall, provided results as if the entire wall was being analysed but at a reduced computational speed. When modelling the wall in this manner, the reaction output in the ATENA Studio postprocessing analysis were multiplied by 2 in order to obtain values that represented what would have been obtained in the entire wall was modelled.

Additional boundary conditions were applied along the base of the wall in the form of pin connections at the mortar interface at the bottom of wall, and a fully fixed condition at the base of the mortar to simulate the effect of the rigid foundation. The pin supports allow for rotational movements along the interface but restricts any vertical and lateral movement that would not be likely to occur in reality. The fully fixed condition at the base restricts displacements in all three directions (x,y and z), and is meant to replicate the interaction between the wall and the rigid foundation it was built upon.

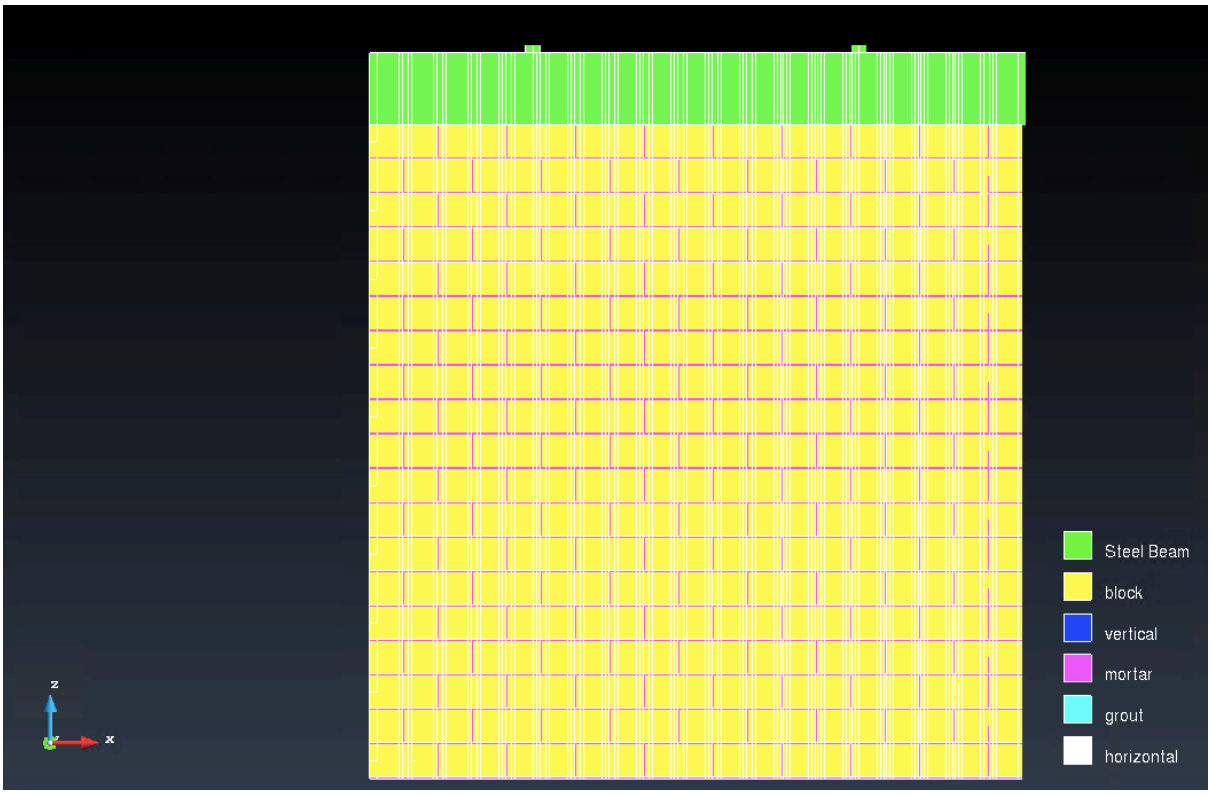

Figure 6.5) Plane XZ view of the complete wall from the front

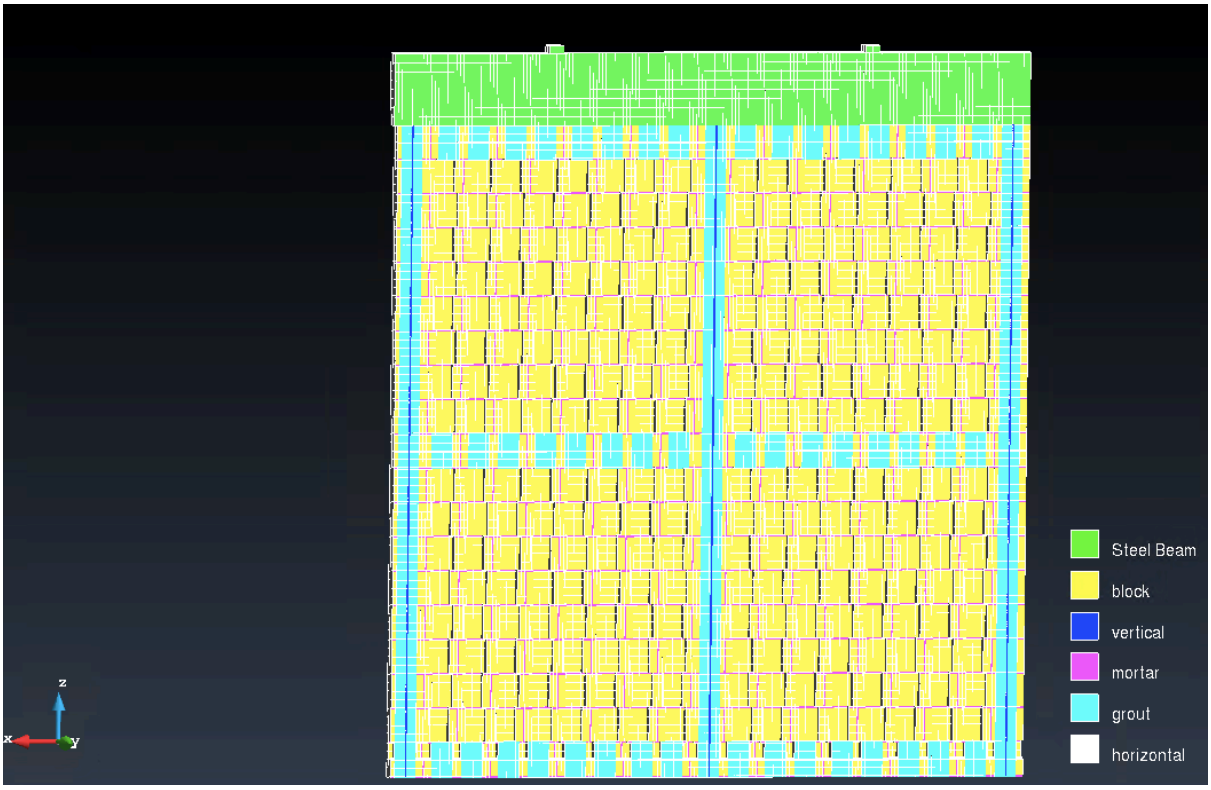

Figure 6.6) Plane XZ view of the completed wall from the back

6.2.5 Finite Element Mesh

Once the geometry of the wall was complete, a finite element mesh was assigned to the model in order to enhance the precision of the results and allow for a more precise response contour along the entirety of the wall. The mesh was generated using the automatic meshing option in the GiD software, which presented some challenges for the model since it was comprised of many individual macro elements that did not always share common nodes with one another. This was purposely done in the model since real life masonry blocks are placed in a staggered arrangement, known as running bond, so as to provide better stability and courses between rows. In order to address this issue, the individual macro elements of the blocks required additional subdividing in order to ensure that the blocks shared common nodes with the rows above and below, which ensured that a mesh could be assigned across the entire wall was relatively constant throughout the model and did not contain any errors in the element discretization process. The final mesh that was assigned to the model comprised of over 15 000 3-D, 8-noded hexahedral elements with a size of 0.5 across the entire wall, a very large number of elements when considering that this model is only half of a single wall specimen that was built in half scale, underscoring the analytical complexity that can associated with the finite element analysis of entire reinforced masonry structures. When conducting a detailed finite element analysis such as this, there exists a fine line between choosing a mesh size that is able to provide appropriate representation of the real structure, while not exceeding the computational complexity of the analysis. To this end, the value of 0.5 for the size of mesh elements was specially chosen as it yielded the most appropriate balance to this condition. In addition, the steel reinforcement bars were modelled as 1D truss elements, however, still had their corresponding dimensions properly assigned in their material definition.

6.2.6 Loading Conditions

The wall was subjected to displacement controlled, fully reversed cyclic loading through the use of a hydraulic actuator that applied the load directly at the wall top. Loading intensity began with a displacement amplitude equal to 0.01 percent drift (0.18mm) and was progressively increased by 150 percent after every cycle. Monitoring points were placed at this location to measure the reactions and displacements from the test, and very cycle was repeated two times in both the push and pull directions. Loading cycles were repeated twice and commenced until failure in the wall occurred, which was defined as when the resistance of the wall had degraded by more than 50 percent of its ultimate strength.

In addition, an applied axial compressive stress of 0.75 MPa was applied to the wall (based on gross area), and was chosen to represent the axial load likely to be resisted by a shear wall contained in a five-storey building. The load was applied in the negative Z direction through two hydraulic jacks located at the top of the wall, and was applied to a steel beam fastened to the top of the wall and connected to the wall through the vertical bars. This was assigned on the wall as two steel plates modelled at coordinates of 0.45m and 1.35m in the x-direction, which allowed for the load to transfer through the steel beam and across the entire wall. The 0.75 MPa stress corresponded to a load of 120 kN however since only half of the wall cross section was modelled for modelling purposes, the value of the applied axial load was also reduced to half, resulting in a total load of 60 kN to be applied in the negative z direction

These loading conditions were applied to the model in two interval steps as displacement-based loading, where the axial load was applied in the first and the monotonic lateral load in the second. The first step applied the axial conditions in one load step and with an interval multiplier of 1. The second load step applied a displacement of 100 mm in 500 steps, corresponding to 0.2 mm per step.

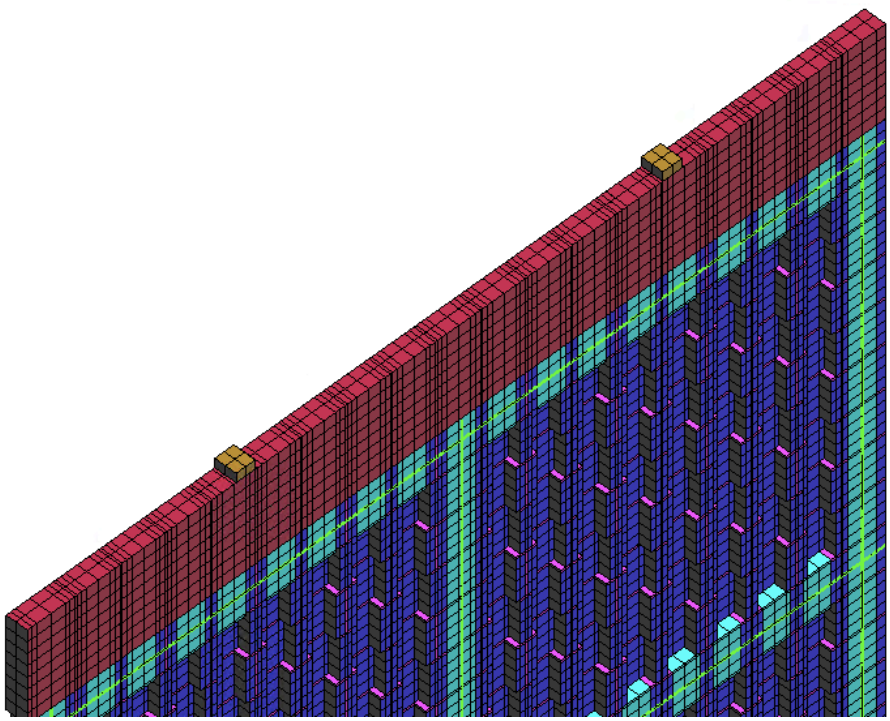

Figure 6.7) Loading beam (red) and steel plates (orange) modelled on top of the wall used for the application of the lateral and axial loads respectively

6.2.7 Analytical Results

Following the analysis of the model, a reaction-displacement output was obtained and compared against the experimentally recorded response. The load-displacement hysteresis loops of the wall recorded in the experiment is provided in Figure 6.8 below, in which a maximum load of 91.21 kN and -96.85 kN was recorded in the push and pull directions at displacements of 2.85 mm (0.158% drift) and -2.98 mm (0.166) respectively.

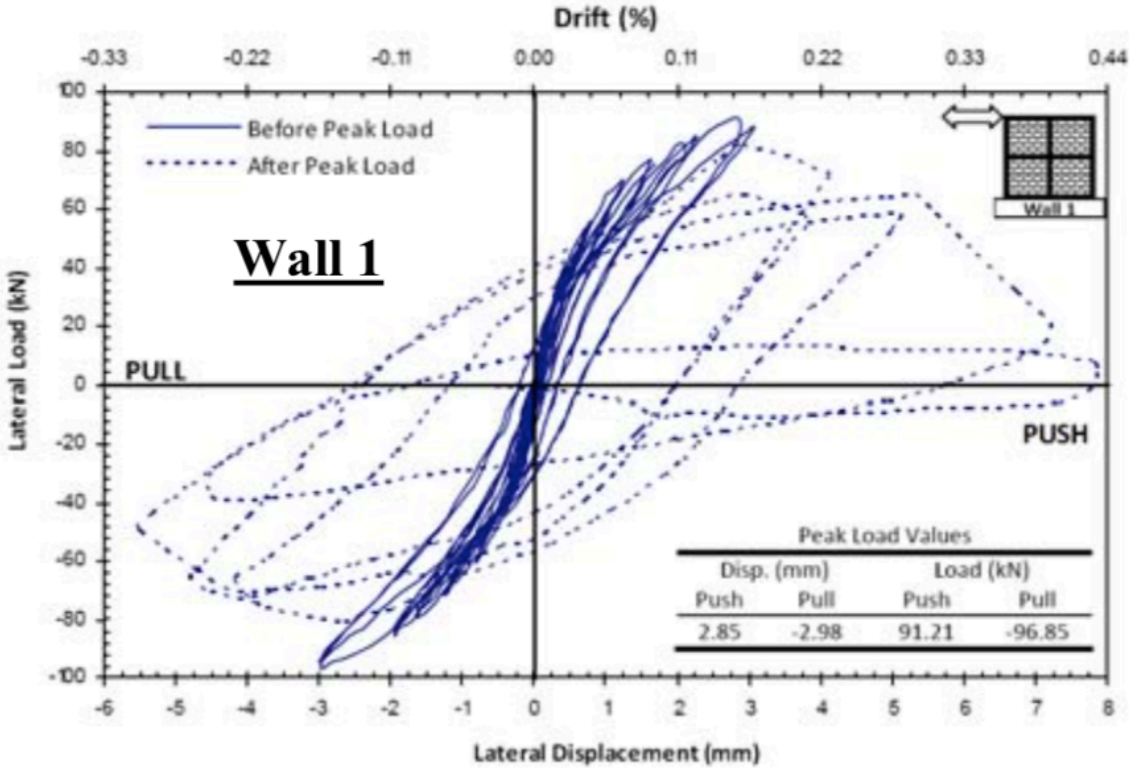

Figure 6.8) Load-displacement hysteresis loops for the tested wall from the experimental report

In comparison to the finite element response that was obtained from the model, a peak strength of 132.2 kN was achieved from the first iteration of the test which was done as a monotonic load. This was done to assess the validity of the model and the level of accuracy that is obtained through running it. This increased analytical strength obtained from the model is expected since it was loading monotonically whereas the experimental test was loaded as a cyclic load.

When a wall is tested from cyclic loads, it experiences fatigue and stresses for a longer period of time as a result of the repeating cycles before it reaches its peak strength, which in turn, weakens the wall and allows for failure to occur more easily. When it is loaded monotonically however, it does not have this same effect from the repeating loading cycles, and therefore, is not prone to this premature exhaustion that occurs during repeating load cycles. Therefore, a next step of the research will be to assess the wall under cyclic loading of the same increasing amplitude that was done in the experiment, so as to fully replicate the loading conditions that were followed in the test, which should predict a lower peak strength value the closer aligns with the experimental value.

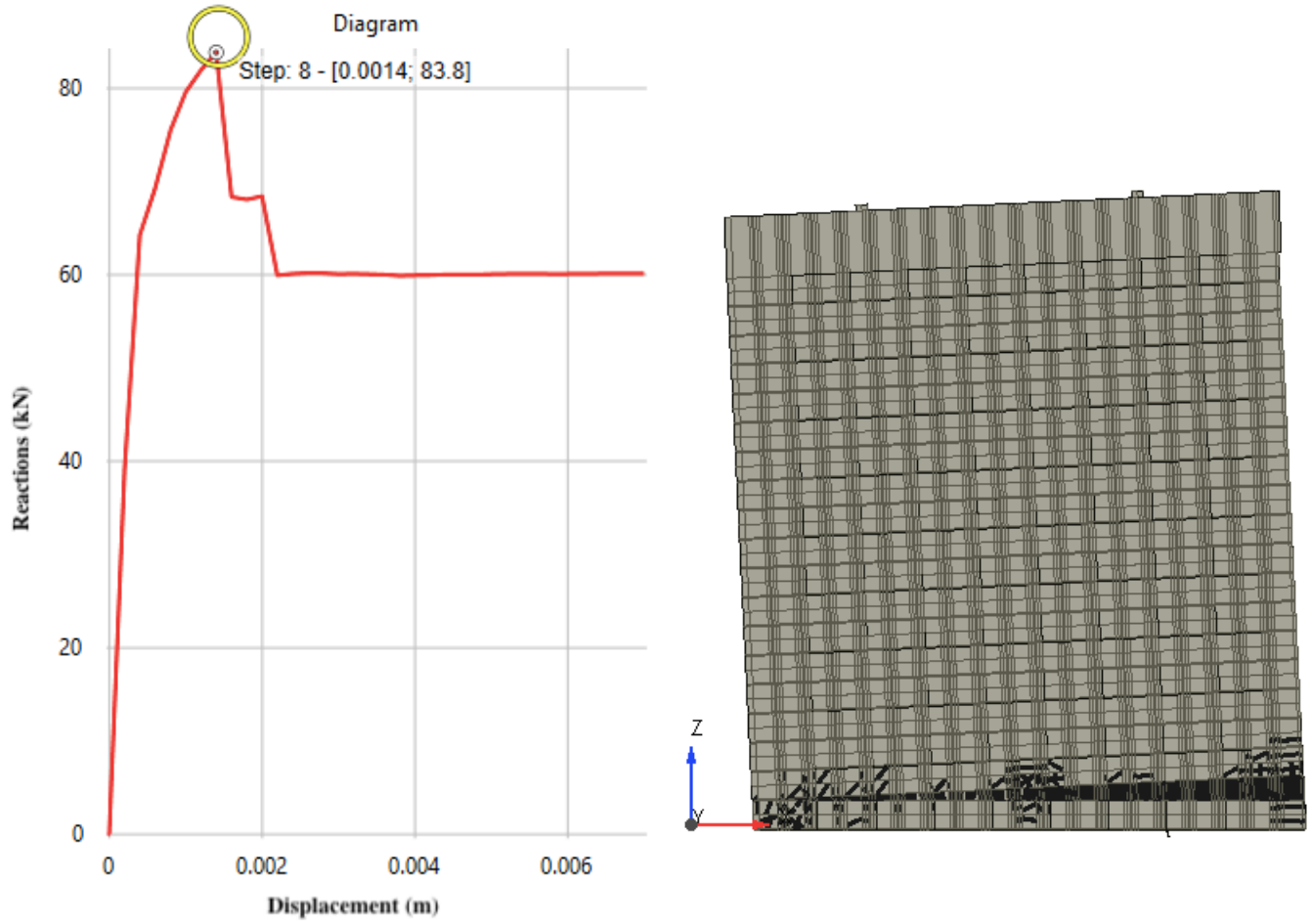

Figure 6.9) Reaction vs. displacement output data obtained from the monotonic loading of the FEA model

6.3 Sensitivity Study

The following section discusses an extension of the prepared analytical model to assess ranges of design parameters that exceeded the ranges of values commonly encountered in Canadian reinforced masonry literature. Primarily, serveral simulations were carried out for varying applied axial loads and vertical and horizontal reinforcement ratios so as to obtain a complete picture of response for a diverse range of values. A comprehensive list of the parametric values for the sensitivity analysis cases investigated is provided in Table 6.1 below:

ID	ρ_v (%)	ρ_h (%)	Axial Load (N)	$\nu = \frac{N}{A_n * f'_w}$
Long 0.2	0.2	0.3	60 000	0.03
Long 0.5	0.5	0.3	60 000	0.03
Long 1.0	1	0.3	60 000	0.03
Tran 1	0.5	0.6	60 000	0.03
Tran 2	0.5	0	60 000	0.03
Tran 3	1	0.6	60 000	0.03
Tran 4	1	0	60 000	0.03

Table 6.1) Parameter Values Used in Sensitivity Study

6.3.1 Longitudinal Reinforcement Ratio

The first three cases that were analysed in this effort were done to contain varying levels of vertical reinforcement ratio in the wall, ranging from values as low as 0.2 percent, to as high as 1.0 percent. To achieve these levels of reinforcement ratios for the specimens, the cross-sectional area of the bars in the model were adjusted while keeping the geometry and loading conditions of the model constant so that only the amount of reinforcement relative to the net area of the wall was changing between cases, thereby adjusting the vertical reinforcement ratio. The horizontal (transverse) reinforcement ratio was also held constant for the tests so as to ensure only the

influence stemming from the vertical reinforcement was being considered as results were compared between the first three cases.

6.3.1.1 Long 0.2

The first sensitivity analysis case contained a longitudinal reinforcement ratio of 0.2 percent and transverse reinforcement ratio of 0.3 which was modelled in the software by assigning cross-sectional areas to the longitudinal and transverse bars of 16.2 mm^2 and 24.3 mm^2 respectively. It is important to note that the true cross-sectional of the bars needed to achieve this level of reinforcement ratio are actually double these values (32.4 mm^2 and 48.6 mm^2), however since only half of the wall was modelled, the amount of reinforcement also required adjustment to adhere to this reduction in the net area of the wall. This procedure was followed for every case of the sensitivity analysis, and was accounted for in the ATENA Studio postprocessing by assigning a multiplier of two the output results.

From the results of the ATENA analysis, a peak strength of 91.1 kN was achieved at a lateral displacement of 0.8 mm, corresponding to a drift of 0.044 percent. As the sensitivity analysis progresses, it can be expected that this level of drift will increase as the larger amounts of longitudinal reinforcement ratios provide enhanced ductility capabilities.

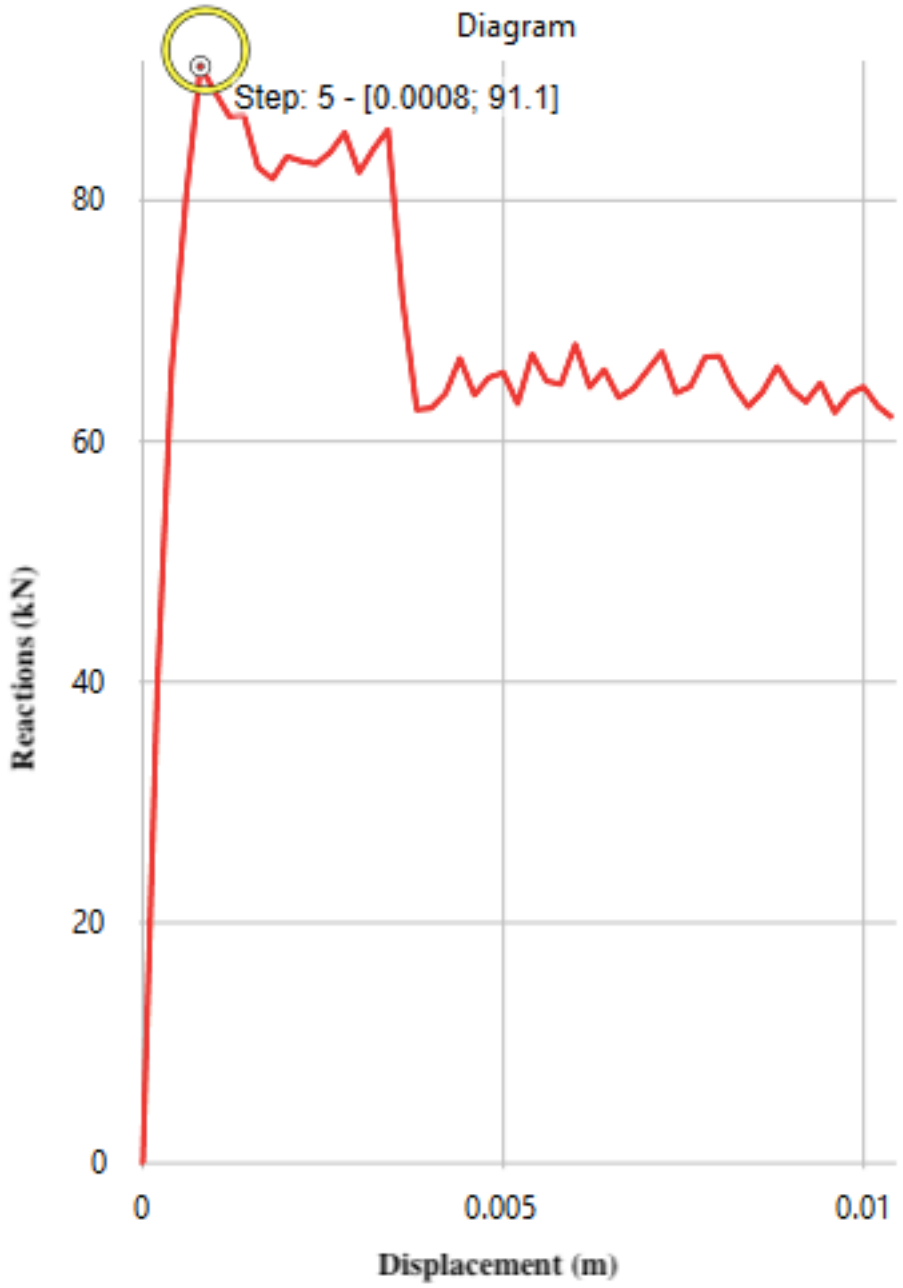

Figure 6.10) Load displacement output plot from ATENA Studio analysis of Long 0.2

The deformed shape model of the wall displays clear flexural cracking at the critical region near the base of the wall, where the largest moments occur. In addition, slight buckling of the vertical reinforcements in the compression zone can be observed.

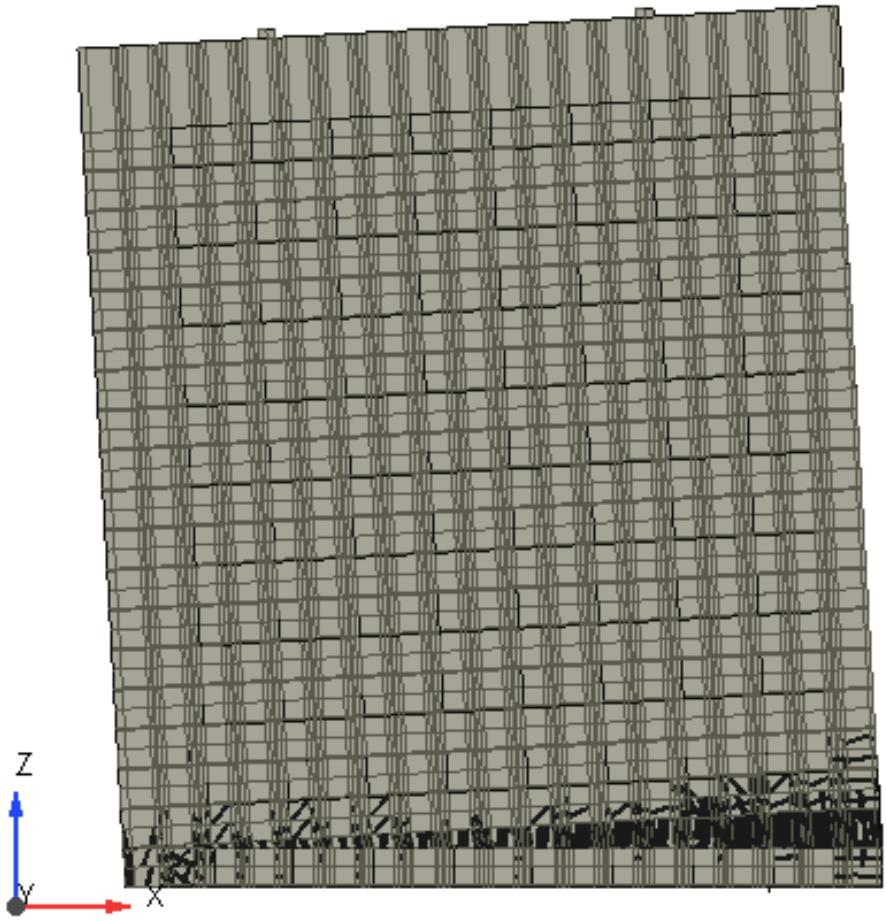

Figure 6.11) Deformed shape cracked model from ATENA Studio analysis of Long 0.2

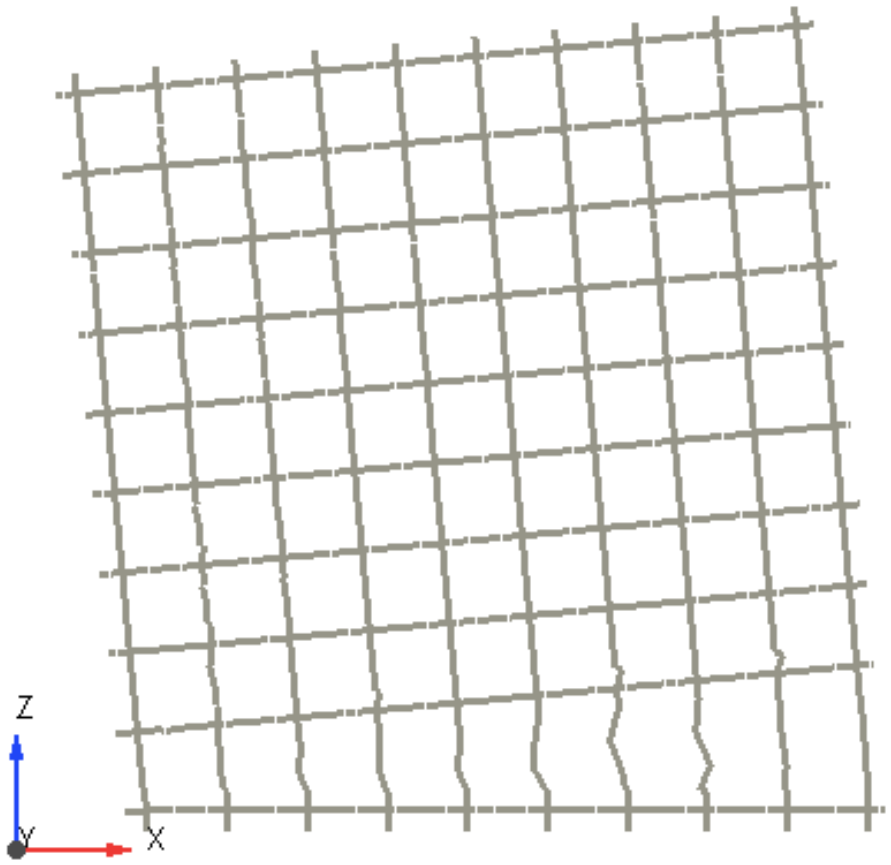

Figure 6.12) Deformed shape 1D model ATENA Studio analysis of Long 0.2

6.3.1.2 Long 0.5

The second trial carried out in the sensitivity analysis was done with an increase in the longitudinal reinforcement ratio to 0.5 percent, while keeping all other design variables consistent with the preceding case. By running though values of progressively greater amounts of transverse reinforcement in the model, the true influence stemming from these reinforcements, in terms of its load carrying capacity and failure mode, can be examined.

As illustrated in the output from the ATENA analysis, peak strength with a magnitude of 111.9 kN was achieved at a lateral displacement of 12 mm, corresponding to a drift of 0.67 percent.

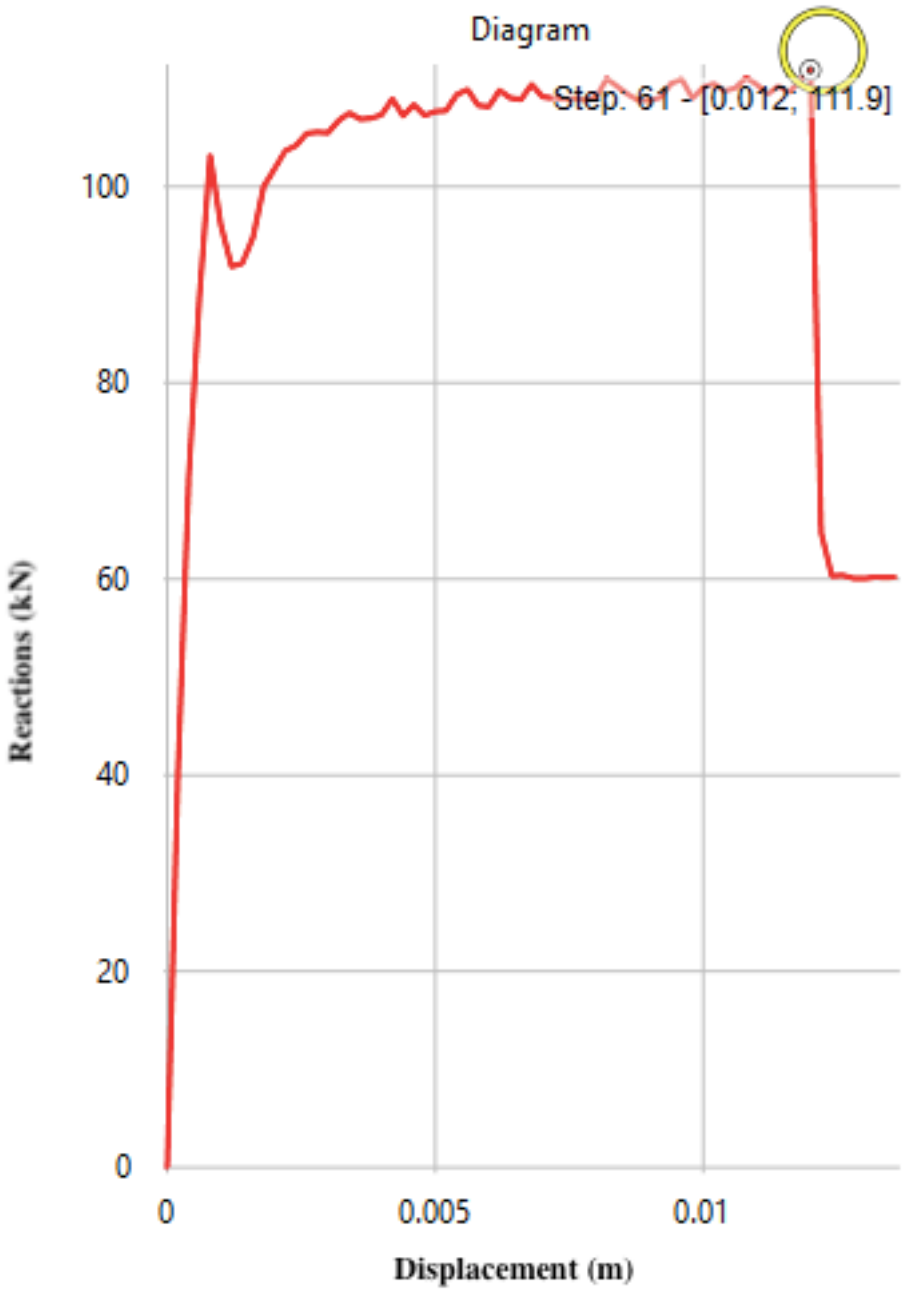

Figure 6.13) Load displacement output plot from ATENA Studio analysis of Long 0.5

Evident in the deformed shape and displayed damage of the wall, flexural cracking in the critical regions towards to base of the wall were observed. In addition, the attainment of the peak strength of the wall occurred much later on as a result of a a greater drift capacity of the wall.

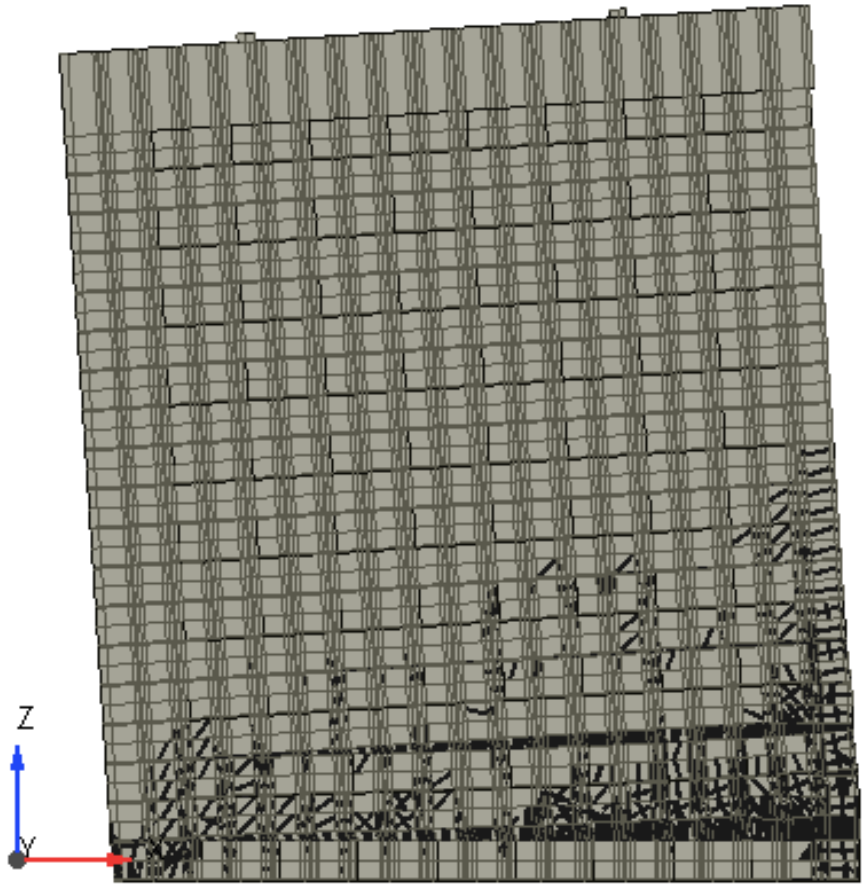

Figure 6.14) Deformed shape cracked model from ATENA Studio analysis of Long 0.5

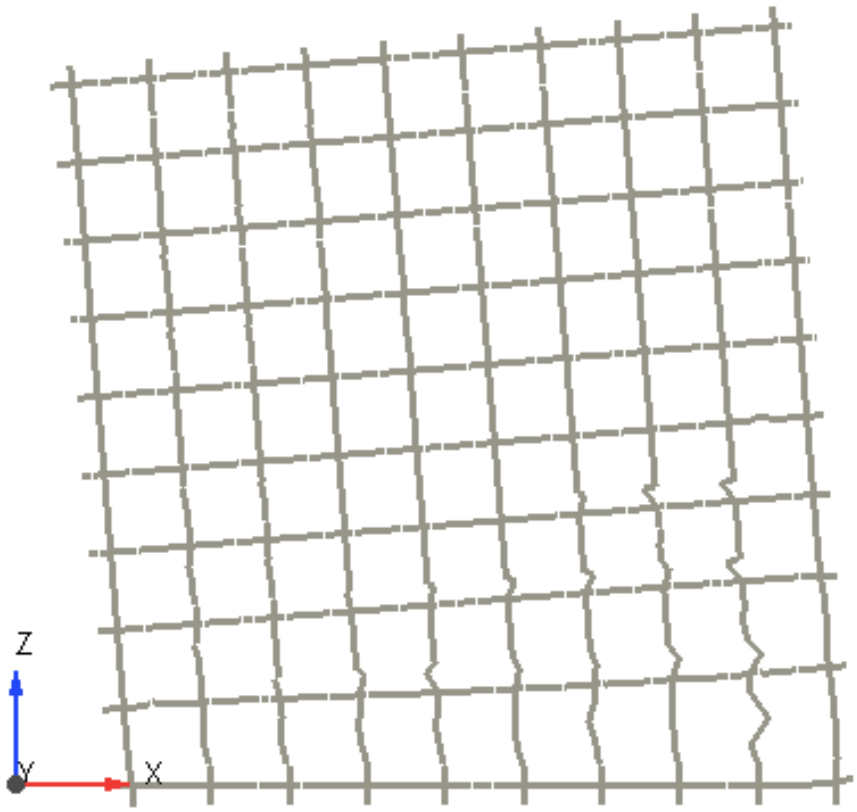

Figure 6.15) Deformed shape 1D model from ATENA Studio analysis of Long 0.5

6.3.1.3 Long 1.0

The third sensitivity simulation contained the greatest longitudinal reinforcement ratio of all cases at a value of 1.0 percent. This increased amount of reinforcement explored the upper bounds of typical values found in the literature, and displayed a much larger peak strength and drift capacity in comparison to the other simulations. As expected, the increase in longitudinal reinforcement allowed the wall to achieve a greater peak strength as well as lateral drift capacity.

The ATENA Studio output results shown below indicate that a peak strength of 152.1 kN that was achieved at a lateral displacement of 10.2 mm, corresponding to a drift ratio of 0.57 percent.

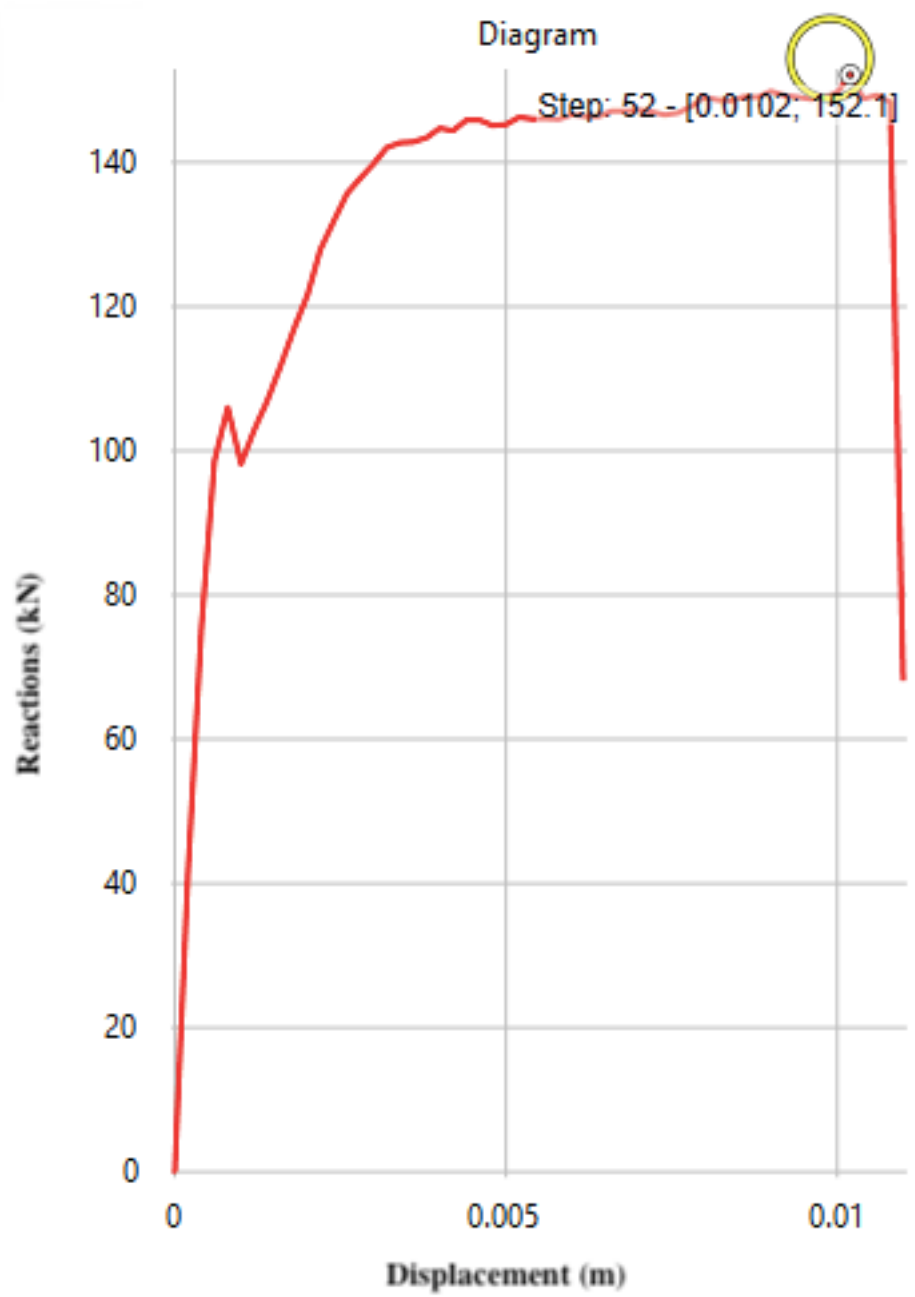

Figure 6.16) Load displacement output plot from ATENA Studio analysis of Long 1.0

The development of damage in the wall displayed flexural cracking across various regions of the wall, primarily in the critical region in the lower section of the wall. In addition, the

deformed model did not display as much of a pronounced diagonal crack as what was observed in the model with a lower transverse reinforcement of 0.5 percent as a result of the more ductile characteristics that come with greater amounts of reinforcement.

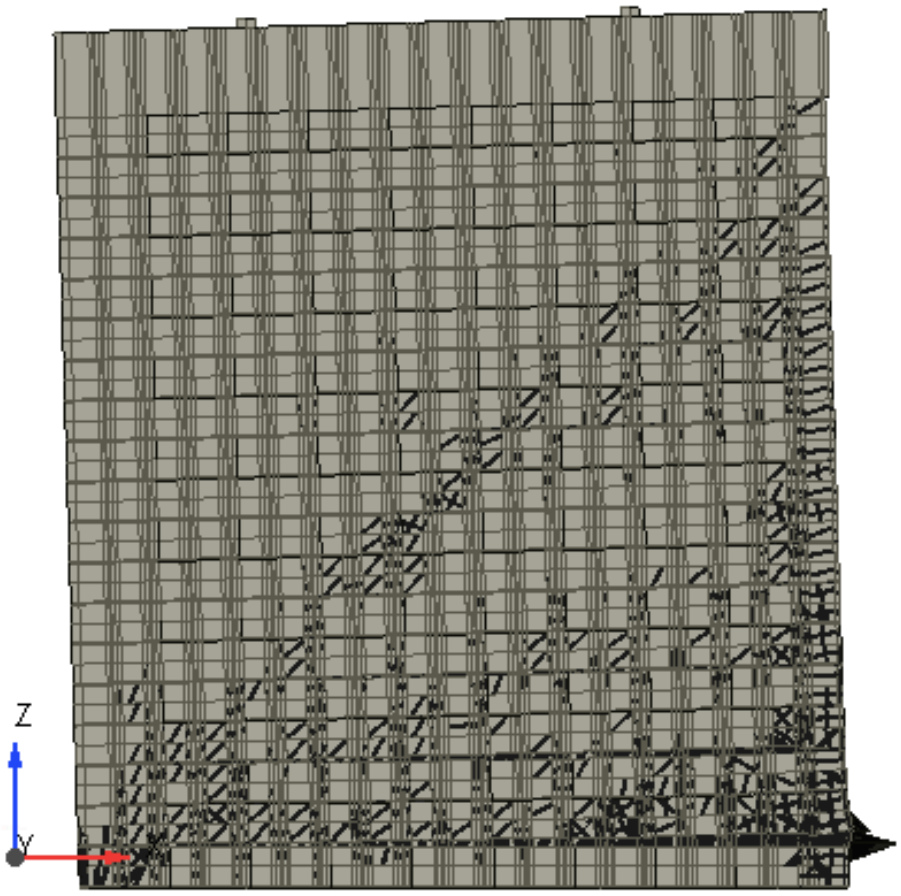

Figure 6.17) Deformed shape cracked model from ATENA Studio analysis of Long 1.0

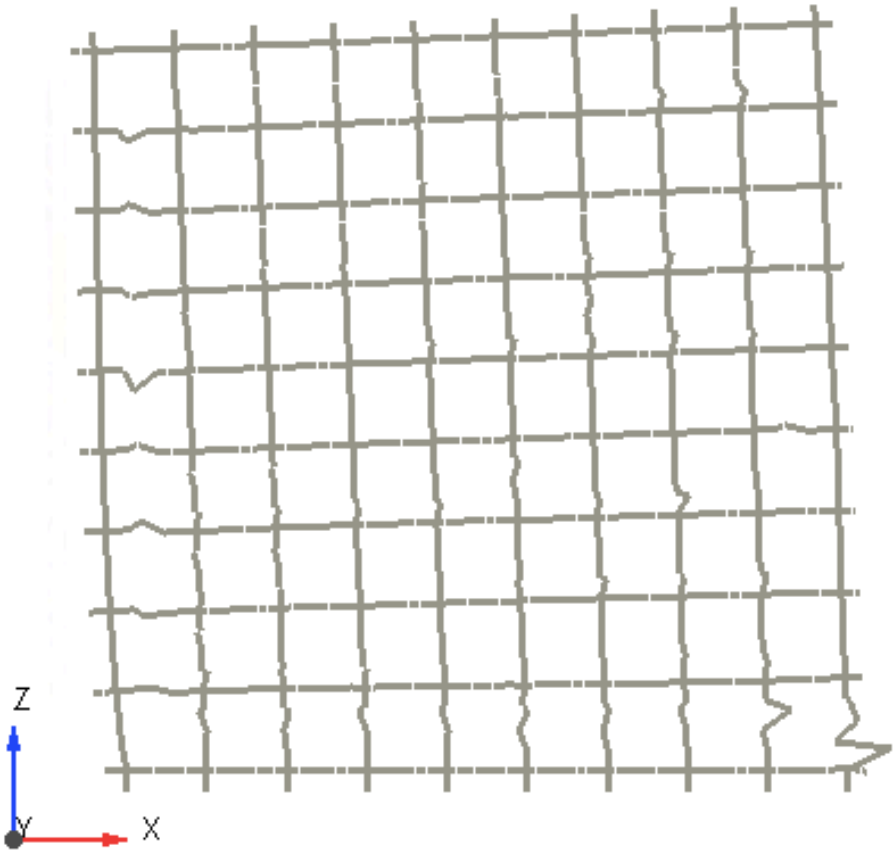

Figure 6.18) Deformed shape 1D model from ATENA Studio analysis of Long 1.0

6.3.1.4 Discussion of Results

Based on these results, it was found that as greater amounts of longitudinal reinforcement ratios were assigned to the model, the peak strength of the wall increased. An interesting observation to be made is that although the specimen with a longitudinal reinforcement ratio of 1 percent outperformed that of the one with 0.5 percent, a greater lateral drift at which this peak was attained at was obtained in the specimen with the lower longitudinal reinforcement ratio.

When comparing the deformed and damaged shape models of the walls, Long 0.2 and 0.5 cases displayed clear flexural behaviour, where the damage was greater in the case with the greater

amount of reinforcement ratio. This was likely due to the fact that failure in the Long 0.2 occurred quite early in the loading processes and did not allow for additional damage to occur.

For the Long 1.0 trial, a clear diagonal tension failure was observed in the deformed model as the excessive amount of vertical reinforcement provided a greatly increased flexural strength capacity, which in turn, ensuring that the mode of failure in the wall was a shear related one as this is the mode it was more under-designed in.

6.3.2 Transverse Reinforcement Ratio

The next set of simulations carried out in the sensitivity analysis investigated the influence that stemmed from the transverse reinforcement. In a similar manner to the preceding cases, various levels of transverse reinforcement were assigned to the model while keeping all other design variables constant.

6.3.2.1 Tran 1

The first simulation in this set of cases contained a transverse reinforcement ratio of 0.6 percent, and a constant axial load and longitudinal reinforcement of 60 kN and 0.5 percent respectively. From this analysis, a peak load of 111.8 kN was achieved at a lateral displacement of 8.2 mm, corresponding to a drift of 0.46 percent.

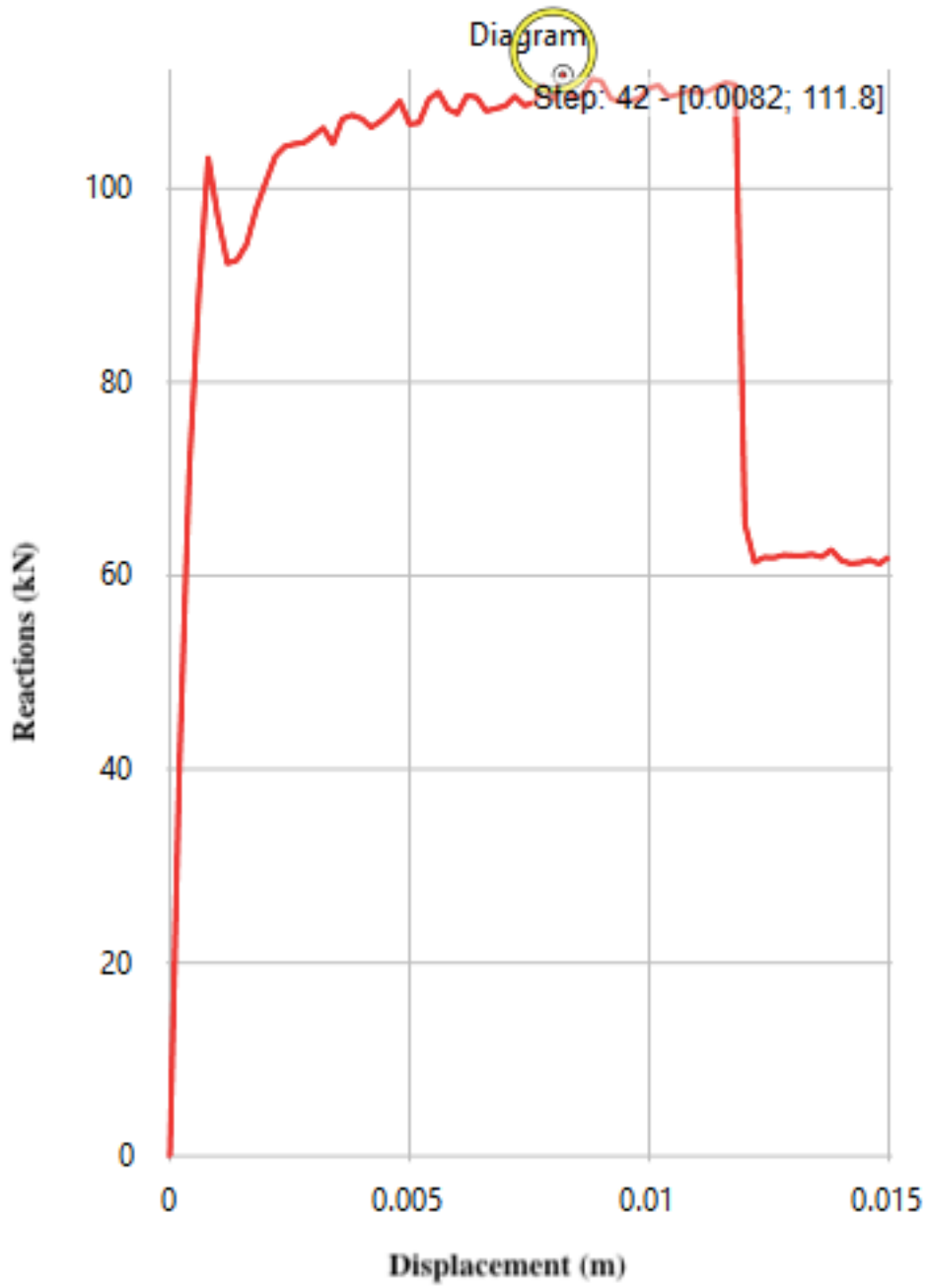

Figure 6.19) Load displacement output plot from ATENA Studio analysis of Tran 1

From the deformed shape model, clear defined flexural cracking in the critical region of the wall, which was located near the bottom of the wall where maximum moment is located, was achieved. In addition, buckling of the vertical reinforcement bars in the compression zones near the application of the lateral load.

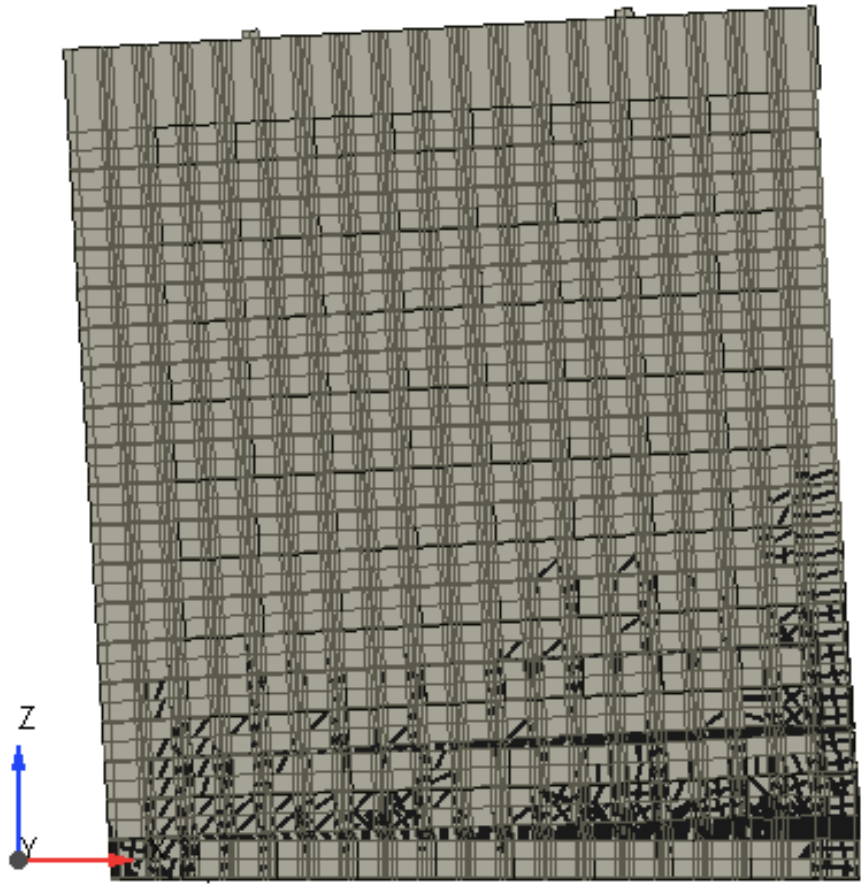

Figure 6.20) Deformed shape cracked model from ATENA Studio analysis of Tran 1

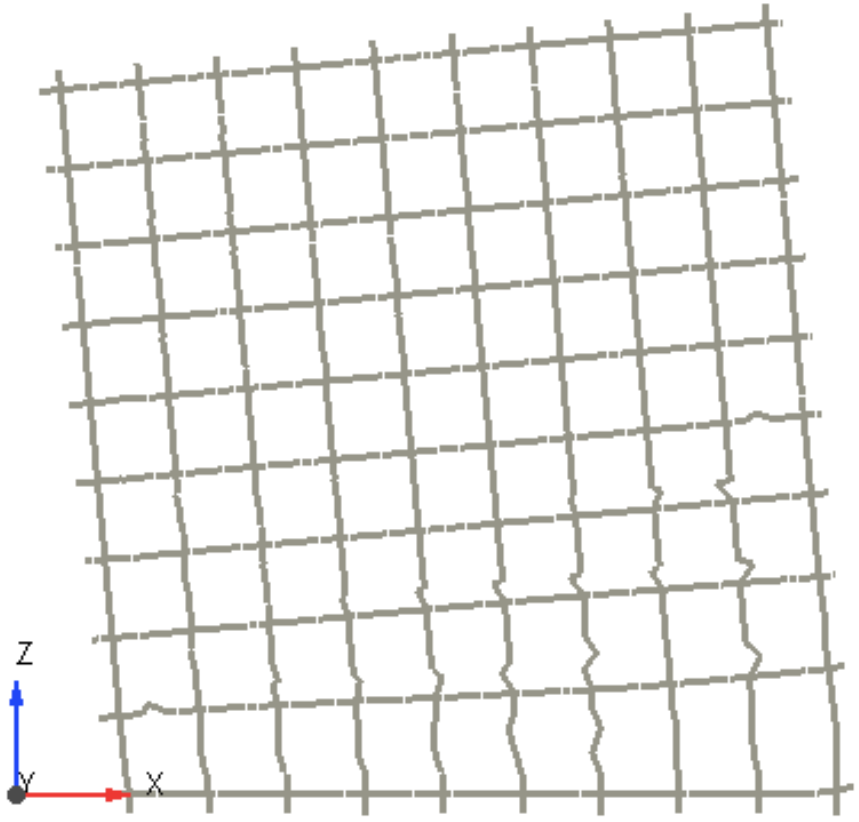

Figure 6.21) Deformed shape 1D model from ATENA Studio analysis of Tran 1

6.3.2.2 Tran 2

The second trial was identical to the previous Tran 1 trial, except the transverse reinforcement ratio was set to zero. By eliminating the contribution from the horizontal reinforcement, the contribution from the longitudinal reinforcement can be isolated and results can be compared with those achieved in the preceding case.

The results of the analysis displayed a peak load of 110.1 kN at a lateral displacement of 10.2 mm, corresponding to a drift of 0.57 percent.

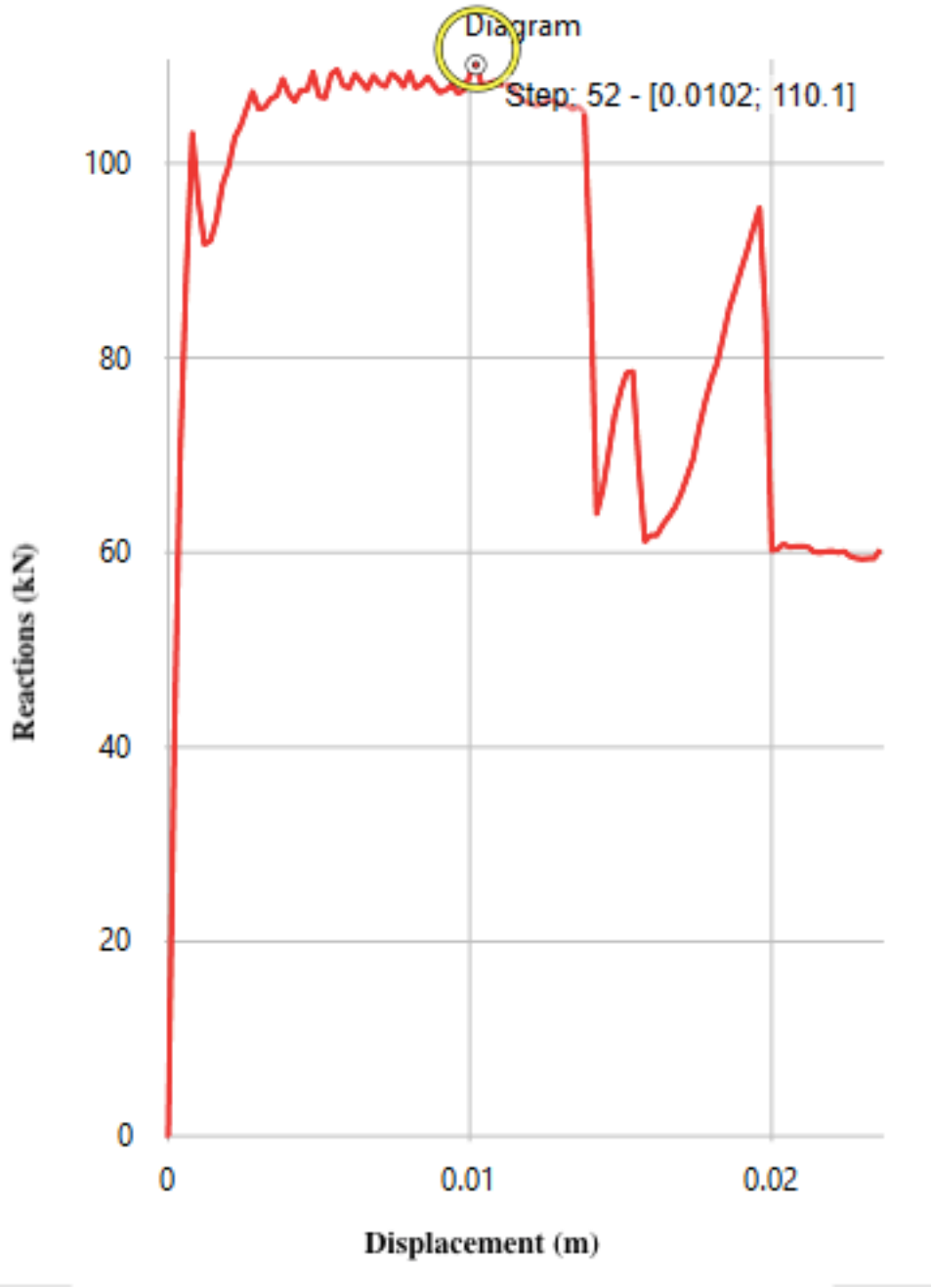

Figure 6.22) Load displacement output plot from ATENA Studio analysis of Tran 2

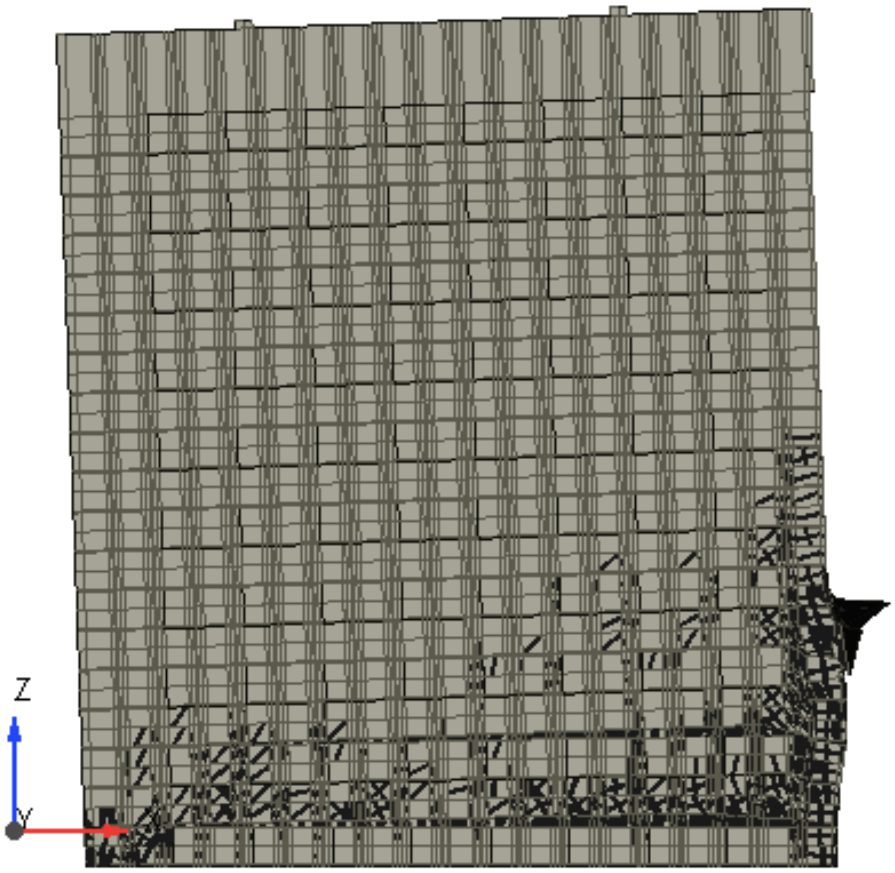

Figure 6.23) Deformed shape cracked model from ATENA Studio analysis of Tran 2

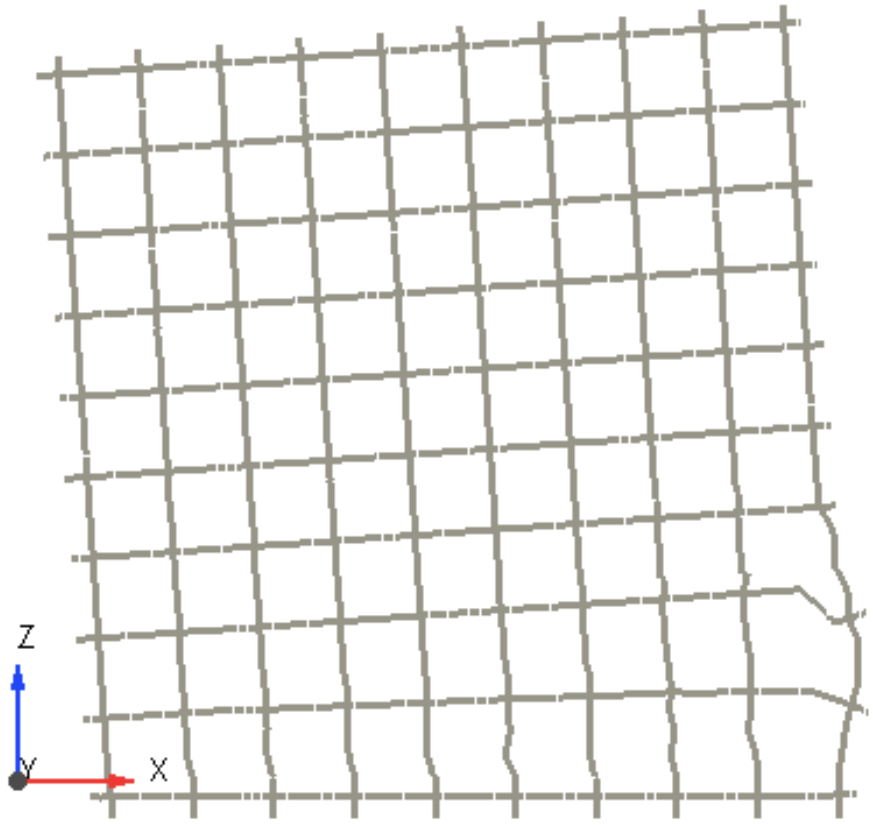

Figure 6.24) Deformed shape 1D model from ATENA Studio analysis of Tran 2

By comparing the results from the Tran 1 and Tran 2 cases, it is evident that the absence of horizontal reinforcement decreased the load carrying capacity of the wall but had a slight increase on the drift capacity at which the peak was attained at. In both cases, flexural cracking was observed in the critical region of the wall, however, the absence of transverse reinforcement in case Tran 2 resulted in substantial yielding and deformation of the reinforcement of the compression face of the wall.

6.3.2.3 Tran 3

The following set of simulations followed a similar trend of the first set to set the transverse reinforcement ratio to zero, however only different in the fact that these models contained an increased longitudinal reinforcement ratio of 1.0 percent as opposed to 0.5 percent. The results of the analysis from this wall, which contained a transverse reinforcement ratio of 0.6 percent, displayed a peak load of 214 kN at a lateral displacement of 4.8 mm, corresponding to a drift of 0.27 percent.

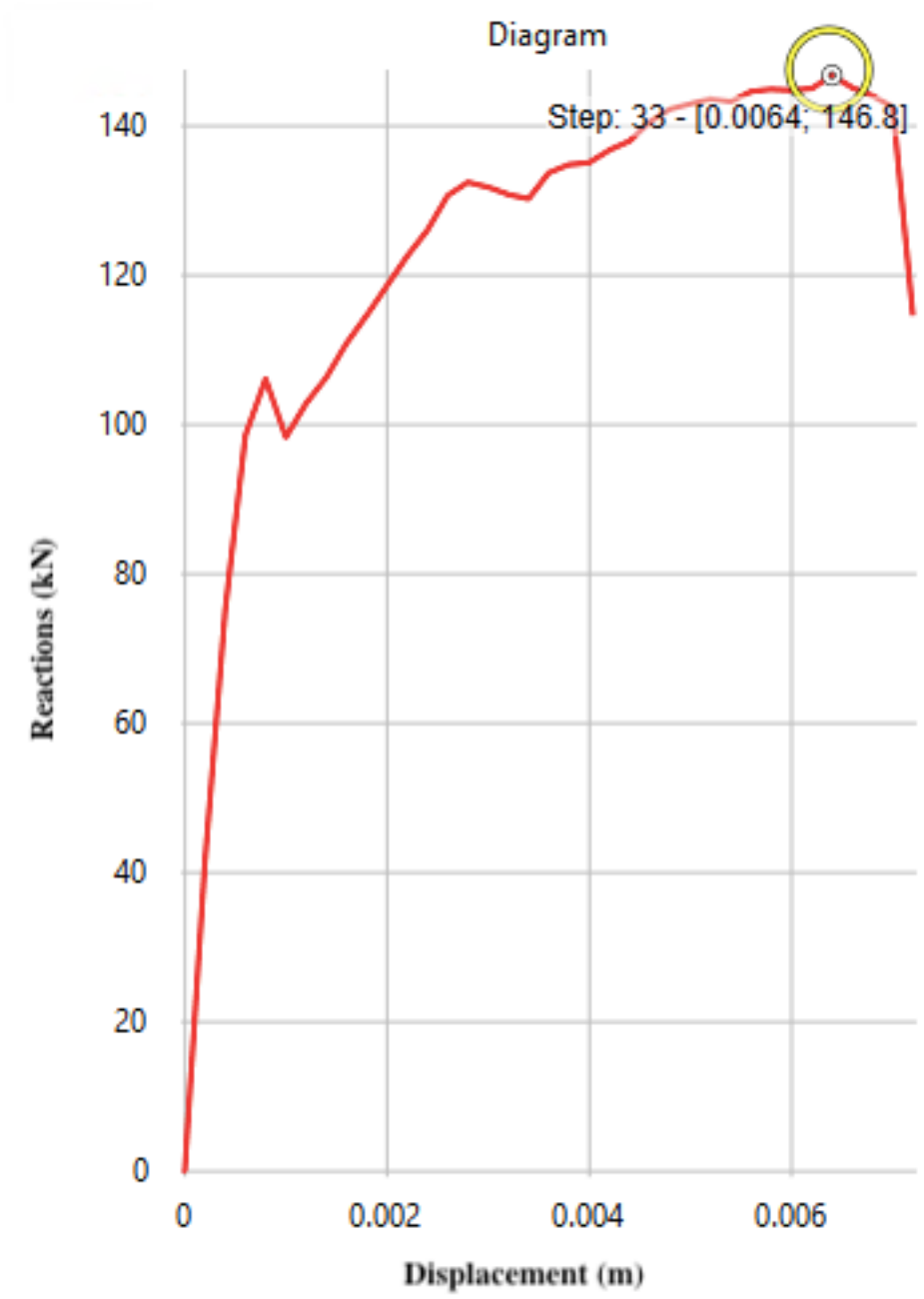

Figure 6.25) Load displacement output plot from ATENA Studio analysis of Tran 3

The deformed shape model wall displays extensive amounts of damage spread out across the entirety of the wall, indicating a wide spread failure mechanism owing to both compressive and tensile failures.

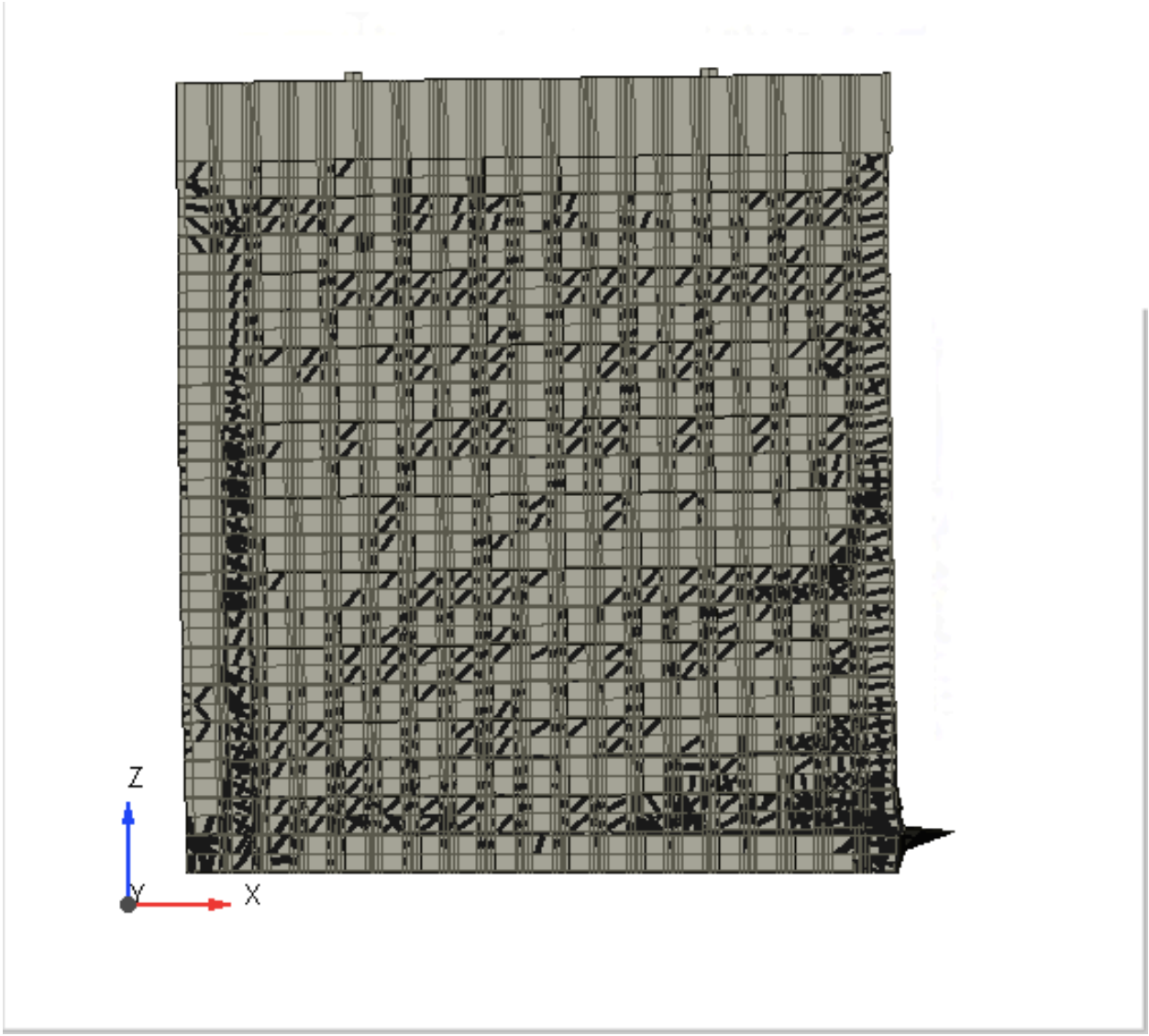

Figure 6.26) Deformed shape cracked model from ATENA Studio analysis of Tran 3

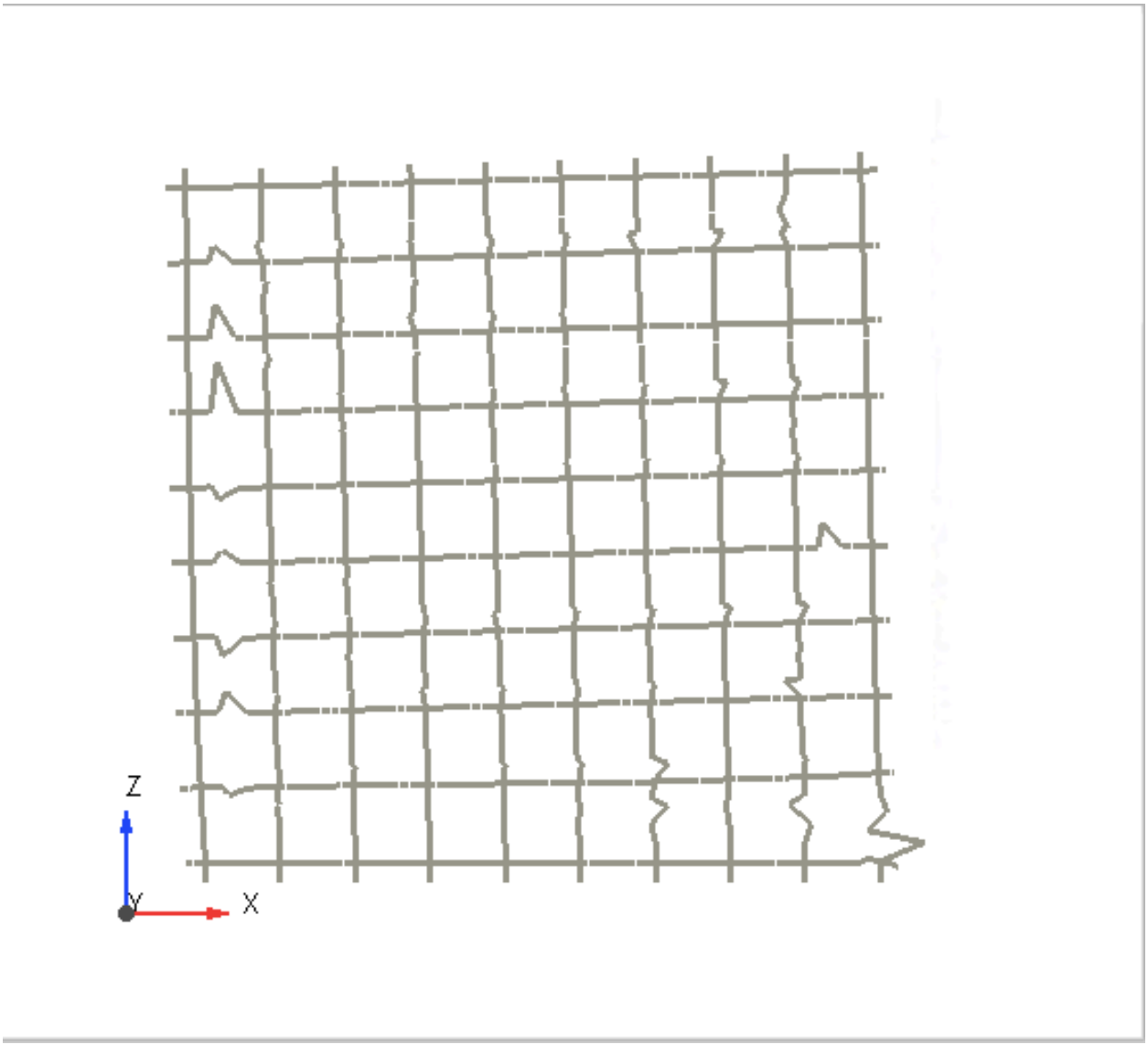

Figure 6.27) Deformed shape 1D model from ATENA Studio analysis of Tran 3

6.3.2.4 Tran 4

The fourth and final trial pertaining to the transverse reinforcement cases was identical to the preceding case except without the presence of any horizontal bars for the purpose of achieving the same comparison made between Tran 1 and Tran 2 cases. From the ATENA analysis, a peak strength of 146.8 kN was attained at a lateral displacement of 6.4 mm, corresponding to a drift of 0.35 percent.

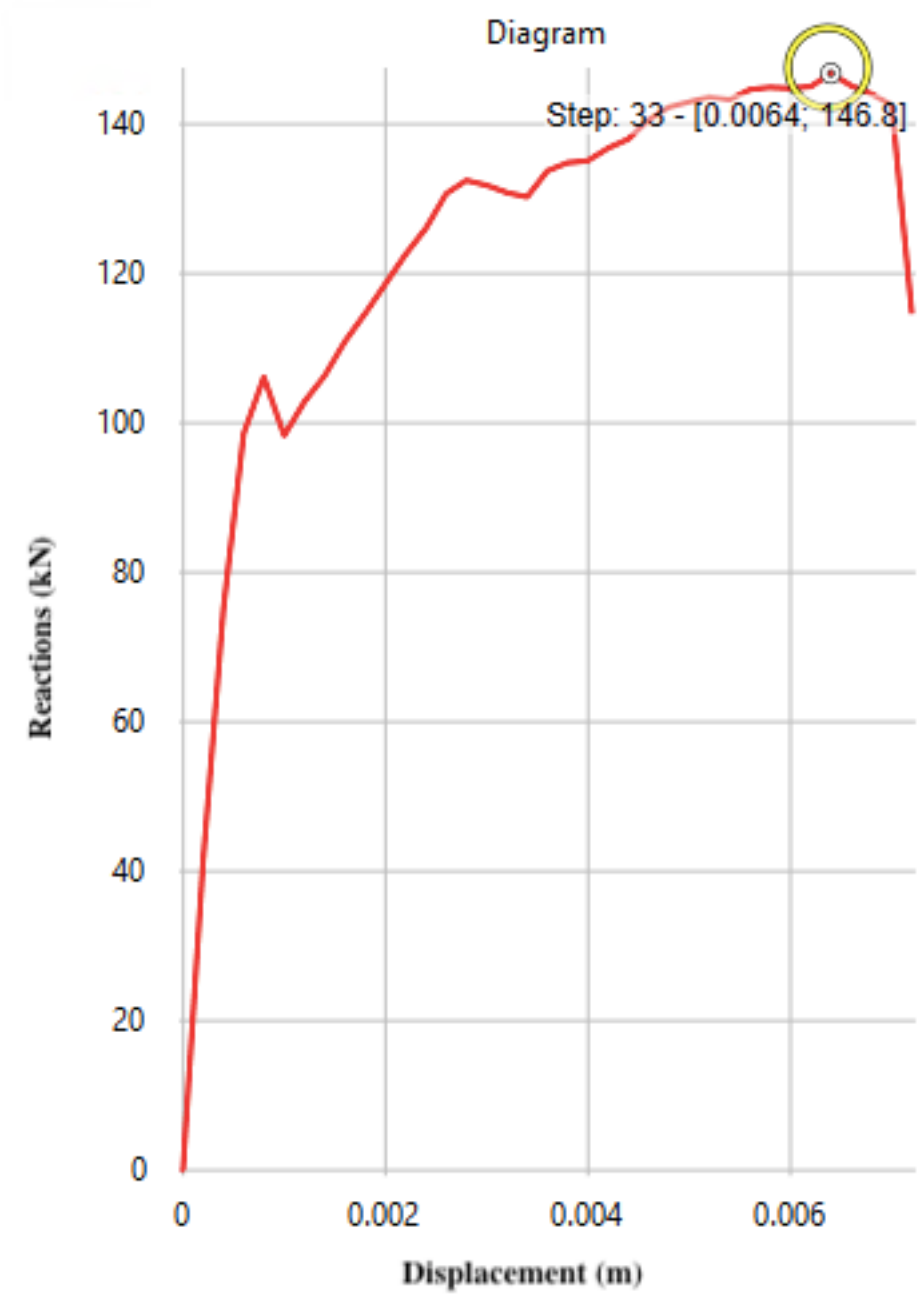

Figure 6.28) Load displacement output plot from ATENA Studio analysis of Tran 4

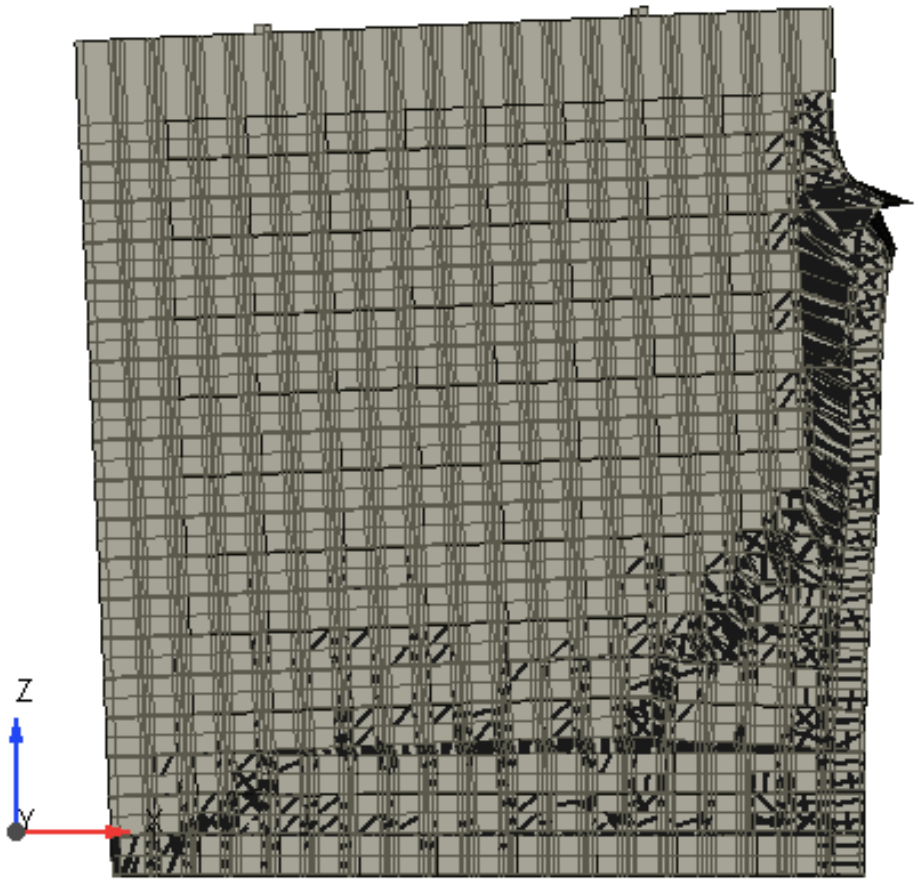

Figure 6.29) Deformed shape cracked model from ATENA Studio analysis of Tran 4

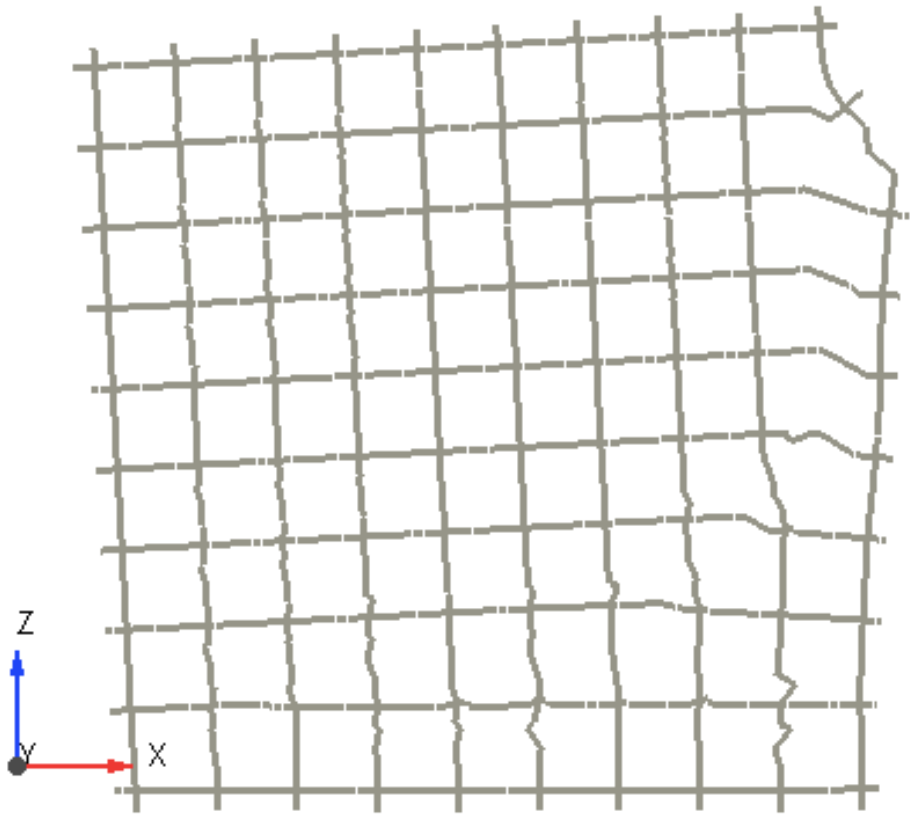

Figure 6.30) Deformed shape 1D model from ATENA Studio analysis of Tran 4

6.3.2.5 Discussion of Results

For the transverse reinforcement ratio sensitivity analysis cases, comparison should be made between cases Tran 1 and 2, and then between Tran 3 and 4. This is because these two sets of cases comprised the same design parameters, except one completely isolated the contribution of the transverse reinforcement.

Between Tran 1 and 2 trials, the removal of transverse reinforcement did not have much of an impact on the peak strength, nor the level of drift at which it was attained at. This can likely be attributed to the fact that both of these walls experienced a flexure dominated failure, and so the

elimination of the transverse reinforcement, which typically impacts the shear resistance of the specimen, did not govern in the performance.

The same was not true when comparing the results obtained Tran 3 and 4 trials, where the removal of the transverse reinforcement saw a quite substantial decrease in the peak strength. For these specimens, the performance was not purely flexural and therefore, the removal of the transverse reinforcement was indeed represented in the results. It is important to note that although case Tran 3, which contained transverse reinforcement, experienced a larger peak strength, case Tran 4 experienced a larger lateral drift capacity. This is an interesting observation because the removal of the transverse reinforcement typically would skew the performance of the wall to a more brittle shear failure, however, the opposite occurred in this case.

Chapter 7

Conclusion and Next Steps

7.1 Findings

Throughout the data vetting and analysis procedures conducted on the experimental database presented in this thesis, several critical findings were identified and investigated regarding various analytical estimations for the seismic behavior of existing reinforced masonry structures in Canada. A summary of the conclusions is as follows:

7.1.1 Empirical vs. Analytical Discrepancies

From the application of the empirically derived expressions for shear and flexure presented in the Canadian standards for masonry design (CSA S304-24), the governing failure mode was determined through the minimum specified strength in either shear or flexure as outlined in Equation 2.17. For several of the specimens in the database, the governing failure mode determined in this manner did not align with what was observed during the experimental investigation, indicating that the values obtained from the equations were inaccurately predicting response. For many of these cases, the inaccuracies were not too severe, but for others the inaccuracies were quite severe.

7.1.2 Influence of Aspect Ratio

As depicted in Figures 5.1, 5.2, 5.4 and 5.4, it was observed that the aspect ratio seems to hold the greatest sensitivity towards the performance of specimens, backed by a strong predictive capability was shown with reference to the peak lateral drift capacities and experienced failure mode of the specimen.

7.1.3 Influence of Axial Load

With reference to Figures 5.10 – 5.13, it was shown that the presence and intensity of an applied lateral load is able to influence the failure mode of walls, where high axial loads tend to provide sufficient of amounts of frictional resistance within the wall that tends to suppress flexural behavior and drift capacities. On the contrary, low amounts of applied axial loads were generally associated with improved ductility, where specimens typically exhibited more flexural behavior through greater lateral drift capacities.

7.1.4 Influence of Vertical Reinforcement Ratio

In accordance with the data shown in Figures 5.6 – 5.9, the influence held by the amount of vertical reinforcement within the wall is apparent in its ability to predict the failure mode of the specimen. Specimens constructed with large amounts of vertical reinforcements clearly exhibited flexural performance, which was accompanied by larger levels of lateral drift, whereas lower amounts of reinforcement limited the response to brittle responses controlled by shear failure.

7.1.5 Shear Failure

It was proven that shear failure was accompanied by lower levels of drift capacities and typically was more prone to occur in specimens with either lower aspect ratios or high levels of applied axial load. It was also found that the CSA S304-24 standards have shown the possibility to both underestimate and overestimate the shear capacity of walls with no indication of which is more likely to occur, however the scenario of overestimating can present severe consequences in the performance of structures.

7.1.6 Flexure Failure

Flexural failures were more pronounced in specimens with greater aspect ratios and lower axial loads, which encouraged greater amounts of deformation capacity through the recorded lateral drift ratios. It was also found that the flexural strength capacity was the most accurate to predict through analytical expressions in comparison to the shear strengths as excellent convergence towards experimental results was observed.

7.1.7 Mixed Failure Modes

Mixed shear-flexural failure was the least reported performance to occur in the experimental literature, and was only achieved in one experimental investigation which directly sought out this form of behaviour in their tests. This is likely due to the fact that research is often carried out for either fully shear or fully flexure dominated specimens to contribute towards the validation of the empirically derived analytical models for the prediction of strength in each form of failure respectively.

7.1.8 Influence of Cracking on Stiffness

The impact of cracking on the effective stiffness of the wall must be considered in the analysis procedures and calculations for structures being exposed to high amounts of loading. When comparing experimental and analytical stiffness values, it was found that the use of cracked section properties, equal to 50 percent of the effective section properties, provided much more realistic values for the analytical stiffness which resulted in between convergence towards experimental values.

7.1.9 Modulus of Elasticity of Masonry (E_m)

The calculation for the modulus of elasticity of masonry (E_m) depends on empirical equations that have been derived based on compressive tests of masonry wall samples and considers a coefficient (α) of 850 for reinforced masonry walls in the Canadian practice (CSA S304-24). When assessing reinforced masonry structures that are being loaded in the lateral direction, such as in the case of during an earthquake, this coefficient seems to be inaccurate in estimating the stiffness of the wall since the strength in the lateral direction is a function of the bond between the masonry and mortar joints, a quantity that does not fully get accounted for during compressive testing, such as the ones that were used in the derivation of the empirical constants. As a result, the stiffness of reinforced masonry walls is at risk of overestimation, leading to inaccurate prediction of their true capacity during service, which in turn can affect the integrity of the structure and the safety of the general public.

7.1.11 Material Factors

Differences in material safety factors are present between the Canadian CSA S304-24 and American TMS 402-22 masonry design codes, such as in the calculation of the steel contribution towards diagonal tension resistance where values of 0.5 and 0.6 are used respectively. In addition, the coefficient (α) used in the estimation for the Modulus of Elasticity of masonry (E_m) in the TMS 402 standard considers a range of values depending on the type of masonry block (700 for clay bricks, 900 for concrete blocks) whereas the CSA S304 assumes a standardized value of 850.

7.1.12 Empirical Equations

The presence of empirically derived analytical equations presents the opportunity of inaccuracy as the equations might not always be applicable for all ranges of possible design parameters since they have typically been derived from a limited set of data. For example, the lack

of data in the literature surrounding walls constructed with flanged sections or boundary elements may often lead to inaccuracies when these empirical equations are applied to such structural configurations.

7.2 Next Steps

These findings obtained from the work presented in this thesis have highlighted key areas for future research to further the development of the assessment criteria for the seismic performance of reinforced masonry structures:

7.2.1 Experimental Pursuit

Future experimental investigations should be done to continue the advancement of the field by continuing to validate and enhance analytical models and empirical relationships. In particular, these research endeavours should attempt to expand on the scope of previously conducted research which would be useful in validating the experiments that these empirical formulae have been derived from as well as providing new research to be added to the datasets.

7.2.2 Moduli Calibration

Expanding on the future experimental investigations of reinforced masonry walls, the empirical definitions of the complex material properties of masonry, such as the Young and Shear Moduli, should continue to be investigated to enhance their applicability in all ranges of data that might have not been considered when the expressions were first being derived. This includes in seismic applications where the compressive strength of the masonry is not the governing failure mechanism of response.

7.2.3 Extended Database Analysis

The database constructed in this thesis should become an open resource in the reinforced masonry analysis field, where it is continuously updated with newly gathered experimental data to further enhance its efficiency. By including newly published data, especially with a level of uniqueness associated to them, such as having distinct design details or boundary element configurations that have not already being considered in the database, further validation of analytical models is possible.

7.2.4 Extended Finite Element Analysis

In addition to the extension of the database, the finite element analysis investigation should be expanded upon in the form of more advanced models of wall specimens that extends into ranges of design parameters where data is scarce. This would help bridge existing gaps in the current knowledge surrounding empirical equations and the precise complex behavior of reinforced masonry.

References

Aly, N., Seif ElDin, H.M., & Galal, K. (2019). Experimental Investigation of Axial Load and Detailing Effects on the Inelastic Response of Reinforced-Concrete Masonry Structural Walls with Boundary Elements. Journal of Structural Engineering.

Albutainy, Mohammed, Galal Khaled. (2021). Experimental investigation of reinforced concrete masonry shear walls with C-shaped masonry units boundary elements. Structures.

American Society of Civil Engineers (ASCE). (2023). Seismic Evaluation and Retrofit of Existing Buildings, ASCE/SEI Standard 41-23. Reston, VA, USA.

Banting, Bennett, Wael W. El-Dakhakhni (2012). Force- and Displacement-Based Seismic Performance Parameters for Reinforced Masonry Structural Walls with Boundary Elements. Journal of Performance of Constructed Facilities.

Banting, Bennett, Wael W. El-Dakhakhni (2012). Seismic performance quantification of reinforced masonry structural walls with boundary elements. Journal of Performance of Constructed Facilities.

Bolhassani, M., Hamid, A.A., & Moon, F.L. (2014). Enhancement of lateral in-plane capacity of partially grouted concrete masonry shear walls. Construction and Building Materials

Robazza, B, Svetlana B. Elwood K., Anderson, D., Yang, T (2015). A Study on the out-of-plane Stability of Ductile Reinforced Masonry Shear Walls Subjected to in-plane reversed Cyclic Loading. 12th North American Masonry Conference.

Canadian Standards Association. (2024). CSA S304.1, Design of Masonry Structures. CSA, Mississauga, ON.

Cervenka, V., & Cervenka, J. (2017). ATENA Program Documentation Part 2-2 User's Manual for ATENA 3D. Prague, Czech Republic.

Clough, R.W., & Penzien, J. (1975). Dynamics of Structures. McGraw-Hill Inc., New York.

Computers & Structures, Inc. (2017). CSi Analysis Reference Manual. Computers & Structures, Inc.

El-Dakhakhni, W., Hussein, W.M., & Siam, A.S. (2013). Seismic Performance Parameter Quantification of Shear-Critical Reinforced Concrete Masonry Squat Walls. Journal of Structural Engineering, ASCE.

FEMA. (2002). Rapid visual screening of buildings for potential seismic hazards: a handbook. (2nd ed.) Applied Technology Council for the Federal Emergency Management Agency, Washington, D.C.

Galal, K. (2017). Effect of reinforcement anchorage end detail and spacing on seismic performance of masonry shear walls. Department of Building, Civil and Environmental, Concordia University.

Ismail, M. (2023). Stress-Strain Models for UHPFRC and Application in Seismic Design and Retrofit of Bridges. York University.

Majid, M. (2008). Behaviour of Partially Grouted Reinforced Masonry Shear Walls Under Cyclic Reversed Loading. McMaster University.

NIST. (2017). NIST GCR 17-917-45. Recommended Modeling Parameters and Acceptance Criteria for Nonlinear Analysis in Support of Seismic Evaluation, Retrofit and Design. National Institute of Standards and Technology, U.S. Department of Commerce, Applied Technology Council.

Pantazopoulou, V.S. (2021). Recommending Modelling Parameters and Acceptance Criteria for Nonlinear Analysis for Seismic Evaluation and Retrofit of Existing Buildings in Canada: Masonry Structures. December 2021, Revised July 2022.

Ramírez, P., Sandoval, C., & Almazán, J.L. (2015). Experimental study on in-plane cyclic response of partially grouted reinforced concrete masonry shear walls. Journal of Structural Engineering.

Rizaee, S., et al. (2020). The effect of the amount, distribution, and end anchorage conditions of bond beam reinforcement on the behaviour of concrete masonry shear walls. Canadian Science Publishing.

Robazza, B.R., Brzev, S., Yang, T.Y., Elwood, K.J., Anderson, D.L., & McEwen, B. (2019). Seismic behaviour and design code provisions for predicting the capacity of ductile slender reinforced masonry shear walls. Journal of Structural Engineering.

Robazza, B.R., Yang, T.Y., Brzev, S., Elwood, K.J., Anderson, D.L., & McEwen, W. (2017). Response of slender reinforced masonry shear walls with flanged boundary elements under in-plane lateral loading: An experimental study. Journal of Engineering Mechanics.

Seif ElDin, H.M., & Galal, K. (2016). In-Plane Seismic Performance of Fully Grouted Reinforced Masonry Shear Walls. Journal of Structural Engineering.

Seif ElDin, H.M., Aly, N., & Galal, K. (2018). In-plane shear strength equation for fully grouted reinforced masonry shear walls. Journal of Structural Engineering.

Seif EIDin. H, Galal, K. "Effect of shear span to depth ratio on seismic performance of reinforced masonry shear walls." Resilient Infrastructure, June 1-4 2016.

Siam, A.S., Hussein, W.M., & El-Dakhakhni, W.W. (2015). Scoring models for reinforced masonry shear wall maximum displacement prediction under seismic loads. Journal of Structural Engineering.

Shedid, M. El-Dakhakhni, W. Drysdale, R.G (2010). Characteristics of Rectangular, Flanged, and End-Confined Reinforced Concrete Masonry Shear Walls for Seismic Design. Journal of Structural Engineering

Siyam, A.M., & Mustafa, A. (2015). Seismic Response Evaluation of Ductile Reinforced Concrete Block Structural Walls. I: Experimental Results and Force-Based Design Parameters. Journal of Performance of Constructed Facilities.

Valadeo, R. Seismic Analysis and Assessment of Historic Unreinforced Masonry (2021), York University, Toronto, Ontario

Appendix

	A	B	C	D	E	F	G	H	I	J	K	L	M	N	O	P	Q	R	S
2	ID #	Paper Title	Specimen	Reference	Grouted	(Mpa)	Scale	Block	tw (mm)	f'c Block (Mpa)	f'c Mortar (Mpa)	fw wall (Mpa)	fy Vertical (Mpa)	fy Horizontal (Mpa)	Less minimum spacings Span	Hw (mm)	lw (mm)	Aspect Ratio	Av Bar
3			W1		Fully Grou	21	Half Scale	Two cell 20 cm ho	90	27.2	21.8	16.4	495		534	3990	1802	2.21	10M
4		"Characteristics of Rectangular, Flanged, and End-Confined	W2		Fully Grou	21	Half Scale	Two cell 20 cm ho	90	27.2	21.8	16.4	495		534	3990	1802	2.21	10M
5			W3		Fully Grou	21	Half Scale	Two cell 20 cm ho	90	27.2	21.8	16.4	495		534	3990	1802	2.21	10M
6		Reinforced Concrete	W4		Fully Grou	21	Half Scale	Two cell 20 cm ho	90	27.2	21.8	16.4	495		534	2660	1802	1.48	10M
7		Masonry Shear Walls for	W5		Fully Grou	21	Half Scale	Two cell 20 cm ho	90	27.2	21.8	16.4	495		534	2660	1802	1.48	10M
8	1	Seismic Design." Journal	W6		Fully Grou	21	Half Scale	Two cell 20 cm ho	90	27.2	21.8	16.4	495		534	2660	1802	1.48	10M
9		Of Structural	W7		Fully Grou	21	Half Scale	Two cell 20 cm ho	90	27.2	21.8	16.4	495		534	2660	1802	1.48	10M
10		R.G., Hamid, A.A., El-	Wall 1		Partially G	40.7	Half Scale	20 cm hollow	90	21.6	21.4	12.4	491.7	690.7	1800	1800	1800	1	10M
11		Damatty, A.A "Behaviour	Wall 2		Partially Grouted		Half Scale	20 cm hollow	90	21.6	21.4	12.4	502.9	743.7	1800	1800	1800	1	#3
12	2	of Partially Grouted	Wall 3		Partially Grouted		Half Scale	20 cm hollow	90	21.6	21.4	12.4	564.7	743.7	1800	1800	1800	1	#4
13		Reinforced Masonry	Wall 4		Partially Grouted		Half Scale	20 cm hollow	90	21.6	21.4	12.4	491.7	743.7	900	900	1800	0.5	10M
14		Shear Walls-	Wall 5		Partially Grouted		Half Scale	20 cm hollow	90	21.6	21.4	12.4	491.7	690.7	2700	2700	1800	1.5	10M
15		Shedid, M. El-	Wall 1		Fully Grouted		Full Scale	190 mm normal w	190	24.8	27.7	14.8	502	502	3600	3600	1800	2	15M
16		Dakhakhni, W. Drysdale,	Wall 2		Fully Grouted		Full Scale	190 mm normal w	190	24.8	27.7	14.8	502	502	3600	3600	1800	2	20M
17		R.G "Behaviour of Fully	Wall 3		Fully Grouted		Full Scale	190 mm normal w	190	24.8	27.7	14.8	502	502	3600	3600	1800	2	25M
18		Grouted Reinforced	Wall 4		Fully Grouted		Full Scale	190 mm normal w	190	24.8	27.7	14.8	502	502	3600	3600	1800	2	25M
19	3	Masonry Shear Walls	Wall 5		Fully Grouted		Full Scale	190 mm normal w	190	24.8	27.7	14.8	502	502	3600	3600	1800	2	25M
20		Failing in Flexure:	Wall 6		Fully Grouted		Full Scale	190 mm normal w	190	24.8	27.7	14.8	624	624	3600	3600	1800	2	25M
21		"Effect of reinforcement	W-Ref		Fully Grou	29.4	Full Scale	Full-scale lightwei	190	16.7	13.7	13.1	430	430	1800	1600	1800	0.8888889	20M
22		anchorage end detail	W-90		Fully Grou	29.4	Full Scale	Full-scale lightwei	190	16.7	13.7	13.1	430	430	1800	1600	1800	0.8888889	20M
23	4	and spacing on seismic	W-Str		Fully Grou	29.4	Full Scale	Full-scale lightwei	190	16.7	13.7	13.1	430	430	1800	1600	1800	0.8888889	20M
24		performance of masonry	W-Sv800		Fully Grou	29.4	Full Scale	Full-scale lightwei	190	16.7	13.7	13.1	430	430	1800	1600	1800	0.8888889	20M
25		shear wall." Department	W-Sh800		Fully Grou	29.4	Full Scale	Full-scale lightwei	190	16.7	13.7	13.1	430	430	1800	1600	1800	0.8888889	30M
26		El-Dakhakhni, Wael, et	W-1		Fully Grouted		Full Scale	Hollow Concrete I	190	35.7	22.7	15.4	425	425	2000	2000	2000	1	20M
27		al. "Seismic	W-2		Fully Grouted		Full Scale	Standard 190 mm	190	21.8	22.7	12.7	425	425	2000	2000	2000	1	20M
28		Performance Parameter	W-3		Fully Grouted		Full Scale	Hollow Concrete I	190	25.7	22.7	15.4	425	425	3000	3000	2000	1.5	25M
29	5	Quantification of Shear-	W-5		Fully Grouted		Full Scale	Standard 190 mm	190	21.8	22.7	12.7	425	425	3000	3000	2000	1.5	25M
30		Critical Reinforced	W-8		Fully Grouted		Full Scale	Standard 190 mm	190	21.8	22.7	12.7	425	425	3000	3000	3000	1	20M
31			Wall 1		Partially Grouted		Full Scale	Hollow Concrete I	190	35.7	22.1	10	450	450	895	1790	1790	1	15M
32			Wall 2		Partially Grouted		Full Scale	Hollow Concrete I	190	35.7	22.1	10	450	450	895	1790	1790	1	15M
33			Wall 3		Partially Grouted		Full Scale	Hollow Concrete I	190	35.7	22.1	10	450	450	895	1790	1790	1	15M
34		Rizaee, Samira et al. "The	Wall 4		Partially Grouted		Full Scale	Hollow Concrete I	190	35.7	22.1	9.8	450	450	895	1790	1790	1	15M
35		effect of the amount,	Wall 5		Partially Grouted		Full Scale	Hollow Concrete I	190	29.3	9.5	13	450	450	1375	1790	1790	1	15M
36		Rizaee, Samira et al. "The	Wall 6		Partially Grouted		Full Scale	Hollow Concrete Bl	190	29.3	9.5	13	450	450	1375	1790	1790	1	15M
37		effect of the amount,	Wall 7		Partially Grouted		Full Scale	Hollow Concrete Bl	190	29.3	11.5	13	450	450	1375	1790	1790	1	15M
38		distribution, and end	Wall 8		Partially Grouted		Full Scale	Hollow Concrete Bl	190	29.3	11.5	13	450	450	1375	1790	1790	1	15M
39		anchorage conditions of	Wall 9		Partially Grouted		Full Scale	Hollow Concrete Bl	190	20.1	11	9.9	450	450	1375	1790	1790	1	15M
40		bond beam reinforcement	Wall 10		Partially Grouted		Full Scale	Hollow Concrete Bl	190	20.1	11	9.9	450	450	1375	1790	1790	1	15M
41		on the behaviour of	Wall 11		Partially Grouted		Full Scale	Hollow Concrete Bl	190	20.1	9.3	9.9	450	450	1375	1790	1790	1	15M
42	6	concrete masonry shear	Wall 12		Partially Grouted		Full Scale	Hollow Concrete Bl	190	20.1	9.3	9.9	450	450	1375	1790	1790	1	15M
43		walls." Canadian Science	Wall 13		Partially Grouted		Full Scale	Hollow Concrete Bl	190	20.1	11.6	9.9	450	450	1375	1790	1790	1	15M
44		Publishing, November	Wall 14		Partially Grouted		Full Scale	Hollow Concrete Bl	190	20.1	11.6	9.9	450	450	1375	1790	1790	1	15M
45	7	2020.	W-M/Vdv1.2		Fully Grouted		Full Scale	Half Scale Concrete	190			13.1	430	430	1250	1600	1800	0.8888889	20M
46		"Effect of shear span to	W-M/Vdv1.8		Fully Grouted		Full Scale	Half Scale Concrete	190			13.1	430	430	1875	1600	1800	0.8888889	20M
47		depth ratio on seismic	W 1		Fully Grouti	18.5	Half Scale	Half Scale	90	26.5	16.6	14.9	496	582.5	3990	3990	2655	1.5028246	10M
48		Banting, Bennett, Wael W.	W 2		Fully Grouti	18.5	Half Scale	Half Scale	90	26.5	16.6	14.9	496	582.5	3990	3990	1235	3.2307692	10M
49		El-Dakhakhni. "Seismic	W 3		Fully Grouti	18.5	Half Scale	Half Scale	90	26.5	16.6	14.9	496	582.5	2660	2660	1235	2.1538461	10M
50	8	performance	W 4		Fully Grouti	18.5	Half Scale	Half Scale	90	26.5	16.6	14.9	496	582.5	2660	2660	1235	2.1538461	10M
51		quantification of	W 5		Fully Grouti	18.5	Half Scale	Half Scale	90	26.5	16.6	14.9	496	582.5	1900	1900	1235	1.5384615	10M
52		reinforced masonry	W-M/Vdv1.8		Fully Grouti	21.67	Half Scale	Half Scale Blocks	95	13.65	19.37	17	460	588	12100	2380	1715	1.3877551	#3
53	9	Albutainy,Mohammed, et	W2-Cs30		Fully Grouti	21.67	Half Scale	Half Scale Blocks	95	13.65	19.37	17	460	588	12100	2380	1715	1.3877551	#3
54		al. "Experimental	W3-Cs45		Fully Grouti	21.67	Half Scale	Half Scale Blocks	95	13.65	19.37	17	460	588	12100	2380	1715	1.3877551	#3
55		Khaled. "In-Plane Seismic	W-ph0		Fully Grouti	21.6	Full Scale	Lightweight knockc	190	16.7	8.5	13.1	430	430	1800	1600	1800	0.8888889	20M
56		Performance of Fully	W-on0		Fully Grouti	21.6	Full Scale	Lightweight knockc	190	16.7	8.5	13.1	430	430	1800	1600	1800	0.8888889	20M
57	10	Grouted Reinforced	W-on1.5		Fully Grouti	21.6	Full Scale	Lightweight knockc	190	16.7	8.5	13.1	430	430	1800	1600	1800	0.8888889	20M
58		Masonry Shear Walls."	W-M/Vdv1.8		Fully Grouti	21.6	Full Scale	Lightweight knockc	190	16.7	8.5	13.1	430	430	1800	1600	1800	0.8888889	20M
59		Aly, Nader, et al.	W7-C4190		Fully Grouted		Half Scale	Half-scale concrete	90	11.3	15.1	8.7	460	535	12100	2380	1715	1.3877551	#3
60		"Experimental	W8-C8190		Fully Grouted		Half Scale	Half-scale concrete	90	11.3	15.1	8.7	460	535	12100	2380	1715	1.3877551	#3
61	11	Investigation of Axial Load	W9-C8290		Fully Grouted		Half Scale	Half-scale concrete	90	11.3	15.1	8.7	460	535	12100	2380	1715	1.3877551	#3
62		Elwood K., Anderson, D.,	Wall 1		Fully Grouti	33.9	Full Scale	Hollow concrete bic	140	25.6	12.5	23.4	400	400	3920	3800	2600	1.4613384	10M & 15M
63		Yang, T "A Study on the	Wall 2		Fully Grouti	33.9	Full Scale	Hollow concrete bic	140	25.6	12.5	23.4	400	400	3800	3800	2600	1.4613384	10M & 15M
64		out-of-plane Stability of	Wall 3		Fully Grouti	33.9	Full Scale	Hollow concrete bic	190	25.6	12.5	27.1	400	400	4000	4000	2600	1.5384615	15M
65	12	Ductile Reinforced	Wall 4		Fully Grouti	33.9	Full Scale	Hollow concrete bic	190	25.6	12.5	27.1	400	400	4000	4000	1400	2.8571428	10M
66		Masonry Shear Walls	Wall 5		Fully Grouti	33.9	Full Scale	Hollow concrete bic	140	25.6	12.5	27.1	400	400	4000	4000	2600	1.5384615	10M & 15M
67		El-Dakhakhni "Force- and	W1		Fully Grouti	20.7	Half Scale	Half-scale concrete	92.5	29.2	21.6	15.9	496.3	582.5	3990	3990	1803	2.2129784	10M
68		Displacement-Based	W2		Fully Grouti	20.7	Half Scale	Half-scale concrete	92.5	29.2	21.6	15.9	496.3	582.5	3990	3990	1803	2.2129784	10M
69	13	Seismic Performance	W3		Fully Grouti	20.7	Half Scale	Half-scale concrete	92.5	29.2	21.6	15.9	496.3	582.5	3990	3990	1803	2.2129784	10M
70		Parameters for Reinforced	W4		Fully Grouti	20.7	Half Scale	Half-scale concrete	92.5	29.2	21.6	15.9	496.3	582.5	3990	3990	1803	2.2129784	10M
71		"Seismic Response	W1		Fully Grouted		One-Third Scale	130mm long, 63 m	63	25.2	18.7	19.3	495	670	2160	2160	1533	1.4090019	D7
72	14	Evaluation of Ductile	W2		Fully Grouted		One-Third Scale	130mm long, 63 m	63	25.2	18.7	19.3	495	670	2160	2160	1533	1.4090019	D7

	T	U	V	W	X	Y	Z	AA	AB	AC	AD	AE	AF	AG	AH	AI
2	Av per bar (mm^2)	Vert Reinf Av (mm^2)	# of Bars in web only	pv (%) - Calculated	pv (%) - From paper	pv * fyv/f'w	Spacing V (mm) -	Ah per bar (mm^2)	otal Horiz Reinf A (mm^2	# of Bars	dv/s	pHoriz (%)	Spacing H (mm) - Vertical	An (mm^2)	An,web (mm^2	Boundary Element
3	100.00	1900	19	1.2012012	1.17	0.36255768	92.5	129	516	4	1.44521	0.3	997.5	162180	158175	None
4	100.00	500	5	0.35329447	0.55	0.10663461	231.25	129	516	4	1.44521	0.3	997.5	162180	141525	Flange
5	100.00	300	3	0.24024024	0.55	0.07251154	323.75	129	516	4	1.44521	0.3	997.5	162180	124875	2 Blocks
6	100.00	1900	19	1.2012012	1.17	0.36255768	92.5	129	1032	8	4.33564	0.6	332.5	162180	158175	None
7	100.00	500	5	0.35329447	0.55	0.10663461	231.25	129	1032	8	4.33564	0.6	332.5	162180	141525	Flange
8	100.00	300	3	0.24024024	0.55	0.07251154	323.75	129	1032	8	4.33564	0.6	332.5	162180	124875	2 Blocks
9	100.00	300	3	0.24024024	0.55	0.07251154	323.75	129	1032	8	4.33564	0.6	332.5	162180	124875	Pilaster Unit
10	100.00	300	3	0.18518519	0.19	0.0734319	855	127	77.4	3	1.68421	0.05	855	162000	162000	No
11	71.00	284	4	0.17530864	0.18	0.07109896	570	71	77.6	4	2.52632	0.05	570	162000	162000	No
12	126.00	252	2	0.15555556	0.16	0.0708405	1710	71	38.8	2	0.84211	0.05	1710	162000	162000	No
13	100.00	300	3	0.18518519	0.19	0.0734319	855	71	142	2	1.68421	0.05	855	162000	162000	No
14	100.00	300	3	0.18518519	0.18	0.0734319	855	127	508	4	1.68421	0.04	855	162000	162000	No
15	200.00	1000	5	0.29239766	0.29	0.09917813	300	100	600	6	2.4	0.08	600	342000	342000	No
16	300.00	2700	9	0.78947368	0.78	0.26778094	180	100	900	9	3.6	0.13	400	342000	342000	No
17	500.00	2500	5	0.73099415	0.73	0.24794531	300	100	900	9	3.6	0.13	400	342000	342000	No
18	500.00	4500	9	1.31578947	1.31	0.44630156	180	100	1800	18	7.2	1.13	200	342000	342000	No
19	500.00	4500	9	1.31578947	1.31	0.44630156	180	100	1800	18	7.2	0.26	200	342000	342000	No
20	500.00	4500	9	1.31578947	1.31	0.55476529	180	100	1800	18	7.2	0.26	200	342000	342000	No
21	300.00	2700	9	0.78947368	0.79	0.25914022	200	100	400	4	3.6	0.13	400	342000	342000	No
22	300.00	2700	9	0.78947368	0.79	0.25914022	200	100	400	4	3.6	0.13	400	342000	342000	No
23	300.00	2700	9	0.78947368	0.79	0.25914022	200	100	400	4	3.6	0.13	400	342000	342000	No
24	300.00	2700	9	0.78947368	0.79	0.25914022	200	200	400	2	1.8	0.13	800	342000	342000	No
25	700.00	2100	3	0.61403509	0.61	0.2015535	800	200	400	2	1.8	0.13	800	342000	342000	No
26	300.00	3000	10	0.78947368	0.79	0.21787423	200	100	100	1	2	0.079	800	380000	380000	No
27	300.00	3000	10	0.78947368	0.79	0.26419395	200	100	400	4	4	0.13	400	380000	380000	No
28	500.00	5000	10	1.31578947	1.32	0.36312372	200	100	600	6	4	0.12	400	380000	380000	No
29	500.00	5000	10	1.31578947	1.32	0.44032325	200	100	200	2	2	0.07	800	380000	380000	No
30	300.00	4500	15	0.78947368	0.79	0.26419395	200	100	200	2	3	0.07	800	570000	570000	No
31	200.00	600	3	0.1764187	0.18	0.07938842	540	200	400	2	1.79	0.12	800	340100	340100	No
32	200.00	600	3	0.1764187	0.18	0.07938842	540	200	400	2	1.79	0.12	800	340100	340100	No
33	200.00	600	3	0.1764187	0.18	0.07938842	540	200	400	2	1.79	0.12	800	340100	340100	No
34	200.00	600	3	0.1764187	0.18	0.08100859	540	200	400	2	1.79	0.12	800	340100	340100	No
35	200.00	600	3	0.1764187	0.18	0.06106801	540	100	200	2	1.79	0.06	800	340100	340100	No
36	200.00	600	3	0.1764187	0.18	0.06106801	540	100	200	2	1.79	0.06	800	340100	340100	No
37	200.00	600	3	0.1764187	0.18	0.06106801	540	100	200	2	1.79	0.06	800	340100	340100	No
35	200.00	600	3	0.1764187	0.18	0.06106801	540	100	200	2	1.79	0.06	800	340100	340100	No
36	200.00	600	3	0.1764187	0.18	0.06106801	540	100	200	2	1.79	0.06	800	340100	340100	No
37	200.00	600	3	0.1764187	0.18	0.06106801	540	100	200	2	1.79	0.06	800	340100	340100	No
38	200.00	600	3	0.1764187	0.18	0.06106801	540	100	200	2	1.79	0.06	800	340100	340100	No
39	200.00	600	3	0.1764187	0.18	0.08019032	540	100	200	2	1.79	0.06	800	340100	340100	No
40	200.00	600	3	0.1764187	0.18	0.08019032	540	100	200	2	1.79	0.06	800	340100	340100	No
41	200.00	600	3	0.1764187	0.18	0.08019032	540	100	200	2	2.38667	0.06	600	340100	340100	No
42	200.00	600	3	0.1764187	0.18	0.08019032	540	100	200	2	2.38667	0.06	600	340100	340100	No
43	200.00	600	3	0.1764187	0.18	0.08019032	540	0	0	0	#DIV/0!	0.03	0	340100	340100	No
44	200.00	600	3	0.1764187	0.18	0.08019032	540	0	0	0	#DIV/0!	0.03	0	340100	340100	No
45	300.00	2700	9	0.78947368	0.79	0.25914022	200	100	400	4	3.6	0.13	400	342000	342000	No
46	300.00	2700	9	0.78947368	0.79	0.25914022	200	100	400	4	3.6	0.13	400	342000	342000	No
47	100.00	1500	15	0.69100541	0.51	0.23002596	95	25.4	254	10	5.58947	0.3	380	238950	217075	End Confined
48	100.00	200	2	0.24338302	0.69	0.08101878	95	25.4	254	10	2.6	0.3	380	111150	82175	End Confined
49	100.00	1300	13	1.58198966	0.69	0.52662206	95	25.4	177.8	7	2.6	0.6	380	111150	82175	End Confined
50	100.00	1300	13	1.58198966	1.17	0.52662206	95	25.4	711.2	28	10.4	0.6	95	111150	82175	End Confined
51	100.00	1300	13	1.58198966	0.69	0.52662206	95	25.4	127	5	2.6	0.6	380	111150	82175	End Confined
52	71.00	284	4	0.2363712	0.79	0.06395927	279	51.67	413.36	8	4.81404	0.83	285	162925	120150	Yes
53	71.00	284	4	0.2363712	0.79	0.06395927	279	51.67	413.36	8	4.81404	1.66	285	162925	120150	Yes
54	300.00	2700	9	0.78947368	0.79	0.25914022	200	0	0	0	#DIV/0!	0	0	342000	342000	No
55	300.00	2700	9	0.78947368	0.79	0.25914022	200	300	900	3	3.6	0.13	400	342000	342000	No
56	300.00	2700	9	0.78947368	0.79	0.25914022	200	300	900	3	3.6	0.13	400	342000	342000	No
57	300.00	2700	9	0.78947368	0.79	0.25914022	200	300	900	3	3.6	0.13	400	342000	342000	No
58	71.00	284	4	0.2363712	0.18	0.12497788	343	51.61	412.88	8	4.81404	0.27	285	154350	120150	190mm C-Shaped Bloc
59	71.00	284	4	0.2363712	0.18	0.12497788	343	51.61	412.88	8	4.81404	0.27	285	154350	120150	190mm C-Shaped Bloc
60	71.00	284	4	0.27559437	0.18	0.14571656	343	51.61	412.88	8	4.81404	0.27	285	154350	103050	290mm C-Shaped Bloc
61	-	1200	-	0.32967033	0.33	0.0563539	400	100	1900	19	10.4	0.36	200	364000	364000	No
62	-	1200	-	0.32967033	0.33	0.0563539	400	100	1900	19	10.4	0.36	200	364000	364000	No
63	200.00	1200	6	0.24291498	0.24	0.03585461	400	100	500	5	2.6	0.26	800	494000	494000	No
64	100.00	400	4	0.15037594	0.15	0.02219571	400	100	500	5	1.4	0.26	800	266000	266000	No
65	-	1200	-	0.32967033	0.33	0.04865983	400	100	1900	19	10.4	0.36	200	364000	364000	No
66	100.00	300	3	0.20639835	0.56	0.06442484	380	25.4	1066.8	42	15.1832	0.3	95	166777.5	145350	Fully grouted 185x185
67	100.00	300	3	0.20639835	0.56	0.06442484	380	25.4	1066.8	42	15.1832	0.3	95	166777.5	145350	Fully grouted 185x185
68	100.00	300	3	0.20639835	0.56	0.06442484	380	25.4	1066.8	42	15.1832	0.3	95	166777.5	145350	Fully grouted 185x185
69	100.00	300	3	0.20639835	0.56	0.06442484	380	25.4	1066.8	42	15.1832	0.3	95	166777.5	145350	Fully grouted 185x185
70	45.36	544.32	12	0.56360078	0.6	0.14455046	133	11.3	203.4	18	12.5785	0.26	97.5	96579	96579	No
71	45.36	317.52	7	0.32876712	0.6	0.0843211	177.666667	11.3	203.4	18	12.5785	0.26	97.5	96579	96579	No

	AR	AT	AU	AW	AX	AY	AZ	BA	BB	BC	BD	BE	BF	BG	BH
2	Axial Stress (Mpa)	N (N)	N/ An*f'w	Qpeak +ve (kN)	θpeak +ve	Qpeak -ve (kN)	θpeak -ve	$Q_{0.8u}$ +ve (kN) Pre	θ0.8u +ve Pre	$Q_{0.8u}$ +ve (kN) Post	θ0.8u +ve Post	$Q_{0.8u}$ -ve (kN) Pre	θ0.8u -ve Pre	$Q_{0.8u}$ -ve (kN) Post	θ0.8u -ve Post
3	1.09	176776.2	0.0664634	177	0.007017544	-177	-0.00877193	141.6	0.003759398	141.6	0.010526316	-141.6	-0.002756892	-141.6	-0.012531328
4	0.89	144340.2	0.0542683	152	0.0160401	-154	-0.010526316	121.6	0.003007519	121.6	0.017794486	-123.2	-0.002005013	-123.2	-0.017293233
5	0.89	144340.2	0.0542683	152	0.029824561	-147	-0.020551378	121.6	0.002255639	121.6	0.030075188	-117.6	-0.002506266	-117.6	-0.025062657
6	1.05	170289	0.0640244	265	0.006766917	-267	-0.004135338	212	0.001879699	212	0.010150376	-213.6	-0.003007519	-213.6	-0.011278195
7	0.88	142718.4	0.0536585	245	0.006766917	-239	-0.012030075	196	0.002255639	196	0.016917293	-191.2	-0.002255639	-191.2	-0.016541353
8	0.88	142718.4	0.0536585	241	0.007518797	-234	-0.018045113	192.8	0.001879699	192.8	0.02593985	-187.2	-0.003007519	-187.2	-0.021804511
9	0.88	142718.4	0.0536585	240	0.018421053	-236	-0.015037594	192	0.00112782	192	0.023308271	-188.8	-0.001879699	-188.8	-0.02481203
10	0.75	121500	0.0604839	91.21	0.001583333	-96.85	-0.001655556	72.968	0.000666667	72.968	0.002833333	-77.48	-0.000861111	-77.48	-0.002305556
11	0.75	121500	0.0604839	103.67	0.002233333	-93.23	-0.002	82.936	0.001222222	82.936	0.003277778	-74.58	-0.001166667	-74.58	-0.003055556
12	0.75	121500	0.0604839	96.7	0.002088889	-86.4	-0.001344444	77.36	0.001	77.36	0.002666667	-69.12	-0.00266667	-69.12	-0.002333333
13	0.75	121500	0.0604839	114.2	0.000966667	-122.9	-0.000888889	91.36	0.00025	91.36	0.001805556	-98.32	-0.000422222	-98.32	-0.001388889
14	0.75	121500	0.0604839	79.1	0.003307407	-84.3	-0.004166667	63.28	0.001481481	63.28	0.004259259	-67.44	-0.002222222	-67.44	-0.005
15	0	0	0	148	0.008777778	-122	-0.009	118.4	0.002638889	118.4	0.023888889	-97.6	-0.002777778	-97.6	-0.021388889
16	0	0	0	278	0.009138889	-246	-0.011666667	222.4	0.003333333	222.4	0.018888889	-196.8	-0.002916667	-196.8	-0.018611111
17	0	0	0	246	0.006722222	-235	-0.010555556	196.8	0.002777778	196.8	0.018055556	-188	-0.003472222	-188	-0.015277778
18	0	0	0	360	0.008277778	-380	-0.008083333	288	0.002916667	288	0.017222222	-304	-0.003333333	-304	-0.015277778
19	0.75	256500	0.0506757	377	0.007027778	-407	-0.009444444	301.6	0.003888889	301.6	0.012638889	-325.6	-0.004861111	-325.6	-0.013055556
20	1.5	513000	0.1013514	541	0.009722222	-558	-0.0095	432.8	0.004166667	432.8	0.015277778	-446.4	-0.005	-446.4	-0.016944444
21	1	342000	0.0763359	418	0.00890625	-409	-0.00875	334.4	0.00303125	334.4	0.0125	-327.2	-0.003	-327.2	-0.0125
22	1	342000	0.0763359	412	0.01003125	-405	-0.01	329.6	0.00303125	329.6	0.0125	-324	-0.003125	-324	-0.01203125
23	1	342000	0.0763359	398	0.00875	-381	-0.00859375	318.4	0.00303125	318.4	0.0109375	-304.8	-0.0028125	-304.8	-0.01125
24	1	342000	0.0763359	384	0.00625	-377	-0.00609375	307.2	0.0028125	307.2	0.0096875	-301.6	-0.00296875	-301.6	-0.00890625
25	1	342000	0.0763359	358	0.005	-346	-0.005	286.4	0.003125	286.4	0.0075	-276.8	-0.001875	-276.8	-0.0075
26	1	380000	0.0649351	407.9	0.004	-408	-0.00175	326.32	0.0009375	326.32	0.0065625	-326.4	-0.000625	-326.4	-0.00375
27	0	0	0	443.1	0.00645	-443.4	-0.00475	354.48	0.002625	354.48	0.00675	-354.72	-0.002375	-354.72	-0.00625
28	0	0	0	450.7	0.0075	-420.9	-0.005833333	360.56	0.00275	360.56	0.010166667	-336.72	-0.0025	-336.72	-0.010666667
29	1	380000	0.0787402	381.6	0.005	-390.8	-0.004133333	305.28	0.0025	305.28	0.005333333	-312.64	-0.001833333	-312.64	-0.004666667
30	0	0	0	548	0.005333333	-569.8	-0.003933333	438.4	0.002	438.4	0.006666667	-455.84	-0.000833333	-455.84	-0.006666667
31	2	680200	0.2	232	0.001675978	-273	-0.003072626	185.6	0.000558659	185.6	0.002960894	-218.4	-0.001927374	-218.4	-0.003351955
32	2	680200	0.2	327	0.001675978	-276	-0.003910615	261.6	0.000977654	261.6	0.002793296	-220.8	-0.001927374	-220.8	-0.004329609
33	2	680200	0.2	346	0.002234637	-276	-0.003910615	276.8	0.000837989	276.8	0.005586592	-220.8	-0.001927374	-220.8	-0.005586592
34	1.96	666596	0.2	282	0.005027933	-334	-0.004469274	225.6	0.000698324	225.6	0.005642458	-267.2	-0.001815642	-267.2	-0.005446927
35	2.6	884260	0.2	232	0.002234637	-216	-0.002234637	185.6	0.000698324	185.6	0.004469274	-172.8	-0.002094972	-172.8	-0.004329609
36	2.6	884260	0.2	191	0.002513966	-215	-0.001117318	152.8	0.000698324	152.8	0.004608939	-172	-0.000558659	-172	-0.001955307
37	2.6	884260	0.2	244	0.002793296	-208	-0.002513966	195.2	0.000837989	195.2	0.004748603	-166.4	-0.000698324	-166.4	-0.004748603
37	2.6	884260	0.2	244	0.002793296	-208	-0.002513966	195.2	0.000837989	195.2	0.004748603	-166.4	-0.000698324	-166.4	-0.004748603
38	2.6	884260	0.2	223	0.002513966	-217	-0.001955307	178.4	0.000782123	178.4	0.005083799	-173.6	-0.000977654	-173.6	-0.003910615
39	1.98	673398	0.2	226	0.003631285	-214	-0.002793296	180.8	0.001256983	180.8	0.004888268	-171.2	-0.000977654	-171.2	-0.00472067
40	1.98	673398	0.2	213	0.002793296	-184	-0.002513966	170.4	0.000726257	170.4	0.00377095	-147.2	-0.000837989	-147.2	-0.004050279
41	1.98	673398	0.2	211	0.002793296	-180	-0.001675978	168.8	0.000698324	168.8	0.004469274	-144	-0.000698324	-144	-0.004469274
42	1.98	673398	0.2	209	0.002513966	-206	-0.002793296	167.2	0.000977654	167.2	0.004581006	-164.8	-0.001117318	-164.8	-0.003910615
43	1.98	673398	0.2	175	0.003351955	-215	-0.003351955	140	0.000698324	140	0.004329609	-172	-0.001396648	-172	-0.004050279
44	1.98	673398	0.2	230	0.003072626	-206	-0.001955307	184	0.001256983	184	0.004469274	-164.8	-0.000977654	-164.8	-0.004050279
45	1	342000	0.0763359	418	0.00875	-409	-0.00875	334.4	0.003	334.4	0.01234375	-327.2	-0.00265625	-327.2	-0.01203125
46	1	342000	0.0763359	315	0.00625	-290	-0.00609375	252	0.00328125	252	0.0121875	-232	-0.0025	-232	-0.013125
47	0.89	212665.5	0.0597315	314.3	0.009398496	-301.8	-0.006340852	251.44	0.002005013	251.44	0.014786967	-241.44	-0.002506266	-241.44	-0.014035088
48	0.89	98923.5	0.0597315	94.2	0.011804511	-91.2	-0.063724696	75.36	0.004511278	75.36	0.037092732	-72.96	-0.004761905	-72.96	-0.032581454
49	0.89	98923.5	0.0597315	132.3	0.011578947	-127	0.014473684	105.84	0.002819549	105.84	0.018045113	-101.6	-0.003759398	-101.6	-0.018796992
50	0.89	98923.5	0.0597315	176.2	0.014285714	-178.9	-0.014323308	140.96	0.004699248	140.96	0.021804511	-143.12	-0.006766917	-143.12	-0.018421053
51	0.89	98923.5	0.0597315	177.4	0.009526316	-181	-0.012578947	141.92	0.002894737	141.92	0.022631579	-144.8	-0.003947368	-144.8	-0.022105263
52	1.5	244387.5	0.0882353	51.67	0.016470588	-51	-0.016806723	41.336	0.002962185	41.336	0.017983193	-40.8	-0.002983193	-40.8	-0.017647059
53	1.5	244387.5	0.0882353	50.39	0.01302521	-43	-0.008613445	40.312	0.002941176	40.312	0.018487395	-34.4	-0.002521008	-34.4	-0.018907563
54	1	342000	0.0763359	365	0.0065625	-367	-0.00625	292	0.0025	292	0.0089375	-293.6	-0.00234375	-293.6	-0.0084375
55	0	0	0	345	0.00625	-336	-0.011875	276	0.00328125	276	0.0109375	-268.8	-0.0029675	-268.8	-0.0096875
56	1.5	513000	0.1145038	458	0.00875	-452	-0.00875	366.4	0.00296875	366.4	0.01078125	-361.6	-0.003125	-361.6	-0.010625
57	1	342000	0.0763359	315	0.00625	-290	-0.00625	252	0.0030625	252	0.012375	-232	-0.00234375	-232	-0.013125
58	2.25	347287.5	0.2586207	64	0.021848739	-60	-0.021848739	51.2	0.00210084	51.2	0.023109244	-48	-0.00210084	-48	-0.022689076
59	2.25	347287.5	0.2586207	82	0.025630252	-81	-0.025630252	65.6	0.002941176	65.6	0.027731092	-64.8	-0.002941176	-64.8	-0.026470588
60	2.25	347287.5	0.2586207	89	0.027310924	-87	-0.028151261	71.2	0.00210084	71.2	0.031092437	-69.6	-0.002310924	-69.6	-0.031092437
61	0.7956	289598.4	0.034	250	0.003947368	-250	-0.004473684	200	0.001315789	200	0.007368421	-200	-0.002105263	-200	-0.007631579
62	0	0	0	220	0.011842105	-200	-0.005263158	176	0.002631579	176	0.017368421	-160	-0.001842105	-160	-0.015
63	0	0	0	200	0.00625	-180	-0.012	160	0.001375	160	0.01875	-144	-0.00125	-144	-0.0175
64	0	0	0	40	0.0095	-50	-0.012	32	0.00075	32	0.012	-40	-0.00025	-40	-0.012
65	0	0	0	185	0.002	-185	-25	148	0.00125	148	0.00625	-148	-0.0025	-148	-0.010125
66	0.45	75049.875	0.0283019	146	0.021052632	-140	-0.020551378	116.8	0.002506266	116.8	0.028822055	-112	-0.001253133	-112	-0.02556391
67	0.45	75049.875	0.0283019	131	0.019799499	-121	-0.019799499	104.8	0.005012531	104.8	0.027568922	-96.8	-0.001253133	-96.8	-0.025062657
68	0.45	75049.875	0.0283019	145	0.021052632	-136	-0.020551378	116	0.002506266	116	0.036340852	-108.8	-0.003759398	-108.8	-0.027568922
69	1.34	223481.85	0.0842767	196.1	0.018045113	-210.7	-0.018796992	156.88	0.003508772	156.88	0.020551378	-168.56	-0.026315789	-168.56	-0.01754386
70	0	0	0	90	0.00787037	-80	-0.005555556	72	0.003935185	72	0.016203704	-64	-0.003472222	-64	-0.013425926
71	0	0	0	120	0.00625	-115	-0.006018519	96	0.003703704	96	0.018518519	-92	-0.003703704	-92	-0.015740741

	BI	BJ	BK	BL	BM	BN	BO	BP	BQ
2	Qo Su +ve [kN] Pre	θ0.5u +ve Pre	Qo Su +ve [kN] Post	θ0.5u +ve Post	Qo Su -ve [kN] Pre	θ0.5u -ve Pre	Qo Su -ve [kN] Post	θ0.5u ve Post	Failure from paper
3	88.5	0.002005013	88.5	0.012781955	-88.5	-0.001253133	-88.5	-0.018045113	Flexure
4	76	0.001002506	76	0.019799499	-77	-0.000501253	-77	-0.018796992	Flexure
5	76	0.000250627	76	0.030075188	-73.5	-0.001253133	-73.5	-0.025313283	Flexure
6	132.5	0.00037594	132.5	0.012030075	-133.5	-0.00075188	-133.5	-0.014285714	Flexure
7	122.5	0.00037594	122.5	0.020300752	-119.5	-0.00075188	-119.5	-0.018421053	Flexure
8	120.5	0.00037594	120.5	0.026691729	-117	-0.00037594	-117	-0.02593985	Flexure
9	120	0.00037594	120	0.02593985	-118	-0.00037594	-118	-0.026691729	Flexure
10	45.605	0.000305556	45.605	0.0035	-48.43	-0.000305556	-48.43	-0.003055556	Diagonal Tension
11	51.835	0.000555556	51.835	0.003833333	-46.62	-0.0001	-46.62	-0.003444444	Diagonal Tension
12	48.35	0.000361111	48.35	0.003222222	-48.35	-0.000277778	-48.35	-0.003	Diagonal Tension
13	57.1	0.000111111	57.1	0.002555556	-61.45	-0.000222222	-61.45	-0.001722222	Diagonal Tension
14	39.55	0.00037037	39.55	0.004814815	-42.15	-0.000592593	-42.15	-0.005555556	Mixed
15	74	0.000833333	74	0.026388889	-61	-0.001111111	-61	-0.026388889	Flexure
16	139	0.001388889	139	0.021666667	-123	-0.001388889	-123	-0.021666667	Flexure
17	123	0.001388889	123	0.019583333	-117.5	-0.002222222	-117.5	-0.018888889	Flexure
18	180	0.002222222	180	0.018888889	-190	-0.001388889	-190	-0.0175	Flexure
19	188.5	0.000694444	188.5	0.014027778	-203.5	-0.002222222	-203.5	-0.014166667	Flexure
20	270.5	0.001388889	270.5	0.015555556	-279	-0.002222222	-279	-0.02	Flexure
21	209	0.00109375	209	0.014375	-204.5	-0.00078125	-204.5	-0.014375	Mixed
22	206	0.0009375	206	0.014375	-202.5	-0.0009375	-202.5	-0.014375	Mixed
23	199	0.000875	199	0.0134375	-190.5	-0.0009375	-190.5	-0.0125	Mixed
24	192	0.00096875	192	0.010625	-188.5	-0.00109375	-188.5	-0.011875	Mixed
25	179	0.00046875	179	0.009375	-173	-0.00075	-173	-0.00921875	Mixed
26	203.95	0.00025	203.95	0.00625	-204	-0.0005	-204	-0.0045	Diagonal Tension
27	221.55	0.0005	221.55	0.007	-221.7	-0.002	-221.7	-0.00675	Diagonal Tension
28	225.35	0.000833333	225.35	0.011666667	-210.45	-0.001	-210.45	-0.0115	Mixed
29	190.8	0.000333333	190.8	0.006	-195.4	-0.001	-195.4	-0.005333333	Diagonal Tension
30	274	0.000666667	274	0.006833333	-284.9	-0.000333333	-284.9	-0.006833333	Mixed
31	116	0.00027933	116	0.003072626	-136.5	-0.000558659	-136.5	-0.003631285	Diagonal Tension
32	163.5	0.00027933	163.5	0.004189944	-138	-0.000558659	-138	-0.004608939	Diagonal Tension
33	173	0.000307263	173	0.005726257	-138	-0.00027933	-138	-0.005893855	Diagonal Tension
34	141	0.00027933	141	0.005865922	-167	-0.000418994	-167	-0.005656425	Diagonal Tension
35	116	0.00027933	116	0.004888268	-108	-0.000558659	-108	-0.004748603	Diagonal Tension
36	95.5	0.000698324	95.5	0.004888268	-107.5	-0.000558659	-107.5	-0.004608939	Diagonal Tension
37	122	0.00027933	122	0.004888268	-104	-0.00027933	-104	-0.005027933	Diagonal Tension
37	122	0.00027933	122	0.004888268	-104	-0.00027933	-104	-0.005027933	Diagonal Tension
38	111.5	0.00027933	111.5	0.005446927	-108.5	-0.00027933	-108.5	-0.005055866	Diagonal Tension
39	113	0.000558659	113	0.005027933	-107	-0.000558659	-107	-0.005167598	Diagonal Tension
40	106.5	0.000418994	106.5	0.004189944	-92	-0.000418994	-92	-0.004329609	Diagonal Tension
41	105.5	0.000418994	105.5	0.004608939	-90	-0.00027933	-90	-0.004608939	Diagonal Tension
42	104.5	0.000418994	104.5	0.004888268	-103	-0.000558659	-103	-0.004748603	Diagonal Tension
43	87.5	0.000418994	87.5	0.004469274	-107.5	-0.000558659	-107.5	-0.004329609	Diagonal Tension
44	115	0.000418994	115	0.004608939	-103	-0.000418994	-103	-0.004469274	Diagonal Tension
45	209	0.00046875	209	0.01390625	-204.5	-0.00109375	-204.5	-0.01421875	Diagonal Tension
46	157.5	0.0009375	157.5	0.0128125	-145	-0.00109375	-145	-0.013125	Diagonal Tension
47	157.15	0.001002506	157.15	0.01754386	-150.9	-0.001253133	-150.9	-0.01566416	Flexure
48	47.1	0.002005013	47.1	0.039849624	-45.6	-0.001253133	-45.6	-0.034586466	Flexure
49	66.15	0.00112782	66.15	0.019548872	-63.5	-0.00093985	-63.5	-0.019172932	Flexure
50	88.1	0.001503759	88.1	0.022556391	-89.45	-0.003007519	-89.45	-0.020676692	Flexure
51	88.7	0.000526316	88.7	0.023684211	-90.5	-0.000526316	-90.5	-0.023684211	Flexure
52	25.835	0.000840336	25.835	0.018907563	-25.5	-0.000840336	-25.5	-0.017647059	Flexure
53	25.195	0.00157563	25.195	0.020168067	-21.5	-0.000840336	-21.5	-0.018907563	Flexure
54	182.5	0.00046875	182.5	0.010625	-183.5	-0.00046875	-183.5	-0.010625	Diagonal Tension
55	172.5	0.0009375	172.5	0.0125	-168	-0.0009375	-168	-0.011875	Diagonal Tension
56	229	0.00046875	229	0.0140625	-226	-0.0009375	-226	-0.011875	Diagonal Tension
57	157.5	0.00046875	157.5	0.013125	-145	-0.0009375	-145	-0.0125	Diagonal Tension
58	32	0.000840336	32	0.023529412	-30	-0.000840336	-30	-0.023529412	Flexure
59	41	0.001260504	41	0.028151261	-40.5	-0.000840336	-40.5	-0.027310924	Flexure
60	44.5	0.00105042	44.5	0.031512605	-43.5	-0.000840336	-43.5	-0.031512605	Flexure
61	125	0.001315789	125	0.008947368	-125	-0.000526316	-125	-0.008684211	Flexure
62	110	0.001315789	110	0.022368421	-100	-0.000263158	-100	-0.019210526	Flexure
63	100	0.00025	100	0.037	-90	-0.00025	-90	-0.0225	Flexure
64	20	0.00025	20	0.01375	-25	-0.00025	-25	-0.01375	Flexure
65	92.5	0.00025	92.5	0.0125	-92.5	-0.00025	-92.5	-0.01375	Flexure
66	73	0.000250627	73	0.037593985	-70	-0.000250627	-70	-0.026315789	Flexure
67	65.5	0.001253133	65.5	0.028822055	-60.5	-0.000501253	-60.5	-0.026315789	Flexure
68	72.5	0.000501253	72.5	0.037593985	-68	-0.001253133	-68	-0.028822055	Flexure
69	98.05	0.001253133	98.05	0.023809524	-105.35	-0.002506266	-105.35	-0.018796992	Flexure
70	45	0.00162037	45	0.018055556	-40	-0.001851852	-40	-0.018981481	Flexure
71	60	0.001851852	60	0.020833333	-57.5	-0.000462963	-57.5	-0.02037037	Mixed

	BG	BH	BI	BJ	BK	BL	BM	BS	BT	BU	BV	BW	BX	BZ	CA
2	Φm	α	β	χ	ξ	He (mm)	c	M1R (Nmm)	M1R (kNm)	Mu Experimental (kN		% Accuracy	M1R/VLs (N)	M1R/VLs (kN)	Qu +ve DataB
3	1	0.85	0.8	1	0.351745	3990	618.015933	614545669.2	614.5456692	706.23		87.01778021	154021.471	154.021471	177
4	1	0.85	0.8	1	0.264636	3990	441.1484329	496902086.3	496.9020863	614.46		80.86809333	124536.8637	124.5368637	154
5	1	0.85	0.8	1	0.258504	3990	442.5594014	520570230	520.57023	606.48		85.83469034	130468.7293	130.4687293	152
6	1	0.85	0.8	1	0.349066	2660	613.3091786	612831698.3	612.8316983	710.22		86.28758671	230387.8565	230.3878565	267
7	1	0.85	0.8	1	0.263763	2660	439.6924084	496141135.1	496.1411351	651.7		76.1302954	186519.2237	186.5192237	245
8	1	0.85	0.8	1	0.257626	2660	441.0557841	519769601.6	519.7696016	641.06		81.07971197	195402.1059	195.4021059	241
9	1	0.85	0.8	1	0.257626	2660	441.0557841	519769601.6	519.7696016	638.4		81.41754411	195402.1059	195.4021059	240
10	1	0.85	0.8	1	0.156897	1800	275.3548261	196354770.9	196.3547709	174.33		112.6339534	109085.9838	109.0859838	96.85
11	1	0.85	0.8	1	0.154953	1800	271.9430234	193562896.2	193.5628962	186.606		103.7281203	107534.9423	107.5349423	103.67
12	1	0.85	0.8	1	0.154737	1800	271.5640945	193252742.3	193.2527423	174.06		111.0265094	107362.6346	107.3626346	96.7
13	1	0.85	0.8	1	0.156897	900	275.3548261	196354770.9	196.3547709	110.61		177.5199086	218171.9676	218.1719676	122.9
14	1	0.85	0.8	1	0.156897	2700	275.3548261	196354770.9	196.3547709	227.61		86.26807736	72723.98921	72.72398921	84.3
15	1	0.85	0.8	1	0.097799	3600	166.7471597	368612408.1	368.6124081	532.8		69.18401052	102392.3356	102.3923356	148
16	1	0.85	0.8	1	0.22813	3600	388.9622262	844645072	844.645072	1000.8		84.39698961	234623.6311	234.6236311	278
17	1	0.85	0.8	1	0.214668	3600	366.0087937	796365488.6	796.3654886	885.6		89.92383566	221212.6357	221.2126357	246
18	1	0.85	0.8	1	0.33234	3600	566.6401496	1210331738	1210.331738	1368		88.47454222	336203.2604	336.2032604	380
19	1	0.85	0.8	1	0.386249	3600	658.5538905	1268877139	1268.877139	1465.2		86.60095132	352465.8719	352.4658719	407
20	1	0.85	0.8	1	0.483904	3600	825.0559225	1437046246	1437.046246	2008.8		71.53754708	399179.5127	399.1795127	558
21	1	0.85	0.8	1	0.315876	1800	538.5677372	867991652.9	867.9916529	752.4		115.3630586	482217.5849	482.2175849	418
22	1	0.85	0.8	1	0.315876	1800	538.5677372	867991652.9	867.9916529	741.6		117.0431031	482217.5849	482.2175849	412
23	1	0.85	0.8	1	0.315876	1800	538.5677372	867991652.9	867.9916529	716.4		121.1601972	482217.5849	482.2175849	398
24	1	0.85	0.8	1	0.315876	1800	538.5677372	867991652.9	867.9916529	691.2		125.5774961	482217.5849	482.2175849	384
25	1	0.85	0.8	1	0.279553	1800	476.6386237	762599832.2	762.5998322	644.4		118.3426183	423666.5735	423.6665735	358
26	1	0.85	0.8	1	0.274219	2000	522.3877533	1124130361	1124.130361	816		137.7610737	562065.1806	562.0651806	408
27	1	0.85	0.8	1	0.224477	2000	427.6288996	886904458.9	886.9044589	886.8		100.0117793	443452.2295	443.4522295	443.4
28	1	0.85	0.8	1	0.285663	3000	544.1880714	1356473826	1356.473826	1352.1		100.3234839	452157.9421	452.1579421	450.7
29	1	0.85	0.8	1	0.411104	3000	783.1534981	1365309558	1365.309558	1172.4		116.4542441	455103.186	455.103186	390.8
30	1	0.85	0.8	1	0.220807	3000	641.4433494	2003485235	2003.485235	1709.4		117.2040034	667828.4116	667.8284116	569.8
31	1	0.85	0.8	1	0.36692	895	621.9292635	566233792.5	566.2337925	244.335		231.7448554	632663.4553	632.6634553	273
32	1	0.85	0.8	1	0.36692	895	621.9292635	566233792.5	566.2337925	292.665		193.4750628	632663.4553	632.6634553	327
33	1	0.85	0.8	1	0.36692	895	621.9292635	566233792.5	566.2337925	309.67		182.8507096	632663.4553	632.6634553	346
34	1	0.85	0.8	1	0.367981	895	623.7274471	556889957.3	556.8899573	298.93		186.2944359	622223.4159	622.2234159	334
35	1	0.85	0.8	1	0.354692	1375	601.2032606	705721150	705.72115	319		221.2292006	513251.7454	513.2517454	232
36	1	0.85	0.8	1	0.354692	1375	601.2032606	705721150	705.72115	295.625		238.7217421	513251.7454	513.2517454	215
37	1	0.85	0.8	1	0.354692	1375	601.2032606	705721150	705.72115	335.5		210.349076	513251.7454	513.2517454	244
38	1	0.85	0.8	1	0.354692	1375	601.2032606	705721150	705.72115	306.625		230.1577334	513251.7454	513.2517454	223
39	1	0.85	0.8	1	0.367445	1375	622.8199661	561562773.9	561.5627739	310.75		180.7120753	408409.2901	408.4092901	226
40	1	0.85	0.8	1	0.367445	1375	622.8199661	561562773.9	561.5627739	292.875		191.7414508	408409.2901	408.4092901	213
41	1	0.85	0.8	1	0.367445	1375	622.8199661	561562773.9	561.5627739	290.125		193.5589053	408409.2901	408.4092901	211
42	1	0.85	0.8	1	0.367445	1375	622.8199661	561562773.9	561.5627739	287.375		195.4111436	408409.2901	408.4092901	209
43	1	0.85	0.8	1	0.367445	1375	622.8199661	561562773.9	561.5627739	295.625		189.9578093	408409.2901	408.4092901	215
44	1	0.85	0.8	1	0.367445	1375	622.8199661	561562773.9	561.5627739	316.25		177.5692566	408409.2901	408.4092901	230
45	1	0.85	0.8	1	0.315876	1250	538.5677372	867991652.9	867.9916529	522.5		166.1228044	694393.3223	694.3933223	418
46	1	0.85	0.8	1	0.315876	1875	538.5677372	867991652.9	867.9916529	590.625		146.9615497	462928.8815	462.9288815	315
47	1	0.85	0.8	1	0.340604	3990	872.7989652	1271713004	1271.713004	1254.057		101.4079108	318725.0637	318.7250637	314.3
48	1	0.85	0.8	1	0.346632	3990	396.0272515	291294108.9	291.2941089	375.858		77.50110651	73006.04233	73.00604233	94.2
49	1	0.85	0.8	1	0.565063	2660	645.5842438	418639742.8	418.6397428	351.918		118.9594573	157383.362	157.383362	132.3
50	1	0.85	0.8	1	0.565063	2660	645.5842438	418639742.8	418.6397428	475.874		87.97281273	157383.362	157.383362	178.9
51	1	0.85	0.8	1	0.565063	1900	645.5842438	418639742.8	418.6397428	343.9		121.7329872	220336.7068	220.3367068	181
52	1	0.85	0.8	1	0.319453	12100	517.5131364	582976387.2	582.9763872	625.207		93.24533909	48179.86671	48.17986671	51.67
53	1	0.85	0.8	1	0.319453	12100	517.5131364	582976387.2	582.9763872	609.719		95.61394465	48179.86671	48.17986671	50.39
54	1	0.85	0.8	1	0.315876	1800	538.5677372	867991652.9	867.9916529	660.6		131.3944373	482217.5849	482.2175849	367
55	1	0.85	0.8	1	0.222319	1800	379.0542999	729202684.4	729.2026844	621		117.4239427	405112.6024	405.1126024	345
56	1	0.85	0.8	1	0.362654	1800	618.3244559	920562977.3	920.5629773	824.4		111.6646018	511423.8763	511.4238763	458
57	1	0.85	0.8	1	0.315876	1800	538.5677372	867991652.9	867.9916529	567		153.0849476	482217.5849	482.2175849	315
58	1	0.85	0.8	1	0.611599	12100	990.7898813	359413267.6	359.4132676	774.4		46.41183724	29703.57584	29.70357584	64
59	1	0.85	0.8	1	0.745792	12100	1208.182497	444457466.7	444.4574667	992.2		44.79514883	36732.02204	36.73202204	82
60	1	0.85	0.8	1	0.775536	12100	1217.591059	433662871.1	433.6628711	1076.9		40.26955809	35839.9067	35.8399067	89
61	1	0.85	0.766	1	0.109304	3920	276.5400475	848298776.6	848.2987766	980		86.56109965	216402.7491	216.4027491	250
62	1	0.85	0.766	1	0.058706	3800	148.5257251	533115862.7	533.1158627	836		63.76984004	140293.6481	140.2936481	220
63	1	0.85	0.729	1	0.040403	4000	101.2106535	544598878.4	544.5988784	800		68.0748598	136149.7196	136.1497196	200
64	1	0.85	0.729	1	0.026241	4000	34.24471306	99229179.38	99.22917938	200		49.61458969	24807.29485	24.80729485	50
65	1	0.85	0.729	1	0.053547	4000	135.4738814	536979843.8	536.9798438	740		72.56484376	134244.961	134.244961	185
66	1	0.85	0.8	1	0.25	3990	368.664475	462809126.3	462.8091263	582.54		79.44675496	115992.2622	115.9922622	146
67	1	0.85	0.8	1	0.21553	3990	368.664475	473621711.4	473.6217114	522.69		90.61235367	118702.1833	118.7021833	131
68	1	0.85	0.8	1	0.21553	3990	368.664475	473621711.4	473.6217114	578.55		81.8635747	118702.1833	118.7021833	145
69	1	0.85	0.8	1	0.296901	3990	507.8494216	547875809.2	547.8758092	840.693		65.16954574	137312.2329	137.3122329	210.7
70	1	0.85	0.8	1	0.132245	2160	198.5663249	161537152.2	161.5371522	194.4		83.09524291	74785.71862	74.78571862	90
71	1	0.85	0.8	1	0.081544	2160	122.4383507	100100072.4	100.1000724	259.2		38.61885509	46342.62611	46.34262611	120

	DE	DI	DJ	DL	DM	DN	DU	DV	DW	DX
2	Vr sliding (fr	Vcrush (4.1	Vr = Vs + Vm - Sl	Vgoverning (kN)	Vflexure (kN	Mixed Mod	Failure (From Pa	Perform	Failure from Analytical P	
3	782093.3	210169.3	182516.15	182.52	154.0215	118.5005	Flexure	Flexure	Flexure	
4	274288.1	210169.3	174407.15	174.41	124.5369	140.0446	Flexure	Flexure	Flexure	
5	204988.1	210169.3	174407.15	174.41	130.4687	133.6774	Flexure	Flexure	Flexure	
6	777552.3	210169.3	235148.75	210.17	230.3879	91.22411	Flexure	Shear	Diagonal Tension	
7	273152.9	210169.3	228256.10	210.17	186.5192	112.6797	Flexure	Flexure	Flexure	
8	203852.9	210169.3	228256.10	203.85	195.4021	104.3248	Flexure	Flexure	Flexure	
9	203852.9	210169.3	228256.10	203.85	195.4021	104.3248	Flexure	Flexure	Flexure	
10	188307	182547.5	156854.17	156.85	109.086	143.7895	Diagonal Tension	Flexure	Flexure	
11	185026.5	182547.5	161105.11	161.11	107.5349	149.8165	Diagonal Tension	Flexure	Flexure	
12	184663.1	182547.5	161105.11	161.11	107.3626	150.057	Diagonal Tension	Flexure	Flexure	
13	188307	273821.2	168759.05	168.76	218.172	77.35139	Diagonal Tension	Shear	Diagonal Tension	
14	188307	182547.5	174674.23	174.67	72.72399	240.1879	Mixed	Flexure	Flexure	
15	351400	421024.1	469609.63	351.40	102.3923	343.1897	Flexure	Flexure	Flexure	
16	948780	421024.1	620209.63	421.02	234.6236	179.4466	Flexure	Flexure	Flexure	
17	878500	421024.1	620209.63	421.02	221.2126	190.3255	Flexure	Flexure	Flexure	
18	1581300	421024.1	1072009.63	421.02	336.2033	125.229	Flexure	Flexure	Flexure	
19	1760850	421024.1	1136134.63	421.02	352.4659	119.451	Flexure	Flexure	Flexure	
20	2324700	421024.1	1419859.63	421.02	399.1795	105.4724	Flexure	Flexure	Mixed	
21	1052100	396106.3	415942.51	396.11	482.2176	82.14265	Mixed	Shear	Diagonal Tension	
22	1052100	396106.3	415942.51	396.11	482.2176	82.14265	Mixed	Shear	Diagonal Tension	
23	1052100	396106.3	415942.51	396.11	482.2176	82.14265	Mixed	Shear	Diagonal Tension	
24	1052100	396106.3	415942.51	396.11	482.2176	82.14265	Mixed	Shear	Diagonal Tension	
25	871500	396106.3	415942.51	396.11	423.6666	93.49482	Mixed	Shear	Diagonal Tension	
26	1158500	477192.9	328377.14	328.38	562.0652	58.42332	Diagonal Tension	Shear	Diagonal Tension	
27	892500	433346.6	343338.66	343.34	443.4522	77.42405	Diagonal Tension	Shear	Diagonal Tension	
28	1487500	477192.9	445877.14	445.88	452.1579	98.61093	Mixed	Mixed	Mixed	
29	1753500	433346.6	353338.66	353.34	455.1032	77.63924	Diagonal Tension	Shear	Diagonal Tension	
30	1338750	650020	345007.99	345.01	667.8284	51.66117	Mixed	Shear	Diagonal Tension	
31	665140	516235.5	556544.20	516.24	632.6635	81.59717	Diagonal Tension	Shear	Diagonal Tension	
32	665140	516235.5	556544.20	516.24	632.6635	81.59717	Diagonal Tension	Shear	Diagonal Tension	
33	665140	516235.5	556544.20	516.24	632.6635	81.59717	Diagonal Tension	Shear	Diagonal Tension	
34	655617.2	511047.1	551067.83	511.05	622.2234	82.13241	Diagonal Tension	Shear	Diagonal Tension	
35	807982	483374.6	504414.85	483.37	513.2517	94.17886	Diagonal Tension	Shear	Diagonal Tension	
36	807982	483374.6	504414.85	483.37	513.2517	94.17886	Diagonal Tension	Shear	Diagonal Tension	
37	807982	483374.6	504414.85	483.37	513.2517	94.17886	Diagonal Tension	Shear	Diagonal Tension	
38	807982	483374.6	504414.85	483.37	513.2517	94.17886	Diagonal Tension	Shear	Diagonal Tension	
39	660378.6	421822.5	427078.51	421.82	408.4093	103.2843	Diagonal Tension	Flexure	Mixed	
40	660378.6	421822.5	427078.51	421.82	408.4093	103.2843	Diagonal Tension	Flexure	Mixed	
41	660378.6	421822.5	427078.51	421.82	408.4093	103.2843	Diagonal Tension	Flexure	Mixed	
42	660378.6	421822.5	427078.51	421.82	408.4093	103.2843	Diagonal Tension	Flexure	Mixed	
43	660378.6	421822.5	337078.51	337.08	408.4093	82.53449	Diagonal Tension	Shear	Diagonal Tension	
44	660378.6	421822.5	337078.51	337.08	408.4093	82.53449	Diagonal Tension	Shear	Diagonal Tension	
45	1052100	517138.8	464355.50	464.36	694.3933	66.87212	Diagonal Tension	Shear	Diagonal Tension	
46	1052100	396106.3	415942.51	396.11	462.9289	85.56526	Diagonal Tension	Shear	Diagonal Tension	
47	669665.9	295155	319183.38	295.16	318.7251	92.60489	Flexure	Shear	Mixed	
48	138686.5	137294.3	227603.60	137.29	73.00604	188.0588	Flexure	Flexure	Flexure	
49	520606.5	137294.3	183217.10	137.29	157.3834	87.2356	Flexure	Shear	Diagonal Tension	
50	520606.5	137294.3	493922.60	137.29	157.3834	87.2356	Flexure	Shear	Mixed	
51	520606.5	137294.3	153626.10	137.29	220.3367	62.31114	Flexure	Shear	Diagonal Tension	
52	262519.3	214962.2	390137.45	214.96	48.17987	446.1661	Flexure	Flexure	Flexure	
53	262519.3	214962.2	390137.45	214.96	48.17987	446.1661	Flexure	Flexure	Flexure	
54	1052100	396106.3	243942.51	243.94	482.2176	50.58764	Diagonal Tension	Shear	Diagonal Tension	
55	812700	396106.3	545442.51	396.11	405.1126	97.77684	Diagonal Tension	Shear	Diagonal Tension	
56	1171800	396106.3	673692.51	396.11	511.4239	77.45166	Diagonal Tension	Shear	Diagonal Tension	
57	1052100	396106.3	630942.51	396.11	482.2176	82.14265	Diagonal Tension	Shear	Diagonal Tension	
58	334549.3	145685.5	365986.86	145.69	29.70358	490.4644	Flexure	Flexure	Flexure	
59	334549.3	145685.5	365986.86	145.69	36.73202	396.6171	Flexure	Flexure	Flexure	
60	334549.3	145685.5	365986.86	145.69	35.83991	406.4895	Flexure	Flexure	Flexure	
61	538718.9	563455.1	1057781.63	538.72	216.4027	248.9427	Flexure	Flexure	Flexure	
62	336000	563455.1	985382.03	336.00	140.2936	239.4977	Flexure	Flexure	Flexure	
63	336000	822927.5	529171.00	336.00	136.1497	246.7871	Flexure	Flexure	Flexure	
64	112000	443114.8	377245.92	112.00	24.80729	451.4801	Flexure	Flexure	Flexure	
65	336000	606367.6	1002547.05	336.00	134.245	250.2887	Flexure	Flexure	Flexure	
66	156757.9	207055.5	722995.67	156.76	115.9923	135.1451	Flexure	Flexure	Flexure	
67	156757.9	207055.5	722995.67	156.76	118.7022	132.0598	Flexure	Flexure	Flexure	
68	156757.9	207055.5	722995.67	156.76	118.7022	132.0598	Flexure	Flexure	Flexure	
69	260660.3	207055.5	760103.66	207.06	137.3122	150.7917	Flexure	Flexure	Flexure	
70	188606.9	135772.4	190586.94	135.77	74.78572	181.5485	Flexure	Flexure	Flexure	
71	110020.7	135772.4	190586.94	110.02	46.34263	237.4071	Mixed	Flexure	Flexure	

	EP	EQ	ER	ES	ET	EU	EV	EW	EX	EY	EZ	FA	FB	FC	FD	FE
2	α	α (%)	β	ϕmLw - Fig	ϕ75Lw - Fig	ϕcLw - Fig	Mmax/fwAr	Qflex (kN) -	Em Modifier	Em (Mpa)	Ie (mm^4)	Icr (mm^4)	Lp (mm)	Av (mm^2)	Gm Modifier	Gm (MPa)
3	0.362558	36.25577	0.066463	0.016902	0.047147	0.076858	0.176608	212.145822	850	13940	4.3886E+10	2.1943E+10	461.486004	129744	0.4	5576
4	0.106635	10.66346	0.054268	0.017249	0.05022	0.070393	0.102804	123.490703	850	13940	4.3886E+10	2.1943E+10	461.486004	129744	0.4	5576
5	0.072512	7.251154	0.054268	0.018189	0.046223	0.048133	0.077426	93.0060128	850	13940	4.3886E+10	2.1943E+10	461.486004	129744	0.4	5576
6	0.362558	36.25577	0.064024	0.017058	0.048007	0.077399	0.175633	316.460849	850	13940	4.3886E+10	2.1943E+10	408.286004	129744	0.4	5576
7	0.106635	10.66346	0.053659	0.017363	0.050341	0.07049	0.102634	184.928367	850	13940	4.3886E+10	2.1943E+10	408.286004	129744	0.4	5576
8	0.072512	7.251154	0.053659	0.018195	0.046205	0.047734	0.077233	139.161394	850	13940	4.3886E+10	2.1943E+10	408.286004	129744	0.4	5576
9	0.072512	7.251154	0.053659	0.018195	0.046205	0.047734	0.077233	139.161394	850	13940	4.3886E+10	2.1943E+10	408.286004	129744	0.4	5576
10	0.073432	7.34319	0.060484	0.018267	0.046444	0.052883	0.079053	158.801214	850	10540	4.374E+10	2.187E+10	372.874764	129600	0.4	4216
11	0.071099	7.109896	0.060484	0.017867	0.046095	0.050335	0.079915	160.532763	850	10540	4.374E+10	2.187E+10	355.935098	129600	0.4	4216
12	0.070841	7.08405	0.060484	0.017823	0.046057	0.050053	0.08001	160.724599	850	10540	4.374E+10	2.187E+10	408.019362	129600	0.4	4216
13	0.073432	7.34319	0.060484	0.018267	0.046444	0.052883	0.079053	317.602428	850	10540	4.374E+10	2.187E+10	336.874764	129600	0.4	4216
14	0.073432	7.34319	0.060484	0.018267	0.046444	0.052883	0.079053	105.867476	850	10540	4.374E+10	2.187E+10	408.874764	129600	0.4	4216
15	0.099178	9.917813	0	0.034667	0.056139	0.063752	0.050016	126.57948	850	12580	9.234E+10	4.617E+10	498.735315	273600	0.4	5032
16	0.267781	26.77809	0	0.022	0.055	0.0767	0.112112	283.734	850	12580	9.234E+10	4.617E+10	536.958666	273600	0.4	5032
17	0.247945	24.79453	0	0.022	0.055	0.0767	0.104178	263.654	850	12580	9.234E+10	4.617E+10	599.208122	273600	0.4	5032
18	0.446302	44.63016	0	0.022	0.055	0.0767	0.183521	464.454	850	12580	9.234E+10	4.617E+10	599.208122	273600	0.4	5032
19	0.446302	44.63016	0.050676	0.017953	0.052306	0.079621	0.203791	515.754	850	12580	9.234E+10	4.617E+10	599.208122	273600	0.4	5032
20	0.554765	55.47653	0.101351	0.014933	0.034558	0.064565	0.267447	676.854	850	12580	9.234E+10	4.617E+10	666.091371	273600	0.4	5032
21	0.25914	25.91402	0.076336	0.016295	0.043535	0.074244	0.13919	623.601	850	11135	9.234E+10	4.617E+10	434.414793	273600	0.4	4454
22	0.25914	25.91402	0.076336	0.016295	0.043535	0.074244	0.13919	623.601	850	11135	9.234E+10	4.617E+10	434.414793	273600	0.4	4454
23	0.25914	25.91402	0.076336	0.016295	0.043535	0.074244	0.13919	623.601	850	11135	9.234E+10	4.617E+10	434.414793	273600	0.4	4454
24	0.25914	25.91402	0.076336	0.016295	0.043535	0.074244	0.13919	623.601	850	11135	9.234E+10	4.617E+10	434.414793	273600	0.4	4454
25	0.201554	20.15535	0.076336	0.016295	0.043535	0.074244	0.116156	520.401	850	11135	9.234E+10	4.617E+10	531.702683	273600	0.4	4454
26	0.217874	21.78742	0.064935	0.016999	0.047688	0.077202	0.118124	691.26	850	13090	1.2667E+11	6.3333E+10	460.293691	304000	0.4	5236
27	0.264194	26.41939	0	0.022	0.055	0.0767	0.110678	534.13	850	10795	1.2667E+11	6.3333E+10	460.293691	304000	0.4	4318
28	0.363124	36.31237	0	0.022	0.055	0.0767	0.150249	586.173333	850	13090	1.2667E+11	6.3333E+10	552.994924	304000	0.4	5236
29	0.440323	44.03232	0.07874	0.016153	0.042638	0.073504	0.212625	684.086667	850	10795	1.2667E+11	6.3333E+10	552.994924	304000	0.4	4318
30	0.264194	26.41939	0	0.022	0.055	0.0767	0.110678	801.195	850	10795	4.275E+11	2.1375E+11	600.293691	456000	0.4	4318
31	0.079388	7.938842	0.2	0.008771	0.003464	0	0.121225	824.5758	850	8500	9.081E+10	4.5405E+10	371.435243	272080	0.4	3400
32	0.079388	7.938842	0.2	0.008771	0.003464	0	0.121225	824.5758	850	8500	9.081E+10	4.5405E+10	371.435243	272080	0.4	3400
33	0.079388	7.938842	0.2	0.008771	0.003464	0	0.121225	824.5758	850	8500	9.081E+10	4.5405E+10	371.435243	272080	0.4	3400
34	0.081009	8.100859	0.2	0.009166	0.00393	0	0.120681	804.455484	850	8330	9.081E+10	4.5405E+10	371.435243	272080	0.4	3332
35	0.061068	6.106801	0.2	0.004301	0	0	0.127381	733.171333	850	11050	9.081E+10	4.5405E+10	390.635243	272080	0.4	4420
36	0.061068	6.106801	0.2	0.004301	0	0	0.127381	733.171333	850	11050	9.081E+10	4.5405E+10	390.635243	272080	0.4	4420
37	0.061068	6.106801	0.2	0.004301	0	0	0.127381	733.171333	850	11050	9.081E+10	4.5405E+10	390.635243	272080	0.4	4420
38	0.061068	6.106801	0.2	0.004301	0	0	0.127381	733.171333	850	11050	9.081E+10	4.5405E+10	390.635243	272080	0.4	4420
39	0.08019	8.019032	0.2	0.008966	0.003695	0	0.120956	530.175636	850	8415	9.081E+10	4.5405E+10	390.635243	272080	0.4	3366
40	0.08019	8.019032	0.2	0.008966	0.003695	0	0.120956	530.175636	850	8415	9.081E+10	4.5405E+10	390.635243	272080	0.4	3366
41	0.08019	8.019032	0.2	0.008966	0.003695	0	0.120956	530.175636	850	8415	9.081E+10	4.5405E+10	390.635243	272080	0.4	3366
42	0.08019	8.019032	0.2	0.008966	0.003695	0	0.120956	530.175636	850	8415	9.081E+10	4.5405E+10	390.635243	272080	0.4	3366
43	0.08019	8.019032	0.2	0.008966	0.003695	0	0.120956	530.175636	850	8415	9.081E+10	4.5405E+10	390.635243	272080	0.4	3366
44	0.08019	8.019032	0.2	0.008966	0.003695	0	0.120956	530.175636	850	8415	9.081E+10	4.5405E+10	390.635243	272080	0.4	3366
45	0.25914	25.91402	0.076336	0.016295	0.043535	0.074244	0.13919	897.98544	850	11135	9.234E+10	4.617E+10	412.414793	273600	0.4	4454
46	0.25914	25.91402	0.076336	0.016295	0.043535	0.074244	0.13919	598.65696	850	11135	9.234E+10	4.617E+10	437.414793	273600	0.4	4454
47	0.230026	23.0026	0.059732	0.017338	0.049474	0.078249	0.120903	286.432319	850	12665	1.4036E+11	7.0182E+10	547.031835	191160	0.4	5066
48	0.081019	8.101878	0.059732	0.019614	0.047614	0.060879	0.07601	38.9637156	850	12665	1.4127E+10	7063698281	405.031835	88920	0.4	5066
49	0.526622	52.66221	0.059732	0.017338	0.049474	0.078249	0.239541	184.188162	850	12665	1.4127E+10	7063698281	351.831835	88920	0.4	5066
50	0.526622	52.66221	0.059732	0.017338	0.049474	0.078249	0.239541	184.188162	850	12665	1.4127E+10	7063698281	351.831835	88920	0.4	5066
51	0.526622	52.66221	0.059732	0.017338	0.049474	0.078249	0.239541	257.863427	850	12665	1.4127E+10	7063698281	321.431835	88920	0.4	5066
52	0.063959	6.395927	0.088235	0.016853	0.044301	0.056208	0.091276	35.8322461	850	14450	3.9933E+10	1.9967E+10	750.568891	130340	0.4	5780
53	0.063959	6.395927	0.088235	0.016853	0.044301	0.056208	0.091276	35.8322461	850	14450	3.9933E+10	1.9967E+10	750.568891	130340	0.4	5780
54	0.25914	25.91402	0.076336	0.016295	0.043535	0.074244	0.13919	623.601	850	11135	9.234E+10	4.617E+10	434.414793	273600	0.4	4454
55	0.25914	25.91402	0	0.022	0.055	0.0767	0.108656	486.801	850	11135	9.234E+10	4.617E+10	434.414793	273600	0.4	4454
56	0.25914	25.91402	0.114504	0.014317	0.030759	0.057719	0.154458	692.001	850	11135	9.234E+10	4.617E+10	434.414793	273600	0.4	4454
57	0.25914	25.91402	0.076336	0.016295	0.043535	0.074244	0.13919	623.601	850	11135	9.234E+10	4.617E+10	434.414793	273600	0.4	4454
58	0.124978	12.49779	0.258621	0.022819	0	0.045	0.154768	29.4568963	850	7395	3.7832E+10	1.8916E+10	750.568891	123480	0.4	2958
59	0.124978	12.49779	0.258621	0.022819	0	0.045	0.154768	29.4568963	850	7395	3.7832E+10	1.8916E+10	750.568891	123480	0.4	2958
60	0.145717	14.57166	0.258621	0.021525	0	0.045	0.148816	28.3239223	850	7395	3.7832E+10	1.8916E+10	750.568891	123480	0.4	2958
61	0.056354	5.63539	0.034	0.012672	0.039248	0.027784	0.077086	435.491564	850	19890	2.0505E+11	1.0253E+11	515.132125	291200	0.4	7956
62	0.056354	5.63539	0	0.006917	0.026933	0.024782	0.06646	387.318278	850	19890	2.0505E+11	1.0253E+11	510.332125	291200	0.4	7956
63	0.035855	3.585461	0	0.063639	0.087547	0.106464	0.039518	343.875399	850	23035	2.7829E+11	1.3914E+11	559.231327	395200	0.4	9214
64	0.022196	2.219571	0	0.059815	0.084405	0.103049	0.048225	121.672749	850	23035	4.3447E+10	2.1723E+10	398.332125	212800	0.4	9214
65	0.04866	4.865983	0	0.067225	0.090492	0.109665	0.031354	201.039768	850	23035	2.0505E+11	1.0253E+11	518.332125	291200	0.4	9214
66	0.064425	6.442484	0.028302	0.015012	0.040815	0.037741	0.072261	86.5884055	850	13515	4.518E+10	2.259E+10	461.905584	133422	0.4	5406
67	0.064425	6.442484	0.028302	0.015012	0.040815	0.037741	0.072261	86.5884055	850	13515	4.518E+10	2.259E+10	461.905584	133422	0.4	5406
68	0.064425	6.442484	0.028302	0.015012	0.040815	0.037741	0.072261	86.5884055	850	13515	4.518E+10	2.259E+10	461.905584	133422	0.4	5406
69	0.064425	6.442484	0.084277	0.016931	0.044679	0.055374	0.089863	107.680437	850	13515	4.518E+10	2.259E+10	461.905584	133422	0.4	5406
70	0.14455	14.45505	0	0.032428	0.058918	0.070267	0.072213	95.5302419	850	16405	1.8914E+10	9457051897	321.541914	77263.2	0.4	6562
71	0.084321	8.43211	0	0.02504	0.046007	0.050232	0.055721	73.7131478	850	16405	1.8914E+10	9457051897	321.541914	77263.2	0.4	6562

	FG	FH	FI	FJ	FK	FL	FM	FN	FO	FP	FQ	FR	FS	FT	FU	FV	FW
	δn-elast	δn-plast	δn-flex	δn - sh	δn		δ75-elast	δ75-plast	δ75-flex	δ75 - sh	δ75		δc-elast	δc-plast	δc-flex (1/m)	δc - sh (1/m)	δc (1/m)
2							0.03479737	0.01100858	0.04580595	1.835E-06	0.04580778		0.05672653	0.01086176	0.07534413	1.2233E-06	0.07534536
3	0.01247467	0.003263	0.01573767	2.4466E-06	0.01574012		0.0370655	0.01193403	0.04899953	1.5965E-06	0.04900113		0.05195497	0.01710041	0.06905537	1.0643E-06	0.06905644
4	0.01273079	0.00349033	0.01622112	2.1287E-06	0.01622325		0.03411556	0.01092249	0.04503805	1.5758E-06	0.04503962		0.03552569	0.01141178	0.04693747	1.0505E-06	0.04693852
5	0.01342451	0.00374307	0.01716758	2.101E-06	0.01716968		0.02362154	0.0099291	0.03355064	2.768E-06	0.03355341		0.03808376	0.01658856	0.05467232	1.8453E-06	0.05467417
6	0.00839314	0.00291683	0.01130997	1.6906E-06	0.01131166		0.02477008	0.01053608	0.03530616	2.5399E-06	0.0353087		0.03468413	0.01510123	0.04978536	1.6933E-06	0.04978706
7	0.00854335	0.00306411	0.01160746	3.3865E-06	0.01161085		0.02273496	0.00961317	0.03234813	2.4984E-06	0.03235063		0.02348718	0.00995954	0.03344672	1.6656E-06	0.03344839
8	0.00895256	0.00326674	0.0122193	3.3312E-06	0.01222263		0.02273496	0.00961672	0.03235168	2.4881E-06	0.03235417		0.02348718	0.00996309	0.03345027	1.6587E-06	0.03345193
9	0.00895256	0.00327029	0.01222285	3.3174E-06	0.01222617		0.01548129	0.00933897	0.02482026	1.3294E-06	0.02482159		0.01762757	0.0106728	0.02830037	8.8627E-07	0.02830126
10	0.00608911	0.00350213	0.00959125	1.7725E-06	0.00959302		0.01536514	0.00882684	0.02419198	1.423E-06	0.02419341		0.0167842	0.00966524	0.02644365	9.4868E-07	0.0264446
11	0.00595582	0.003245	0.00920082	1.8974E-06	0.00920272		0.01535227	0.01013194	0.02548421	1.3273E-06	0.02548554		0.01668434	0.01103779	0.02772213	8.8489E-07	0.02772301
12	0.00594105	0.00373201	0.00967306	1.7698E-06	0.00967483		0.00774064	0.00853044	0.01627109	1.687E-06	0.01627277		0.00881379	0.00973549	0.01854928	1.1246E-06	0.0185504
13	0.00304456	0.00325713	0.00630169	2.2493E-06	0.00630394		0.02322193	0.01014612	0.03336805	1.1571E-06	0.0333692		0.02644136	0.01160872	0.03805008	7.7142E-07	0.03805085
14	0.00913367	0.00374574	0.01287942	1.5428E-06	0.01288096		0.03742632	0.01509735	0.05252367	8.0624E-07	0.05252448		0.0425014	0.01720662	0.05970802	5.375E-07	0.05970855
15	0.02311162	0.00914798	0.0322596	1.075E-06	0.03226057		0.03666667	0.01548184	0.05214851	1.5144E-06	0.05215003		0.05113333	0.02155518	0.07308851	1.0096E-06	0.07308952
16	0.01466667	0.0056376	0.02030427	2.0192E-06	0.02030629		0.03666667	0.0173955	0.05406216	1.3401E-06	0.0540635		0.05113333	0.02461928	0.07575262	8.3941E-07	0.07575351
17	0.01466667	0.00641002	0.02107668	1.7868E-06	0.02107847		0.03666667	0.01689782	0.05356449	2.0701E-06	0.05356656		0.05113333	0.02412161	0.07525494	1.3801E-06	0.07525632
18	0.01466667	0.00591234	0.02057901	2.7601E-06	0.02058177		0.03487072	0.01590076	0.05077147	2.2172E-06	0.05077369		0.05308047	0.02499362	0.07807408	1.4781E-06	0.07807556
19	0.01196853	0.00446478	0.01643331	2.9562E-06	0.01643626		0.02303865	0.01048448	0.03352313	9.0398E-06	0.03352617		0.04304349	0.02158869	0.06463218	2.0265E-06	0.0646342
20	0.0099552	0.00322217	0.01317737	4.053E-06	0.01318142		0.01451153	0.00987093	0.02438246	2.5726E-06	0.02438503		0.02474795	0.01728235	0.0420303	1.7151E-06	0.04203202
21	0.00543173	0.00329694	0.00872867	3.4301E-06	0.0087321		0.01451153	0.00988006	0.02439158	2.5357E-06	0.02439412		0.02474795	0.01729148	0.04203943	1.6904E-06	0.04204112
22	0.00543173	0.00330606	0.0087378	3.3809E-06	0.00874118		0.01451153	0.00990135	0.02441288	2.4495E-06	0.02441533		0.02474795	0.01731277	0.04206072	1.633E-06	0.04206235
23	0.00543173	0.00332735	0.00875909	3.266E-06	0.00876236		0.01451153	0.00992264	0.02443417	2.3633E-06	0.02443653		0.02474795	0.01733406	0.04208201	1.5756E-06	0.04208359
24	0.00543173	0.00334865	0.00878038	3.1511E-06	0.00878353		0.01451153	0.00994393	0.02445546	2.2833E-06	0.02445829		0.02474795	0.01735546	0.04210341	1.4689E-06	0.04210488
25	0.00543173	0.00414699	0.00957872	2.9378E-06	0.00958166		0.01451153	0.01219324	0.02670476	2.2033E-06	0.02670697		0.02474795	0.01126446	0.04601241	1.4689E-06	0.04601388
26	0.00566639	0.00345924	0.00912563	2.5632E-06	0.00912819		0.01589587	0.01052209	0.02641796	1.9224E-06	0.02641988		0.02573392	0.01731469	0.04304861	1.2816E-06	0.04304989
27	0.00733333	0.00446619	0.01179952	3.3778E-06	0.0118029		0.01833333	0.01206103	0.03039437	2.5334E-06	0.0303969		0.02556667	0.01705522	0.04262189	1.6889E-06	0.04262358
28	0.011	0.00518105	0.01618105	2.8315E-06	0.01618388		0.0275	0.01430546	0.04180546	2.1236E-06	0.04180758		0.03835	0.02030546	0.05865546	1.4157E-06	0.05865687
29	0.00807669	0.00351808	0.01159477	2.9771E-06	0.01159775		0.0213191	0.01084106	0.03216016	2.2329E-06	0.0321624		0.03675195	0.01937535	0.0561273	1.4886E-06	0.05612878
30	0.00733333	0.00395744	0.01129078	2.8938E-06	0.01129367		0.01833333	0.01056067	0.02889401	2.1704E-06	0.02889618		0.02556667	0.0149028	0.04046946	1.4469E-06	0.04047091
31	0.0014618	0.00158483	0.00304663	2.9511E-06	0.00304958		0.00057731	0.00048362	0.00106093	2.2133E-06	0.00106314		0	-0.0002352	-0.0002352	1.4756E-06	-0.0002337
32	0.0014618	0.00153832	0.00300012	3.5349E-06	0.00300365		0.00057731	0.00043711	0.00101442	2.6511E-06	0.00101707		0	-0.0002817	-0.0002817	1.7674E-06	-0.0002799
33	0.0014618	0.00152195	0.00298375	3.7402E-06	0.00298749		0.00057731	0.00042074	0.00099805	2.8052E-06	0.00100086		0	-0.000298	-0.000298	1.8701E-06	-0.0002962
34	0.00152768	0.00160845	0.00313613	3.6842E-06	0.00313982		0.00065508	0.00052203	0.00117711	2.7632E-06	0.00117987		0	-0.0002936	-0.0002936	1.8421E-06	-0.0002917
35	0.00110118	0.00069016	0.00179133	1.9292E-06	0.00179326		0	-0.0002484	-0.0002484	1.4469E-06	-0.0002469		0	-0.0002484	-0.0002484	9.6458E-07	-0.0002474
36	0.00110118	0.00070836	0.00180953	1.7878E-06	0.00181132		0	-0.0002302	-0.0002302	1.3409E-06	-0.0002288		0	-0.0002302	-0.0002302	8.939E-07	-0.0002293
37	0.00110118	0.00067731	0.00177849	2.0289E-06	0.00178052		0	-0.0002612	-0.0002612	1.5217E-06	-0.0002597		0	-0.0002612	-0.0002612	1.0145E-06	-0.0002602
38	0.00110118	0.00069979	0.00180097	1.8543E-06	0.00180282		0	-0.0002387	-0.0002387	1.3907E-06	-0.0002373		0	-0.0002387	-0.0002387	9.2716E-07	-0.0002378
39	0.00229588	0.00163906	0.00393493	2.4677E-06	0.0039374		0.00094606	0.00048862	0.00143468	1.8509E-06	0.00143653		0.01718608	0.01659155	0.03377763	1.7151E-06	0.03377934
40	0.00229588	0.00165733	0.00395321	2.3258E-06	0.00395553		0.00094606	0.00050689	0.00145296	1.7443E-06	0.0014547		0	-0.0002594	-0.0002594	1.1629E-06	-0.0002983
41	0.00229588	0.00166014	0.00395602	2.3039E-06	0.00395832		0.00094606	0.00050971	0.00145577	1.728E-06	0.0014575		0	-0.0002966	-0.0002966	1.152E-06	-0.0002955
42	0.00229588	0.00166295	0.00395883	2.2821E-06	0.00396111		0.00094606	0.00051252	0.00145858	1.7116E-06	0.0014629		0	-0.0002938	-0.0002938	1.1411E-06	-0.0002927
43	0.00229588	0.00165452	0.0039504	2.3476E-06	0.00395274		0.00094606	0.00050408	0.00145015	1.7607E-06	0.0014519		0	-0.0003022	-0.0003022	1.1738E-06	-0.0003011
44	0.00229588	0.00163343	0.00392931	2.5114E-06	0.00393182		0.00094606	0.000483	0.00143906	1.8836E-06	0.0014304		0	-0.0003233	-0.0003233	1.2557E-06	-0.0003221
45	0.00377204	0.0033144	0.00708843	3.4301E-06	0.00708986		0.01007745	0.00955546	0.01963291	2.5726E-06	0.01963549		0.01718608	0.01659155	0.03377763	1.7151E-06	0.03377934
46	0.00563806	0.00345735	0.00911154	2.5849E-06	0.00911799		0.01511617	0.01007674	0.02519291	1.9387E-06	0.02519485		0.02577911	0.01753934	0.04331846	1.2925E-06	0.04331975
47	0.00868519	0.00280045	0.01148564	3.2455E-06	0.01148888		0.02478345	0.0094217	0.03420515	2.4341E-06	0.03420758		0.03919839	0.01535059	0.05454898	1.6228E-06	0.0545506
48	0.02112234	0.00473083	0.02585317	2.0912E-06	0.02585526		0.05127661	0.01391386	0.06519047	1.5684E-06	0.06519204		0.06556188	0.01826423	0.08382612	1.0456E-06	0.08382716
49	0.0124476	0.00355523	0.01600284	2.9369E-06	0.01600577		0.03551961	0.01271027	0.04822987	2.2027E-06	0.04823208		0.05617907	0.020908	0.07708707	1.4685E-06	0.07708854
50	0.0124476	0.00306774	0.01551535	3.9714E-06	0.01551932		0.03551961	0.01222278	0.04774239	2.9786E-06	0.04774536		0.05617907	0.02042051	0.07659958	1.9857E-06	0.07660156
51	0.00889114	0.00327685	0.012168	4.018E-06	0.01217202		0.02537115	0.01164085	0.03701199	3.0135E-06	0.03701501		0.0401279	0.01913026	0.05925816	2.009E-06	0.05926017
52	0.03963401	0.0057491	0.04538311	6.8586E-07	0.04538379		0.1041878	0.01776201	0.12194981	5.1439E-07	0.12195033		0.13218945	0.02297287	0.15516232	3.4293E-07	0.15516267
53	0.03963401	0.00578939	0.0454234	6.6887E-07	0.04542407		0.1041878	0.0178023	0.1219901	5.0165E-07	0.1219906		0.13218945	0.02301317	0.15520262	3.3443E-07	0.15520295
54	0.00543173	0.00337451	0.00880624	3.0116E-06	0.00880925		0.01451153	0.0099485	0.02446039	2.2587E-06	0.02446229		0.02474795	0.01735992	0.04210787	1.5058E-06	0.04210938
55	0.00733333	0.00478477	0.01211811	2.8311E-06	0.01212094		0.01833333	0.01274904	0.03108238	2.1233E-06	0.0310845		0.02556667	0.01798615	0.04355282	1.4155E-06	0.04355424
56	0.00477229	0.00275864	0.00753094	3.7584E-06	0.0075347		0.01025308	0.00672687	0.01697994	2.8188E-06	0.01698276		0.01923982	0.01323349	0.03247331	1.8792E-06	0.03247519
57	0.00543173	0.0034536	0.00888533	2.5849E-06	0.00888792		0.01451153	0.01002759	0.02453912	1.9387E-06	0.02454106		0.02474795	0.01743901	0.04218696	1.2925E-06	0.04218826
58	0.0536652	0.00583142	0.05949662	1.7522E-06	0.05949837		0	-0.0041552	-0.0041552	1.3142E-06	-0.0041539		0.1058309	0.01553901	0.12136991	8.761E-07	0.12137079
59	0.0536652	0.00466276	0.05832796	2.245E-06	0.05833021		0	-0.0053239	-0.0053239	1.6838E-06	-0.0053222		0.1058309	0.01437035	0.12020125	1.1225E-06	0.12020238
60	0.0506234	0.00364223	0.05426563	2.4367E-06	0.05426807		0	-0.0057784	-0.0057784	1.8275E-06	-0.0057765		0.1058309	0.01391587	0.11974678	1.2183E-06	0.119748
61	0.00636867	0.00226319	0.00863187	1.0791E-06	0.00863294		0.01972472	0.00752859	0.02725331	8.0931E-07	0.02725412		0.01396319	0.00525721	0.01922204	5.395E-07	0.01922094
62	0.00336998	0.00114853	0.00451851	9.4958E-07	0.00451946		0.01312138	0.00507731	0.01819869	7.1219E-07	0.0181904		0.01207331	0.00465505	0.01672835	4.748E-07	0.01672883
63	0.03263553	0.01354853	0.04618406	5.4924E-07	0.04618461		0.04489567	0.01869072	0.06358639	4.1193E-07	0.0635868		0.05459674	0.02275958	0.07735632	2.7462E-07	0.07735659
64	0.05696648	0.01685948	0.07382595	2.5501E-07	0.07382621		0.08038573	0.02385596	0.10424168	1.9125E-07	0.10424188		0.09814184	0.02916058	0.12730241	1.275E-07	0.12730254
65	0.03447423	0.01323942	0.04771365	6.895E-07	0.04771434		0.04640603	0.01787789	0.06428392	5.1712E-07	0.06428444		0.05623844	0.02170023	0.07793867	3.4475E-07	0.07793902
66	0.01107369	0.00296452	0.01403821	2.0242E-06	0.01404024		0.03010759	0.00957495	0.03968254	1.5181E-06	0.03968405		0.02784032	0.00878753	0.03662785	1.0121E-06	0.03662887
67	0.01107369	0.00305507	0.01412876	1.8162E-06	0.01413058		0.03010759	0.00966549	0.03977309	1.3622E-06	0.03977445		0.02784032	0.00887808	0.0367184	9.0811E-07	0.03671931
68	0.01107369	0.00297056	0.01404425	2.0103E-06	0.01404626		0.03010759	0.00958098	0.03968857	1.5077E-06	0.03968008		0.02784032	0.00879357	0.03683389	1.0052E-06	0.0368349
69	0.01248946	0.00306563	0.01555511	2.9212E-06	0.01555803		0.03295765	0.0101742	0.04313185	2.1909E-06	0.04313404		0.04084704	0.01291416	0.0537612	1.4606E-06	0.05376266
70	0.01523015	0.00639867	0.02162881	1.7751E-06	0.02163059		0.02767185	0.01195496	0.03962681	1.3314E-06	0.03962814		0.033002	0.01433533	0.04733732	8.8757E-07	0.04733821
71	0.0117605	0.00471487	0.01647538	2.3669E-06	0.01647774		0.02160798	0.00911262	0.0307206	1.7751E-06	0.03072237		0.02359242	0.00999884	0.03359126	1.1834E-06	0.03359245

	HH	HI	HJ	HK	HL	HM	HN	HO	HP	HQ	HR	HS	HT
2	a = 1%	a = 5%	a = 10%	a= 15%	a = 20%	φmLw - 1%	φmLw 1% < α < 5%	φmLw 5% < α < 10%	φmLw - 10% < α < 15%	φmLw - 15% < α < 20%	φmLw - α	φmLw	
3	0.03729441	0.02892478	0.02187571	0.01826528	0.01690177	0	0	0	0	0	0.016902	0.016902	
4	0.04332177	0.03416808	0.02385727	0.02031823	0.01770486	0	0	0	0.01724879	0	0	0.017249	
5	0.04332177	0.03416808	0.02385727	0.02031823	0.01770486	0	0	0.01818869	0	0	0	0.018189	
6	0.03844277	0.02990681	0.02225536	0.01865445	0.01705763	0	0	0	0	0	0.017058	0.017058	
7	0.04364188	0.03445211	0.02396181	0.0204279	0.01774658	0	0	0	0.01736291	0	0	0.017363	
8	0.04364188	0.03445211	0.02396181	0.0204279	0.01774658	0	0	0.01819456	0	0	0	0.018195	
9	0.04016056	0.03139162	0.02396181	0.0204279	0.01774658	0	0	0.01819456	0	0	0	0.018195	
10	0.04016056	0.03139162	0.02282129	0.01923844	0.01728811	0	0	0.01826734	0	0	0	0.018267	
11	0.04016056	0.03139162	0.02282129	0.01923844	0.01728811	0	0	0.01786746	0	0	0	0.017867	
12	0.04016056	0.03139162	0.02282129	0.01923844	0.01728811	0	0	0.01782316	0	0	0	0.017823	
13	0.04016056	0.03139162	0.02282129	0.01923844	0.01728811	0	0	0.01826734	0	0	0	0.018267	
14	0.0788	0.0676	0.02282129	0.01923844	0.01728811	0	0	0.01826734	0	0	0	0.018267	
15	0.0788	0.0676	0.0352	0.0327	0.022	0	0	0.03466743	0	0	0	0.034667	
16	0.0788	0.0676	0.0352	0.0327	0.022	0	0	0	0	0	0.022	0.022	
17	0.0788	0.0676	0.0352	0.0327	0.022	0	0	0	0	0	0.022	0.022	
18	0.04523353	0.03587155	0.0352	0.0327	0.022	0	0	0	0	0	0.022	0.022	
19	0.02399357	0.01852403	0.02448072	0.02097406	0.01795279	0	0	0	0	0	0.017953	0.017953	
20	0.03293787	0.02529011	0.01735668	0.01387056	0.0149328	0	0	0	0	0	0.014933	0.014933	
21	0.03293787	0.02529011	0.02042405	0.01679941	0.0162952	0	0	0	0	0	0.016295	0.016295	
22	0.03293787	0.02529011	0.02042405	0.01679941	0.0162952	0	0	0	0	0	0.016295	0.016295	
23	0.03293787	0.02529011	0.02042405	0.01679941	0.0162952	0	0	0	0	0	0.016295	0.016295	
24	0.03293787	0.02529011	0.02042405	0.01679941	0.0162952	0	0	0	0	0	0.016295	0.016295	
25	0.03801066	0.02953625	0.02042405	0.01679941	0.0162952	0	0	0	0	0	0.016295	0.016295	
26	0.0788	0.0676	0.02211263	0.01850789	0.01699916	0	0	0	0	0	0.016999	0.016999	
27	0.0788	0.0676	0.0352	0.0327	0.022	0	0	0	0	0	0.022	0.022	
28	0.03194775	0.02448759	0.0352	0.0327	0.022	0	0	0	0	0	0.022	0.022	
29	0.0788	0.0676	0.02009119	0.01646899	0.01615339	0	0	0	0	0	0.016153	0.016153	
30	0.018	0.026	0.0352	0.0327	0.022	0	0	0	0	0	0.022	0.022	
31	0.018	0.026	0.0138	0.0133	0.012	0	0	0.00877077	0	0	0	0.008771	
32	0.018	0.026	0.0138	0.0133	0.012	0	0	0.00877077	0	0	0	0.008771	
33	0.018	0.026	0.0138	0.0133	0.012	0	0	0.00877077	0	0	0	0.008771	
34	0.018	0.026	0.0138	0.0133	0.012	0	0	0.0091661	0	0	0	0.009166	
35	0.018	0.026	0.0138	0.0133	0.012	0	0	0.00430059	0	0	0	0.004301	
36	0.018	0.026	0.0138	0.0133	0.012	0	0	0.00430059	0	0	0	0.004301	
37	0.018	0.026	0.0138	0.0133	0.012	0	0	0.00430059	0	0	0	0.004301	
38	0.018	0.026	0.0138	0.0133	0.012	0	0	0.00430059	0	0	0	0.004301	
39	0.018	0.026	0.0138	0.0133	0.012	0	0	0.00896644	0	0	0	0.008966	
40	0.018	0.026	0.0138	0.0133	0.012	0	0	0.00896644	0	0	0	0.008966	
41	0.018	0.026	0.0138	0.0133	0.012	0	0	0.00896644	0	0	0	0.008966	
42	0.018	0.026	0.0138	0.0133	0.012	0	0	0.00896644	0	0	0	0.008966	
43	0.018	0.026	0.0138	0.0133	0.012	0	0	0.00896644	0	0	0	0.008966	
44	0.03293787	0.02529011	0.0138	0.0133	0.012	0	0	0.00896644	0	0	0	0.008966	
45	0.03293787	0.02529011	0.02042405	0.01679941	0.0162952	0	0	0	0	0	0.016295	0.016295	
46	0.04053333	0.03171617	0.02042405	0.01679941	0.0162952	0	0	0	0	0	0.016295	0.016295	
47	0.04053333	0.03171617	0.02294381	0.01936543	0.01733773	0	0	0	0	0	0.017338	0.017338	
48	0.04053333	0.03171617	0.02294381	0.01936543	0.01733773	0	0	0.0196136	0	0	0	0.019614	
49	0.04053333	0.03171617	0.02294381	0.01936543	0.01733773	0	0	0	0	0	0.017338	0.017338	
50	0.04053333	0.03171617	0.02294381	0.01936543	0.01733773	0	0	0	0	0	0.017338	0.017338	
51	0.02830865	0.0216346	0.02294381	0.01936543	0.01733773	0	0	0	0	0	0.017338	0.017338	
52	0.02830865	0.0216346	0.01885571	0.01526574	0.01561592	0	0	0.01685264	0	0	0	0.016853	
53	0.03293787	0.02529011	0.01885571	0.01526574	0.01561592	0	0	0.01685264	0	0	0	0.016853	
54	0.0788	0.0676	0.02042405	0.01679941	0.0162952	0	0	0	0	0	0.016295	0.016295	
55	0.02049571	0.01637222	0.0352	0.0327	0.022	0	0	0	0	0	0.022	0.022	
56	0.03293787	0.02529011	0.01609534	0.01278245	0.01431688	0	0	0	0	0	0.014317	0.014317	
57	0.03656457	0.05625636	0.02042405	0.01679941	0.0162952	0	0	0	0	0	0.016295	0.016295	
58	0.03656457	0.05625636	0.01813995	0.02125826	0.01210107	0	0	0	0.0228188	0	0	0.022819	
59	0.03656457	0.05625636	0.01813995	0.02125826	0.01210107	0	0	0	0.0228188	0	0	0.022819	
60	0.0549184	0.0447248	0.01813995	0.02125826	0.01210107	0	0	0	0.02152541	0	0	0.021525	
61	0.0788	0.0676	0.0276112	0.0243224	0.0191712	0	0	0.01267236	0	0	0	0.012672	
62	0.0788	0.0676	0.0352	0.0327	0.022	0	0	0.00691733	0	0	0	0.006917	
63	0.0788	0.0676	0.0352	0.0327	0.022	0	0.06363929	0	0	0	0	0.063639	
64	0.0788	0.0676	0.0352	0.0327	0.022	0	0.0598148	0	0	0	0	0.059815	
65	0.05853371	0.04810694	0.0352	0.0327	0.022	0	0.06722475	0	0	0	0	0.067225	
66	0.05853371	0.04810694	0.02877013	0.02558127	0.01961303	0	0	0.01501193	0	0	0	0.015012	
67	0.05853371	0.04810694	0.02877013	0.02558127	0.01961303	0	0	0.01501193	0	0	0	0.015012	
68	0.02977321	0.02276266	0.02877013	0.02558127	0.01961303	0	0	0.01501193	0	0	0	0.015012	
69	0.0788	0.0676	0.01935544	0.01574766	0.01583561	0	0	0.0169312	0	0	0	0.016931	
70	0.0788	0.0676	0.0352	0.0327	0.022	0	0	0	0.03242752	0	0	0.032428	
71	0.0788	0.0676	0.0352	0.0327	0.022	0	0	0.02504007	0	0	0	0.02504	

	HU	HV	HW	HX	HY	HZ	IA	IB	IC	ID	IE	IF
2	a = 1%	a = 5%	a = 10%	a= 15%	a = 20%	φ75Lw - 1%	φ75Lw 1% < α < 5%	φ75Lw 5% < α < 10%	10% < α < 15%	15% < α < 20%	φ75Lw - α	φ75Lw
3	0.101982	0.055222	0.049413	0.048527	0.047147	0	0	0	0	0	0.047147	0.047147
4	0.120884	0.060757	0.051379	0.050758	0.051232	0	0	0	0.05022	0	0	0.05022
5	0.120884	0.060757	0.051379	0.050758	0.051232	0	0	0.046223	0	0	0	0.046223
6	0.105762	0.056293	0.049829	0.048987	0.048007	0	0	0	0	0	0.048007	0.048007
7	0.121829	0.061046	0.05147	0.050865	0.051419	0	0	0	0.050341	0	0	0.050341
8	0.121829	0.061046	0.05147	0.050865	0.051419	0	0	0.046205	0	0	0	0.046205
9	0.121829	0.061046	0.05147	0.050865	0.051419	0	0	0.046205	0	0	0	0.046205
10	0.11125	0.05788	0.050412	0.049642	0.049222	0	0	0.046444	0	0	0	0.046444
11	0.11125	0.05788	0.050412	0.049642	0.049222	0	0	0.046095	0	0	0	0.046095
12	0.11125	0.05788	0.050412	0.049642	0.049222	0	0	0.046057	0	0	0	0.046057
13	0.11125	0.05788	0.050412	0.049642	0.049222	0	0	0.046444	0	0	0	0.046444
14	0.11125	0.05788	0.050412	0.049642	0.049222	0	0	0.046444	0	0	0	0.046444
15	0.1	0.0908	0.0567	0.0587	0.055	0	0	0.056139	0	0	0	0.056139
16	0.1	0.0908	0.0567	0.0587	0.055	0	0	0	0	0	0.055	0.055
17	0.1	0.0908	0.0567	0.0587	0.055	0	0	0	0	0	0.055	0.055
18	0.1	0.0908	0.0567	0.0587	0.055	0	0	0	0	0	0.055	0.055
19	0.126453	0.062473	0.051904	0.051384	0.052306	0	0	0	0	0	0.052306	0.052306
20	0.048308	0.04185	0.042229	0.041243	0.034558	0	0	0	0	0	0.034558	0.034558
21	0.086679	0.051067	0.047615	0.046602	0.043535	0	0	0	0	0	0.043535	0.043535
22	0.086679	0.051067	0.047615	0.046602	0.043535	0	0	0	0	0	0.043535	0.043535
23	0.086679	0.051067	0.047615	0.046602	0.043535	0	0	0	0	0	0.043535	0.043535
24	0.086679	0.051067	0.047615	0.046602	0.043535	0	0	0	0	0	0.043535	0.043535
25	0.086679	0.051067	0.047615	0.046602	0.043535	0	0	0	0	0	0.043535	0.043535
26	0.104351	0.055891	0.049675	0.048816	0.047688	0	0	0	0	0	0.047688	0.047688
27	0.1	0.0908	0.0567	0.0587	0.055	0	0	0	0	0	0.055	0.055
28	0.1	0.0908	0.0567	0.0587	0.055	0	0	0	0	0	0.055	0.055
29	0.082953	0.0501	0.047149	0.046117	0.042638	0	0	0	0	0	0.042638	0.042638
30	0.1	0.0908	0.0567	0.0587	0.055	0	0	0	0	0	0.055	0.055
31	0.020515	0.0238	0.0094	0.0134	0.057	0	0	0.003464	0	0	0	0.003464
32	0.020515	0.0238	0.0094	0.0134	0.057	0	0	0.003464	0	0	0	0.003464
33	0.020515	0.0238	0.0094	0.0134	0.057	0	0	0.003464	0	0	0	0.003464
34	0.020515	0.0238	0.0094	0.0134	0.057	0	0	0.00393	0	0	0	0.00393
35	0.020515	0.0238	0.0094	0.0134	0.057	0	0	-0.001812	0	0	0	0
36	0.020515	0.0238	0.0094	0.0134	0.057	0	0	-0.001812	0	0	0	0
37	0.020515	0.0238	0.0094	0.0134	0.057	0	0	-0.001812	0	0	0	0
38	0.020515	0.0238	0.0094	0.0134	0.057	0	0	-0.001812	0	0	0	0
39	0.020515	0.0238	0.0094	0.0134	0.057	0	0	0.003695	0	0	0	0.003695
40	0.020515	0.0238	0.0094	0.0134	0.057	0	0	0.003695	0	0	0	0.003695
41	0.020515	0.0238	0.0094	0.0134	0.057	0	0	0.003695	0	0	0	0.003695
42	0.020515	0.0238	0.0094	0.0134	0.057	0	0	0.003695	0	0	0	0.003695
43	0.020515	0.0238	0.0094	0.0134	0.057	0	0	0.003695	0	0	0	0.003695
44	0.020515	0.0238	0.0094	0.0134	0.057	0	0	0.003695	0	0	0	0.003695
45	0.086679	0.051067	0.047615	0.046602	0.043535	0	0	0	0	0	0.043535	0.043535
46	0.086679	0.051067	0.047615	0.046602	0.043535	0	0	0	0	0	0.043535	0.043535
47	0.112416	0.058222	0.050533	0.049779	0.049474	0	0	0	0	0	0.049474	0.049474
48	0.112416	0.058222	0.050533	0.049779	0.049474	0	0	0.047614	0	0	0	0.047614
49	0.112416	0.058222	0.050533	0.049779	0.049474	0	0	0	0	0	0.049474	0.049474
50	0.112416	0.058222	0.050533	0.049779	0.049474	0	0	0	0	0	0.049474	0.049474
51	0.112416	0.058222	0.050533	0.049779	0.049474	0	0	0	0	0	0.049474	0.049474
52	0.068235	0.046449	0.045201	0.044139	0.039118	0	0	0.044301	0	0	0	0.044301
53	0.068235	0.046449	0.045201	0.044139	0.039118	0	0	0.044301	0	0	0	0.044301
54	0.086679	0.051067	0.047615	0.046602	0.043535	0	0	0	0	0	0.043535	0.043535
55	0.1	0.0908	0.0567	0.0587	0.055	0	0	0	0	0	0.055	0.055
56	0.041424	0.037757	0.03892	0.038149	0.030759	0	0	0	0	0	0.030759	0.030759
57	0.086679	0.051067	0.047615	0.046602	0.043535	0	0	0	0	0	0.043535	0.043535
58	0.014839	0.026903	-0.018866	-0.008216	0.171186	0	0	0	-0.002886	0	0	0
59	0.014839	0.026903	-0.018866	-0.008216	0.171186	0	0	0	-0.002886	0	0	0
60	0.014839	0.026903	-0.018866	-0.008216	0.171186	0	0	0	-0.007303	0	0	0
61	0.1187	0.070944	0.054021	0.054103	0.056153	0	0	0.039248	0	0	0	0.039248
62	0.1	0.0908	0.0567	0.0587	0.055	0	0	0.026933	0	0	0	0.026933
63	0.1	0.0908	0.0567	0.0587	0.055	0	0.087547	0	0	0	0	0.087547
64	0.1	0.0908	0.0567	0.0587	0.03	0	0.084405	0	0	0	0	0.084405
65	0.1	0.0908	0.0567	0.0587	0.03	0	0.090492	0	0	0	0	0.090492
66	0.115566	0.07403	0.054623	0.054962	0.056924	0	0	0.040815	0	0	0	0.040815
67	0.115566	0.07403	0.054623	0.054962	0.056924	0	0	0.040815	0	0	0	0.040815
68	0.115566	0.07403	0.054623	0.054962	0.056924	0	0	0.040815	0	0	0	0.040815
69	0.074371	0.047938	0.046034	0.044975	0.040576	0	0	0.044679	0	0	0	0.044679
70	0.1	0.0908	0.0567	0.0587	0.055	0	0	0	0.058918	0	0	0.058918
71	0.1	0.0908	0.0567	0.0587	0.055	0	0	0.046007	0	0	0	0.046007

	IH	II	IJ	IK	IL	IM	IN	IO	IP	IQ	IR	IS	IT	IU	IV	IW	IX	IY	IZ	JA	JB	JC	JD	JE	JF	JG	JH	JI
2	a = 1%	a = 5%	a = 10%	a= 15%	a = 20%	ϕcLw - 1%	ϕcLw 1% < α < 5%	ϕcLw 5% < α < 10%	ϕcLw - 10% < α < 15%	ϕcLw - 15% < α < 20%	ϕcLw - α >	ϕcLw			a = 1%	a = 5%	a = 10%	a= 15%	a = 20%	Mmax/fwAr	Mmax/fwAr nLw 1% <	Mmax/fwAr nLw 5% <	Mmax/fwAr nLw - 10%	Mmax/fwAr nLw - 15%	Mmax/fwAr	Mmax/fwAr	Qflex (kN) NIST	Qflex (kN) Paper
3	0.165549	0.130213	0.081626	0.07444	0.076858	0	0	0	0	0	0.076858	0.076858			0.031585	0.052765	0.071168	0.089939	0.108646	0	0	0	0	0	0.176608	0.176608	212.1458	177
4	0.198476	0.143018	0.081793	0.075688	0.079145	0	0	0	0.070393	0	0	0.070393			0.026707	0.04868	0.067229	0.08628	0.10539	0	0	0	0.102804	0	0	0.102804	123.4907	154
5	0.198476	0.143018	0.081793	0.075688	0.079145	0	0	0.048133	0	0	0	0.048133			0.026707	0.04868	0.067229	0.08628	0.10539	0	0	0.077426	0	0	0	0.077426	93.00601	152
6	0.172134	0.132774	0.081779	0.074766	0.077399	0	0	0	0	0	0.077399	0.077399			0.03061	0.051948	0.07038	0.089207	0.107995	0	0	0	0	0	0.175633	0.175633	316.4608	267
7	0.200122	0.143659	0.081762	0.075725	0.079232	0	0	0	0.07049	0	0	0.07049			0.026463	0.048476	0.067032	0.086098	0.105227	0	0	0	0.102634	0	0	0.102634	184.9284	245
8	0.200122	0.143659	0.081762	0.075725	0.079232	0	0	0.047734	0	0	0	0.047734			0.026463	0.048476	0.067032	0.086098	0.105227	0	0	0.077233	0	0	0	0.077233	139.1614	241
9	0.200122	0.143659	0.081762	0.075725	0.079232	0	0	0.047734	0	0	0	0.047734			0.026463	0.048476	0.067032	0.086098	0.105227	0	0	0.077233	0	0	0	0.077233	139.1614	240
10	0.181694	0.136492	0.081894	0.075171	0.07811	0	0	0.052883	0	0	0	0.052883			0.029194	0.050762	0.069236	0.088145	0.107049	0	0	0.079053	0	0	0	0.079053	158.8012	96.85
11	0.181694	0.136492	0.081894	0.075171	0.07811	0	0	0.050335	0	0	0	0.050335			0.029194	0.050762	0.069236	0.088145	0.107049	0	0	0.079915	0	0	0	0.079915	160.5328	103.67
12	0.181694	0.136492	0.081894	0.075171	0.07811	0	0	0.050053	0	0	0	0.050053			0.029194	0.050762	0.069236	0.088145	0.107049	0	0	0.08001	0	0	0	0.08001	160.7246	96.7
13	0.181694	0.136492	0.081894	0.075171	0.07811	0	0	0.052883	0	0	0	0.052883			0.029194	0.050762	0.069236	0.088145	0.107049	0	0	0.079053	0	0	0	0.079053	317.6024	122.9
14	0.181694	0.136492	0.081894	0.075171	0.07811	0	0	0.052883	0	0	0	0.052883			0.029194	0.050762	0.069236	0.088145	0.107049	0	0	0.079053	0	0	0	0.079053	105.8675	84.3
15	0.12	0.11	0.0645	0.0697	0.0767	0	0	0.063752	0	0	0	0.063752			0.005	0.0305	0.0497	0.07	0.0909	0	0	0.050016	0	0	0	0.050016	126.5795	148
16	0.12	0.11	0.0645	0.0697	0.0767	0	0	0	0	0	0.0767	0.0767			0.005	0.0305	0.0497	0.07	0.0909	0	0	0	0	0	0.112112	0.112112	283.734	278
17	0.12	0.11	0.0645	0.0697	0.0767	0	0	0	0	0	0.0767	0.0767			0.005	0.0305	0.0497	0.07	0.0909	0	0	0	0	0	0.104178	0.104178	263.654	246
18	0.12	0.11	0.0645	0.0697	0.0767	0	0	0	0	0	0.0767	0.0767			0.005	0.0305	0.0497	0.07	0.0909	0	0	0	0	0	0.183521	0.183521	464.454	380
19	0.208176	0.146791	0.081559	0.075874	0.079621	0	0	0	0	0	0.079621	0.079621			0.02527	0.047476	0.066068	0.085203	0.10443	0	0	0	0	0	0.203791	0.203791	515.754	407
20	0.074257	0.093581	0.072937	0.065613	0.064565	0	0	0	0	0	0.064565	0.064565			0.045541	0.064453	0.082436	0.100405	0.117961	0	0	0	0	0	0.267447	0.267447	676.854	558
21	0.138893	0.119847	0.080402	0.072732	0.074244	0	0	0	0	0	0.074244	0.074244			0.035534	0.056073	0.074356	0.092901	0.111282	0	0	0	0	0	0.13919	0.13919	623.601	418
22	0.138893	0.119847	0.080402	0.072732	0.074244	0	0	0	0	0	0.074244	0.074244			0.035534	0.056073	0.074356	0.092901	0.111282	0	0	0	0	0	0.13919	0.13919	623.601	412
23	0.138893	0.119847	0.080402	0.072732	0.074244	0	0	0	0	0	0.074244	0.074244			0.035534	0.056073	0.074356	0.092901	0.111282	0	0	0	0	0	0.13919	0.13919	623.601	398
24	0.138893	0.119847	0.080402	0.072732	0.074244	0	0	0	0	0	0.074244	0.074244			0.035534	0.056073	0.074356	0.092901	0.111282	0	0	0	0	0	0.13919	0.13919	623.601	384
25	0.138893	0.119847	0.080402	0.072732	0.074244	0	0	0	0	0	0.074244	0.074244			0.035534	0.056073	0.074356	0.092901	0.111282	0	0	0	0	0	0.116156	0.116156	520.401	358
26	0.169675	0.131818	0.081729	0.074649	0.077202	0	0	0	0	0	0.077202	0.077202			0.030974	0.052253	0.070674	0.089481	0.108238	0	0	0	0	0	0.118124	0.118124	691.26	408
27	0.12	0.11	0.0645	0.0697	0.0767	0	0	0	0	0	0.0767	0.0767			0.005	0.0305	0.0497	0.07	0.0909	0	0	0	0	0	0.110678	0.110678	534.13	443.4
28	0.12	0.11	0.0645	0.0697	0.0767	0	0	0	0	0	0.0767	0.0767			0.005	0.0305	0.0497	0.07	0.0909	0	0	0	0	0	0.150249	0.150249	586.1733	450.7
29	0.132402	0.117323	0.079957	0.072222	0.073504	0	0	0	0	0	0.073504	0.073504			0.036496	0.056878	0.075133	0.093622	0.111924	0	0	0	0	0	0.212625	0.212625	684.0867	390.8
30	0.12	0.11	0.0645	0.0697	0.0767	0	0	0	0	0	0.0767	0.0767			0.005	0.0305	0.0497	0.07	0.0909	0	0	0	0	0	0.110678	0.110678	801.195	569.8
31	0.049	-0.01	-0.0175	-0.0015	-0.0163	0	0	-0.020592	0	0	0	0			0.085	0.0975	0.1143	0.13	0.1443	0	0	0.121225	0	0	0	0.121225	824.5758	273
32	0.049	-0.01	-0.0175	-0.0015	-0.0163	0	0	-0.020592	0	0	0	0			0.085	0.0975	0.1143	0.13	0.1443	0	0	0.121225	0	0	0	0.121225	824.5758	327
33	0.049	-0.01	-0.0175	-0.0015	-0.0163	0	0	-0.020592	0	0	0	0			0.085	0.0975	0.1143	0.13	0.1443	0	0	0.121225	0	0	0	0.121225	824.5758	346
34	0.049	-0.01	-0.0175	-0.0015	-0.0163	0	0	-0.020349	0	0	0	0			0.085	0.0975	0.1143	0.13	0.1443	0	0	0.120681	0	0	0	0.120681	804.4555	334
35	0.049	-0.01	-0.0175	-0.0015	-0.0163	0	0	-0.02334	0	0	0	0			0.085	0.0975	0.1143	0.13	0.1443	0	0	0.127381	0	0	0	0.127381	733.1713	232
36	0.049	-0.01	-0.0175	-0.0015	-0.0163	0	0	-0.02334	0	0	0	0			0.085	0.0975	0.1143	0.13	0.1443	0	0	0.127381	0	0	0	0.127381	733.1713	215
37	0.049	-0.01	-0.0175	-0.0015	-0.0163	0	0	-0.02334	0	0	0	0			0.085	0.0975	0.1143	0.13	0.1443	0	0	0.127381	0	0	0	0.127381	733.1713	244
38	0.049	-0.01	-0.0175	-0.0015	-0.0163	0	0	-0.02334	0	0	0	0			0.085	0.0975	0.1143	0.13	0.1443	0	0	0.127381	0	0	0	0.127381	733.1713	223
39	0.049	-0.01	-0.0175	-0.0015	-0.0163	0	0	-0.020471	0	0	0	0			0.085	0.0975	0.1143	0.13	0.1443	0	0	0.120956	0	0	0	0.120956	530.1756	226
40	0.049	-0.01	-0.0175	-0.0015	-0.0163	0	0	-0.020471	0	0	0	0			0.085	0.0975	0.1143	0.13	0.1443	0	0	0.120956	0	0	0	0.120956	530.1756	213
41	0.049	-0.01	-0.0175	-0.0015	-0.0163	0	0	-0.020471	0	0	0	0			0.085	0.0975	0.1143	0.13	0.1443	0	0	0.120956	0	0	0	0.120956	530.1756	211
42	0.049	-0.01	-0.0175	-0.0015	-0.0163	0	0	-0.020471	0	0	0	0			0.085	0.0975	0.1143	0.13	0.1443	0	0	0.120956	0	0	0	0.120956	530.1756	209
43	0.049	-0.01	-0.0175	-0.0015	-0.0163	0	0	-0.020471	0	0	0	0			0.085	0.0975	0.1143	0.13	0.1443	0	0	0.120956	0	0	0	0.120956	530.1756	215
44	0.049	-0.01	-0.0175	-0.0015	-0.0163	0	0	-0.020471	0	0	0	0			0.085	0.0975	0.1143	0.13	0.1443	0	0	0.120956	0	0	0	0.120956	530.1756	230
45	0.138893	0.119847	0.080402	0.072732	0.074244	0	0	0	0	0	0.074244	0.074244			0.035534	0.056073	0.074356	0.092901	0.111282	0	0	0	0	0	0.13919	0.13919	897.9854	418
46	0.138893	0.119847	0.080402	0.072732	0.074244	0	0	0	0	0	0.074244	0.074244			0.035534	0.056073	0.074356	0.092901	0.111282	0	0	0	0	0	0.13919	0.13919	598.657	315
47	0.183725	0.137282	0.081902	0.075247	0.078249	0	0	0	0	0	0.078249	0.078249			0.028893	0.05051	0.068993	0.087919	0.106848	0	0	0	0	0	0.120903	0.120903	286.4323	314.3
48	0.183725	0.137282	0.081902	0.075247	0.078249	0	0	0.060879	0	0	0	0.060879			0.028893	0.05051	0.068993	0.087919	0.106848	0	0	0.07601	0	0	0	0.07601	38.96372	94.2
49	0.183725	0.137282	0.081902	0.075247	0.078249	0	0	0	0	0	0.078249	0.078249			0.028893	0.05051	0.068993	0.087919	0.106848	0	0	0	0	0	0.239541	0.239541	184.1882	132.3
50	0.183725	0.137282	0.081902	0.075247	0.078249	0	0	0	0	0	0.078249	0.078249			0.028893	0.05051	0.068993	0.087919	0.106848	0	0	0	0	0	0.239541	0.239541	184.1882	178.9
51	0.183725	0.137282	0.081902	0.075247	0.078249	0	0	0	0	0	0.078249	0.078249			0.028893	0.05051	0.068993	0.087919	0.106848	0	0	0	0	0	0.239541	0.239541	257.8634	181
52	0.106765	0.107353	0.077631	0.069845	0.070186	0	0	0.056208	0	0	0	0.056208			0.040294	0.060059	0.0782	0.096471	0.114459	0	0	0.091276	0	0	0	0.091276	35.83225	51.67
53	0.106765	0.107353	0.077631	0.069845	0.070186	0	0	0.056208	0	0	0	0.056208			0.040294	0.060059	0.0782	0.096471	0.114459	0	0	0.091276	0	0	0	0.091276	35.83225	50.39
54	0.138893	0.119847	0.080402	0.072732	0.074244	0	0	0	0	0	0.074244	0.074244			0.035534	0.056073	0.074356	0.092901	0.111282	0	0	0	0	0	0.13919	0.13919	623.601	367
55	0.12	0.11	0.0645	0.0697	0.0767	0	0	0	0	0	0.0767	0.0767			0.005	0.0305	0.0497	0.07	0.0909	0	0	0	0	0	0.108656	0.108656	486.801	345
56	0.067023	0.079771	0.066502	0.060263	0.057719	0	0	0	0	0	0.057719	0.057719			0.050802	0.068859	0.086685	0.104351	0.121473	0	0	0	0	0	0.154458	0.154458	692.001	458
57	0.138893	0.119847	0.080402	0.072732	0.074244	0	0	0	0	0	0.074244	0.074244			0.035534	0.056073	0.074356	0.092901	0.111282	0	0	0	0	0	0.13919	0.13919	623.601	315
58	0.049	0.048	0.045	0.045	0.044	0	0	0	0.045	0	0	0.045			0.108448	0.117138	0.133234	0.147586	0.159952	0	0	0	0.154768	0	0	0.154768	29.4569	64
59	0.049	0.048	0.045	0.045	0.044	0	0	0	0.045	0	0	0.045			0.108448	0.117138	0.133234	0.147586	0.159952	0	0	0	0.154768	0	0	0.154768	29.4569	82
60	0.049	0.048	0.045	0.045	0.044	0	0	0	0.045	0	0	0.045			0.108448	0.117138	0.133234	0.147586	0.159952	0	0	0	0.148816	0	0	0.148816	28.32392	89
61	0.1812	0.1372	0.07878	0.075657	0.080644	0	0	0.027784	0	0	0	0.027784			0.0186	0.04189	0.060682	0.0802	0.099778	0	0	0.077086	0	0	0	0.077086	435.4916	250
62	0.12	0.11	0.0645	0.0697	0.0767	0	0	0.024782	0	0	0	0.024782			0.005	0.0305	0.0497	0.07	0.0909	0	0	0.06646	0	0	0	0.06646	387.3183	220
63	0.12	0.11	0.0645	0.0697	0.0767	0	0.106464	0	0	0	0	0.106464			0.005	0.0305	0.0497	0.07	0.0909	0	0.039518	0	0	0	0	0.039518	343.8754	200
64	0.12	0.11	0.0645	0.0697	0.0767	0	0.103049	0	0	0	0	0.103049			0.005	0.0305	0.0497	0.07	0.0909	0	0.048225	0	0	0	0	0.048225	121.6727	50
65	0.12	0.11	0.0645	0.0697	0.0767	0	0.109665	0	0	0	0	0.109665			0.005	0.0305	0.0497	0.07	0.0909	0	0.031354	0	0	0	0	0.031354	201.0398	185
66	0.170943	0.132642	0.077193	0.075175	0.080547	0	0	0.037741	0	0	0	0.037741			0.016321	0.039981	0.058842	0.078491	0.098457	0	0	0.072261	0	0	0	0.072261	86.58841	146
67	0.170943	0.132642	0.077193	0.075175	0.080547	0	0	0.037741	0	0	0	0.037741			0.016321	0.039981	0.058842	0.078491	0.098457	0	0	0.072261	0	0	0	0.072261	86.58841	131
68	0.170943	0.132642	0.077193	0.075175	0.080547	0	0	0.037741	0	0	0	0.037741			0.016321	0.039981	0.058842	0.078491	0.098457	0	0	0.072261	0	0	0	0.072261	86.58841	145
69	0.117453	0.111509	0.07871	0.070906	0.071646	0	0	0.055374	0	0	0	0.055374			0.038711	0.058733	0.076921	0.095283	0.113402	0	0	0.089863	0	0	0	0.089863	107.6804	210.7
70	0.12	0.11	0.0645	0.0697	0.0767	0	0	0	0.070267	0	0	0.070267			0.005	0.0305	0.0497	0.07	0.0909	0	0	0	0.072213	0	0	0.072213	95.53024	90
71	0.12	0.11	0.0645	0.0697	0.0767	0	0	0.050232	0	0	0	0.050232			0.005	0.0305	0.0497	0.07	0.0909	0	0	0.055721	0	0	0	0.055721	73.71315	120